OPTIMIZATION STUDIES ON ONE-PART GEOPOLYMER MIXES (PASTES, MORTARS AND CONCRETES)

Thesis

submitted in partial fulfilment of the requirements for the degree of

DOCTOR OF PHILOSOPHY

by

ANIL SAGAR S

(187006CV003)

DEPARTMENT OF CIVIL ENGINEERING

NATIONAL INSTITUTE OF TECHNOLOGY KARNATAKA

SURATHKAL, MANGALORE – 575 025

AUGUST, 2024

OPTIMIZATION STUDIES ON ONE-PART GEOPOLYMER MIXES (PASTES, MORTARS AND CONCRETES)

Thesis

submitted in partial fulfilment of the requirements for the degree of

DOCTOR OF PHILOSOPHY

by

ANIL SAGAR S

(187006CV003)

Under the Guidance of

Prof. Subhash C Yaragal

&

Prof. K Swaminathan

DEPARTMENT OF CIVIL ENGINEERING

NATIONAL INSTITUTE OF TECHNOLOGY KARNATAKA

SURATHKAL, MANGALORE – 575 025

AUGUST, 2024

DECLARATION

I hereby declare that the Research Thesis entitled "**OPTIMIZATION STUDIES ON ONE-PART GEOPOLYMER MIXES (PASTES, MORTARS AND CONCRETES)**", which is being submitted to the National Institute of Technology Karnataka, Surathkal in partial fulfilment of the requirements for the award of the **Degree of Doctor of Philosophy** in **Civil Engineering**, is *a bonafide report of the work carried out by me*. The material contained in this Research Thesis has not been submitted to any University or Institution for the award of any degree.

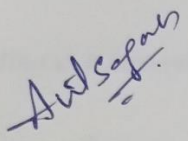

ANIL SAGAR S

Register No. 187006CV003

Department of Civil Engineering

NITK, Surathkal

CERTIFICATE

This is to certify that the Research Thesis entitled "**OPTIMIZATION STUDIES ON ONE-PART GEOPOLYMER MIXES (PASTES, MORTARS AND CONCRETES)**" submitted by **ANIL SAGAR S (Register Number: 187006CV003)** as the record of the work carried out by him, is accepted as the Research Thesis submission in partial fulfilment of the requirements for the award of degree of **Doctor of Philosophy**.

Research Supervisors

Prof. Subhash C. Yaragal & Prof. K Swaminathan
Department of Civil Engineering
NITK Surathkal – 575 025

राष्ट्रीय प्रौद्योगिकी संस्थान कर्नाटक, सुरत्कल
सिविल अभियांत्रिकी विभाग
Dept. of Civil Engineering
National Institute of Technology Karnataka, Surathkal

HOD/Chairman – DRPC
Department of Civil Engineering
NITK Surathkal – 575 025
Karnataka, India.

Chairman (DRPC)
Department of Civil Engineering
National Institute of Technology Karnataka
Surathkal, Mangalore - 575 025, Karnataka, INDIA

ACKNOWLEDGEMENT

I take this opportunity to express my sincere gratitude to my research supervisors Dr. Subhash C Yaragal and Dr. K Swaminathan, for their constant support, patience, motivation, enthusiasm, and guidance during the entire journey of my research work.

I wish to extend my sincere thanks to Dr. M C Narasimhan, Professor, Department of Civil Engineering, and Dr. Anandhan Srinivasan, Professor, Department of Metallurgical and Materials Engineering, for being the Research Progress Assessment Committee (RPAC) members and for their valuable suggestions at various stages of the research.

I wish to thank Dr. Subhash C. Yaragal, Head of the Civil Engineering Department, former Heads of the Civil Engineering Department, Dr. Varghese George, Dr. K Swaminathan, and Dr. B. R. Jayalekshmi for their support during various stages of this work.

For the support and facilities extended, I would also like to thank Dr. B B Das, Faculty-in-Charge of Civil Engineering Materials Laboratory, and Dr. T Palanisamy, Faculty-in-Charge of Structural Engineering Laboratory.

This research work would not have been possible without the support and cooperation of the laboratory staff of Civil Engineering, Mr. Geethesh Shetty, Mr. Ramanath Acharya, Mr. Ranjith, and Mr. Manmohan Shetty.

I would also like to extend my sincere thanks to the concerned faculty and staff of Central Research Facility and Department of Metallurgical and Materials Engineering, NITK for providing necessary facilities for conduct of microstructural studies.

I place on record the faculty members of Civil Engineering Department, for their valuable suggestions and guidance.

Finally, I am thankful to my family and friends who have encouraged me during the progress of the research work.

ANIL SAGAR S

ABSTRACT

The consumption of ordinary Portland cement (OPC) to meet the enormous need for concrete production all over the world, is a global threat for climate change. To reduce massive carbon dioxide emissions associated with the manufacturing of OPC, the geopolymerization process has given rise to the transformation of industrial wastes into strong and durable construction materials such as geopolymer binders. However, these geopolymer binders are based on aluminosilicate by-products and alkali activators. The activators involved in alkali activation process are concentrated aqueous solutions, which are viscous, corrosive and caustic. In addition, complexity in transportation and impracticalities in site such as, difficulty in handling, not user friendly, and hard to use for mass production. This study reports on development of a novel 'one-part' or 'just-add water' geopolymer binder produced by dry blending the solid aluminosilicate precursors, solid alkali source and then adding free water to the blended dry mix to produce a binder as similar to OPC.

One-part geopolymers (OPG) have immense potential in large-scale structures owing to their improved safety and convenience of handling over the conventional geopolymer mixing procedure. This study aims to optimize the mixes by understanding, assessing the influence of binder content, activator dosage and water to geopolymer solids (W/GS) ratio on the fresh and hardened properties of one-part geopolymer mixes (namely pastes, mortars and concretes). Various fly ash and slag-based OPG mixes have been developed and studied. The GGBS substitution was chosen as 25, 50, and 75% by volume of fly ash. The activator dosage was taken as 8, 12, and 16% by mass of total binder content and at varied W/GS ratios of 0.35, 0.40, and 0.45. The test results were utilized to develop models which can predict the desired properties of mixes and optimize the mix proportions of OPG mixes using the response surface method (RSM). The microstructural characterization adopting techniques like Scanning Electron Microscope (SEM), X-Ray Diffraction (XRD), Thermal Gravimetric Analysis (TGA) and Fourier Transform Infrared (FTIR) was carried out to study microstructural changes, mineral phases, thermal mass loss and molecular bonding of OPG mixes. The elevated temperature studies, ecological and cost analysis studies were also performed.

Based on the material characterization observations, the change in GGBS addition, activator dosage, and W/GS ratio were observed to have a considerable impact on both the fresh and hardened properties. The optimum mix proportion of OPG paste obtained was 51.4% GGBS substitution, 12.4% activator content, and 0.32 W/GS ratio with 191 mm flow, 68.6 MPa of compressive strength, 59 and 191 mins of initial and final setting times, respectively. The optimum mix proportion of OPG mortar obtained consists of 49.8% GGBS, 13.6% activator dosage, and 0.37 W/GS ratio. This mix achieved 170.4 mm flow, 57.8 MPa and 5.9 MPa compressive and flexural strengths, respectively and also 1626 microstrain of 180 days drying shrinkage. The optimum mix composition of OPG concrete for achieving a 125 mm slump while maximizing strengths comprises of 75% GGBS, activator dosage of 13.8%, and W/GS ratio of 0.34. This optimized mix achieved compressive, flexural, and split tensile strengths of 73 MPa, 6.2 MPa and 3.9 MPa, respectively. The verification of experimental values of proposed optimized mix are within the absolute deviation of 10% of predicted values, indicating the accuracy of the models and effectiveness of RSM in designing the optimum mix proportions of OPG mixes. Elevated temperature endurance of OPGC mixes increases with both GGBS content and activator dosage. Embodied CO_2eq (ECO_2eq) and embodied energy (EEeq) increases with increase in activator dosage. The ECO_2eq and EEeq of OPG concrete mixes are lower compared to OPC based concrete mixes. Hence the OPG mixes can be considered as more eco-friendly and sustainable materials, as against conventional OPC based mixes.

Keywords: One-part geopolymer, Optimization, Response surface method, Solid activator, Ecological studies

TABLE OF CONTENTS

LIST OF FIGURES

LIST OF TABLES

NOMENCLATURE

Abbreviations

AAB	:	Alkali Activated Binder
AAM	:	Alkali-Activated Material
AASC	:	Alkali-Activated Slag Concrete
BBD	:	Box-Behnken Design
C-A-S-H	:	Calcium-Aluminium-Silicate-Hydrate
CCD	:	Central Composite Design
CpS	:	Compressive Strength
C-S-H	:	Calcium-Silicate-Hydrate
DrS	:	Drying Shrinkage
DTG	:	Differential Thermogravimetry
ECO_2e	:	Equivalent Carbon Dioxide Emissions
EDS	:	Energy Dispersive Spectroscopy
EE	:	Embodied Energy
EIA	:	Environmental Impact Assessment
FA	:	Fly Ash
FFD	:	Full Factorial Design
FrS	:	Flexural Strength
FTIR	:	Fourier Transform Infrared
GGBS	:	Ground-Granulated Blast-Furnace Slag
GWP	:	Global Warming Potential
HCFA	:	High Calcium Fly Ash
LCA	:	Life Cycle Analysis
N-A-S-H	:	Sodium-Aluminium-Silicate-Hydrate
OPC	:	Ordinary Portland Cement
OPG	:	One-Part Geopolymer
OPGB	:	One-Part Geopolymer Binders
RSM	:	Response Surface Method
SEM	:	Scanning Electron Microscope
SpS	:	Split Tensile Strength

TGA	:	Thermal Gravimetric Analysis
W/GS	:	Water-To-Geopolymer Solids Ratio
XRD	:	X-Ray Diffraction

CHAPTER 1

INTRODUCTION

1.1 GENERAL

Nowadays, Concrete no doubt is the most popular building material in the building sector because of its wide application to meet the needs of the general populace. Concrete is advantageous in its use due to its mouldability, strength, durability, resistance to natural disasters, cost-effectiveness, and low maintenance requirements. These benefits make it a versatile material used in various applications and an economically viable option. The primary constituents of concrete are cement, water, and aggregates. Ordinary Portland Cement (OPC) is the primary binding ingredient in producing mortar and concrete. OPC can set, strengthen, and adhere to various building materials, such as bricks, tiles, stones, and reinforced steel, among others. The cement production significantly utilizes natural resources such as limestone, chalk, shells, clay, and other minerals. The rapid depletion of natural resources is a consequence of the extensive utilization of stated resources in the production of OPC. The manufacturing process involves the calcination of limestone and the combustion of fossil fuels during manufacturing, which results in significant carbon dioxide (CO_2) emissions into the atmosphere, ultimately contributing to global warming and climate change. As environmental protection and sustainable developments are concerned, the researchers are motivated to explore sustainable solutions for replacing conventional cement and to investigate the potential for incorporating value-added industrial by-products as part/full replacement to OPC.

1.2 CEMENT

The cement industry is a crucial contributor to the economic growth of a nation, as it generates significant revenue for the government and provides employment opportunities in infrastructure development and urban housing. The construction industry heavily relies on cement as the primary material of consumption. India holds the position of being the second-largest cement producer globally. The demand for cement in different sectors in India during FY21 is depicted in Figure 1.1. Cement

consumption and production in India from FY16 to FY22 are illustrated in Figure 1.2 (Source: ibef.org). The per capita demand for cement in India is 195 kg annually, whereas 1000 kg in China (Bureau of energy efficiency, Ministry of Power, Government of India).

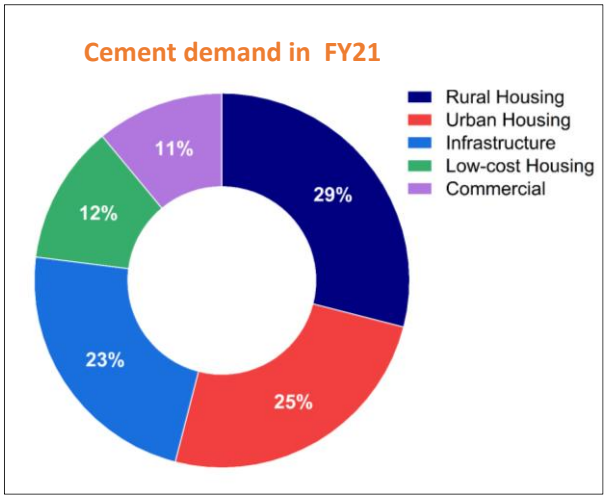

Figure 1.1 Cement demand in India during FY21 (Source: ibef.org; 06.01.2024)

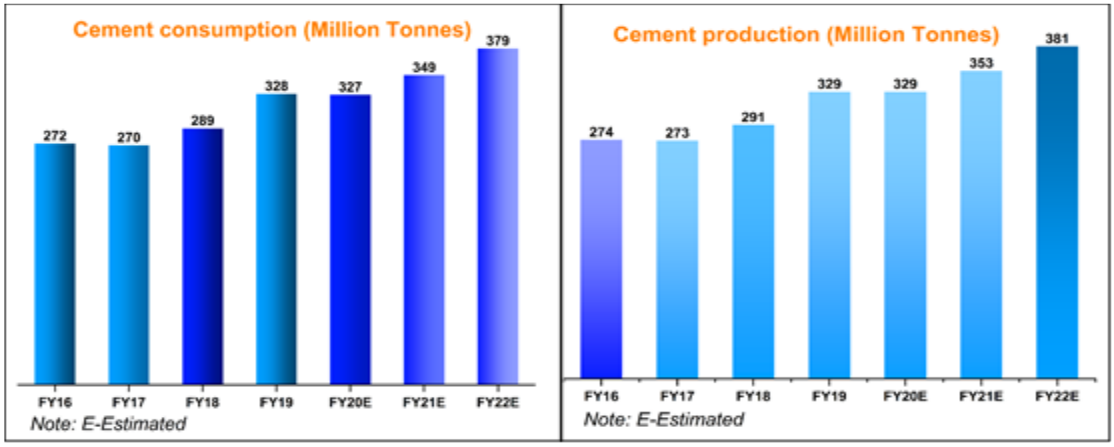

Figure 1.2 Cement consumption and production in India (Source: ibef.org; 06.01.2024)

In recent updates, global cement production is reported to be responsible for 8% of the world`s CO_2 emission. The total emission of CO_2 per kg of cement clinker produced is about 0.55 kg for the decarbonation of calcite, 0.33 kg from the burning phase and about 0.12 kg by the energy required for power supply, making a total about one tonne. As a result, cement production is regarded as an energy-intensive process, with each tonne of OPC produced emitting around 1 tonne of CO_2 (Rehan and Nehdi

2005). In cement production, energy inputs account for 50-60% (Wang et al. 2009) of total cost, with thermal energy accounting for about 20-25%, and typical electrical energy consumption of a modern cement plant is about 110-120 kWh per tonne of cement, accounting for 30-40% of cement production cost (Madlool et al. 2011). The main thermal energy is used during the burning process, while electrical energy is used for cement grinding. Hence, the cement industries across the world are blamed for contributing more CO_2 in all the stages of cement production. Therefore, sustainable and eco-friendly research and development is urgently needed to mitigate the concern. This necessitates the development of new, practical technologies that could efficiently cut down on the use of energy, natural resources, and CO_2 emissions. However, it is essential to ensure these developments do not impair the concretes strength and durability characteristics.

1.3 GEOPOLYMER BINDERS

Geopolymer binders have developed as a possible alternative to standard OPC in recent years, spurred by the need for sustainable and environmentally friendly construction materials. These cutting-edge binders have special qualities and advantages that make them suited for a variety of uses, including the manufacturing of concrete, soil stabilisation, and waste encapsulation.

Geopolymers refer to inorganic polymers synthesized from different aluminosilicate materials such as fly ash, slag, or clay activated with strong alkaline activators, typically sodium silicate (Na_2SiO_3), potassium silicate (K_2SiO_3), sodium hydroxide (NaOH), and potassium hydroxide (KOH) or mixture of these. Alkaline activation causes the aluminosilicate components to dissolve and reform into a three-dimensional polymeric network. Geopolymer binders are synthesized through a chemical process known as geopolymerization (Duxson and Provis 2008; Pacheco-Torgal et al. 2008). The geopolymer based concrete known for the exceptional mechanical and durability comparable to or even surpassing conventional concrete (Fu et al. 2011; Kong and Sanjayan 2010; Ryu et al. 2013). This strength is attributable to the creation of a highly interconnected and rigid structure during geopolymerization, resulting in improved performance and structural integrity (Singh et al. 2015). Geopolymer binders are noted for having a low carbon footprint, which is an important

benefit in the context of sustainable construction. Geopolymer binders utilise industrial by-products and need less energy during synthesis, lowering both energy consumption and greenhouse gas emissions. This attribute is consistent with worldwide efforts to reduce climate change and move to a more sustainable future (Rehan and Nehdi 2005).

However, various parameters influence the strength and durability of geopolymer binders. These parameters include the curing regime, type of curing, total water content, water to binder ratio, type of source materials, type of alkaline activators, dosage and activator modulus of alkaline activators, etc. All of these factors play a crucial role in determining the overall performance and longevity of geopolymer binders (Rashad 2013). Numerous research investigations have found that geopolymer binders outperform traditional OPC in terms of mechanical and durability characteristics. As a result, geopolymer binders have emerged as a possible alternative to OPC in various applications. Some of the recent construction projects which have incorporated geopolymer based concrete include the following: University of Queensland's Global Change Institute (2013, Australia); Toowoomba Well camp Airport (2014, Australia); and Transnet's City Deep Container Terminal (2015, South Africa).

In spite of several advantages and practical applications, geopolymer binder materials have demonstrated their impracticalities, drawbacks, and limitations in major engineering applications. These limitations arise from the utilization of highly corrosive, substantial volumes of viscous, and hazardous liquid alkali activators, which possess high causticity and lack of user-friendliness. The use of geopolymers in construction demands the implementation of stringent protection procedures during workers' operations, transportation, storage, and handling of the alkaline solution. These procedures necessitate the adoption of additional safety measures, leading to a slower pace in bulk production and increased costs. As a result, researchers have recently shown interest in novel one-part geopolymer binders, similar to OPC, and can be used by simply adding water. One-part geopolymers offer a significant advancement over two-part systems by addressing key challenges associated with the use of liquid activators. One-part geopolymers use solid activators, which are much safer to handle compared to caustic liquid activators. This significantly reduces health and safety risks.

The mixing process is simplified as the solid activator is pre-mixed with the aluminosilicate source. This eliminates the need for handling and mixing liquid chemicals on-site. Pre-mixing ensures a more consistent and homogeneous distribution of the activator throughout the material, leading to more predictable and reliable performance. Solid activators are easier and safer to transport compared to liquid chemicals. They do not require specialized containers and are less prone to spillage and leakage. Solid activators have more stable during storage, reducing waste and lowering costs. Overall, one-part geopolymers provide a safer, more user-friendly, and environmentally sustainable alternative, making the technology more accessible and practical for widespread use in construction and other applications.

1.4 ONE-PART GEOPOLYMER BINDERS

The concept of "just add water" has led to the development of a new category of non-Portland cementitious materials known as one-part geopolymer binders (OPGB). These binders offer a convenient and straightforward application method, as they require only the addition of water. Unlike traditional two-part geopolymer binders, which have certain limitations, OPGBs are designed to address these drawbacks. They are produced by dry mixing solid aluminosilicate precursors with solid alkali activators, and the mixture is then activated by simply adding water.

The most commonly used aluminosilicate precursors in OPGBs are either fly ash, a residue from coal combustion, or blast furnace slag, a by-product of pig iron manufacture. Blast furnace slag contains silicate and aluminate impurities derived from iron ore and coke. Solid activators such as sodium metasilicate powders, sodium hydroxide powder, sodium carbonate powder, and others reported in (Elzeadani et al. 2022; Luukkonen et al. 2018a) are utilized in the process. Following the addition of water to one-part geopolymer mixtures, the sequence of four steps is observed: (i) ion exchange, (ii) hydrolysis, (iii) network breakdown, and (iv) release of Silica and Alumina (Matalkah et al. 2017). Subsequent to these stages, the development of one-part geopolymers likely involves similar key steps as observed in two-part geopolymers: speciation, gelation, reorganization, and polymerization (Duxson et al. 2007). The primary distinction between one-part and two-part geopolymers lies in the rate of release and accessibility of silica and alumina. One-part geopolymer (OPG)

mixtures typically involve solid silica sources with slower reactivity compared to soluble silicate solutions. Moreover, the availability of alumina plays a crucial role as a significant parameter influencing various properties of geopolymers, including setting, strength development, acid resistance, and microstructural changes. However, the chemical reactions, hydration products, physical properties, and mechanical and durability characteristics (which will be discussed in the literature survey chapter) are good comparable results to two-part geopolymers. Therefore, OPGs are currently gaining significant attention, particularly for in situ applications, where handling alkali solutions can be challenging as in two-part geopolymers.

The research interest in developing OPGBs has accelerated over the past five years due to their exceptional behaviour and adaptability as cast in-situ materials. The number of articles published based on interest in developing OPGs is presented in Figure 1.3, which shows that OPG is key engineering material that can be replaced in place of conventional geopolymers. The research communities are continuously involved in developing OPG and studying reaction mechanics with various binder materials. This illustrates that the intensity of research in this area is increasing and needs additional efforts and dedicated work to develop OPG as a more sustainable material.

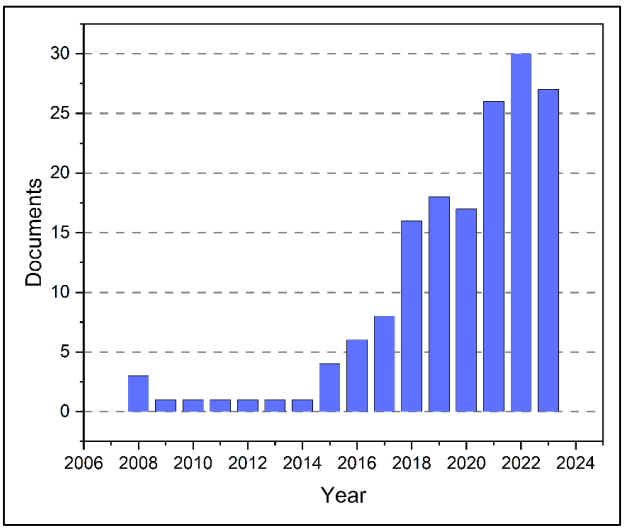

Figure 1.3 Documents reported on one-part geopolymer annually (Source: https://www.scopus.com/term/analyzer; 20.07.2024)

1.5 OPTIMIZATION OF MIXTURE PROPORTIONS

The formulation of geopolymer-based materials involves combining different components in varying forms and quantities. The performance of these materials in terms of their fresh and hardened states is significantly influenced by the proportions of their mixtures. Therefore, it is imperative to acquire the optimal blend ratios of geopolymer-based materials in accordance with the target benchmarks of various properties. The growing requirement for more sustainable construction practices has increased the necessity of investigating the experimental optimization of geopolymers.

1.5.1 Optimization approach

The process of optimizing experimental design entails iteratively selecting suitable proportions of raw materials to formulate a geopolymer-based mixture that fulfils specific desired properties in both fresh and hardened states. In the realm of mixture design optimisation, conventional methods can generally be classified into two main categories: prescriptive approaches and performance-based approaches (Li et al. 2021). The prescriptive approach involves determining the mixture proportions by adhering to predefined guidelines, standards, or established rules like. The approach employed in this method is predicated based upon the utilization of specialized expertise and empirical correlations in order to ascertain the optimal composition of the mixture. Engineers and researchers adhere to established protocols in order to determine the appropriate ratios of individual components, with the objective of satisfying specific performance criteria or requirements (DeRousseau et al. 2018). Although this methodology can be characterized by its simplicity and efficiency in terms of time, it may not consistently yield the most optimized blend in all circumstances.

On the other hand, the performance-based approach places emphasis on attaining specific material properties and performance characteristics. Instead of conforming to predetermined regulations, this approach employs empirical data and modeling methodologies to evaluate the impact of various factors on the performance of the mixes. Through the process of quantifying the correlation between input factors and output responses, researchers are able to ascertain the optimal combination of

materials that will yield the desired performance (DeRousseau et al. 2018). The performance-based approach frequently incorporates statistical techniques, design of experiments (DoE), and optimization algorithms to methodically investigate the design space and identify the most optimal mixture proportions.

1.5.2 Response surface method

Response Surface Methodology (RSM) is an optimization strategy that combines statistical and mathematical techniques to experimental design, fitting models, regression analysis, and analyzing independent variable interactions (Li et al. 2021). RSM can resolve the persistent response issue when multiple factors and levels are involved by establishing a functional relationship among contextual variables and response values. It fits the regression equation to draw the response surface and contour line for each factor level. In Parallel, the optimum prediction value is found based on each factor level's response, which offers optimization design advantages over the single factor control variable technique and orthogonal test. The Central Composite Design (CCD), Box-Behnken Design (BBD) or full factorial designs of RSM are widely used in multi-objective optimization in the area of material engineering (Chen et al. 2022; Shahmansouri et al. 2021). This study employs RSM to obtain the optimum mix proportions of one-part geopolymer pastes, mortars, and concretes based on the comprehensive experimental assessments and statistical approaches.

1.6 SIGNIFICANCE OF THE STUDY

This study represents pioneering research in the field of one-part geopolymers, with several key novel aspects. It is the first comprehensive study to optimize one-part geopolymer mixes, offering a detailed methodology and results that lay the groundwork for future research. Additionally, it is the first to investigate the performance of OPGs under elevated temperature conditions, addressing a significant gap in the existing literature. Furthermore, the study evaluates the ecological and cost benefits of OPGs, providing new insights into their potential advantages over traditional materials.

1.7 AIM AND OBJECTIVES OF THE WORK

This study aims to minimize the impracticalities of conventional geopolymer mixes in practical applications and to minimize the environmental problems associated with production of binder materials. This can be achieved by replacing activator solutions by solid activators and by optimizing the one-part geopolymer mixes with respect to fresh, mechanical and durability properties. The following objectives are formulated to envisage the proposed purpose.

1. Optimization of one-part geopolymer pastes, mortars and concretes based on fresh and hardened properties.
2. Performance of one-part geopolymer mixes (namely pastes, mortars, and concretes) subjected to elevated temperatures.
3. Microstructure studies on select one-part geopolymer mixes (namely pastes, mortars, and concretes) at ambient/room temperature and at elevated temperatures.
4. Ecological and cost analysis studies on developed one-part geopolymer concretes.

1.8 SCOPE OF THE WORK

The current research focuses on development of optimized mix proportions of parameters involved in the production of OPG mixes. The parameters considered are GGBS substitution in percentage, water to geopolymer solids ratio, and percentage of activator addition. The optimization studies are conducted on one-part geopolymer paste, mortar and concrete mixes. The best mix proportion of these mixes is suggested based on the outcomes of response surface method. The microstructural characterization has been carried out for selected mixes to study the microstructural changes and reaction mechanisms in these mixes with various factors and levels. The elevated temperature studies, ecological, and cost analysis have also been performed.

1.9 ORGANIZATION OF THESIS

This thesis presents a comprehensive analysis of the optimization methods employed in one-part geopolymer mixes. There are eight chapters in this thesis, and then a reference section. The following are brief descriptions of these chapters:

CHAPTER 1

This chapter provides a concise overview of the significance of sustainable development associated with cement manufacturing. The brief introduction of conventional and one-part geopolymers are presented. The use of optimization methods and scope of the work are detailed.

CHAPTER 2

This chapter provides comprehensive review of pertinent literature. The need and objectives of the study are outlined.

CHAPTER 3

In this chapter, physical and chemical properties of FA, GGBS, solid activator, aggregates, and water used in the preparation of OPG mixes are presented. Testing procedure for mechanical properties, microstructure studies, and optimization methods used for OPG mixes in the present thesis is also detailed comprehensively.

CHAPTER 4

Here, the results of experimental investigation, optimization study and microstructural analysis of one-part geopolymer pastes are presented and discussed.

CHAPTER 5

The results of experimental investigation, optimization study and microstructural analysis of one-part geopolymer mortars are presented and discussed in detail.

CHAPTER 6

In this chapter, the results of experimental investigation, optimization study and microstructural analysis of one-part geopolymer concretes are presented and discussed.

CHAPTER 7

The results of experimental investigation and microstructural analysis of one-part geopolymer concretes subjected to elevated temperatures are presented and discussed. The ecological and cost analysis of one-part geopolymer concretes are performed and discussed.

CHAPTER 8

The major conclusions based on the present investigation and the scope for future studies are presented in this chapter.

1.10 CLOSURE

This chapter emphasizes the significance of sustainable concrete construction by highlighting the use of industrial wastes in cement production. A brief on geopolymer binders, solid activators, and concept of optimization is presented. Scope of work and the organization of thesis have been presented.

CHAPTER 2

LITERATURE REVIEW

2.1 GENERAL

This chapter discusses the brief history and chemical background of conventional geopolymers. Further, it reports a concise overview of the existence, reaction mechanism, and development of OPGs. The literature of various research works on advancing OPGs using various raw materials is reviewed. Additionally, the significance and few works on using optimization techniques in obtaining the optimized mix proportions of various constituents are reported. Finally, the literature summary and the present work's scope and objectives are presented.

2.2 GEOPOLYMERS

The term 'geopolymer' was coined in the 1970s by Prof. Joseph Davidovits, a French scientist. It was used to describe a category of solid materials that are produced through the chemical reaction between an alumina-silicate powder and an alkaline solution (Davidovits 1991). Geopolymers belong to the category of inorganic polymers and are characterized by their chain-like structures that are primarily composed of aluminium (Al) and silicon (Si) ions. Geopolymer materials exhibit a chemical composition that is analogous to that of natural zeolite materials. Both geopolymer and zeolite materials are classified as aluminosilicates due to the presence of Al, Si, and oxygen atoms within their chemical composition. However, the primary distinction resides within their microstructure. The inherent structure of natural zeolite materials is characterized by a crystalline microstructure, denoting a state in which the constituent atoms are organized meticulously and repetitively, thereby establishing distinct and well-defined crystal lattices. In contrast, geopolymer materials possess an amorphous microstructure. This implies that the atomic arrangement exhibits a lack of long-range order and does not exhibit the formation of regular crystal lattices. Conversely, the atoms exhibit a random distribution, leading to the formation of a disordered yet stable network (Palomo et al. 1999).

The amorphous microstructure observed in geopolymers can be attributed to the geopolymerization process, in which aluminosilicate precursors undergo a reaction with alkaline activators, leading to the formation of an amorphous three-dimensional geopolymer gel. The gel is the primary binding agent, imparting cohesiveness and structural integrity to the substance (Davidovits 1994). Polymerization occurs through a rapid chemical reaction in strongly alkaline conditions on Si-Al minerals, leading to the formation of a three-dimensional polymeric chain and ring structure characterized by Si-O-Al-O bonds. A geopolymer can exist in one of three fundamental forms (Davidovits 1999): Poly (sialate) featuring [-Si-O-Al-O-], Poly (sialate-siloxo) with [-Si-O-Al-O-Si-O-], and Poly (sialate-disiloxo) characterized by [-Si-O-Al-O-Si-O-Si-O-]. "Sialate" serves as an abbreviation for silicon-oxo-aluminate. The molecular structures of these sialate forms are depicted in Figure 2.1.

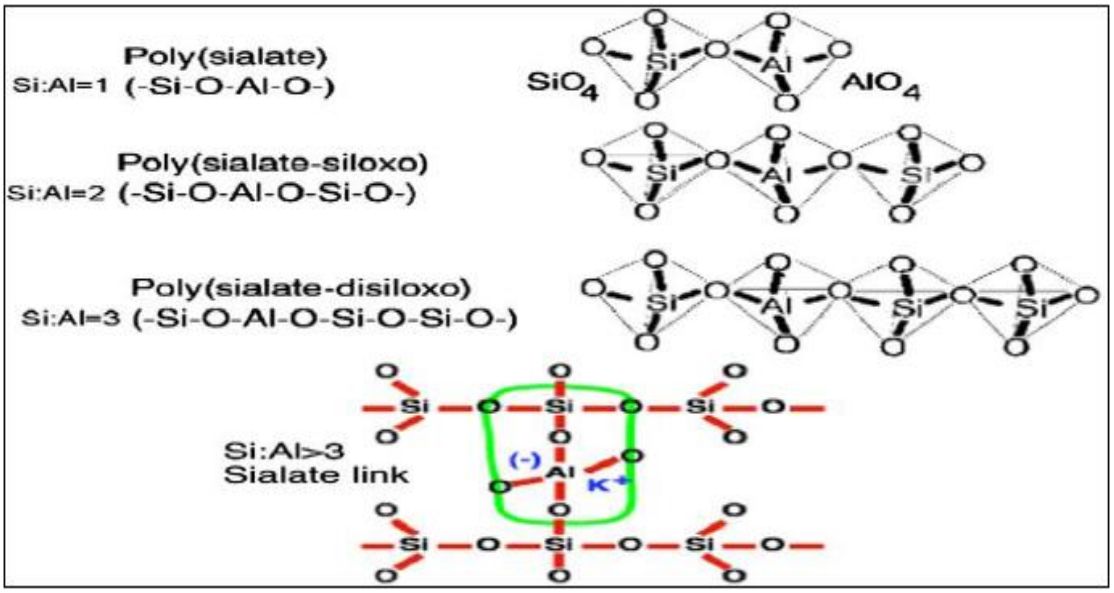

Figure 2.1 Molecular structure of geopolymer (Davidovits 2005).

The selection of the Si:Al atomic ratio in geopolymer polysialate is tailored to specific applications, with lower Si:Al ratios proving suitable for a majority of civil engineering applications. Low-calcium fly ash, classified as ASTM Class F, is prevalent and can be utilized in the production of geopolymer concrete. Typically, approximately 80% of the fly ash particles are smaller than 50μm. Duxson et al. (2007) provided a concise overview of the conceptual model of geopolymerization, as illustrated in Figure 2.2.

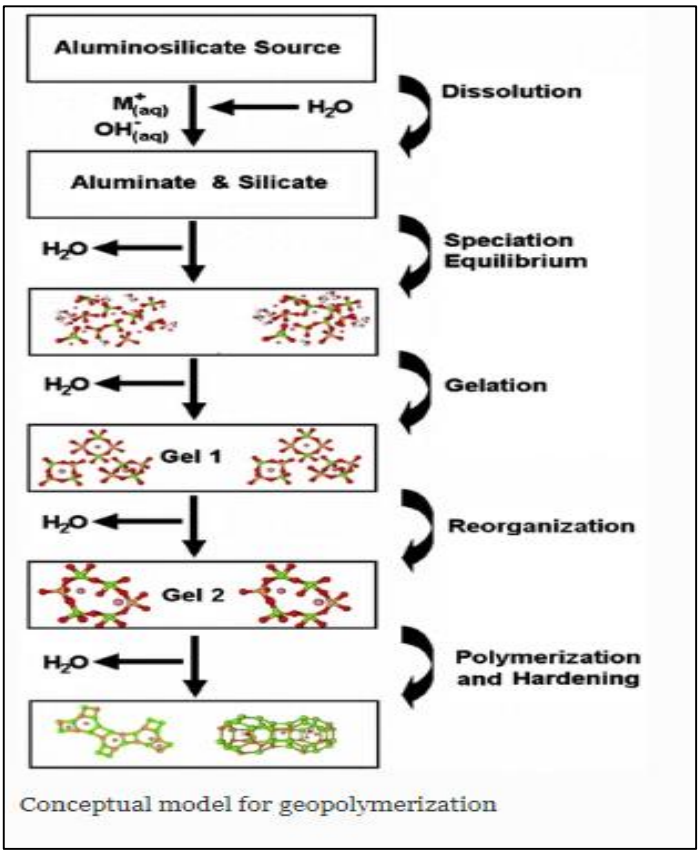

Figure 2.2 Model of geopolymerization (Duxson et al. 2007).

2.3 ONE-PART GEOPOLYMERS

To address the challenges associated with the impracticalities and occupational risks related to the handling, storage, and transportation of highly viscous and often corrosive alkali-activator solutions - typically comprising concentrated aqueous alkali hydroxide and/or silicate - various one-part materials activated by alkali (such as dry-mix or "just add water" formulations) have been the subject of growing research. OPGs employ a solid powder form of alkali-activator, and the reactions commence upon the addition of water. The mix formulation of OPGs involves a small quantity of solid activator instead of substantial amounts of activator solutions, significantly enhancing the commercial feasibility and broad-scale applicability of the developed geopolymer within the construction industry (Bong et al. 2020). The detailed literature on the OPG mix with respect to raw materials, polymerization and binding phases, properties are discussed in the following sections.

2.3.1 Reaction mechanism and binding phases

When water is introduced to the dry one-part mixture, the solid activator dissolves, resulting in an exothermic reaction. The process of precursor wetting and disintegration of amorphous phases happens simultaneously. After water is added to OPG mixes, it is proposed that the following four steps take place: (1) ion exchange, (2) hydrolysis, (3) network disintegration, and (4) release of Si and Al (Matalkah et al. 2017). Following these processes, the production of one-part geopolymers is expected to proceed in a similar manner as two-part geopolymers, involving speciation, gelation, reorganization, and polymerization. The processes involved in the activation of aluminosilicates by alkali, which occur in two halves, have been previously explained in preceding sections.

Matalkah et al. (2017) identified and categorized three exothermic processes that occurred when water was added to a fly ash–based one-part mixture using iso-thermal calorimetry. The process involves three main steps: (1) the dissolution of NaOH and the hydration of CaO immediately after water is added, (2) the attack of OH^- on the Si-O and Al-O bonds after approximately 130 minutes, and (3) polymerization after approximately 170 minutes. These steps are responsible for the mechanochemical transformation and hydration of aluminosilicate precursors and alkaline activators into hydraulic cement, as depicted in Figure 2.3. In their study, Wang et al. (2017) observed one-part mixture reactions using calorimetry and identified only two distinct peaks. They proposed that these peaks were linked to the dissolution of raw materials, specifically the breaking of Si-O-Si and Al-O-Al bonds. This process resulted in the release of Ca, Si, and Al, as well as the formation of a gel that covered the unreacted slag particles.

In OPGs, similar sodium-aluminum-silicate-hydrate (N-A-S-H) binding phase are found after addition of water and curing, as per two-part geopolymer. No discernible disparities were observed in the resulting substances of fly-ash geopolymers, whether the compounds were synthesized using one or two parts, regardless of the similarity in their mixing ratios. Crystalline calcium-silicate-hydrate (C-S-H) has been identified as the primary binding phase in high-calcium systems, which can be detected by X-ray diffraction (Ye et al. 2016). Calcium-aluminum-silicate-hydrate (C-A-S-H gel is

expected to be formed in high-calcium one-part systems as well (Yousefi Oderji et al. 2019).

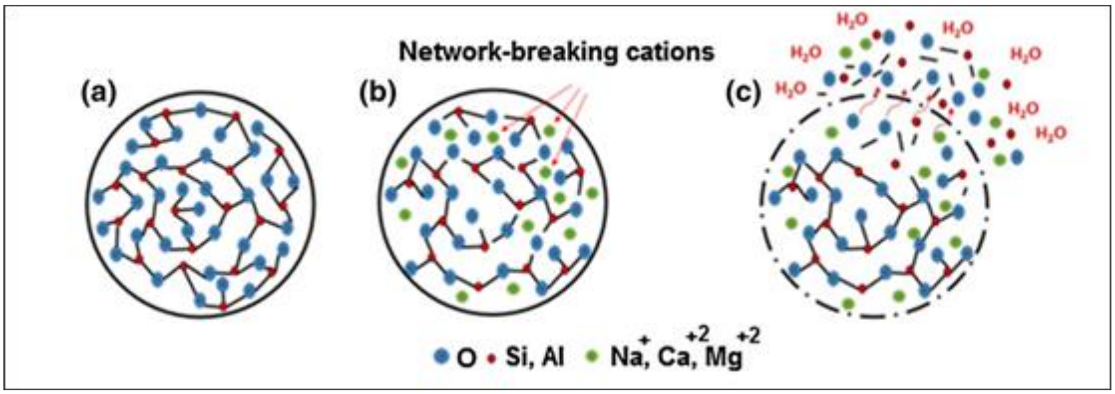

Figure 2.3 Schematics of mechanochemical transformation and hydration of aluminosilicate precursors and alkaline activators into hydraulic cement: (Matalkah et al. 2017)

(a) Ordered aluminosilicate precursor

(b) Disordered and reactive alkali earth/alkali metals aluminosilicate cement

(c) Dissolution of an aluminosilicate glass during the early stages of hydration

Furthermore, several studies have recognized various zeolites and unspecified amorphous substances as the resulting products of hydration. These studies have also identified the presence of calcium silicate and sodium aluminosilicate in red mud that endured thermal treatment with NaOH at a temperature of 800 °C and exhibited hydration upon contact with water (Ke et al. 2015). Hajimohammadi and van Deventer (2017) proposed that one-part geopolymers may exhibit a reduced propensity for zeolite formation compared to two-part geopolymers. Matalkah et al. (2017) observed that the formation of portlandite was absent when coal fly ash, which had a CaO content of 14.3%, was subjected to milling with alkali activators (quick lime, NaOH, and MgO) before adding water. Nevertheless, the process of milling independently led to the creation of portlandite. Furthermore, a multitude of crystalline secondary hydration products were detected. The nature of the (secondary) hydration products cannot be determined with certainty due to the paucity of research that has systematically compared the reaction products of one-part and two-part geopolymers. However, it is important to understand the fundamental distinctions between one-part and two-part geopolymer mixtures, as illustrated in Table 2.1 below.

Table 2.1 General differences between two-part and one-part geopolymer mixes.

Particulars	**Two-part geopolymer**	**One-part geopolymer**	**References**
Activators	Liquid form	Solid form	(Luukkonen et al. 2018a)
Mixing method	Solution kept for dissolution in water before 24 hours used for mixing with alumino-silicate precurosrs	Direct dry mixing with alumino-silicate precursors	(Abdollahnejad et al. 2015)
Availability of silica	Faster since dissolved solution is added to mix	Slow due to direct mixing method	(Hajimohammadi et al. 2011)
Alumina release rate	Rapid in rate	Slow release	(Hajimohammadi et al. 2010)
Time required to achieve the desired mix proportions for the practical application or execution	1 day prior to cast	Cast in-situ	(Duxson and Provis 2008)
Handling	Difficult and non-user friendly	Easy and user friendly	(Luukkonen et al. 2018a)
Material transportation cost	Expensive	Less for dry materials	(Bong et al. 2020)
Environmental Impact	60% impact of OPC	24% impact of OPC	(Ouellet-Plamondon and Habert 2015)
Work suitability	Pre cast	Cast in-situ	(Luukkonen et al. 2018a)

2.3.2 Factors affecting the properties of one-part geopolymer mixes

Geopolymer science initially studied in a limited number of institutions over 25 years, but research has significantly expanded globally in the past decade. Recent advancements include the development of one-part geopolymer technology. Challenges and considerations in using geopolymer, including mixing methods and factors, have been highlighted through previous studies on geopolymer mortar and concrete mixes.

Based on previous research, various factors influence the properties of one-part geopolymer mixes. These factors include the type and usage of aluminosilicate precursors, type and amount of solid activators, alkali activator modulus, curing conditions, and water-to-geopolymer solids ratio (W/GS). The impact of the above mentioned factors on the properties of one-part geopolymer mixes are reviewed from the earlier reported studies.

2.3.2.1 Aluminosilicate precursors used in one-part geopolymer mix

Fly ash, typically derived from coal combustion either alone or in partial combination with blast furnace slag, serves as the predominant solid aluminosilicate precursor in one-part geopolymer mixes. Most of the fly ashes utilized as precursors belong to class F, characterized by low calcium content according to ASTM standard C618 (Nematollahi et al. 2017a; Wang et al. 2017; Yousefi Oderji et al. 2019; Haruna et al. 2021). Class C fly ash, which contains higher calcium content, is less commonly employed in geopolymer binders due to its tendency for rapid setting and limited availability (Chindaprasirt et al. 2012; Mohammed et al. 2019a).

Traditionally, fly ashes have been used in one-part mixes without pretreatment; however, (Matalkah et al. 2017) employed a mechanochemical activation approach, wherein fly ash was ball-milled with dry-blended activators (CaO, MgO, and NaOH). Their findings indicated that the addition of Na, Ca, and Mg to the fly ash structure resulted in the breaking of aluminosilicate bonds, which in turn led to improved characteristics such as higher strength, better resistance to moisture, and a finer microstructure. This was in contrast to the raw materials that were individually milled and then mixed together.

(Hajimohammadi and van Deventer 2017) examined the impact of changes in water content and Si/Al ratio on the response mechanisms and physical characteristics of one-part-mix systems that utilize fly ash. The quantities of Si and Al nutrients supplied for the reaction do not always accurately reflect the quantities of Si and Al that actually participate in the reaction. The rates at which they are released can significantly impact their availability for the reaction and their level of involvement in the structure of the geopolymer gel. Modifying the mixture of initial substances can result in reduced crystallinity, accelerated nanostructural transformations over time, elevated Si/Al ratio

of the ultimate binder in later reaction stages, and a more compact microstructure of the final binder (Geraldo et al. 2022). Typically, these modifications are beneficial in enhancing the mechanical characteristics of the end product, which consists of a one-part mixture binder. They concluded that the absence of typical crystalline phases in fly ash geopolymers. Moreover, they found that increasing the Si/Al ratio reduced the Si contribution in the final geopolymer gel, with a greater involvement of Si observed in both stages of gel formation in samples with lower water content. An acceptable level of mechanical strength is attained, reaching a peak value of 65 MPa. Thus, fly ash is regarded as a potentially useful aluminosilicate precursor in the manufacturing of a one-part geopolymer mixture.

Ground-granulated blast-furnace slag (GGBS) serves as a frequently utilized calcium-rich aluminosilicate precursor in alkali-activated materials. Blast furnace slag, which is a by-product of pig iron manufacturing at blast furnaces, consists of silicate and aluminate impurities present in iron ore and coke. Blast furnace slag is commonly blended with class F fly ash in one-part geopolymer mixtures, although it can also be utilized independently. The utilization of blast furnace slag enhances the reactivity of low-calcium content fly ash (Elzeadani et al. 2022; Perumal et al. 2021). Typically, calcium-rich aluminosilicate or calcium hydroxide would accelerate setting and promote high early strength (Li et al. 2013; Haruna et al. 2020a). However, substituting a portion of the slag with calcium hydroxide led to a reduction in both compressive strength and workability in a one-part geopolymer (Nematollahi et al. 2015).

Wang et al. (2017) determined that a ratio of 5:1 (by weight) of blast furnace slag to solid water glass yielded optimal compressive strength, while ratios of 4:1 and 6:1 resulted in reduced strength. Nematollahi et al. (2017a) employed both "typical" and "gypsum-free" slags in developing a one-part strain-hardening geopolymer composite. The use of "typical slag" resulted in a decreased relative slump value, significantly increased thixotropic property, greater elastic modulus, less brittle structure, and improved uniaxial tensile performance. This indicates that the presence of gypsum in slag is unfavorable.

Reactive amorphous silica and alumina are typically obtained from aluminosilicate precursors like fly ash, metakaolin, or slags. However, they are often

complemented with an aqueous solution of sodium or potassium silicate (known as water glass) or aluminate in traditional two-part geopolymers. One-part mixes incorporate various solid amorphous silica sources, including rice hull and husk ash, silica residue from chlorosilane production, geothermal silica, and silica fume (or microsilica). Additionally, solid sodium aluminate is commonly used as an activator and a source of reactive alumina (Elzeadani et al. 2022).

Researchers conducted numerous investigations by developing one-part blends with additional sources of silica and alumina. Sturm et al. (2016) incorporated rice husk and hull as supplementary silica sources in the formulation of one-part mixes activated with solid sodium aluminate. They observed that after only one day of curing, the compressive strength reached a relatively high level (30 MPa), with nearly complete reaction of the rice husk ash. Gluth et al. (2013) investigated the utilization of silica residue from the waste treatment of chlorosilane production, combined with solid sodium aluminate, in one-part geopolymerization. They identified the reaction product as a geopolymer containing zeolite, suggesting that the residue can be effectively utilized in geopolymers production. However, they observed no significant further progress in reaction after three days of curing and noted a slight decrease in strength.

Hajimohammadi et al. (2008) utilized geothermal silica, while (Ye et al. 2016) employed silica fume (also known as microsilica) as supplementary silica sources in their respective studies. Both studies concluded that the inclusion of these additional silica sources resulted in improved performance of one-part geopolymers. Yong-Jie et al. (2023) investigated the utilization of ladle furnace slag with combination of low calcium fly ash and reported the achievement of compressive strength of 38.8 MPa after 28 days. However, many studies reported using various aluminosilicate precursors, among many the combination of fly ash and blast furnace slag achieved outstanding mechanical strength properties.

2.3.2.2 Effects of solid alkali activators on properties of one-part geopolymer mix

In one-part geopolymer mixes, alkali sources (i.e., activators), encompass any substance capable of supplying alkali cations, elevating the pH of the reaction mixture, and aiding in dissolution. In literatures, found many cations sources employed in one-part geopolymer mixes namely, solid sodium hydroxide (NaOH), Solid sodium meta

silicate (Na_2SiO_3), Sodium silicate pentahydrate ($Na_2SiO_3.5H_2O$), Sodium carbonates (Na_2CO_3), Sodium aluminate ($NaAlO_2$), Calcium sulphate ($CaSO_4$), Sodium sulphate (Na_2SO_4), Potassium hydroxide (KOH), red mud, maize stalk and cob ash. The molar ratio of SiO_2/Na_2O in commercial solid sodium silicates has ranged from 0.93 to 3.32 in the reported one-part geopolymer investigations (Duxson and Provis 2008; Nematollahi et al. 2017b; Hajimohammadi and van Deventer 2017).

Dong et al. (2020) endeavoured to develop OPG mixture utilizing sodium metasilicate pentahydrate as a solid activator, comparing it to water and a hybrid activator solution comprising sodium silicate and sodium hydroxide. They examined binders composed of fly ash and GGBS, with varying percentages of fly ash (80%, 40%, and 0%) and different water-to-binder ratios (0.31, 0.34, and 0.37). They used solid ground metasilicate and as-received (rocks like) metasilicate pentahydrate to develop one part mixes and in comparison with conventional two part mix geopolymer mortars by maintaining the consistent silica modulus ratio as Ms = 0.97, mix design performed for the same Ms for all 20 mixes. The mortar cube specimens were cured both in ambient and water curing method and mechanical properties are noted. By comparing 18 one-part geopolymer mixes with conventional geopolymer mixes, they concluded that solid activator using sodium metasilicate pentahydrate in one part mix has gained good compressive strength compared to liquid activator mixes by lowering the water to binder ratio which interns results in lower efflorescence compared to two part mix. The compressive strength decreased and efflorescence increased dramatically as the metasilicate concentration exceeded Na_2O = 6%, 9%, and 12% in XRD, indicating that the additional activator did not participate in the processes but instead boosted CO_2 absorption from the atmosphere. Decrease in fineness of metasilicate result in creating air voids. More metasilicate dissolved in higher W/B ration results in reduced compressive strength and severe shrinkage cracking.

Anhydrous sodium metasilicate (Na_2SiO_3) exhibited superior compressive strength and improved workability compared to sodium silicate pentahydrate ($Na_2SiO_3.5H_2O$) when employed to activate fly ash and blast furnace slag, with or without hydrated lime, in a one-part geopolymer system (Nematollahi et al. 2015; Oderji et al. 2019).

. Hajimohammadi and van Deventer (2017) focused on formulating a one-part geopolymer mix based on fly ash, utilizing solid sodium metasilicate as the activator with molar ratios of Na_2O/SiO_2, SiO_2/Al_2O_3, and Na_2O/Al_2O_3 set at 0.8, 1.8, and 1.5, respectively. They attained a compressive strength of 65 MPa.

Bong et al. (2020) investigates the impact of anhydrous sodium metasilicate powder with a modulus (Ms) of 0.9 (where Ms = $nSiO_2/nNa_2O$, SiO_2 = 46 wt% and Na_2O = 51 wt%), with partial substitution of wollastonite as sand or geopolymer precursor substitutes on the characteristics of a one-part geopolymer mortar. This resulted in an increase in flexural strength, while compressive strength remained unchanged. Moreover, the workability and setting time of the mixtures were significantly reduced.

Luukkonen et al. (2020) employed sodium silicate powders with varying SiO_2/Na_2O ratios (silica modulus), assessing their solubility rate, pH, and chemical structure using Si MAS-NMR, and compared their performance in the formulation of one-part (or dry-mix) alkali-activated blast furnace slag mortar. A low SiO_2/Na_2O ratio suggests the advantageous presence of less polymerized silica, leading to quicker dissolution. Consequently, employing sodium silicates with SiO_2/Na_2O ratios of 0.9, 2.1, and 3.4 yielded 28-day compressive strengths of 103, 80, and 2 MPa, respectively, accompanied by prolonged setting times and reduced heat release in isothermal calorimetry. Adjusting the activator modulus SiO_2/Na_2O from 2.1 or 3.4 to 0.9 by incorporating NaOH powder led to varying changes in the mechanical properties of the mortar, depending on the initial silica modulus. However, these properties did not match those achieved with sodium silicate initially having a SiO_2/Na_2O of 0.9. Depending on the scenario, the additional NaOH may be utilized for dissolving the sodium silicate activator, slag, or the formation of (C,N)-(A)-S-H gel.

Mohammed et al. (2019b) conducted an experimental investigation on geopolymer cement that used high calcium fly ash (HCFA). This cement was then utilized in the manufacturing of OPG binders. The HCFA was activated using anhydrous sodium metasilicate powder and cured in ambient conditions, comprising 8-16% of the total precursor materials. The study examined the properties of density, flowability, setting time, compressive strength, splitting tensile strength, and molar

ratio impact. Higher activator content was found to shorten the setting time of the developed OPG paste. The experimental results demonstrated that the resistance of OPG cement paste increases with a higher activator content. Increasing the granular activator above 12 percent by the weight of fly ash reduces the strength and workability of the developed OPG cement. The optimal weight ratio of fly ash was determined to be 12 percent. After 28 days of curing, the OPG paste achieved the highest compressive strength, measuring over 50 MPa. The density of the OPG paste remains consistent across all mixes. In conclusion, they suggest that the strength development of OPG cement is comparable to that of Portland cement.

Askarian et al. (2019) examined OPG formulations manufactured using either 100% fly ash or a combination of fly ash and slag as the precursor materials. Various solid activators in powder form, including sodium silicate, potassium carbonate calcium hydroxide, lithium hydroxide, sodium oxide or their combinations, were utilized. The mixtures underwent both ambient and heat curing to evaluate the impact of curing conditions. The study evaluated the impact of different solid activators and their combinations on the workability, initial and ultimate strength, density, and microstructure of these geopolymer formulations. Incorporating slag into the binder enhanced the early and final strength of the mixes while decreasing workability. Additionally, the type or combination of solid activators influences the microstructure of the geopolymer gels, consequently affecting the mechanical properties. In the studied ambient-cured geopolymers, a significant compressive strength of 38 MPa at 28 days was achieved when the geopolymer precursor comprised 50 wt% fly ash and 50 wt% slag, activated using a combination of sodium silicate, calcium hydroxide, and lithium hydroxide.

Ma et al. (2019) incorporated sodium sulfate into a one-part geopolymer to partially replace Na_2SiO_3 - anhydrous, and investigated its effects and mechanisms through property measurements and microscopic characterization. The findings suggest that as the replacement level of sodium sulfate increases, the strength decreases. Sodium sulfate lowers the initial rate of heat release and moderately extends the induction period. Initially, during the hydration process, a portion of sodium sulfate is present in a crystalline form with water molecules, leading to initial volume expansion.

Subsequently, sodium sulfate participates in hydration, as detected by X-Ray Diffraction (XRD) analysis, despite no new hydration products being detected in the geopolymer. Sodium sulfate significantly reduces drying shrinkage, primarily because of the early-term volume expansion resulting from the phase change of sodium sulfate. Its presence also increases the overall porosity, particularly the proportion of deleterious pores in OPG. Sodium sulfate has been demonstrated to be a more appropriate activator for producing environmentally friendly OPG, as it leads to a reduction of at least 20% in potential CO_2 emissions after its addition.

The unconfined compressive strength of OPG exhibits a broad range, with the highest recorded 28-day compressive strength reaching up to 80 MPa, while occasional reports indicate very low values (Luukkonen et al. 2018a). In certain instances, the compressive strength of one-part geopolymers has been lower compared to similar compositions of two-part geopolymers (Nematollahi et al. 2015). However, higher values have also been documented following the calcination of low-quality kaolin, which contains a significant amount of quartz, with NaOH or Na_2CO_3. Subsequently, cement pastes were synthesized from the ground precursor powders by solely adding water and cured at 80 °C for 3 days, followed by ambient environment curing for 25 days (Peng et al. 2014).

Yousefi Oderji et al. (2019) noted that the concentration of Na_2SiO_3 significantly impacts the mechanical strength of samples. The compressive strength of mixtures experienced a sharp decline when the percentage of Na_2SiO_3 was decreased below 8%. The decrease in strength due to a reduction in activator concentration can be attributed to alterations in Na_2O content and related molar ratios, which are critical factors influencing strength gain through alkali activation reactions.

Sadeghian et al. (2022) aimed to assess the drying shrinkage of one-part alkali-activated slag concrete (AASC) over a period of 180 days, influenced by various mix design parameters. The study investigated the effects of water-to-binder ratio, silica fume-to-binder ratio, alkaline activator-to-slag ratio, and curing regime (water curing vs. sealed plastic bag curing) on drying shrinkage. Results indicated that approximately 75% of the 180-day shrinkage occurred within the first 20 days. Additionally, the addition of silica fume significantly reduced drying shrinkage, while AASC samples

cured in sealed plastic bags experienced at least a 5.9% increase in drying shrinkage. The highest drying shrinkage was observed in a mix design with the highest water-to-binder ratio and zero silica fume content, regardless of curing type. These findings suggest that the incorporation of silica fume as a co-binder effectively mitigates drying shrinkage in AASC.

The workability of fresh OPG paste, as determined by the slump test or spread flow test, has been documented to range from 3.52 to 3.69 as the relative slump value (Nematollahi et al. 2017a; b). Observations revealed that blast furnace slag without gypsum yielded a higher relative slump value compared to slag containing gypsum in one-part geopolymers (Nematollahi et al. 2017a).

One-part geopolymers containing fly ash and blast furnace slag were noted to exhibit thixotropic behavior, demonstrating good workability during mixing and vibration (Nematollahi et al. 2017b). Augmenting the quantity of sodium silicate activator in OPGs comprised of fly ash and blast furnace slag led to a notable reduction in workability (Nematollahi et al. 2015). Conversely, augmenting the water content enhanced workability, albeit at the expense of decreased compressive strength. The workability of OPGs was approximately 35% inferior compared to similar compositions of two-part geopolymers (Nematollahi et al. 2015).

Additionally, incorporating slag into fly ash-based mixes enhances compressive and flexural strength due to its higher CaO composition. However, this addition leads to decreased workability due to the angularity of slag particles and the rapid formation of network structures, resulting in the formation of C-A-S-H or N-A-S-H gel during alkali activation. These gels are responsible for strength gain, resulting in dense and uniform microstructures in the OPG binder system (Yousefi Oderji et al. 2019; Shah et al. 2020). The initial and final setting times of OPG mixes have ranged from 23 to 150 minutes and 69 to 230 minutes, respectively (Matalkah et al. 2017; Wang et al. 2017).

Li et al. (2020) measured the setting time of slag-based OPG mixes activated with anhydrous Na_2SiO_3 at room temperature. They observed a decrease in setting time as the activator dosage increased from 10% to 25% of the binder content (with the ratio of activator to geopolymer solids ranging from 0.10 to 0.25).

Nematollahi et al. (2015) found that increasing the blast furnace slag content in OPG mixture containing fly ash resulted in a reduction of the setting time. Higher CaO content in the precursor typically leads to rapid setting. The faster dissolution rate of CaO, compared to SiO_2 and Al_2O_3, creates nucleation sites early in the process, resulting in shorter setting times and rapid hardening (Haruna et al. 2020a).

It has been observed that the setting mechanism of low-CaO and high-CaO precursors varies in alkaline environments. Typically, the former sets through a gel percolation approach, whereas the latter sets through the localized precipitation of C-A-S-H gels (Rasuli et al. 2022). Yang et al. (2008) noted that alkali-activated blast furnace slag exhibited slower hardening when a solid activator was utilized instead of a solution.

2.3.2.3 Curing regimes

One-part geopolymers have undergone curing at ambient temperatures as well as elevated temperatures ranging from 40 to 80 °C, depending on the precursors and mix design. In certain instances, the compressive strength of one-part geopolymers has exhibited a decline with increasing curing duration. This phenomenon has been attributed to depolymerization, carbonation, or efflorescence (Ye et al. 2016).

Peng et al. (2017) found notably lower 28-day compressive strength in one-part samples cured for 3 days at 20°C compared to heat curing, which accelerates early strength development of geopolymers. Additionally, they emphasized the importance of controlling relative humidity during curing. Sealing geopolymer concrete is generally preferred to prevent dehydration, which can lead to efflorescence, micro-cracking, and a subsequent decrease in compressive strength. The heat generated upon adding water to one-part geopolymers typically promotes water loss, underscoring the importance of sealing. Optimal curing conditions involve saturated conditions (i.e., relative humidity of 100%), eliminating the need for additional water during curing. Additionally, besides curing in air, one-part geopolymers have also been cured in water tanks (Nematollahi et al. 2017a).

2.4 ELEVATED TEMPERATURE STUDIES

Elevated temperatures, refers to temperatures that are higher than normal or ambient conditions. Specifically, this term is often used to describe temperatures that are significantly above room temperature but below the thresholds typically associated with fires. However, these temperature conditions can significantly weaken cementitious materials. This kind of exposure can shorten the lifespan of a structure and greatly hinder its performance. The behavior of cementitious materials when exposed to high temperatures depends on various parameters, such as the type of cement, composition of the aggregate, amount of aggregate, size of the aggregate, and the microstructure and mineral composition of the material.

OPC-based mortars typically disintegrate when exposed to temperatures reaching 900°C. However, incorporating 5% graphite by weight of OPC has shown resilience, allowing mortar specimens to remain intact at elevated temperatures. Although adding graphite may reduce compressive strength under normal conditions, its ability to withstand high temperatures exceeds that of conventional OPC-based mortars (Cülfik and Özturan 2002).

Karahan and Yakupoğlu (2011) investigated the effects of elevated temperatures on alkali-activated materials, taking into account the concentration of alkaline solution. Following preconditioning and exposure to elevated temperatures, alkali activated slag mortar specimens were evaluated for residual compressive strength. Mortars prepared with sodium silicate (Na_2SiO_3)-based alkaline solutions demonstrated superior mechanical strength compared to those prepared with sodium hydroxide (NaOH) and sodium carbonate (Na_2CO_3)-based solutions. Moreover, an increase in alkaline solution concentration further enhanced the residual compressive strength under elevated temperatures.

Yazici et al. (2012) investigated the impact of using fly ash, silica fume, and pumice as binders in OPC-based mortar mixtures subjected to elevated temperatures up to 750°C. Their findings indicated that OPC mortar mixtures containing fly ash performed notably well under elevated temperatures compared to other binder alternatives.

Nadeem et al. (2013) investigated the mechanical properties of OPC mortars incorporating fly ash and metakaolin when exposed to elevated temperatures. They found that mortars containing 20% FA showed superior performance at high temperatures. Conversely, MK-based OPC mortars were more susceptible to the effects of elevated temperatures, requiring caution when exposed to temperatures exceeding 400°C.

Rashad and Sadek (2017) investigated the impact of GGBS in alkali-activated materials (AAMs). AAMs incorporating GGBS showed reduced micro-cracking under elevated temperatures and displayed higher residual compressive strength compared to AAMs containing siliceous-based natural fine aggregates. Zhang et al. (2020) examined the properties of recycled glass materials in AAMs under elevated temperatures, demonstrating improved temperature resistance with the addition of recycled glass.

Jiang et al. (2020) conducted a comprehensive comparative analysis on the influence of elevated temperatures (up to 1200°C) on geopolymer pastes derived from Class C and Class F fly ash. The results indicate that Class F fly ash-based geopolymer pastes exhibit superior mechanical properties and thermo-physical performance when subjected to heating temperatures below 500°C. Conversely, Class C fly ash-based geopolymer specimens demonstrate enhanced thermal performance and a higher retention ratio of strengths after exposure to higher temperatures (>800°C).

Qu et al. (2020) evaluated the synergistic impacts of preloading damage and elevated temperatures on fly ash and GGBS -based geopolymer mortars. They observed that a higher GGBS content led to improved compressive strength at room temperature. However, under the combined conditions, mortars with a lower GGBS content exhibited better performance.

Luo et al. (2022) explored the physicochemical properties of alkali-activated fly ash up to 800°C and elucidates their synergistic impact on thermal behaviour. A quantitative analysis of cracking behaviour is developed to understand the cracking mechanism. The results indicate a linear relationship between crack density and ultrasonic pulse velocity. Furthermore, crack density and compressive strength exhibit a positive correlation below 100°C but a negative relationship beyond this temperature.

The addition of slag to geopolymers mitigates certain geopolymeric behaviours such as further geopolymerization and viscous sintering but exacerbates thermal damage due to the compact structure and unstable hybrid gel.

2.5 ECOLOGICAL STUDIES ON ONE-PART GEOPOLYMERS

Life cycle analysis (LCA) analysis is commonly used to assess the environmental impact of OPC concretes and geopolymers. The "cradle to grave" approach is a standardized method employed by both industry and academia. The LCA should comprehensively assess all potential environmental consequences associated with a product, spanning from the procurement of raw materials to its ultimate disposal. Geopolymers are commonly evaluated and contrasted with OPC based concrete regarding their net CO_2 reduction and global warming potential (GWP). Other environmental impact categories besides GWP include abiotic depletion, ozone layer depletion, human toxicity, various forms of ecotoxicity (freshwater, marine, terrestrial), photochemical oxidation, acidification, and eutrophication. Generally, these classifications are less significant for construction materials compared to their importance in the agriculture business (Rockström et al. 2009).

Ali Shah et al. (2021) conducted an environmental impact assessment (EIA) on a specific type of AAMs that utilized lithium slag as a binder. The EIA was conducted using carbon dioxide emissions as a measure of strength performance. The results indicate that the ECO_2eq (equivalent carbon dioxide emissions) of the lithium slag based AAM is considerably lower in comparison to the combination based on OPC.

In general, the published findings exhibit some inconsistency: the net change in GWP of geopolymers has been documented to vary widely, ranging from a reduction of 96% to an increase of 20% compared to OPC concrete. Geopolymers exhibit a somewhat moderate positive or negative influence in comparison to OPC concrete in many environmental impact categories such as abiotic depletion. The average environmental impact of one-part geopolymers is 24%, while that of two-part geopolymers is 60% compared to the environmental impact of OPC. Therefore, one-part geopolymers have the potential to be more environmentally benign compared to two-part geopolymers (Luukkonen et al. 2018a).

2.6 OPTIMIZATION - RESPONSE SURFACE METHOD

Response surface method addresses the challenge of obtaining consistent responses when multiple factors and levels are involved by establishing a functional relationship between contextual variables and response values. It achieves this by determining response values for each factor level through fitting a regression equation and visualizing the response surface and contour lines. Simultaneously, the optimal prediction value is identified by considering the response values corresponding to each factor level, offering distinct advantages over single-factor control variable methods and orthogonal testing in terms of optimization (Rajput and Datta 2019).

The CCD and BBD are two standard designs of RSM widely used in multi-objective optimization in the area of material engineering (Shahmansouri et al. 2021; Chen et al. 2022).

Mohammed et al. (2012) utilized response surface statistical methodology to create a model that examines the impact of paper-mill residuals, with and without Class F fly ash replacement, on the slump and compressive strength of concrete. The factors examined in this study encompassed the water/cement ratio, the amount of paper-mill residual, and the proportion of fly ash to total cementitious material. The contour diagrams were utilized to further discuss the effectiveness of the obtained models in achieving a favorable balance between workability and compressive strength. The findings demonstrated that the compressive strength of concrete incorporating paper-mill residuals may be accurately estimated based on the corresponding slump value.

Mermerdaş et al. (2017) used RSM to optimize the parameters involved in production of light-weight geopolymer mortars. These mortar mixes were developed using fly ash and GGBS. The test results demonstrate that increasing the binder content leads to a higher compressive strength of light-weight geopolymer mortars. The strength is directly proportional to both the curing temperature and curing period. The experimental verification demonstrated a high level of concurrence with the optimized outcomes.

Ye et al. (2016) studied strength optimization of red mud based one-part geopolymer mixes. Shi et al. (2022) used BBD to design the tests and to establish the

regression models of geopolymer mortar by adopting 3 independent variables and 4 responses. (Mohammed et al. 2019a) developed the prediction models of cast in-situ alkali activated binders with Face-centered central composite design FCCD) for two factors with two levels of each, keeping W/GS ratio constant as 0.25 for all mixes. However, there are limited optimization studies on development of prediction models for low calcium FA based and GGBS based one-part geopolymer pastes synthesized by solid anhydrous sodium metasilicate powder and effect of water to geopolymer solid ratio for reaction mechanism of OPG mixes. This has limited the application of one-part geopolymers and the standardization of its manufacturing process.

2.7 SUMMARY OF THE LITERATURE

Several research works on fly ash based and slag based geopolymers have been carried out in recent years. Most of the researchers have focused on the physical, mechanical and microstructural properties of the geopolymer mortar varying the following parameters: concentration of NaOH solution, ratio of Na_2SiO_3 solution to NaOH solution, temperature for heat curing, duration of heat curing, ratio of alkaline liquid to fly ash/slag etc. Based on literatures, chemical activator consisted of Na_2SiO_3 and NaOH is found to be the most effective to produce geopolymer matrix with proper mechanical properties. However, the practical application of geopolymer concrete are numbered due to these solutions storage and handling issues. Hence, few researchers came up with an idea of "just add water" concept same as OPC which is known as one-part geopolymer mix by dry mixing solid sodium metasilicate and solid sodium hydroxide activators with aluminosilicate precursors such as fly ash or slag. Many researchers replaced fly ash with GGBS by percentage by weight in the production of OPG, but the development of optimal mix proportion are not reported in any literature. The usage of optimization techniques to optimize the parameters involved in the production of OPG are rarely reported. Hence, the attempt has made to develop optimized OPG mixes by employing response surface method.

The elevated temperature studies on OPG mixes are not reported yet. Most existing studies focus on conventional geopolymer or Portland cement-based systems. In practical applications, materials used in construction are often exposed to elevated temperatures, either due to environmental conditions or accidental fires. Understanding

how OPG mixes behaves under these conditions is critical for ensuring the safety and durability of structures. OPGs is a relatively new material, and its behavior under extreme conditions is not yet fully understood. Investigating its performance at elevated temperatures fills a significant knowledge gap and contributes to the advancement of material science. Hence, efforts are made to study the high temperature effects on OPG mixes. The study provides a basis for comparing the performance of OPGC with traditional Portland cement-based concretes, highlighting the potential advantages and limitations of using OPG in fire-prone environments. Furthermore, the ecological studies and cost analysis are plan to report as for now only few literatures are available.

2.8 RESEARCH GAPS BASED ON LITERATURE

Based on the comprehensive literature review, several significant research gaps have been identified, which form the basis of this thesis:

1. **Optimization of OPG Mixes:** While there have been studies on the development of one-part geopolymers, comprehensive optimization of OPG mixes remains underexplored. This study aims to fill this gap by providing a detailed methodology for optimizing OPG mixes.
2. **Performance Under Elevated Temperatures:** There is a lack of research on the performance of OPGs under elevated temperature conditions. This study addresses this gap by investigating the behavior and durability of OPGs when exposed to high temperatures.
3. **Ecological and Cost Analysis:** Limited research has been conducted on the ecological impact and cost-effectiveness of OPGs. This thesis includes analysis of these aspects, highlighting the potential benefits of OPGs over traditional materials.
4. **Microstructural Characterization:** Although some studies have explored the microstructural properties of OPGs, there is a need for more comprehensive and detailed characterization using advanced techniques. This research includes an in-depth microstructural analysis to better understand the material properties.

2.9 CLOSURE

This chapter presents a brief note on geopolymer technology and development of OPG systems. The effects of various factors on properties of OPG mixes at fresh and hardened state are discussed. In addition, works pertaining to elevated temperature studies, ecological and cost analysis are reviewed. Further, literature on employment of optimization methods in development of various types of one-part and two-part geopolymer mixes have been discussed in detail. Finally, the summary of detailed literature review is presented and the chapter sets forth specific research objectives designed to address gaps in knowledge and highlight areas that require further investigation.

CHAPTER 3

MATERIALS AND METHODOLOGY

3.1 INTRODUCTION

In the present investigation, class F fly ash and GGBS as aluminosilicate precursors, anhydrous sodium metasilicate powder as solid activator, fine aggregate, coarse aggregate and water were have been used to develop one-part geopolymer mixes. Their important physical and chemical properties are presented. Also the methodology and different test conducted are detailed.

3.2 ALUMINOSILICATE PRECURSORS

The aluminosilicate precursors used in this study are Fly ash (FA) and ground granulated blast-furnace slag (GGBS). FA is a residual substance generated by the burning of pulverized coal in coal-fired furnaces, commonly found in thermal power plants. The present investigation employed low calcium FA (class F) confirming to ASTM C618 from Udupi Thermal Power Plant in Karnataka, India. GGBS is a by-product material derived from iron and steel manufacturing. It is acquired by rapidly cooling molten iron slag from a blast furnace using either water or steam. Following the quenching process, the granular product is subjected to drying and subsequent grinding, forming a finely powdered material. The present investigation employed GGBS confirming to ASTM C989 sourced from M/s JSW Iron and Steel Company, Bellary, Karnataka, India.

The chemical composition of FA and GGBS obtained by X-ray Fluorescence spectroscopy is presented in Table 3.1. The rate of the GGBS hydration modulus [HM = $(CaO + MgO + Al_2O_3)/SiO_2$] is 1.85. The activity coefficient $H_o = (Al_2O_3/SiO_2) = 0.51 > 0.25$ of slag is considered to be high activity slag. The alkalinity coefficient $M_o = (CaO+ MgO)/(SiO_2 + Al_2O_3) = 0.88 > 1.0$ corresponds to acid slag. The X-Ray Diffraction (XRD) technique was used to determine the crystallinity and phase of FA and GGBS as shown in Figure 3.1. The XRD spectra reveals that the principal crystalline peaks in the FA include quartz, mullite, calcite, and hematite whereas the amorphous structure of GGBS is observed with slight traces of Gehlenite which is in

the form of silicates. The Scanning Electron Microscope (SEM) micrographs of FA and GGBS are shown in Figure 3.2. From SEM images it is evident that FA particles exhibited spherical shape with varying dimensions, enabling them to efficiently blend with in the mixture and GGBS particles show irregular sequence of angular grains.

Table 3.1 Chemical oxide compositions of Fly ash and GGBS.

Oxides (% by weight)	Fly ash	GGBS
SiO_2	60.65	32.45
Al_2O_3	28.62	16.72
CaO	1.70	33.75
Fe_2O_3	3.19	1.22
MgO	1.84	9.61
SO_3	1.26	0.85
Na_2O	1.11	0.15
K_2O	0.11	0.06
LOI[a]	4.52	0.4
Specific gravity	2.25	2.91
Blaine fineness (m^2/kg)	381	417

[a] Loss on ignition

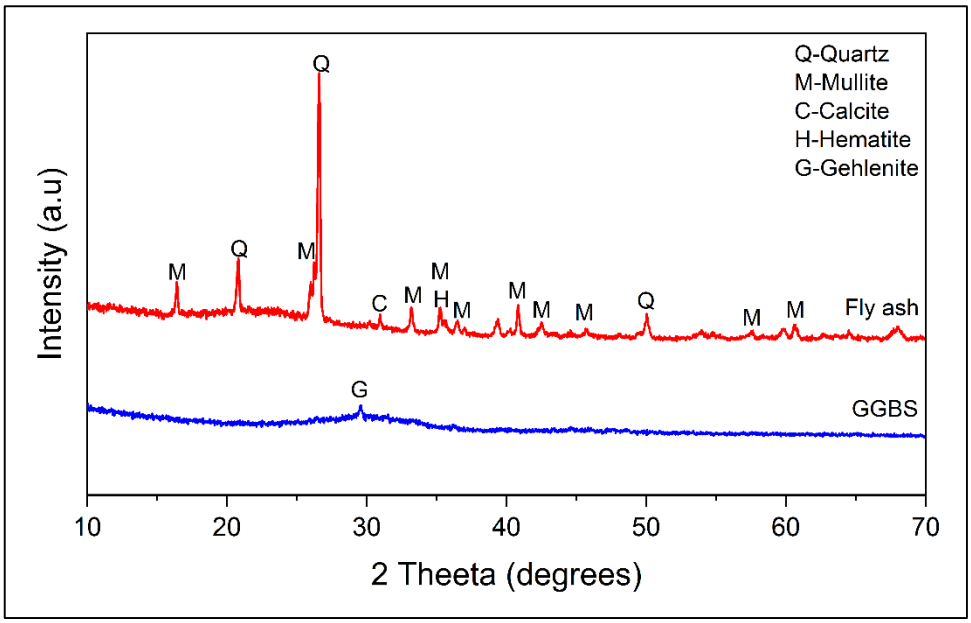

Figure 3.1 XRD patterns of fly ash and GGBS.

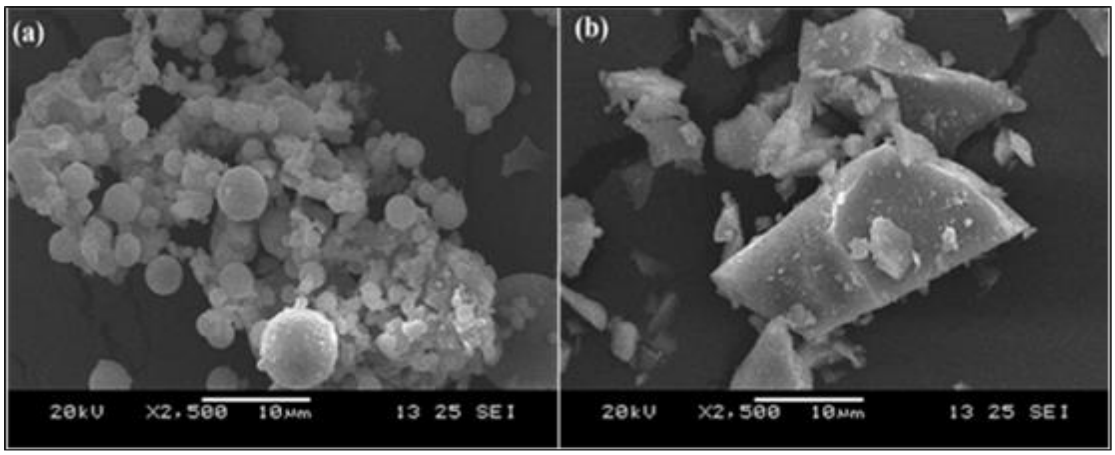

Figure 3.2 SEM images of (a) fly ash (b) GGBS.

3.3 ALKALI SOURCES

Activator anhydrous sodium metasilicate powder was used as a solid alkali activator to synthesize the one-part geopolymer mix, which provides alkali cations, raises the pH of the reaction mixture and facilitates dissolution. The chemical contents of the anhydrous sodium metasilicate powder are 48% Na_2O and 47% SiO_2 by weight resulting in a modulus ratio (Ms) of 0.97 (where Ms = SiO_2/Na_2O). Solid alkali activators procured from a local supplier/dealer of Mangalore in bulk. The properties of anhydrous sodium metasilicate powder are given in Table 3.2. Solid Alkali activators will be added to aluminosilicates precursors directly by dry mixing for about 2 – 3 minutes. Solid activator used in this study is shown in Figure 3.3.

Figure 3.3 Solid activator used in OPG mixes.

Table 3.2 Properties of anhydrous sodium metasilicate powder.*

Properties	Results
SiO_2 comprised	47 % by weight
Na_2O comprised	48% by weight
H_2O comprised	<5% by weight
pH	12.5 (1% solution)
Melting Point/Freezing Point	1089°C
Molecular Weight	122.062 g/mol
Specific gravity	2.61
Physical state	Solid granules or powder
Colour	White

* provided by the manufacturer

3.4 AGGREGATES

3.4.1 Fine aggregates

Locally available river sand conforming to Zone II of IS: 383-2016 has been used as fine aggregate to produce OPG mixes. The physical properties of sand are given in Table 3.3. The fine aggregate passing through 4.75 mm and retained on 150 microns sieve has been considered for the study.

3.4.2 Coarse aggregates

Crushed granite stone conforming to IS 383-2016 has been used as coarse aggregate to produce OPG concrete mixes. The physical properties of coarse aggregates are given in Table 3.3. The coarse aggregate of (20-10 mm) and (10-4.75 mm) i.e., 20 mm and 10 mm maximum size aggregates are used for this study.

3.4.3 Water

Tap water sourced from the laboratory of the institute was used to produce OPG mixes.

Table 3.3 Physical properties of fine and coarse aggregates.

Aggregates	Specific gravity	Bulk density (kg/m^3)		Fineness modulus	Water absorption (%)
		Loose	Dense		
Fine aggregate (4.75-0.15 mm)	2.66	1412	1679	3.04	1.02
Coarse aggregate (20-10 mm)	2.71	1365	1568	5.95	0.51
Coarse aggregate (10-4.75 mm)	2.69	1475	1693	5.43	0.62

3.5 METHODOLOGY

The methodology adopted includes the following steps:

1. The preliminary investigation on the suitability and performance of FA and GGBS along with solid activator to achieve desired fresh and hardened properties.
2. Experimental assessments are to be carried out for one – part geopolymer mixes (namely one-part geopolymer pastes, mortars, and concretes) to arrive at an optimized mix designs.
3. Performance of one-part geopolymer mixes (namely pastes, mortars, and concretes) subjected to elevated temperatures of 200 °C, 400 °C, 600 °C and 800 °C.
4. Microstructural characterization studies are conducted to analyze the effect of considered factors to OPG mix in improvising the interfacial bond or aggregate interfacial transition zone and in quantifying the amount of strength with respect to the gel formed.
5. Finally, ecological studies on developed OPG concrete mixes and cost analysis are performed.

3.5.1 Casting of specimen

3.5.1.1 One-part geopolymer pastes (OPGP)

The OPGP mixes were developed using low calcium fly ash, GGBS, anhydrous sodium metasilicate powder, and water. OPGP mixes were uniformly produced by dry blending solid aluminosilicate with a solid activator manually for 2-3 min. After that, the calculated amount of water was added to the mix after transferring the dry blends to the Hobart mixer and thoroughly mixed for about 3-4 min at 65 rpm. The mixing continued until consistent and homogenous mixes were obtained. Then, the wet mixture was subjected to flow test, and setting time of the OPGP mixes were also obtained. Further, steel molds were used to cast 50 mm cube specimens to find the compressive strength of the OPGPs. After 24 hours, the de-molded specimens were kept for ambient air curing until the test period.

3.5.1.2 One-part geopolymer mortars (OPGM)

The experiments on of OPGM have been carried out by employing low calcium fly ash, GGBS, anhydrous sodium metasilicate powder, and fine aggregates. A uniform mixture of OPGM was achieved by means of manual dry mixing of FA and GGBS with a solid activator for a period of 2-3 minutes. Fine aggregates (in 1:2 binder to sand ratio) was added to the dry blend and mixed uniformly. The dry mixes were combined with the appropriate quantity of water in the Hobart mixer, and subsequently agitated for a duration of 3-4 minutes until a homogeneous mixture was achieved. The mixtures were thoroughly blended until all visible differences were eliminated. Following this, the blend was relocated into molds for specimen preparation. After 24-hour duration, the specimen were carefully retrieved from their molds and then exposed to ambient curing until the scheduled testing phase.

3.5.1.3 One-part geopolymer concretes (OPGC)

The OPGC mixes were developed using low calcium fly ash, GGBS, anhydrous sodium metasilicate powder, and aggregates. A homogeneous blend of OPGC was obtained through the manual dry blending of FA and GGBS with a solid activator for a duration of 2-3 minutes. The dry blend was uniformly mixed with coarse and fine aggregates in a proportion of 65% and 35%, respectively, by mass of the total aggregate content. The

coarse aggregates used in the study consisted of two sizes: 20 mm and 10 mm. These sizes were combined in a ratio of 60% and 40% respectively, based on the mass of the total coarse aggregate content. The dry blends were mixed with the appropriate quantity of water in the concrete mixer and agitated for 3-4 minutes until a uniform OPGC mixture was obtained. The mixtures were thoroughly blended to eliminate any noticeable distinctions. Subsequently, the mixture was transferred into molds to produce specimen. The specimen were de-molded after 24 hours of casting and stored under ambient laboratory conditions until the test period.

3.5.2 Tests on pastes, mortars and concrete mixes

3.5.2.1 Flow and slump

The workability of OPG mixes refers to their ease of usage, which can be quantified by evaluating the flow and slump values of the mixes. Flow test of OPGP and OPGM mixes were conducted using flow table apparatus shown in Figure 3.4. The diameter of the OPGP and OPGM flow was measured at its fresh state following the guidelines outlined in ASTM C1437. The slump test for workability of OPGC mixes were performed by using slump cone at fresh state following the guidelines outlined in ASTM C143.

Figure 3.4 Flow table test apparatus.

3.5.2.2 Setting time

The initial and final setting time of OPGP mixes was recorded using Vicat apparatus. Initial and final setting time readings were taken every 5 and 30 minutes, respectively, according to ASTM C191-21.

3.5.2.3 Compressive strength

The compressive strength (CpS) of all the OPG mixes were recorded for a test period of 7 days and 28 days. The CpS of three test cube specimen, which were cast using different OPG mixtures, was determined by calculating the average strength of the tested specimen. The CpS of the OPGP mixes were performed using 50 mm cube specimen, according to the test procedure of ASTM C 109. The CpS of the OPGM mixes was evaluated by using 70.6 mm cube specimen in accordance with the IS 4031-part 6. The CpS of the OPGC mixes were evaluated using 100 mm cube specimen, following the guidelines outlined in (IS:516-6 2021). The size of the test specimen adhered to the standards specified in (IS 1199 (Part 5) 2018) and (IS 10086 2021).

3.5.2.4 Flexural strength

The Flexural strength (FrS) of all the OPG mixes were recorded for a test period of 7 days and 28 days. The FrS of three test prism specimen, which were cast using different OPG mixtures, was determined by calculating the average strength of the tested specimen. The FrS of the OPGM mixes were recoded using 40 × 40 × 160 mm prism specimen according to the test procedure of ASTM C348-97. The FrS of the OPGC mixes were evaluated using 100 × 100 × 500 mm prism specimen, following the guidelines outlined in (IS:516-6 2021). The size of the test specimen adhered to the standards specified in (IS 1199 (Part 5) 2018) and (IS 10086 2021).

3.5.2.5 Split tensile strength test

The split tensile strength (SpS) of OPGC mixes were obtained for a test period of 7 days and 28 days. The SpS of three test cylindrical samples, which were cast using different OPGC mixtures, was determined by calculating the average strength of the tested specimen. The SpS of the OPGC mixes were evaluated using 150 mm diameter

and 300 mm length cylindrical specimen, following the guidelines outlined in (IS:516-6 2021). The size of the test specimen adhered to the standards specified in (IS 1199 Part 5: 2018) and (IS 10086 2021).

3.5.2.6 Drying shrinkage

Drying shrinkage (DrS) is a phenomenon in which the volume of a matrix varies due to the evacuation of interior water produced by the humidity gradient between the external and internal regions. The measurement of DrS in the OPGM cast specimen involved assessing the change in length along the longer direction, which occurred as a result of moisture loss from the materials. The experiment pertaining to DrS was conducted by utilizing prismatic specimen with a length of 285 mm and a cross-sectional area of 25 × 25 mm, as per the guidelines outlined in ASTM C596. The length of each prism specimen was measured with a length comparator immediately following the removal from the mold. Figure 3.5 shows the cast specimen and testing apparatus used to obtain the DrS of the OPGM mixes. Subsequently, all samples were subjected to the prescribed curing method. Then, the specimens were subjected to length measurements to determine the variations in length throughout different time intervals, specifically at ages of 3, 7, 28, 56, 90, 120, 150, and 180 days. In this investigation, DrS was measured and represented as micro-strain for each OPGM mix.

Figure 3.5 Drying shrinkage test setup and cast prism samples.

3.5.2.7 Elevated temperature exposure

After 56 days of curing at room temperature, the specimen were exposed to higher temperatures in a programmable electric furnace. The programmable electric furnace shown in Figure 3.6 was employed in this investigation. The positioning of the samples was arranged such that there was a small space between the bottom of the furnace chamber and the samples. Additionally, the samples were placed at a significant distance from the heating coils. This arrangement was done to ensure that heat was evenly distributed to the specimens and to prevent any potential harm to the furnace coils in the event of severe spalling. The specimens were exposed to a controlled heating process at a rate of 5 °C per minute until they reached the desired temperature of maximum 800 °C at intervals of 200 °C. After attaining the desired test temperature, the specimens were maintained for 30 minutes retention period. Subsequently, the power supply to the furnace was switched off, leading to the furnace cooling of the specimen to ambient room temperature. The specimens were subjected to laboratory conditions for 20 hours before the commencement of the compression test (Hiremath and Yaragal 2018; Yaragal et al. 2020).

Figure 3.6 Programmable electric furnace.

3.5.3 Microstructural, phase and chemical analysis

Field emission scanning electron microscopy (HR-FESEM, GEMINI 300, Carl Zeiss, Germany) was used to analyze the crack surface of the OPG mixes by capturing SEM micrographs of unpolished samples that were sputtered with gold. The elemental composition of the OPGC was determined using the PV 7600 SU A EDAX Octane super EDS System-SDD 70mm Energy Dispersive Spectroscopy (EDS). Mineralogical

changes in the system were analysed using advanced X-Ray Diffraction (XRD) analysis. The XRD analysis was conducted using the Empyrean 3rd Gen XRD instrument manufactured by Malvern PANalytical in the Netherlands. The analysis was performed within 10° to 70°, 2θ angles range, with a scanning rate of 0.01° per step. The Thermal Gravimetric Analysis (TGA) and Fourier Transform Infrared (FTIR) analysis were conducted to study the thermal decomposition profile and chemical bond shifts, respectively. The TGA 4000 and Spectrum 2 FT-IR Spectrometer (PerkinElmer, Singapore) were used to obtain the data. SEM and EDS analyses were conducted on small fragments of a 28-day cured concrete specimen. The specimen was ground and pulverized until it could pass through a 75μ sieve for XRD and FTIR-TGA analysis.

3.6 OPTIMIZATION METHODS

Optimization methods are widely employed across many disciplines as a fundamental and adaptable collection of strategies to identify the optimal solution from a given set of available possibilities. These methods aim to maximize or minimize a specific objective, while adhering to certain constraints. Design of Experiments (DOE) supplements optimization through its structured methodology for conducting experiments and gathering data. It enables engineers to investigate how different design parameters and variables influence project performance, quality, and efficiency. DOE provides engineers with the tools to unravel the interconnections among various factors, facilitating the creation of robust, reliable, and efficient designs.

Response Surface Methodology is one of the optimization technique that combines statistical and mathematical techniques to experimental design, fitting models, regression analysis, and analyzing independent variable interactions (Li et al. 2021). RSM has been employed in this study to investigate the combined influence of independent variables x_1, x_2,.., x_n and establish an association between the variables and the output responses y_1, y_2,..,y_k by developing a functional model. RSM can examine the effects of several input variables on the response while keeping low test costs and optimizing the responses. A different set of models were used in the response surface analysis to develop statistical associations among the responses and the independent variables. RSM employs the nonlinear fitting model method to generate the fitting

equation. The quadratic polynomial in RSM fits the factor relationship with the interaction in Eq. (3.1), and the fitting equation finds the optimal value.

$$y = \beta_0 + \sum_{i=1}^{k} \beta_i x_i + \sum_{i=1}^{k} \beta_{ii} x_i^2 + \sum_{j=2}^{k} \sum_{i=1}^{j-1} \beta_{ij} x_i x_j + \varepsilon \qquad (3.1)$$

Where x_i and x_j are the variables, y is the response, k is the number of experimental parameters, β is the regression coefficient estimated from the experimental data, and ε is the random error. RSM optimization results are predictions that must be tested by experiments. The optimization by response surface analysis is successful, if the test and predicted results are in good agreement. Empirical models are derived from experimental data and are further analysed using statistical techniques such as multiple regression. Additionally, Analysis of variance (ANOVA) is used to assess the impact of each factor by analyzing the established regression model.

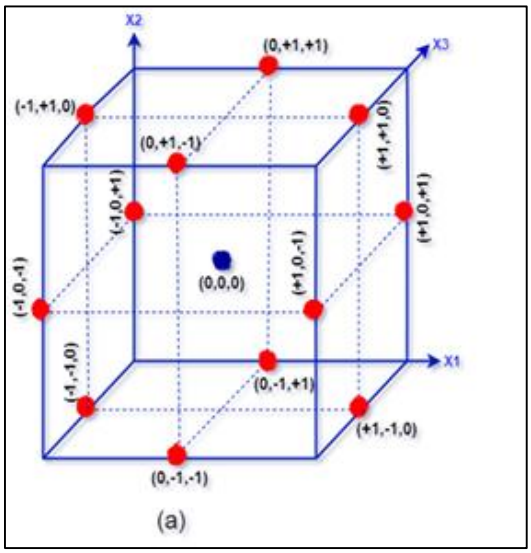

Figure 3.7 Coded design of BBD for 3 independent variables.

In this study, Box-Behnken Design (BBD) and full factorial designs (FFD) of RSM are used in multi-objective optimization of OPG mixes. BBD and FFD are two different experimental designs used in the context of RSM for optimizing processes and understanding the relationships between factors and responses. BBD is a fractional factorial design, which means it uses only a fraction of the total number of possible combinations. It does not test all possible factor level combinations, making it more efficient in terms of the number of experiments conducted. Whereas in FFD, all possible

combinations of factor levels are tested. This means that each factor is studied at all levels, resulting in a comprehensive set of experiments. The BBD of three-dimensional space and the arrangement of coded test points are shown in Figure 3.7. To optimize a problem using RSM, three key stages are typically undertaken. The initial stage involves the statistical design of experiments. Subsequently, the factors are predicted through mathematical modelling. Finally, the response is predicted and the model's viability is evaluated within the experimental setup. The procedure of RSM modeling approach to obtain optimal design parameters is shown in Figure 3.8.

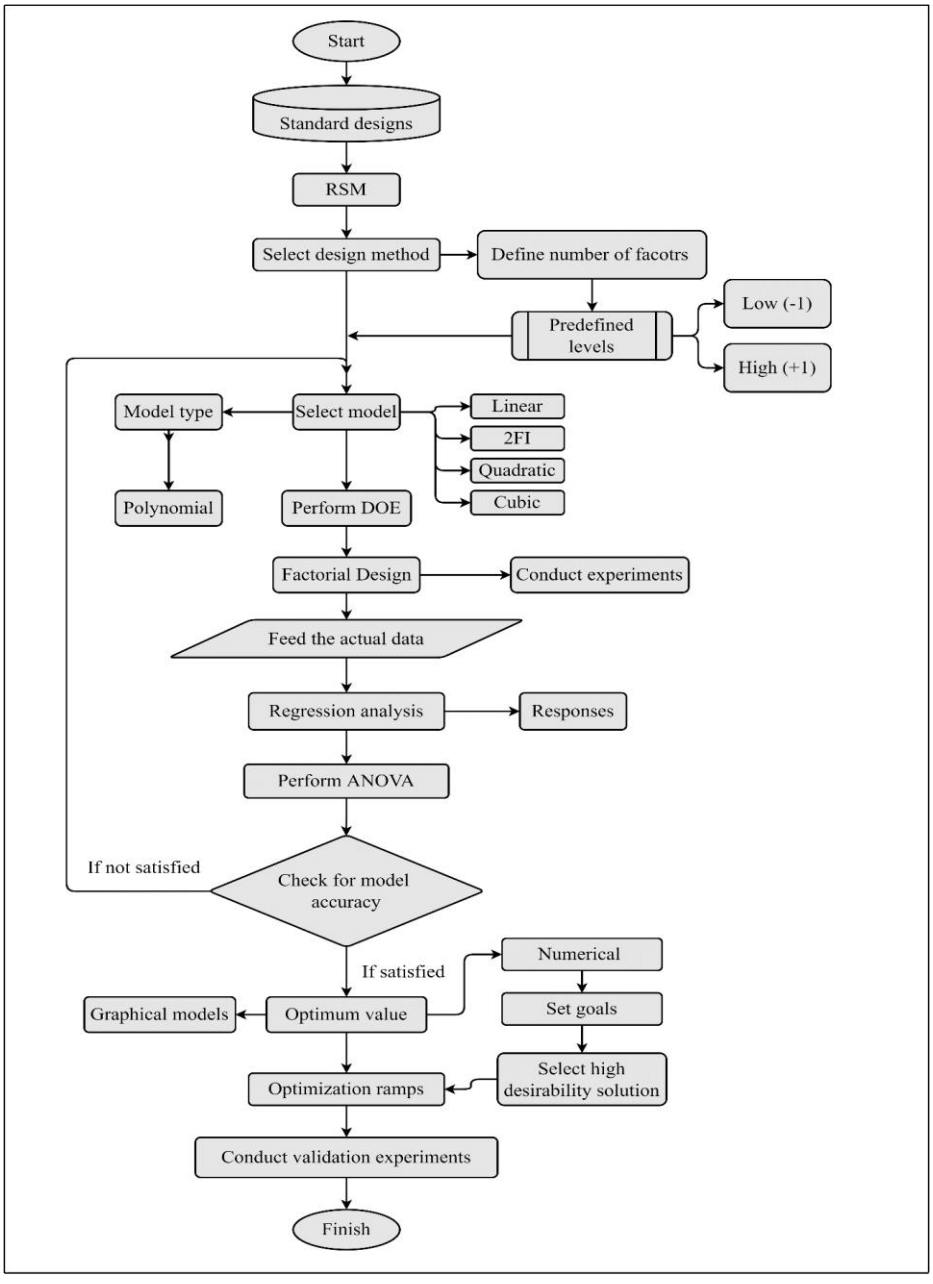

Figure 3.8 Response surface method flow chart.

3.7 CLOSURE

In this chapter, the physical and chemical properties of FA, GGBS, solid activator, aggregates, and water used in the development of OPG mixes are presented. Testing procedure for mechanical properties, microstructure studies, and optimization methods used for OPG mixes in the present work also detailed comprehensively.

CHAPTER 4

ONE-PART GEOPOLYMER PASTES

4.1 GENERAL

In this chapter, experimental evaluation and optimization studies on one-part geopolymer pastes are discussed. Furthermore, the investigation of microstructure and mineralogy is conducted in order to determine the development of various hydration products, utilizing SEM and XRD techniques.

4.2 MIX PROPORTIONS DESIGNED BY RESPONSE SURFACE METHOD

Response surface method is used to investigate the effect of three parameters on the fresh and hardened characteristics of OPG mixes. The role of GGBS is predominant in the strength development of OPGs, but it inhibits workability (Ma et al. 2018; Yousefi Oderji et al. 2019). High water content results in the reduced strength of the OPG mix (Dong et al. 2020). The amount of solid activator in the mix also has an impact on the rheological and hardened properties of the proposed mix (Li et al. 2020). For this optimization study, the influencing factors taken are GGBS substitution in percentage (A), water to geopolymer solid ratio W/GS (B), and the dosage of activator as a percentage of the total binder (C). The three levels were considered to optimize these factors for desired properties of OPG mixes, are illustrated in Table 4.1.

The BBD of RSM is used, which has three factors and three levels. The experimental runs from BBD are shown in Table 4.2. BBD designs for a total of 17 runs, including 12 design test points and five center points, to estimate the experimental error. Figure 4.1 shows the BBD test points for the three factors of designed OPG paste with coded and uncoded values. The mixture proportions designed by BBD of RSM are listed in Table 4.3. The response values recorded for one-part geopolymer paste are flow values (y_1), compressive strength (y_2), initial setting time (y_3), and final setting time (y_4). Design-Expert software was used to perform Box-Behnken design and to develop a prediction model for the responses.

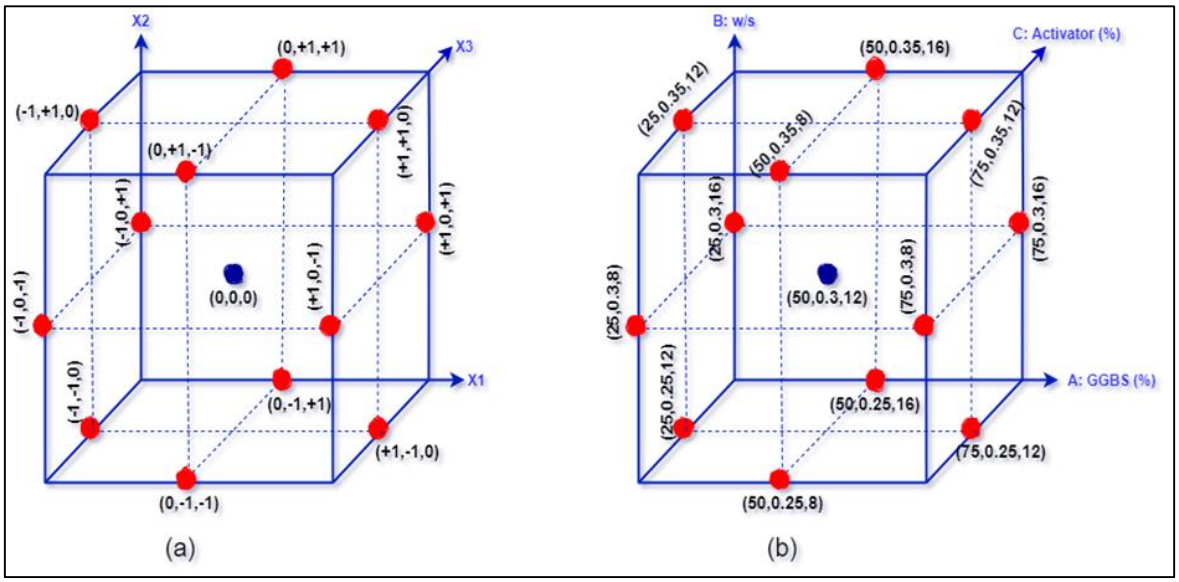

Figure 4.1 BBD for 3 independent variables of designed OPG paste based on (a) coded and (b) uncoded values.

Table 4.1 Coded and level of actual factors in BBD.

Levels	**Actual factors**			**Coded factors**		
	Substitution of GGBS, % (A)	**W/GS (B)**	**Activator, % (C)**	**Z_1**	**Z_2**	**Z_3**
Low	25	0.25	08	-1	-1	-1
0	50	0.30	12	0	0	0
High	75	0.35	16	1	1	1

Table 4.2 Experimental runs from BBD.

Design summary			
Factors	3	Base Runs	17
Responses	4	Base blocks	1
Design test points	13	Replicates	1
Center points	5	Total runs	17

Table 4.3 Design and RSM test results of the one-part geopolymer paste.

Std. order	Mix ID	Fly Ash (%)	A: GGBS (%)	B: W/GS	C: Activator (%)	y_1: Flow in mm	y_2: Compressive strength in MPa		y_3: Setting Time in min	
							7 day	28 day	Initial	Final
1	$G_{25}W_{0.25}A_{12}$	75	25	0.25	0.12	136	52.9	67.7	46	142
2	$G_{75}W_{0.25}A_{12}$	25	75	0.25	0.12	115	59.2	79.3	25	126
3	$G_{25}W_{0.35}A_{12}$	75	25	0.35	0.12	218	23.1	29.5	112	300
4	$G_{75}W_{0.35}A_{12}$	25	75	0.35	0.12	180	41.5	53.8	65	166
5	$G_{25}W_{0.3}A_{8}$	75	25	0.30	0.08	166	13.7	19.1	74	215
6	$G_{75}W_{0.3}A8$	25	75	0.30	0.08	135	35.2	39.0	53	114
7	$G_{25}W_{0.3}A_{16}$	75	25	0.30	0.16	214	39.9	50.2	63	144
8	$G_{75}W_{0.3}A_{16}$	25	75	0.30	0.16	181	55.7	78.5	40	125
9	$G_{50}W_{0.25}A_{8}$	50	50	0.25	0.08	110	29.4	41.7	45	163
10	$G_{50}W_{0.35}A_{8}$	50	50	0.35	0.08	175	21.9	30.6	89	242
11	$G_{50}W_{0.25}A_{16}$	50	50	0.25	0.16	142	49.3	64.5	31	144
12	$G_{50}W_{0.35}A_{16}$	50	50	0.35	0.16	210	43.5	56.4	62	184
13	$G_{50}W_{0.3}A_{12}$	50	50	0.30	0.12	170	51.3	70.3	47	175
14	$G_{50}W_{0.3}A_{12}$	50	50	0.30	0.12	168	52.8	71.2	46	168
15	$G_{50}W_{0.3}A_{12}$	50	50	0.30	0.12	171	50.2	69.1	51	175
16	$G_{50}W0_{.3}A_{12}$	50	50	0.30	0.12	169	49.1	67.7	48	171
17	$G_{50}W_{0.3}A_{12}$	50	50	0.30	0.12	172	52.2	73.7	53	177

4.3 RESULTS AND DISCUSSION

4.3.1 Response model development using RSM

The RSM has been employed to analyze the relationship between the responses and the independent variable. Table 4.3 shows the flowability, strength, and setting time of each of the developed one-part geopolymer paste. The data in Table 4.3 clearly shows that adding GGBS significantly increases the strength of the FA-based one-part geopolymers and reduces the flow values. The maximum 7-day and 28-day compressive strengths of 59.2 and 79.3 MPa respectively, were achieved for $G_{75}W_{0.25}A_{12}$ mix, i.e., mix comprising of 75% GGBS, 0.25 W/GS ratio with 12% activator with. Due to higher CaO content present in GGBS, it results in the formation of C-A-S-H gel under the influence of an alkali activator. For the same, a lower flow of 115 mm was recorded because of the angular and irregular shape of GGBS particles and for their nature of immediate reaction with activators. The higher flow value of 218 mm is recorded for $G_{25}W_{0.35}A_{12}$ with a higher W/GS ratio of 0.35, lower GGBS, and a 12% activator. The shortest initial setting time of 25 mins, and final setting time of 114 mins were recorded for $G_{75}W_{0.25}A_{12}$ and $G_{75}W_{0.3}A_{8}$, respectively, where mixes comprised of a higher percentage of GGBS. The lower 7-day and 28-day compressive strengths of 13.7 and 19.1 Mpa, respectively, were obtained for lower GGBS and 0.3 W/GS ratio based mix.

The software "Design Expert" was used to model the experimental results to find the polynomial function that best fits the data. Nonlinear fitting of various models is performed using model summary statistics, the sum of squares of the deviation, and fitting error (Li et al. 2021). The quadratic polynomial models are developed with the coefficient of parameters given by multiple regression analysis. The variable relationships and influence for their actual quantities and responses were obtained using ANOVA. The present results agree well with the findings already reported in the literature (Dong et al. 2020; Oderji et al. 2019). The regression models for each response are shown in Eq. (4.1)-(4.4).

$$\textbf{\textit{Flowability }}(y_1) = -496.625 - 0.095A + 3525B + 3.4062C - 3.4AB - 0.005AC + 3.75BC + 0.0056A^2 - 4500B^2 + 0.0312C^2 \quad (4.1)$$

Compressive strength (y_2) $= -246.8315 + 0.5526A + 961.955B + 26.2276C + 2.568AB + 0.0211AC + 3.8375BC - 0.0115A^2 - 2239.3B^2 - 1.0295C^2$ (4.2)

Initial setting time (y_3) $= 82.7916 - 0.035A - 544.1667B + 1.1667C - 5.2667AB - 0.005AC - 17.5BC + 0.0111A^2 + 2450B^2 + 0.0963C^2$ (4.3)

Final setting time (y_4) $= 276.4916 + 5.114A - 2658.1667B + 18.027C - 23.6667AB + 0.2058AC - 49.1667BC - 0.0183A^2 + 8706.6667B^2 - 0.7437C^2$ (4.4)

Table 4.4 ANOVA response models of experimental results.

Model	**Responses**			
	y_1	y_2	y_3	y_4
Standard deviation	4.29	7.05	6.15	11.78
Mean	166.59	56.66	55.88	172.37
Coefficient of variation (%)	2.57	12.44	11.01	6.84
R^2 value	0.9918	0.9373	0.9626	0.9711
Adeq Precisior	34.0501	9.7927	16.0795	19.2549
F value	94.09	11.64	20.03	26.12
p-value (model)	<0.0001	0.0019	0.0003	0.0001
Lack of fit (model)	0.0110	0.0060	0.0189	0.0055
p-value (Prob > F) of factor, interaction of factor and square of factor				
A: GGBS (%)	<0.0001	0.0039	0.0003	<0.0001
B: W/GS	<0.0001	0.0043	<0.0001	<0.0001
C: SM/b	<0.0001	0.0006	0.0075	0.0045
AB	0.0879	0.3927	0.0696	0.0015
AC	0.8223	0.5674	0.8755	0.0101
BC	0.7368	0.8338	0.2927	0.1390
A^2	0.1379	0.0735	0.0533	0.0856
B^2	0.0010	0.1472	0.0804	0.0068
C^2	0.8178	0.0020	0.6230	0.0769

All regression models were statistically examined and validated by analysis of variance (ANOVA). To evaluate the significance of experimental factors, the analysis was performed at 5% significance level. The R^2 (regression coefficient) value, which

depicts the distinction between response function and actual value, was used to test how well the model fit. The obtained p-values of all the models are less than 0.05, which indicates that all factors were statistically significant at 95% confidence level as shown in Table 4.4. The factor is very significant if the p-value is less than 0.01, indicating a substantial regression effect. The higher R^2 values of 0.9918, 0.9373, 0.9626, and 0.9711 for flowability, compressive strength, and initial and final setting time models, respectively, indicate a significant level of agreement between predicted and actual values and show that the fitting effect of the equation is good. The CV (coefficient of variation) of 2.57, 12.44, 11.01, and 6.84% for responses y_1, y_2, y_3, and y_4, respectively, are in good agreement, indicating that the developed model is more feasible. All models have precision values greater than 4, as shown in Table 4.4, indicating that they could be used to explore the design space.

A normal probability plot shows data distribution and sufficiency (Mohammed et al. 2018). The distribution of the points for all dependent variables shown in Figure 4.2, is almost perfectly straight, demonstrating the normal distribution of the data for all residual responses. A graphical analysis of the expertise and fitness of the models developed is shown by a plot of predicted results as the ordinate and actual results as the abscissa. The plot in Figure 4.3 shows that the predicted response model was accurate, and every point lies close to the straight line. The smooth fit of the points to a straight line indicates that the experimental and predicted results follow established models fairly well and fit the data well.

The statistics shown in Table 4.4 reveal that the three variables significantly affect flowability, compressive strength, and setting time, and their interaction has an influence on the outcomes. The influence of each variable on flowability of OPG paste is as follows: B > A > C > AB > BC > AC. The influence of each variable on compressive strength is as follows: C > A > B > AB > AC > BC. The influence of each variable on initial and final setting are B > A > C > AB > BC > AC and B > A > AB > C > AC > BC, respectively.

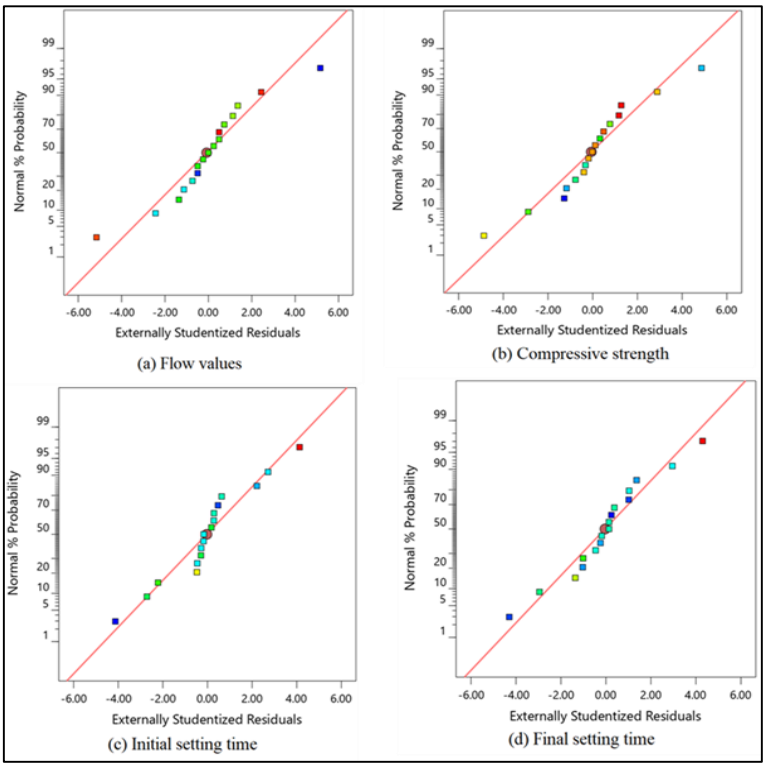

Figure 4.2 Normal plot of the residual response models of OPG pastes.

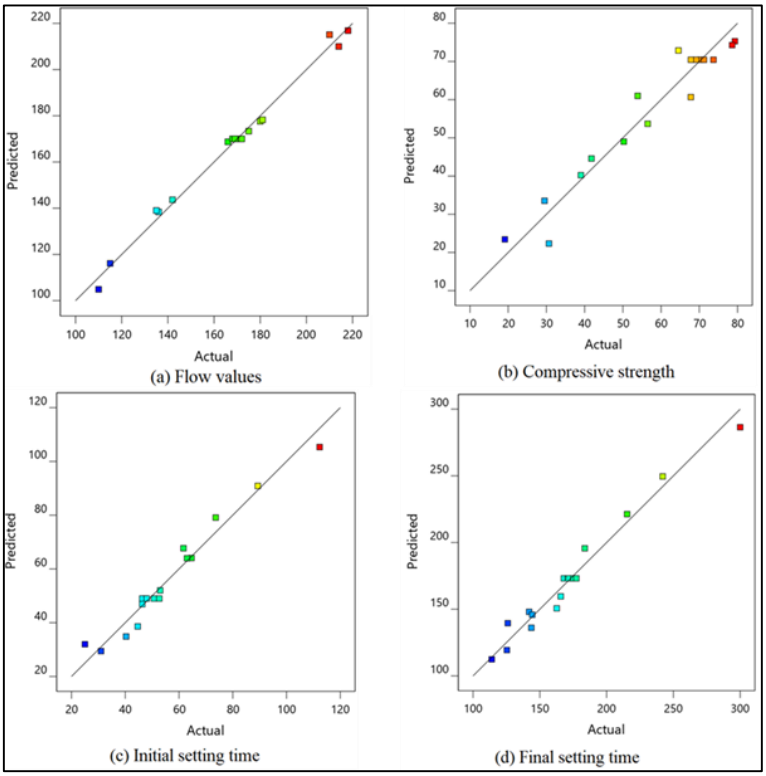

Figure 4.3 Comparison of the predicted and actual values of OPG pastes.

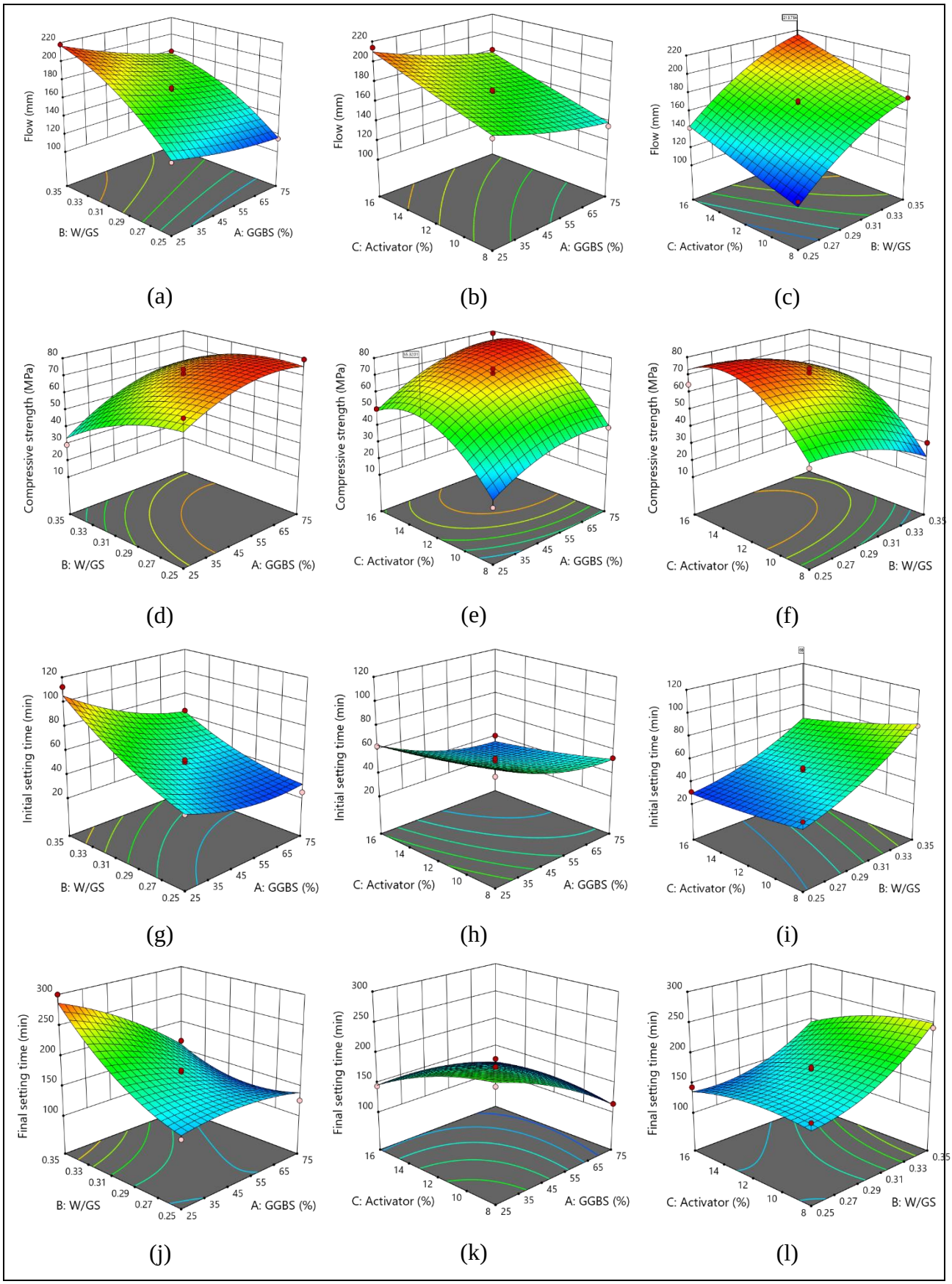

Figure 4.4 3D response surface plots for flowability, compressive strength, initial and final setting time of OPG pastes.

It can be observed that all individual factors significantly affect the flowability of a one-part system. The interaction of GGBS substitution and W/GS ratio has a greater effect on flow and strength of the mixes. Flow value increases with increase in water content and decreases with increase in GGBS substitution due to higher specific surface area and irregular shape of slag particles, which hinders the flow (Yousefi Oderji et al. 2019). The activator dosage followed by GGBS substitution has a greater influence on the compressive strength of the mix due to the rapid reaction of slag particles, resulting in a faster polymerization process with sufficient alkalis to form C-A-S-H gel which is responsible for the strength gain of the OPG mixes (Ma et al. 2018). The setting time of OPG mixes is greatly affected by the W/GS ratio followed by GGBS substitution. The higher water content results in delayed setting time, and higher GGBS substitution results in the quick setting of the one-part mixes due to higher calcium in slag, leading to quick gel formation and fastening hardening rate (Elzeadani et al. 2022; Li et al. 2020). The combined effect of AB is highly significant in all responses compared to other factor interactions.

4.3.2 3D surface response plots

Response surface plots, including contour and surface plots, help in determining appropriate response value systems and operating conditions. The response surface plots can explicitly represent the combined effects of two variables on the obtained response values. The significance of the effect of factor interaction increases with increasing response surface curvature; otherwise, there is no discernible impact (Li et al. 2021). The response surface plots are generated by 'Design Expert' software. Figure 4.4 illustrates the effect of three factors on response values of one-part geopolymer pastes.

4.3.2.1 Flowability

The impact of GGBS substitution and W/GS ratio on the flow values of OPG paste is depicted in Figure 4.4a. When the GGBS substitution increases for constant W/GS ratio, flow decreases by 15-20%, approximate linear decrement seen in the plot. This is because of the greater explicit surface region and irregular shape of the slag particle, which slows down the flow and rapid reaction process of slag particles (Yousefi Oderji

et al. 2019). At constant GGBS substitution, the flow increases significantly as the W/GS ratio increases. The surface of the curve is steep, that increases the maximum flow diameter by 60.3%. The lowest flow was recorded for maximum GGBS substitution and least W/GS ratio, and the maximum flow is found for least value of GGBS substitution and maximum W/GS ratio. This demonstrates that the W/GS ratio is the fundamental factor influencing the flow values of the paste, followed by GGBS substitution. This is because, as water content increases, the mix becomes less viscous, which results in a higher flowability (Dong et al. 2020). Figure 4.4b shows the interaction effect of GGBS substitution and dosage of activator on flow of OPG paste. At constant GGBS substitution, activator dosage positively correlates with flow and the rate of flow increases by 34.1%. When the activator content is low, the flow values decrease gradually with an increase in GGBS substitution. At the point when GGBS replacement is high, the flow values increase marginally with an increment of activator content. This is attributed to excess sodium silicate activator that impedes the dissolving of high modulus raw materials, leading to a less cohesive paste (Jafari Nadoushan and Ramezanianpour 2016). Figure 4.4c shows the impact of the W/GS ratio being positively related to flow values irrespective of the activator dosage. The lower flow values are recorded for lower W/GS ratio and activator content. For constant activator dosage, flow values significantly increases by 59.1% with increase in W/GS ratio. When W/GS is unchanged, the flow values gradually increases as the activator content increases and the increase is 21.7%. It is noticed that the influence on the flow is that, the W/GS ratio > activator dosage, which is consistent with the ANOVA results presented in Table 4.4.

4.3.2.2 Compressive strength

The influence of GGBS substitution and W/GS ratio on the OPG paste compressive strength is shown in Figure 4.4d. With a constant W/GS ratio, GGBS replacement improves compressive strength and the increase is about 76.5%. When GGBS is unaltered, W/GS ratio is inversely linked with compressive strength, and it reduces by 69.4%. This implies that the GGBS replacement significantly influences the compressive strength of the OPG pastes. Since more prominent GGBS substitution results in higher calcium concentration in the mixture, it results in more C-A-S-H gel

development affected by an alkali activator, and that exists together with Sodium-Alumina-Silica-Hydrate (N-A-S-H) gel. Furthermore, higher calcium accelerates the polycondensation process forming tetrahedral structures of silica and aluminum, which later forms three-dimensional network that results in higher compressive strength (Askarian et al. 2019; Ma et al. 2018). Figure 4.4e demonstrates the effect of GGBS and activator dosage on OPG paste compressive strength. It reveals that, for constant GGBS substitution, the observed curved surface shows that compressive strength increases with activator concentration and reaches a peak at some point. Strength declines by 10-15% from the maximum strength recorded. This is due to a higher activator dosage consisting of excess Na_2O that prevents the development of binding phases and thereby increases the likelihood of activator leaching and efflorescence, both of which contribute to matrix deterioration and lower strength (Dong et al. 2020; Yousefi Oderji et al. 2019).

However, regardless of activator dosage, the strength increases as the GGBS content increase. On the other side, Figure 4.4f shows that for unchanged activator content, strength declines as the W/GS ratio increases and the strength change is small. The curve shows the decrease in strength after attaining the maximum strength as activator content increases, irrespective of the W/GS ratio. This indicates that the effect of activator dosage dominates the W/GS ratio in compressive strength of OPG pastes.

4.3.2.3 Setting time

Figure 4.4g and 4.4j demonstrate the interaction between the GGBS substitution and the W/GS ratio, as well as the effect on the setting time. The initial and final setting times increase by 102.7% and 110.2%, respectively, as the W/GS ratio increases when the GGBS replacement is left unaltered. The prolonged setting time of OPG paste was recorded due to increase in water content in the mix. This is because of a viscosity change that the Vicat needle cannot detect, and water acts as a reaction medium. The excess water negatively affects the polymerization process, which results in delayed setting time (Ranjbar et al. 2020). When the W/GS ratio remains constant, increasing the GGBS replacement reduces the initial and final setting times by 72.3% and 81.1%, respectively. However, at a lower W/GS ratio, the recorded decrement of setting time was small. This is because precursors with a greater CaO concentration result in a faster

dissolution rate than SiO_2 and Al_2O_3, which provides a nucleation site at an early age, leading to rapid hardening and shorter setting time (Pangdaeng et al. 2014). Also, the slag particles have a higher activity rate for their amorphous phase, faster charge neutralization, and stronger electrostatic attraction of ca^{2+} ions that hydrates rapidly in an alkaline media to generate C-A-S-H gel, which specifies the starting time of the paste hardening (Elzeadani et al. 2022). The combined impact of the GGBS and activator dosage on the setting time is shown in Figure 4.4h and 4.4k. When the activator content is constant, the GGBS replacement negatively correlates with the setting time, reducing the initial setting time by 39.6%, and final setting time by 33.0%. When the GGBS replacement is constant, both the setting times decrease as the activator content increases, proving that a larger activator dosage contains more silica, which facilitates polymerization of dissolved active compounds of precursors (Li et al. 2020; Nath and Sarker 2014). Figure 4.4i and 4.4l shows the effect of W/GS ratio and activator interaction on setting time of OPG paste. When the activator content is constant, the initial and final setting times increase by 89.8% and 49.9%, respectively, as the W/GS ratio increases. When the W/GS ratio is unaltered, the decrease in initial setting time by 23.6% and final setting time by 18.5% with the increase of activator content is observed.

4.3.3 Optimization and validation study

By using the numerical multi-objective optimization technique, the response surface fitting model, and the desirability function, the optimum amount of GGBS substitution, W/GS ratio, and activator dosage were determined with the aim of maximizing the flow, compressive strength, and setting time of the developed OPG pastes by considering all responses with equal importance. The optimization research is concerned with determining the desirable values of independent variables to achieve the optimization benchmark. The desirability function (D) of a single solution ranges from 0 to 1, with 0 representing the unsatisfactory response value and 1 representing the desired response value. The goal of multi-objective optimization is to maximize the desirability function. Table 4.5 summarizes the optimization criteria. The RSM approach was used to improve the responses impacted by various factors. As a result, the following ratio is found to be ideal: GGBS substitution 51.4%, W/GS ratio 0.32, and activator dosage

12.4% for a desirability function value of 0.629, showing that the projected value is very reliable (Aydin 2013).

Table 4.6 displays the outcomes of numerical optimization solutions based on the objective of the optimization. The prediction error for optimizing OPG mix proportions is less than 10%, with reference to the actual value, which reveals higher model accuracy. However, the model validation was done by calculating response prediction values using individual response models and obtaining the absolute deviations from the actual values. Eq.4.5 gives the absolute relative deviations of predicted and actual values. Figure 4.5 shows the model significance with actual and predicted values of flow values and compressive strength of all OPG mixes. The predicted and actual values of setting time are shown in Figure 4.6. The independent variables and responses were visually represented by the optimization ramps illustrated in Figure 4.7.

Table 4.5 Factors and the optimization benchmarks for individual responses.

Factors	**Goal**	**Lower limit**	**Upper limit**
A: GGBS Substitution (%)	In range	25	75
B: W/GS ratio	In range	0.25	0.35
C: Activator dosage (%)	In range	8	16
Benchmarks for individual responses			
y_1: Flowability (mm)	Maximize	110	218
y_2: Compressive strength (MPa)	Maximize	19.13	79.31
y_3: Initial setting time (min)	Maximize	25	112
y_4: Final setting time (min)	Maximize	114	300

Table 4.6 Model verification.

Responses	**GGBS (%)**	**W/GS ratio**	**Activator (%)**	**Predicted value**	**Experimental value**	**Error (%)**
Flow (mm)	51.39	0.32	12.35	187	191	2.1
Compressive strength (MPa)	51.39	0.32	12.35	64.8	68.5	5.5
IST (min)	51.39	0.32	12.35	62	59	5.1
FST (min)	51.39	0.32	12.35	198	191	3.7

$$Error\ (\%) = \frac{Actual\ value\ -\ predictive\ value}{Actual\ value} \times 100\% \quad (4.5)$$

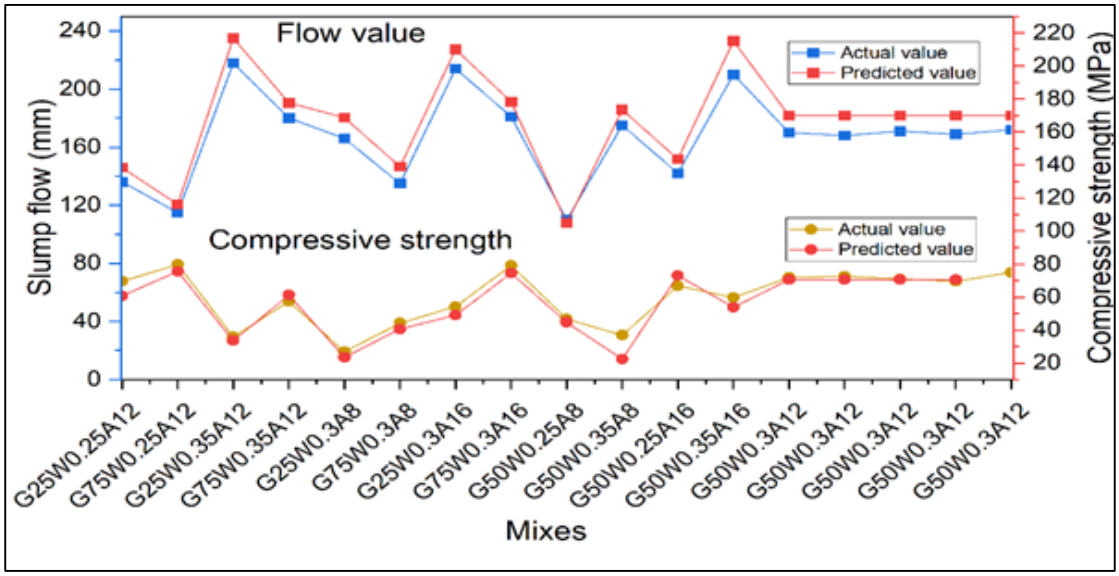

Figure 4.5 Model significance with actual and predicted values of flow value and compressive strength responses.

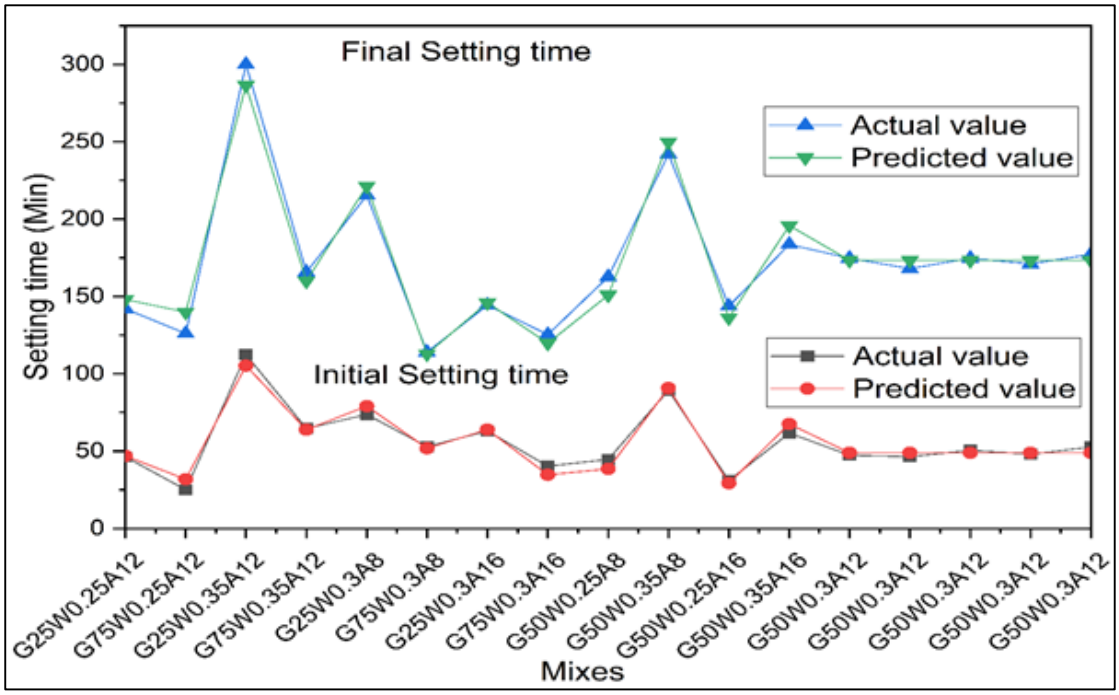

Figure 4.6 Model significance with actual and predicted values of initial and final setting time responses.

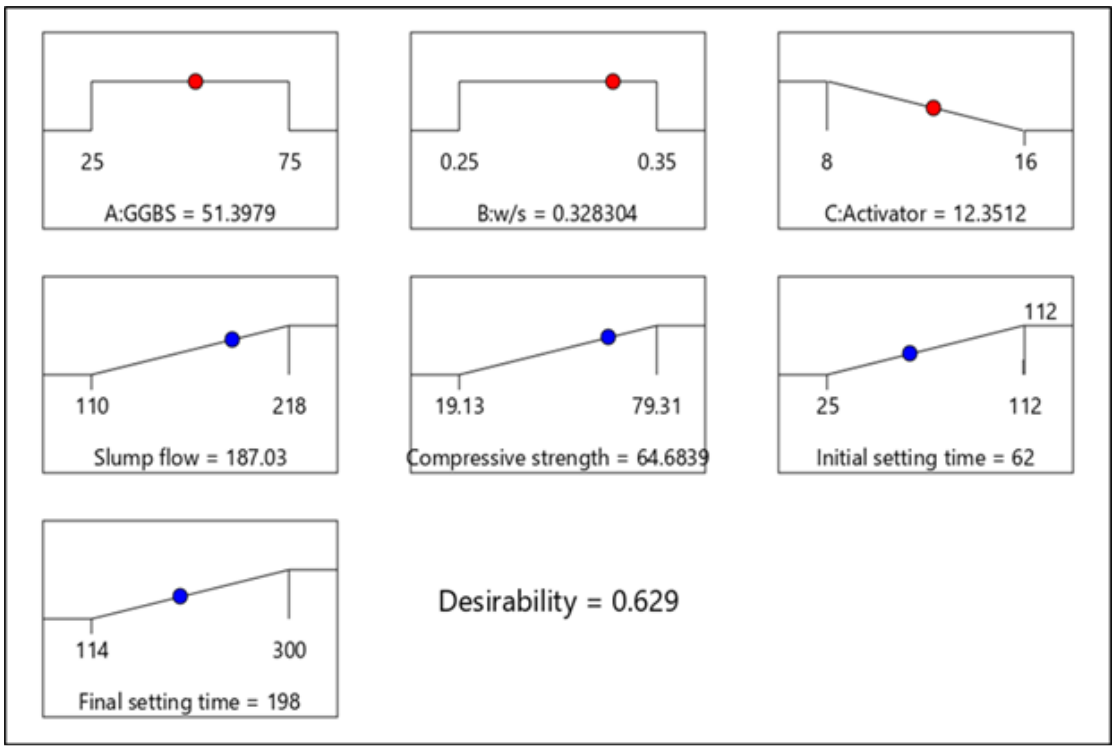

Figure 4.7 Optimization ramps.

4.4 MICROSTRUCTURES AND MINERALOGY

4.4.1 SEM and EDS analysis

To study the individual and combined effect of factors, SEM micrographs of chosen specimens were evaluated at 28 days, are shown in Figure 4.8 and Figure 4.9. It can be observed in Figure 4.8a, that the binder with a lower W/GS ratio clearly exhibits a less quantity of un-reacted particles than the binder with a higher W/GS ratio shown in Figure 4.8b. This resulted in less gel synthesis in samples with a higher W/GS ratio, which accounts for the drastic decrease in compressive strength represented in Table 4.3 and the same observations were reported by Oderji et al. (Oderji et al. 2019). Lower W/GS ratio in the system exacerbates self-desiccation by causing pore dryness owing to water consumption for hydration reactions, resulting in increased voids (Li et al. 2014) as observed in Figure 4.8a. The heat emitted during the dissolution of the anhydrous sodium metasilicate activator might be responsible for the voids (Ma et al. 2019). Along with the geopolymer products, varying amounts of unreacted FA and GGBS particles are present for each mix, as observed in the micrographs. An increased GGBS content in the mix exhibits a highly uniform, dense, and compact microstructure,

leading to the formation of C-A-S-H gel, which contributed to greater increase in strength, as observed in Figure 4.8a and 4.8c and is in line with studies reported earlier (Yousefi Oderji et al. 2019). In some regions, there is partial development of C-A-S-H gel due to the inequitable distribution of the sodium metasilicate grains, resulting in varying silica availability in the matrix. However, a few minor cracks were noticed in the micrographs, which could be attributed to the gel drying shrinkage. This shrinkage might be caused by water evaporation and non-uniform internal pressure during the polycondensation process, which creates capillary tension inside the gel matrices (Das and Rout 2021).

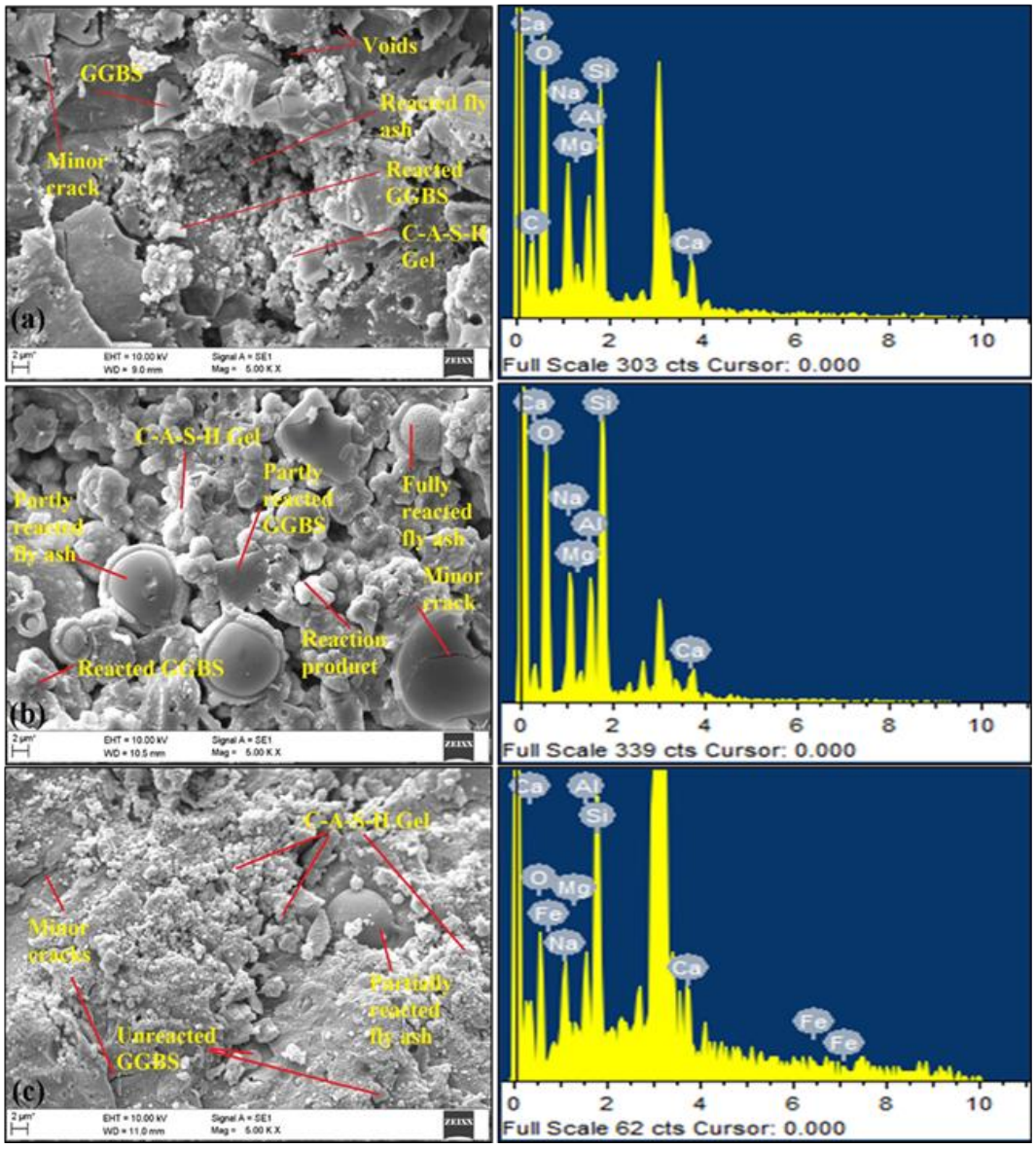

Figure 4.8 SEM and EDS images of (a) $G_{75}W_{0.25}A_{12}$, (b) $G_{25}W_{0.35}A_{12}$, and (c) $G_{50}W_{0.3}A_{12}$

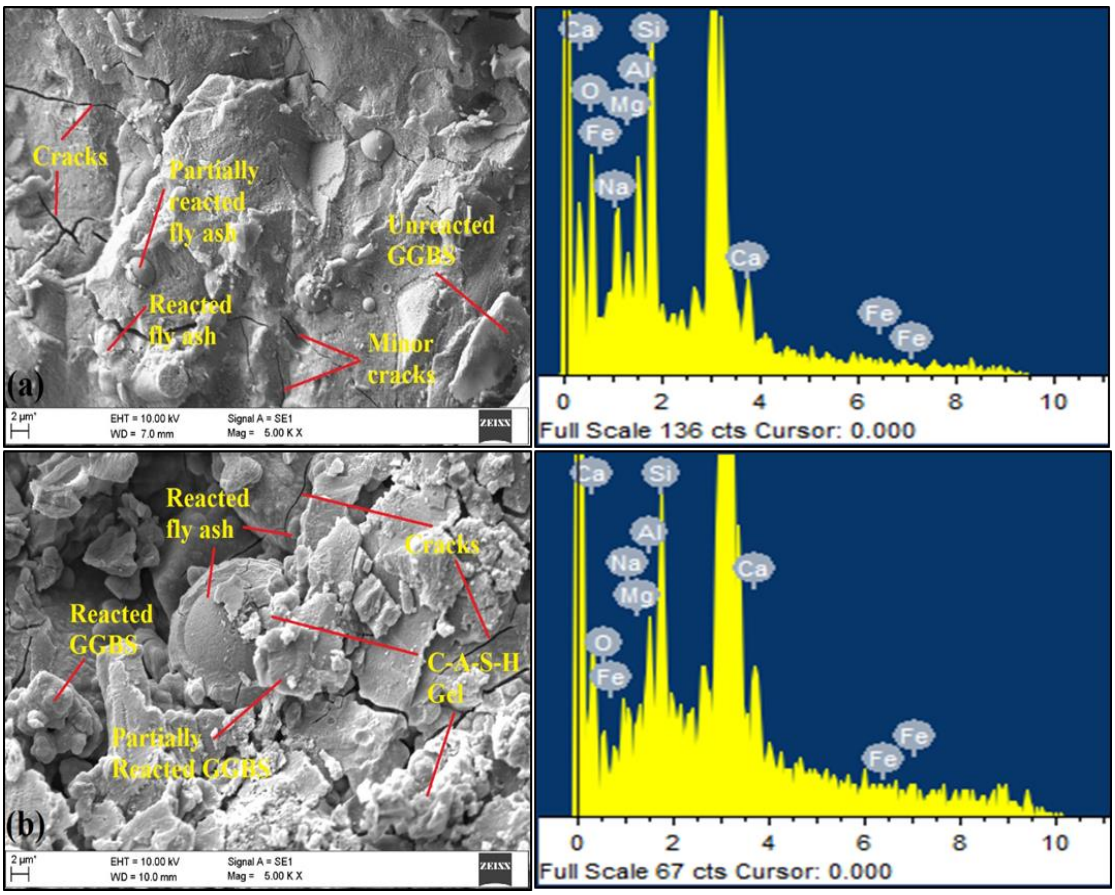

Figure 4.9 SEM and EDS images of (a) $G_{75}W_{0.3}A_8$ and (b) $G_{75}W_{0.3}A_{16}$

Figure 4.9 shows the micrographs of change in activator dosage of mixes. From Figure 4.9a, it can be noticed that the mix with lower activator content mix consists of more unreacted fly ash and GGBS particles compared to higher activator content mix as is observed in Figure 4.9b. The amount of reacted product in the mix $G_{75}W_{0.3}A_8$ is very less compared to the mix $G_{75}W_{0.3}A_{16}$. This is attributed to the insufficient amount of activator content required for dissolution of precursors, leading to more unreacted particles in the mix. The mix with higher activator content shows a very dense and uniform matrix. However, longer micro cracks were observed as in Figure 4.9b. This can be related to the more Na_2O content in the system at a higher activator dosage which generates more reaction heat during the polymerization process and results in a rise in ionic species concentration, which decreases ion mobility and slows down the development of coagulated formations (Haruna et al. 2021). The SEM micrographs of $G_{50}W_{0.3}A_{12}$ are shown in Figure 4.8c exhibits denser microstructure with smaller unreacted particles and larger formation of C-A-S-H gel which are well correlated with

the compressive strength properties of one-part geopolymer mixes. Energy dispersive spectroscopy analysis (EDS) was carried out for chosen specimens to observe the silicate activated geopolymerization products shown in Figure 4.8 andFigure 4.9. The presence of calcium, silicon, sodium, and aluminum phases with interparticle bonds among elements has been revealed in the EDS analysis. These substances were found to be present, indicating the presence of C-(N) -A-S-H gels. The Ca/Si and Al/Si ratio of mixes were found to be in the range of 1.03 to 1.71 and 0.21 to 0.69, respectively. The Ca/Si and Al/Si ratio of mix $G_{50}W_{0.3}A_{12}$, are 1.68 and 0.61, respectively which indicates the presence of C-A-S-H gel and exhibits the denser microstructure properties. As residues in the paste, additional amounts of calcium, iron, and magnesium were observed. The element residues did not entirely dissolve throughout the reaction process, and they exhibited a morphology and composition similar to that of a two-part geopolymer (Ali et al. 2018; Puligilla and Mondal 2013).

4.4.2 XRD analysis

The XRD peaks of FA replacement with GGBS mix with varied W/GS ratio and alkali activator mixture contents between $2\theta = 10^{\circ}$ to 70° are illustrated in Figure 4.10. No new peak appears in the one-part geopolymer paste crystal phase results compared to the raw ingredients; however, the diffraction peak intensity is different. The presence of inert elements like quartz, mullite, and hematite in the FA based OPG paste suggests that not all aluminosilicate precursors are involved in the reaction. As observed in the XRD graph, the intensity of quartz increases with increase in fly ash content which resembles the presence of non-reactive silica in the form of quartz in fly ash. A shift in peak intensity at about 29° is the only statistically significant difference between the peaks observed for the mixes which resemble the presence of C-S-H gel and calcium carbonate phase, which is in agreement with the work reported by T. Luukkonen et.al (Luukkonen et al. 2018b) and shown in Figure 4.10. At $2\theta = 20^{\circ}$ to 40°, C-(N)-A-S-H gels peaks have appeared that indicates the strength development of the paste (Kim et al. 2013).

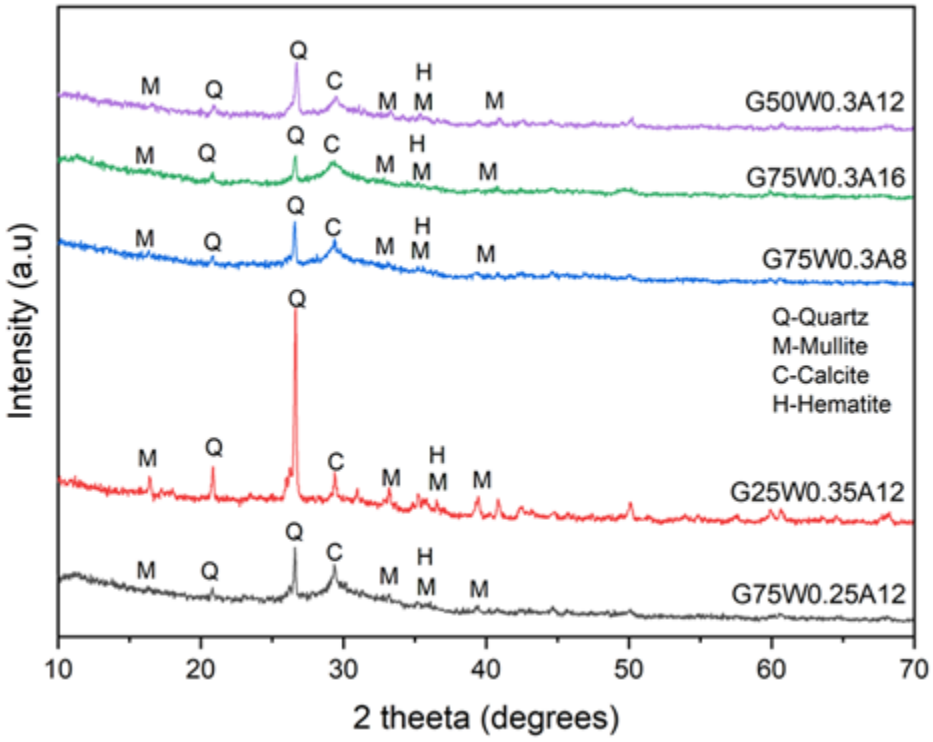

Figure 4.10 XRD patterns of OPG pastes.

The C-(A)-S-H phase exists in OPG or conventional geopolymer system due to a complex polymerization reaction mechanism (Bernal and Provis 2014; Yousefi Oderji et al. 2019). Among all the mixes, $G_{50}W_{0.3}A_{12}$ mix shows a better smooth curve indicating fewer unreacted particles in the system, which recorded a compressive strength of 73 MPa and denser microstructures (Dong et al. 2020). Increased GGBS substitution results in the rapid development of C-S-H gel which accelerates the Si and Al dissolution present in the precursor that greatly enhances geopolymer functionality.

4.5 CLOSURE

In this chapter, the experimental programme and optimization studies on one-part geopolymer pastes are reported. The combined interaction effects of considered variables on properties of paste systems are presented. The detailed microstructural and mineralogical changes in the behavior of one-part geopolymer pastes are examined.

CHAPTER 5

ONE-PART GEOPOLYMER MORTARS

5.1 GENERAL

This chapter focuses on the experimental evaluation and optimization of one-part geopolymer mortars. Further, the microstructural characterization adopting techniques like SEM, XRD, TGA and FTIR was carried out to study microstructural changes, mineral phases, thermal mass loss and molecular bonding of one-part geopolymer mortar mixes.

5.2 MIX PROPORTIONS DESIGNED BY RESPONSE SURFACE METHOD

Experiments on one-part geopolymer mortars was carried out by employing low calcium fly ash, GGBS, anhydrous sodium metasilicate powder, and fine aggregates. In this study, 3 influential factors of 3 levels each, were considered to develop OPGM mixes. The various factors taken are substitution of GGBS by 25%, 50% and 75% by volume of fly ash, and activator dosage of 8%, 12%, and 16% by mass of binder with W/GS ratio of 0.35, 0.40, and 0.45. According to 3-level factorial design, a total of 27 number of mixes were designed. The comprehensive information regarding the mix proportions of OPGMs is given in Table 5.1. Mix proportions are denoted for convenience, for example $G_{25}A_8W_{0.35}$, where G_{25}, $A_{8,}$ and $W_{0.35}$ indicates 25% GGBS substitution, 8% activator dosage, and W/GS ratio of 0.35 respectively.

Table 5.1 Mix proportions for 1 m^3 of one-part geopolymer mortars.

Mix No.	Mix ID	W/GS	A* (%)	FA (%)	GGBS (%)	B/S*	FA (kg/m^3)	GGBS (kg/m^3)	A* (kg/m^3)	Water (kg/m^3)	Sand (kg/m^3)
M1	$G_{25}A_8W_{0.35}$	0.35	8	75	25	2	569.3	245.4	70.8	309.9	1943
M2	$G_{50}A_8W_{0.35}$			50	50	2	379.5	490.8	75.7	331.1	1943
M3	$G_{75}A_8W_{0.35}$			25	75	2	189.8	736.2	80.5	352.3	1943
M4	$G_{25}A_{12}W_{0.35}$		12	75	25	2	544.5	234.7	106.3	309.9	1943
M5	$G_{50}A_{12}W_{0.35}$			50	50	2	363.0	469.5	113.5	331.1	1943
M6	$G_{75}A_{12}W_{0.35}$			25	75	2	181.5	704.2	120.8	352.3	1943
M7	$G_{25}A_{16}W_{0.35}$		16	75	25	2	519.8	224.1	141.7	309.9	1943
M8	$G_{50}A_{16}W_{0.35}$			50	50	2	346.5	448.1	151.4	331.1	1943
M9	$G_{75}A_{16}W_{0.35}$			25	75	2	173.3	672.2	161.0	352.3	1943
M10	$G_{25}A_8W_{0.40}$	0.40	8	75	25	2	569.3	245.4	70.8	354.2	1943

M11	$G_{50}A_8W_{0.40}$			50	50	2	379.5	490.8	75.7	378.4	1943
M12	$G_{75}A_8W_{0.40}$			25	75	2	189.8	736.2	80.5	402.6	1943
M13	$G_{25}A_{12}W_{0.40}$		12	75	25	2	544.5	234.7	106.3	354.2	1943
M14	$G_{50}A_{12}W_{0.40}$			50	50	2	363.0	469.5	113.5	378.4	1943
M15	$G_{75}A_{12}W_{0.40}$			25	75	2	181.5	704.2	120.8	402.6	1943
M16	$G_{25}A_{16}W_{0.40}$		16	75	25	2	519.8	224.1	141.7	354.2	1943
M17	$G_{50}A_{16}W_{0.40}$			50	50	2	346.5	448.1	151.4	378.4	1943
M18	$G_{75}A_{16}W_{0.40}$			25	75	2	173.3	672.2	161.0	402.6	1943
M19	$G_{25}A_8W_{0.45}$	0.45	8	75	25	2	569.3	245.4	70.8	398.5	1943
M20	$G_{50}A_8W_{0.45}$			50	50	2	379.5	490.8	75.7	425.7	1943
M21	$G_{75}A_8W_{0.45}$			25	75	2	189.8	736.2	80.5	452.9	1943
M22	$G_{25}A_{12}W_{0.45}$		12	75	25	2	544.5	234.7	106.3	398.5	1943
M23	$G_{50}A_{12}W_{0.45}$			50	50	2	363.0	469.5	113.5	425.7	1943
M24	$G_{75}A_{12}W_{0.45}$			25	75	2	181.5	704.2	120.8	452.9	1943
M25	$G_{25}A_{16}W_{0.45}$		16	75	25	2	519.8	224.1	141.7	398.5	1943
M26	$G_{50}A_{16}W_{0.45}$			50	50	2	346.5	448.1	151.4	425.7	1943
M27	$G_{75}A_{16}W_{0.45}$			25	75	2	173.3	672.2	161.0	452.9	1943

* A: Activator; B/S: Binder to sand ratio;

5.3 RESULTS AND DISCUSSION

The test results obtained for the OPGM mixes of various fly ash/GGBS ratios and dosages of activator content at different water to geopolymer solids ratios are presented in Figure 5.1 - Figure 5.4.

5.3.1 Flowability

The flow values of all the designed OPGM mixes are shown in Figure 5.1. The observed results indicate the change in the flowability of the mixes relies on the W/GS ratio regardless of GGBS content and activator dosage in the mix. The flowability of the mixes increases as W/GS ratio increases. The maximum flow value of 244 mm was noted for the mix with 0.45 W/GS ratio at 16% activator with 25% GGBS content, and 169 mm flow was noted for the mix with W/GS ratio of 0.35 for same activator and GGBS content. Flowability increases by approximately 19-31% and 44-52%, as the W/GS ratio changes from 0.35 to 0.40 and 0.45, respectively regardless of activator and GGBS content in the mix. This phenomenon can be ascribed to the inverse relationship between water content and viscosity in the mix, whereby an increase in water content leads to a decrease in viscosity, consequently yielding higher flowability which is in line with earlier literatures (Dong et al. 2020). It can be observed from Figure 5.1 that

the OPGM flow values showed an increase by approximately 14% and 25% when the dosage of activator was varied from 8% to 12% and 16%, respectively irrespective of W/GS ratio. This is due to overabundance of anhydrous Na_2SiO_3 content, which restricts the dissolution of high-modulus raw materials, resulting in a reduced cohesive paste (Jafari Nadoushan and Ramezanianpour 2016). Further Figure 5.1 depicts the effect of GGBS content on the flowability of the OPGMs. With increase in GGBS content, the flowability of the OPGMs decreased irrespective of the activator content and W/GS ratio. With GGBS replacement level varied from 25% to 50% and 75%, the fluidities of the OPGMs decreases by approximately 8% and 23%, respectively. The lowest flow value of 109 mm was recorded for the mix comprising of high level of GGBS content with lower level of activator dosage at the least W/GS ratio. It is clear that GGBS had a negative effect on the flow properties of the OPGM mixes, which is in line with the conclusions of previous studies (Li et al. 2020; Perumal et al. 2021). This performance can be attributed to the larger specific surface area and erratic shape of the slag particles, that restrict the flow and rapid reaction kinetics of the slag particles (Yousefi Oderji et al. 2019).

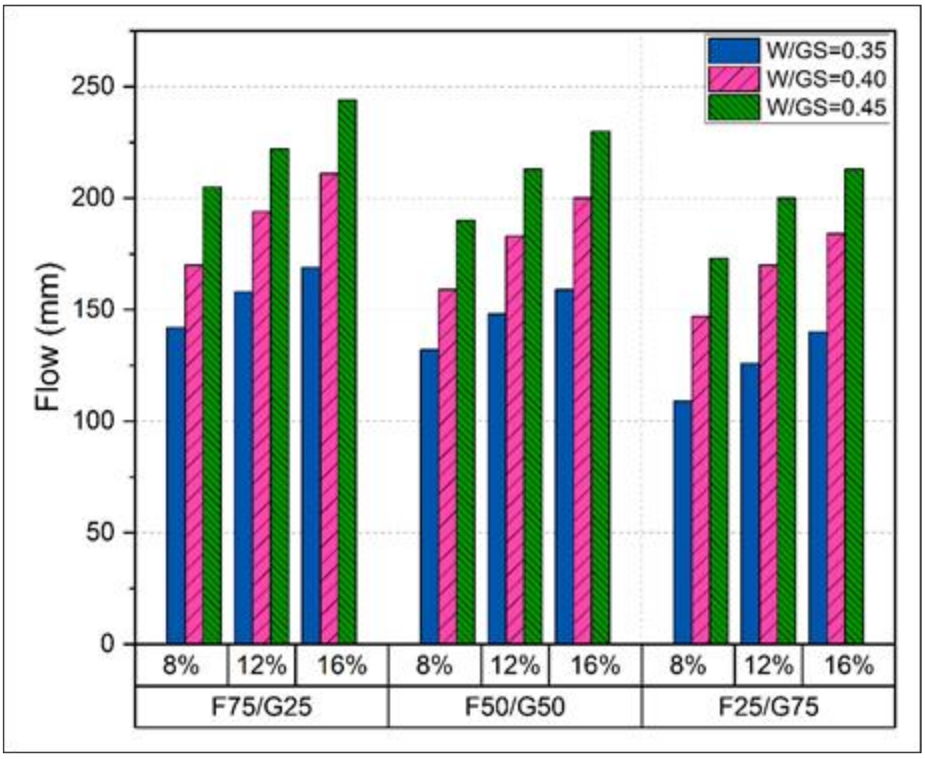

Figure 5.1 Flow values of one-part geopolymer mortars.

5.3.2 Compressive and flexural strengths

The compressive strength (CpS) and flexural strength (FrS) results of OPGMs for various factors and levels are presented in Figure 5.2. The strengths of all blends after 7 days achieved approximately 65-70% of the 28 days strength of OPGM. The CpS and FrS of OPGMs was observed to considerably decrease when W/GS ratio increased. The rise in W/GS ratio hinders the geopolymerization process resulting in strength drop. The lowest 28 day CpS and FrS of 10.05 MPa and 2.16 MPa, respectively were recorded for the OPGM mix $G_{25}A_8W_{0.45}$ comprised of higher W/GS ratio of 0.45, at least activator content with 75% fly ash as precursor. Whereas, the highest CpS of 64.8 MPa and FrS of 6.2 MPa were recorded for the OPGM mix $G_{75}A_{12}W_{0.35}$ comprising of lower W/GS ratio of 0.35 at 12% activator dosage with 75% GGBS content. However, the variability in CpS and FrS has been observed with increase in the W/GS ratio, which can be attributed to the significant influence of fluctuations in the proportions of fly ash and GGBS within the OPGM mixes. The similar observations are reported in the literature (Askarian et al. 2018; Prusty and Pradhan 2020; Yousefi Oderji et al. 2019). On comparing CpS and FrS for contemporary mixes with rise in W/GS from 0.35 to 0.40 and 0.45, the CpS drops by 5-31% and 11-59%, and FrS drops by 10-25% and 15-42%, respectively. The strength drop is because, an increase in the W/GS ratio results in a rise in the water content in the mix, which affects the polymerization process. The amount of water in one part geopolymer is determined by the quantity necessary to achieve complete activator breakdown; any excess water over this limit results in an increased porosity resulting in strength degradation (Ye et al. 2016; Yousefi Oderji et al. 2019).

It is evident that increase in GGBS content leads to increased CpS and FrS of the OPGMs, regardless of the activator content and W/GS ratio in the mixes. The CpS increased by 10-35% and 25-80% when the GGBS content increased from 25% to 50% and 75%, respectively in the mixes. The percentage of increment in FrS of OPGMs is minimal when slag content is beyond 50% in the mix. This means that the GGBS replacement has a substantial influence on the strength of the OPGMs. Various researchers have documented concordant findings regarding the CpS and FrS of the

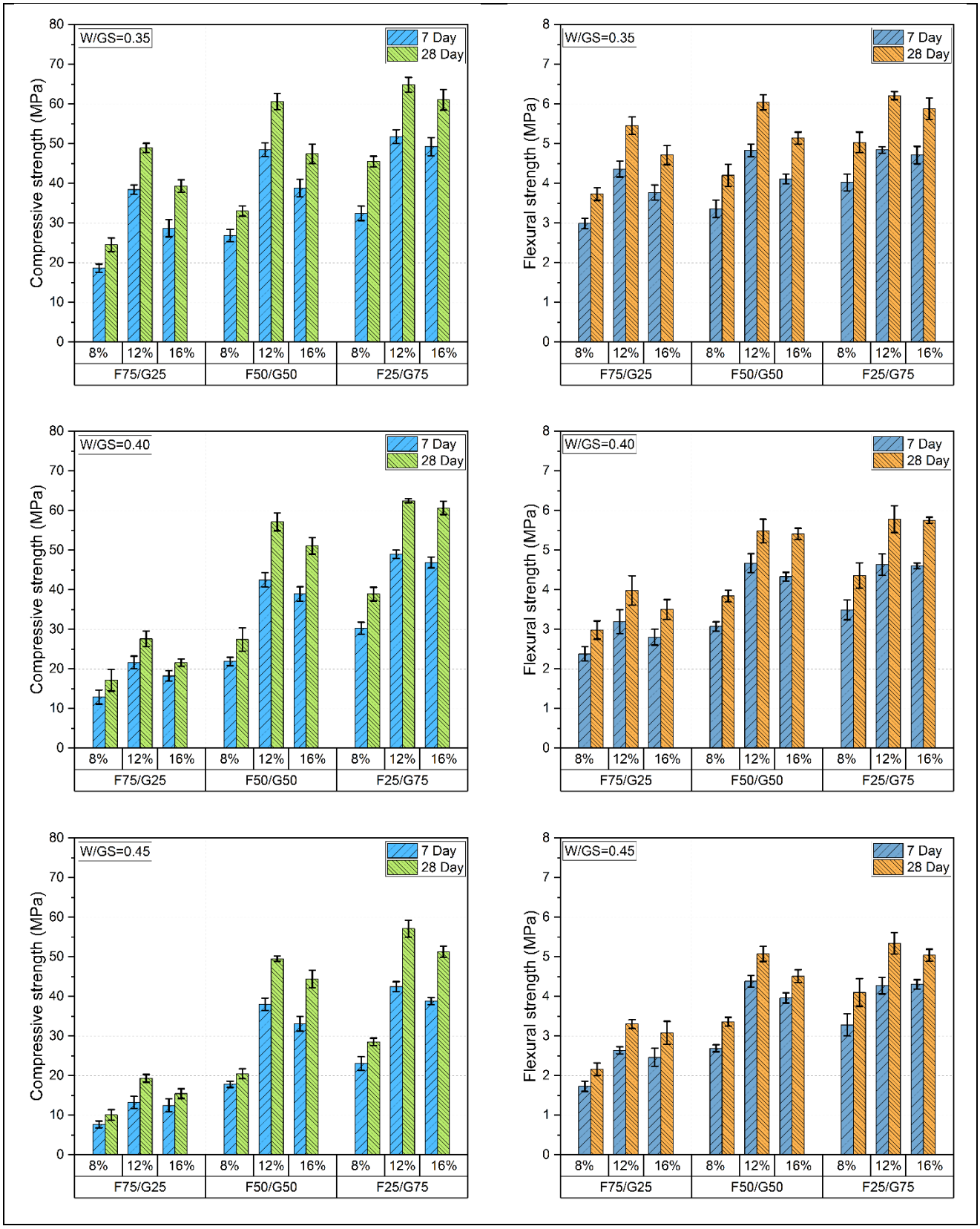

Figure 5.2 Compressive and flexural strengths of one-part geopolymer mortars.

OPGM mixes (Guo et al. 2021; Ma et al. 2023)(Haruna et al. 2020a). The substantial variation in CpS and FrS among OPGM mixes at a specific age can be linked primarily to the notable impact of the GGBS replacement percentage. This is because, more significant GGBS replacement leads to higher calcium content in the mix, which results in improved CpS and FrS of OPGM mixes. The significant calcium content leads to greater C-A-S-H gel formation impacted by an alkali activator occurs alongside N-A-S-H gel (Mohammed et al. 2019a). Moreover, the greater calcium speeds up the polycondensation process that results in formation of tetrahedral silica and aluminium structures, which eventually form a 3-D network with higher CpS (Wang et al. 2021) (Askarian et al. 2018; Elzeadani et al. 2022; Prusty and Pradhan 2020; Yousefi Oderji et al. 2019).

It is noted that, regardless of the W/GS ratio and slag content the CpS and FrS development were found approximately 2 times and 1.5 times, respectively when activator dosage is increased to 12% from 8%. At lower activator content, the reduced degree of polycondensation leads to a decrease in strength of the OPGM mixes. On the contrary, an increased activator leads to a more extensive dissolution of Al, Si, and Ca species, thereby enhancing the extent of the geopolymerization process. This leads to the creation of a stable aluminosilicate network, along with the formation of C-S-H gel within the mixture, resulting in higher CpS for the blends (Elzeadani et al. 2022; Ma et al. 2019). However, increase in activator content beyond 12% results in marginal decrement in the CpS and FrS of OPGMs. This behaviour can be linked to a larger activator dosage, notably an excess of Na_2O, which inhibits the formation of binding phases and enhances the likelihood of activator leaching and efflorescence. These causes leads to matrix degradation and a decrease in strength (Dong et al. 2020). The slag content and dosage of activator plays an important role in the strength development of OPGMs.

A power regression analysis was conducted to investigate the correlation between the CpS and FrS of one-part geopolymer mortars derived from experimental data. The results of the regression analysis, displaying both the correlation and sample data are obtained from the study which are represented in Figure 5.3. The regression analysis revealed a significant power relationship between CpS and FrS, as indicated

by a highly significant correlation coefficient with R^2 = 0.97432 in the context of CpS and FrS. The obtained R^2 value is well correlated with the significant relationship between FrS and CpS in conventional geopolymers reported in earlier literature, with R^2 values of 0.9435 (Huseien et al. 2019), 0.91 (Kaya 2022), 0.87 (Ruiz-Santaquiteria et al. 2013), and 0.7823 (Kaya et al. 2020). In the equation shown in Figure 5.3, where y and x represents FrS and CpS, respectively and 0.731 is the constant factor, the calculated R^2 value indicates how well the regression line can explain the variations in the y variable (FrS). Sofi et.al. and Diaz-Loya et al. proposed the relation between FrS and CpS of geopolymer concrete obtaining constant factor as 0.6 (Sofi et al. 2007) and 0.69 (Diaz-Loya et al. 2011), respectively. The constant factor obtained in the present prediction model is in close agreement with the relation between FrS and CpS of OPC based concrete constant factor of 0.7 recommended by code IS 456 (BIS 456:(2000) 2000). However, given the limited availability of data on OPG mixes, the derived prediction model can be effectively employed to estimate the FrS of OPG mixes based on its CpS.

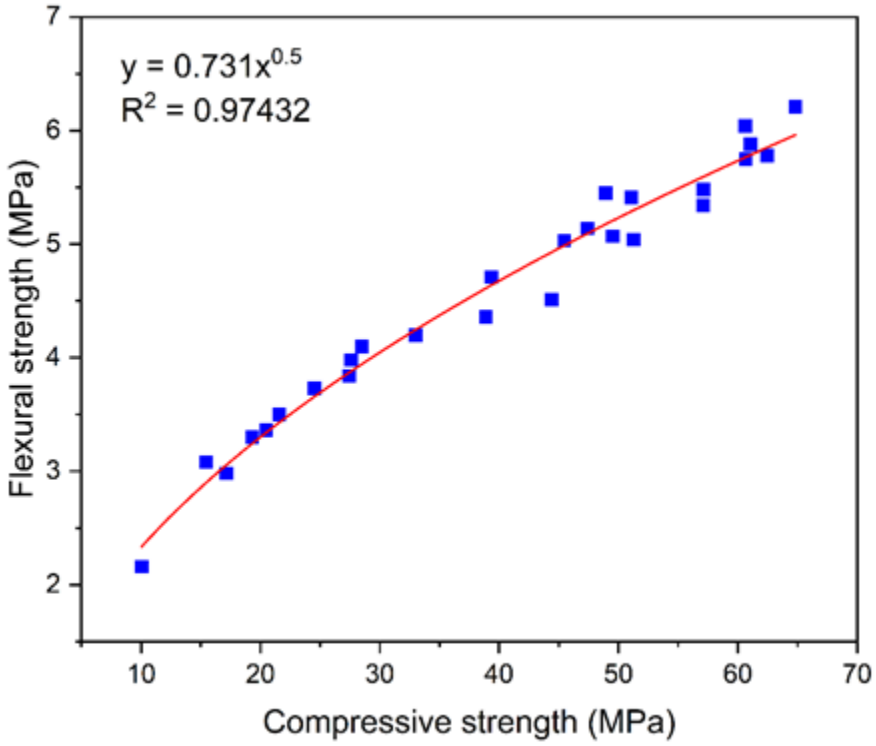

Figure 5.3 Correlation between 28-day flexural and compressive strength of one-part geopolymer mortars.

5.3.3 Drying shrinkage

The drying shrinkage (DrS) results of OPGMs for various factors and levels are plotted in Figure 5.4. The graphs are presented as a matrix to clearly observe the effect of GGBS substitution, activator dosage and W/GS ratio on DrS strain of OPGMs from 1 day to 180 days. The columns and rows indicates the chosen W/GS ratio and activator dosage, respectively.

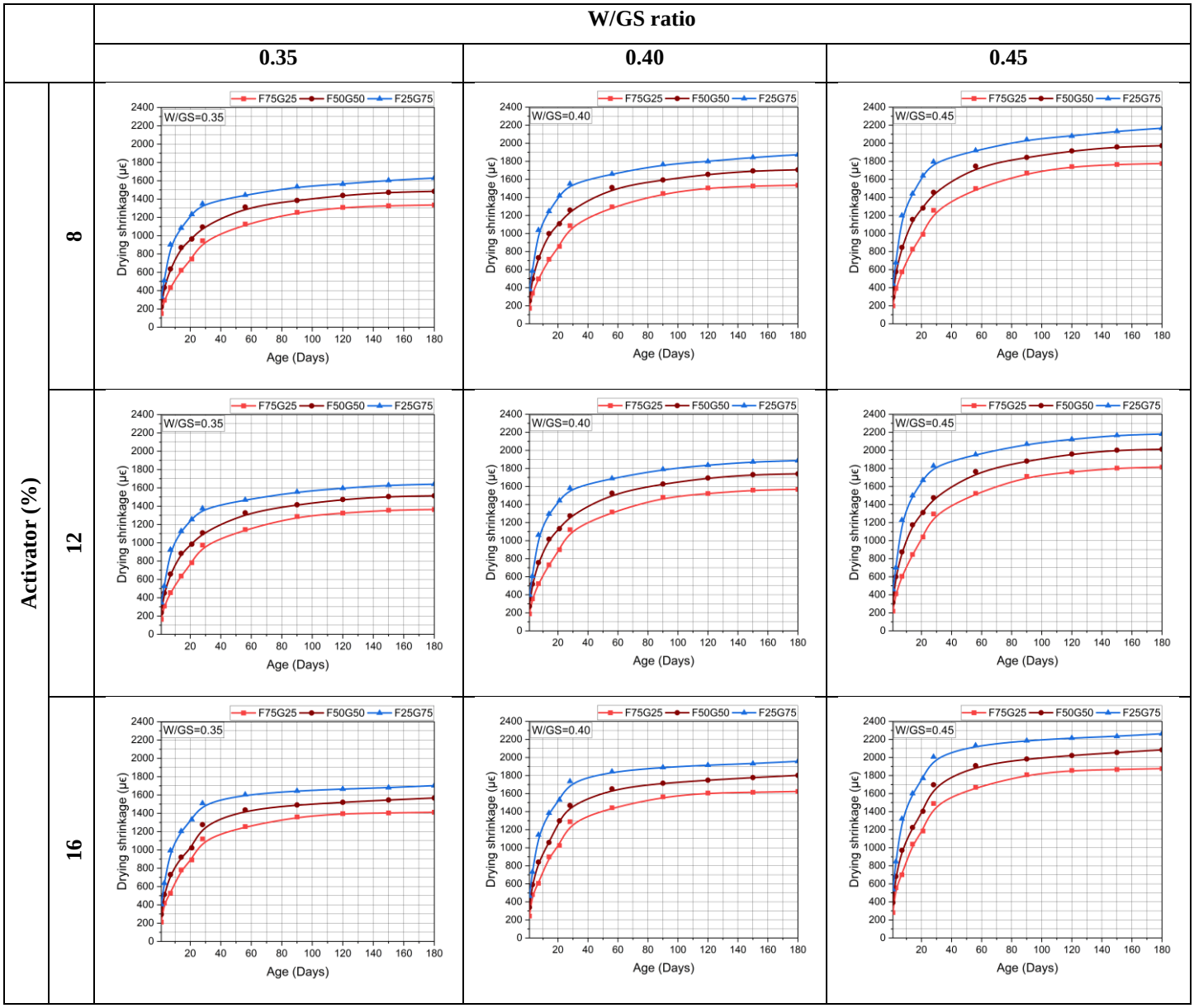

Figure 5.4 Drying shrinkage of one-part geopolymer mortars.

It is noticed that, the amount of DrS increases rapidly in early phases, followed by gradual and minor rise as time progresses, which is in agreement with earlier reports (Melo Neto et al. 2008; Palacios and Puertas 2007). Regardless of the W/GS ratio and activator content, mix with 75% GGBS content exhibited the greater shrinkage compared to mix with 25% and 50% because of higher capillary stress associated with fine pore structure as slag content rises. This phenomenon can be ascribed to the reduction in the hydraulic volume occurring during the hydration process of slag, particularly during the later stages of the curing period, which is in agreement with earlier findings (Zhou et al. 2020). The increased fly ash content in the mix results in decreased shrinkage rate as the spherical form of fly ash particles adds to a coarser porosity structure. As a result, the surface tension decreases, and existence of a less interlinked capillary network within the geopolymeric matrix resulting in less DrS (Mastali et al. 2018). Hence, the mix with a higher fly ash component shrinks less.

The maximum DrS of 2263 microstrain was recorded for the mix with higher level of W/GS ratio at 16% activator dosage. As W/GS ratio rises, rate of shrinkage also increases substantially. The surplus water content present in the mix evaporates with age, leading to creation of cavities and pores in the system, resulting in increased drying shrinkage (Mastali et al. 2018; Sadeghian et al. 2022). The rate of DrS in OPGM specimen increased as activator dosage increases. The DrS of OPGMs was 5-10% more than mixes activated with lower activator dosage. This is because, as dosage of activator increases, the heat of hydration also increases, which results in densification of mixtures leading to a finer pore structures causes increase in capillary stresses associated with the shrinkage (Duran Atiş et al. 2009; Thomas et al. 2017). Nonetheless, the curing method also impacts the rate of drying shrinkage, especially when exposed to ambient temperatures with a relatively high quantity of unbound water that has the potential to excessively evaporate and thus exacerbate drying shrinkage (Mastali et al. 2018). Whereas employing curing temperatures exceeding 100 °C leads to the disintegration of the granular structure of the geopolymer, contraction of the gel, and the absence of transformation into a semi-crystalline state that enhances early-age compressive strength and significantly expedites the development of strength as reported by

Bakharev et al. (IS 4031 (Part 5) 2002). From the observations, it is clear that all the factors are significantly affecting the drying shrinkage properties of OPGMs.

5.4 OPTIMIZATION PROGRAMME

5.4.1 Modelling and Statistical evaluation

The RSM has been utilized for conducting a multi-objective optimization analysis based on the previous test outcomes. The aim was to determine the optimal values of slag content, activator dosage and W/GS ratio. The optimization study was conducted by considering the goals of maximizing the flow and strength properties, and minimizing the drying shrinkage properties of OPGMs. The experimental results were modelled using the software "Design Expert" to identify the polynomial function that best fit the data. Model summary statistics, the sum of squares of the deviation, and fitting error are used to execute nonlinear fitting of various models. The quadratic polynomial models were formulated by estimating the coefficients of the parameters through multiple regression analysis (Kaya 2022). Analysis of variance (ANOVA) is employed to assess the robustness of outcomes and to compare the means and effects of multiple factors. The general polynomial regression model is shown in Eq.5.1. The regression model developed for all responses are shown in Eqs. 5.2-5.5 with actual coefficients, and the coded coefficients of each responses are given in Table 5.2.

$$Response = a + b\times A + c\times B + d\times C + e\times AB + f\times AC + g\times BC + h\times A^2 + i\times B^2 + j\times C^2 \quad (5.1)$$

$$Flowability = - 292.27778 - 0.358889\times A + 3.02778\times B + 1594.4444\times C + 0.000833\times AB + 0.60000\times AC + 14.16667\times BC - 0.004533\times A^2 - 0.177083\times B^2 - 1400.0000\times C^2 \quad (5.2)$$

$$Compressive\ strength = - 36.07704 + 0.081822\times A + 20.78194\times B - 173.33889\times C + 0.029533\times AB + 2.23333\times AC + 3.02083\times BC - 0.007822\times A^2 - 0.892847\times B^2 - 147.55556\times C^2 \quad (5.3)$$

$$Flexural\ strength = 4.57315 + 0.007433\times A + 1.33972\times B - 34.52778\times C + 0.000908\times AB + 0.213333\times AC + 0.420833\times BC - 0.000708\times A^2 - 0.058924\times B^2 - 10.88889\times C^2 \quad (5.4)$$

$$Drying\ shrinkage = 1384.05556 + 0.654444 \times A - 28.30556 \times B - 3637.22222 \times C - 0.010833 \times AB + 18.93333 \times AC + 32.08333 \times BC - 0.014400 \times A^2 - 1.13542 \times B^2 - 9133.33333 \times C^2 \quad (5.5)$$

Where *a-j* are coded coefficients, A, B and C are GGBS content, activator dosage, and W/GS ratio, respectively. To ensure that each regression analysis produced good results within an acceptable range, various statistical metrics such as p-values, lack of fit assessments, and R^2 (regression coefficient) values were computed. Table 5.3 shows the model terms used in the computations, as well as the results of the ANOVA performed for each response and descriptive statistics for each model. According to the results shown in Table 5.3, all response models and individual factors show statistical significance at the 95% confidence level, as demonstrated by p-values less than 0.05. A notable influence on a response variable can be deduced when the F-value is significant, and the corresponding P-value is equal to or less than 0.05. The F-value represents the ratio of the mean square effect to the mean square error, analogous to the ratio of the average variation among groups to the average variation within groups (Bingol et al. 2010). The higher F- values of GGBS content, activator dosage and W/GS ratio of 157.19, 55.82, and 43.20, respectively, shows that these independent variables has a significant effect in the CpS of OPGMs. A P-value of less than 0.050 verified the validity of this assertion (Shi et al. 2022). These independent variables had a significant influence on the flowbility, FrS, and DrS as well. The R^2 value of flowability, CpS, FrS, and DrS of the OPGMs was 0.9958, 0.9509, 0.9485 and 0.9997, respectively. The R^2 value quantifies the relationship between observed experimental results and the predicted results from the model equation. As a result, when R^2 approaches unity, the precision of the generated model equation improves. The difference between the anticipated R^2 and adjusted R^2 values for all the models is less than 0.2, indicating that the models' fitness and reliability are within acceptable limits. The CV% (coefficient of variation) values of 1.55, 11.52, 6.68 and 0.3273 for responses flowability, CpS, FrS, and DrS, respectively, show that the constructed model is more viable. According to Table 5.3, all of the models possess precision values exceeding 4, suggesting their suitability for examining the design space.

Table 5.2 Coded coefficients of responses.

Coefficients		Response			
		Flowability	**Compressive strength**	**Flexural strength**	**Drying shrinkage**
Coded	*a*	183.56	53.21	5.53	1737.22
	b	-14.06	13.68	0.8206	166.44
	c	17.94	8.15	0.5572	44.94
	d	33.72	-7.17	-0.5050	250.06
	e	0.0833	2.95	0.0908	-1.08
	f	0.7500	2.79	0.2667	23.67
	g	2.83	0.6042	0.0842	6.42
	h	-2.83	-4.89	-0.4428	-9.00
	i	-2.83	-14.29	-0.9428	18.17
	j	-3.50	-0.3689	0.0272	22.835.53

The residual normal probability plots that show data sufficiency and distribution for all the response models are shown in Figure 5.5. These plots show that the data points align along a linear trend, showing that the residuals adhere to a normal distribution after the response variables were transformed appropriately, providing satisfactory results. The expertise and fitness of the developed models are visually assessed through a graphical analysis, where the predicted results are plotted on the y-axis against the actual results on the x-axis. The graphic in Figure 5.6 shows the precision of the projected response model, with each point closely aligned to the straight line. The consistent alignment of the data set with the straight line suggests that the test and predicted outcomes conform well to the existing models, demonstrating a strong agreement with the data. The 3D response surface plots are shown in Figure 5.7 for the models of flowability, CpS, FrS, and DrS. The response surface plots demonstrates the variation in independent factors which include GGBS content, activator dosage, and W/GS ratio, and their individual effect and interaction effects on the responses like flowability, drying shrinkage, compressive and flexural strength. The significance level of combined factor effects on responses of OPGMs are given in Table 5.4.

Table 5.3 ANOVA models.

Model	**Responses**			
	Flowability	**Compressive strength**	**Flexural strength**	**Drying shrinkage**
p-value (model)	<0.0001	<0.0001	<0.0001	<0.0001
F-value	443.53	36.61	34.80	5612.50
R^2	0.9958	0.9509	0.9485	0.9997
Adjusted R^2	0.9935	0.9250	0.9213	0.9995
Predicted R^2	0.9884	0.8697	0.8754	0.9991
Adeq precision	78.6613	21.9320	22.0589	263.4737
Std. deviation	2.75	4.63	0.3087	5.76
Mean	177.44	40.19	4.62	1758.56
C.V (%)	1.55	11.52	6.68	0.3273
p-value (Prob > F) of factors, their interrelations and squares				
A: GGBS (%)	<0.0001	<0.0001	<0.0001	<0.0001
B: Activator (%)	<0.0001	<0.0001	<0.0001	<0.0001
C: W/GS	<0.0001	<0.0001	<0.0001	<0.0001
AB	0.9175	0.0412	0.3224	0.5231
AC	0.3573	0.0521	0.0082	<0.0001
BC	0.0023	0.6570	0.3582	0.0013
A^2	0.0217	0.0192	0.0027	0.0013
B^2	0.0217	<0.0001	<0.0001	<0.0001
C^2	0.0062	0.8476	0.8316	<0.0001

Table 5.4 Significance level of combined factors.

Responses	**Significance of combined factors**
Flowability	BC > AC > AB
Compressive strength	AB > AC > BC
Flexural strength	AC > AB > BC
Drying shrinkage	AC > BC > AB
A: GGBS content, B: Activator dosage, C: W/GS ratio	

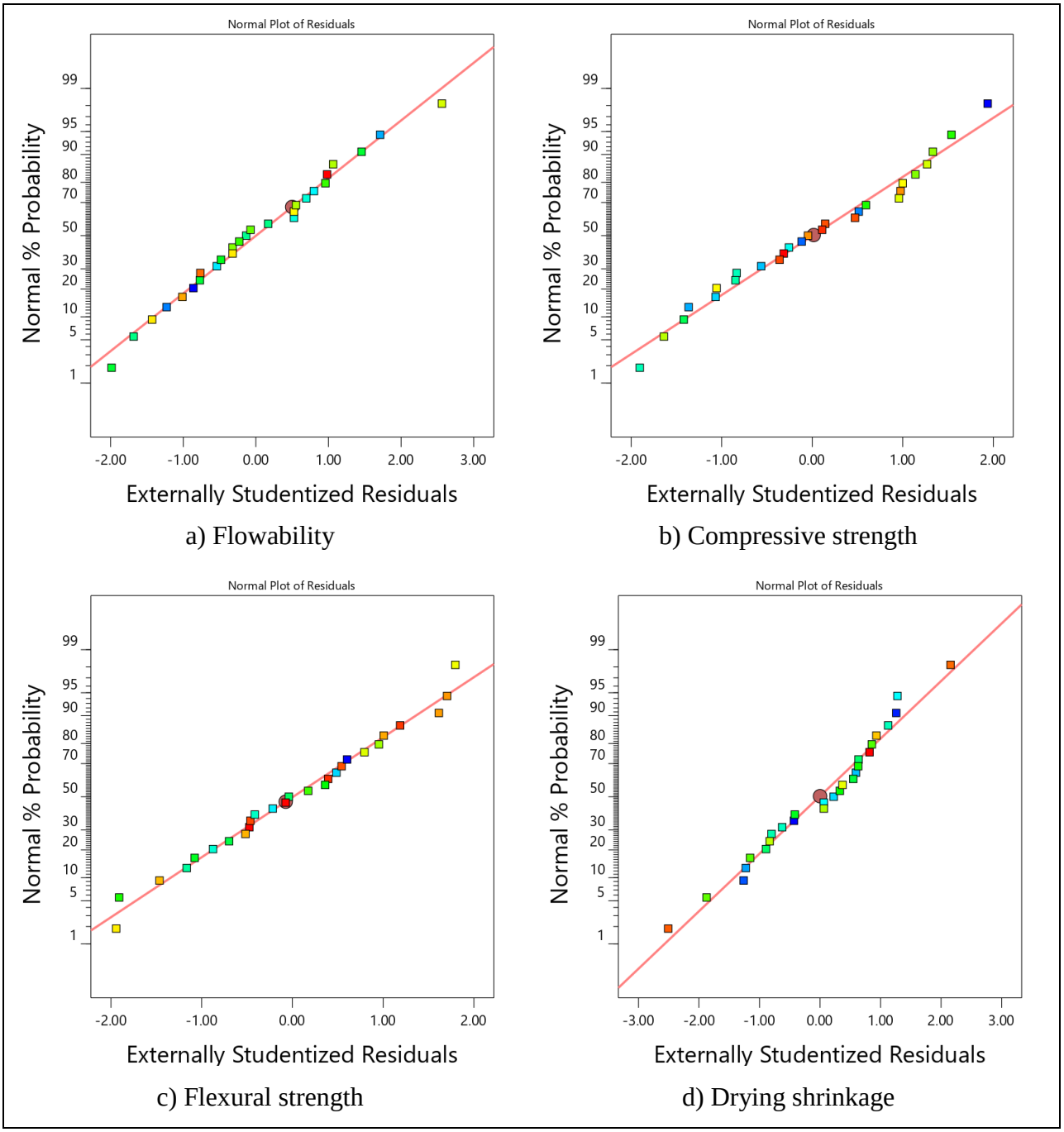

Figure 5.5 (a)-(d) Normal probability plots of response models of one-part geopolymer mortars.

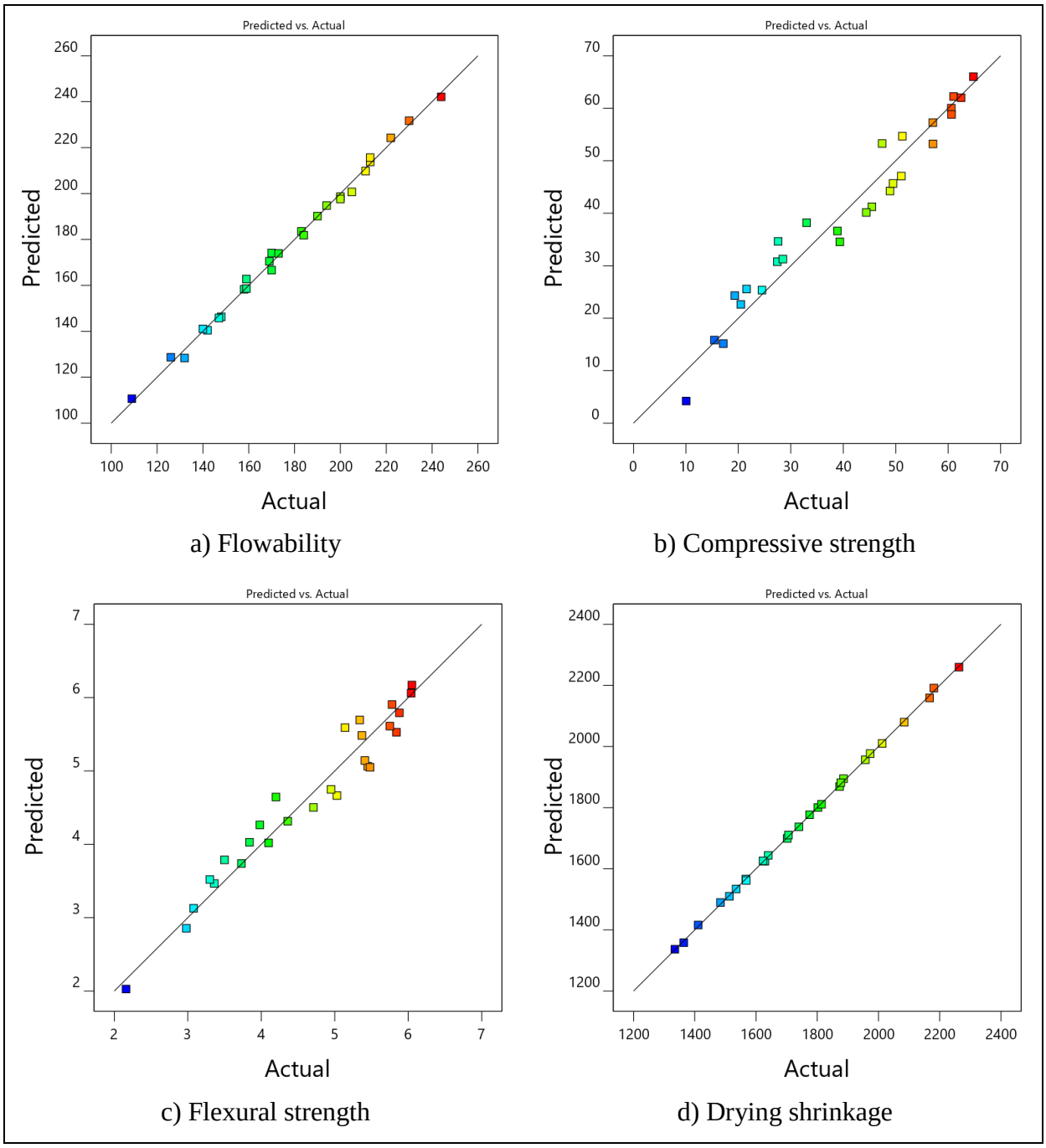

Figure 5.6 (a)-(d) Predicted and actual values of one-part geopolymer mortar responses.

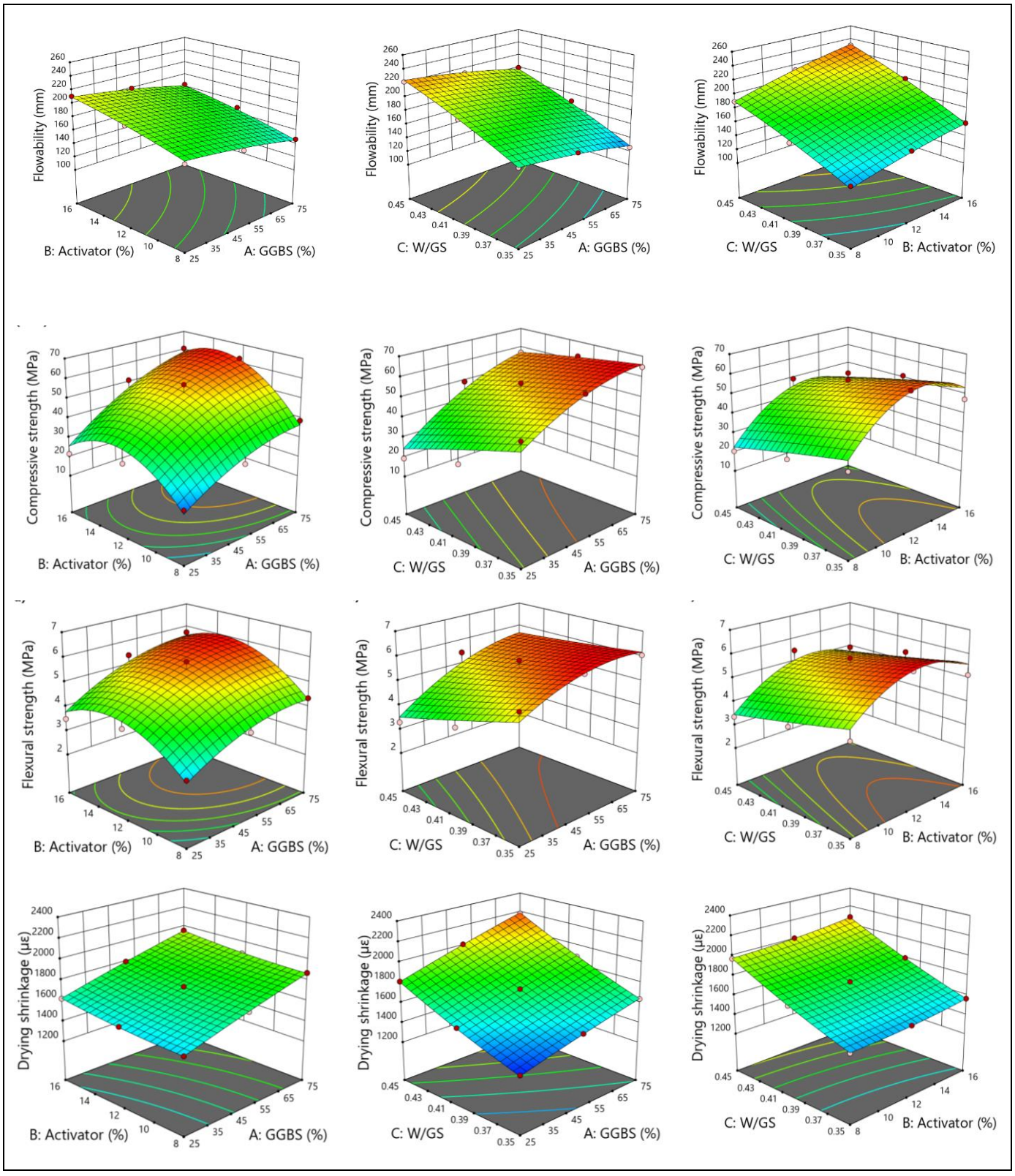

Figure 5.7 Response surface plots for one-part geopolymer mortar mixes.

5.4.2 Optimization and validation study

Response surface method was utilized to examine the interaction or combined effect of the factors on the properties of OPGMs along with drawing the relationships between the considered variables and responses. The optimal values for the amount of GGBS content, activator dosage and W/GS were determined using a computational multi-objective optimization technique, response surface fitting model, and the desirability function. The goal was to maximize the flowability, compressive and flexural strength, and to minimize the drying shrinkage of the developed one-part geopolymer mortars while assigning equal importance to all responses. The goal of optimization research is to determine the preferred values of independent factors in order to attain the optimal performance criteria. The desirability function (D) assigns a numerical value ranging from 0 to 1 to a single solution, where zero indicates an unsatisfactory response value and one signifies the desired response value. The aim of multi-objective optimization is to maximize the desirability function. The optimization goals and benchmarks are given in Table 5.5. To improve responses influenced by many factors, the RSM technique was used. As a result, the following optimum ratios were determined: GGBS content of 49.8%, activator dosage at 13.6%, and W/GS ratio at 0.37. These results correspond to a desirable function value of 0.713, indicating high reliability, and the expected outcome is quite reliable.

Table 5.5 Optimization goals and benchmarks.

Independent variables and responses	Goal	Lower limit	Upper limit
A: GGBS (%)	In range	25	75
B: Activator (%)	In range	8	16
C: W/GS	In range	0.35	0.45
R1: Flowability	Maximize	109	244
R2: Compressive strength	Maximize	10.05	64.81
R3: Flexural strength	Maximize	2.16	6.05
R4: Drying shrinkage	Minimize	1335	2263

The numerical optimization solutions, which were aimed at optimizing a certain goal, are illustrated in Table 5.6. Regarding the optimum OPGMs proportions, the prediction error for optimization is less than 10%, indicating high model accuracy. To validate the model, individual response models were used to calculate response prediction values and the absolute deviations from the test values. The error percentage

between experimental and predicated values are given in Table 5.6 where, the maximum deviation is noted for the compressive strength response of 6.61% which is less than 10% that shows the accuracy of the model is high (Shi et al. 2022). However, the test values of the optimum mix can be interpreted with the mixes considered for the optimization study, where the lower limit and upper limit values of each responses are considered for the optimization study and also it was observed that test values of the validation mix were within the range of respective responses. Figure 5.8 depicts the optimization ramps, visually representing the independent variables and responses in the study.

Table 5.6 Optimum mix model verification.

Responses	GGBS (%)	Activator (%)	W/GS	Predicted value	Test value	Error (%)
Flowability (mm)	49.81	13.6	0.37	170.3	165.5	2.7
Compressive strength (MPa)	49.81	13.6	0.37	57.7	61.8	6.6
Flexural strength (MPa)	49.81	13.6	0.37	5.8	6.0	3.1
Drying shrinkage (με)	49.81	13.6	0.37	1626	1538	5.7

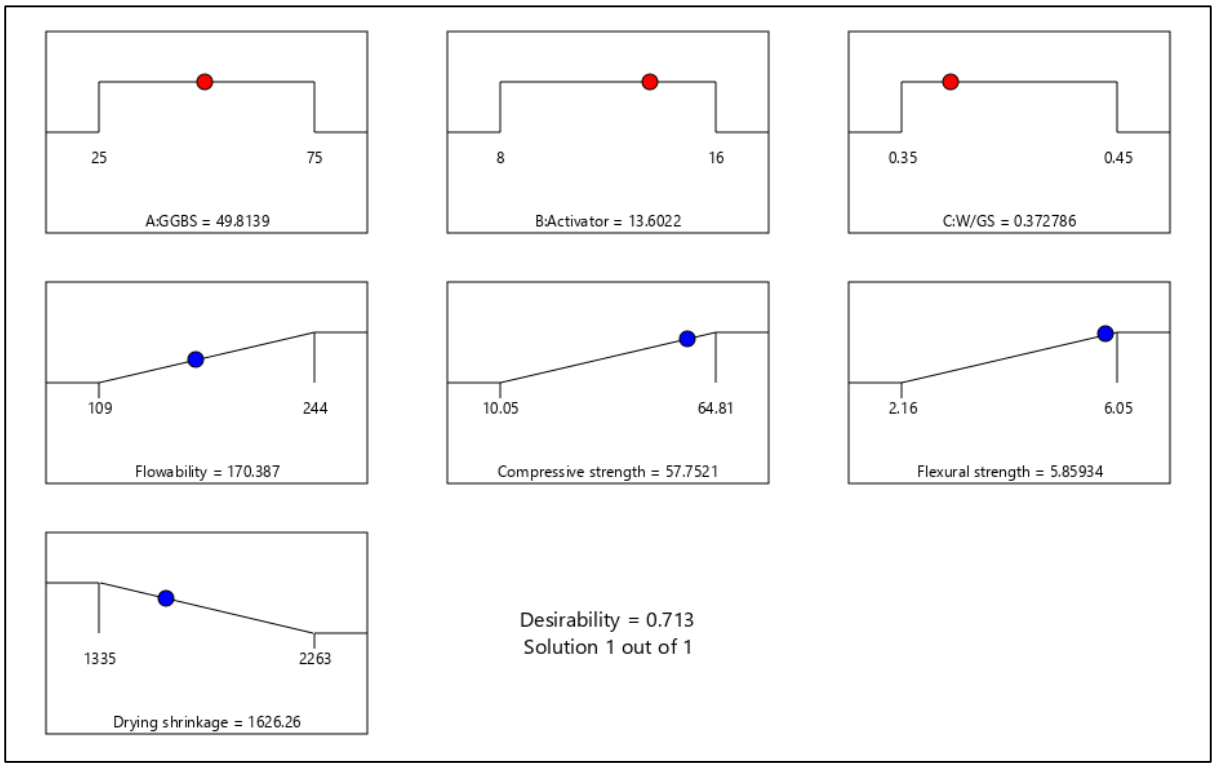

Figure 5.8 Optimization ramps.

5.5 MICROSTRUCTURAL, PHASE AND CHEMICAL ANALYSIS

The microstructural characterization like SEM, EDS, XRD, TGA/DTG and FTIR were studied for selected OPGM mixes. To study the individual and interaction factor effects on microstructural properties of OPGMs, the test samples after 28 days of curing were subjected for characterization. The chosen mixes were $G_{50}A_{12}W_{0.45}$, $G_{50}A_{16}W_{0.40}$, and $G_{75}A_{12}W_{0.40}$, to compare and analyze the test results with the validated mix which was developed for optimum mix proportion i.e. $G_{49.81}A_{13.60}W_{0.37}$.

5.5.1 SEM morphology and EDS analysis

The SEM micrographs and EDS results of the selected OPGMs are shown in Figure 5.9. The SEM and EDS images of OPGM developed for optimum mix proportions $G_{49.81}A_{13.60}W_{0.37}$ is shown in Figure 5.9a, and the other mixes namely $G_{50}A_{12}W_{0.45}$, $G_{50}A_{16}W_{0.40}$, and $G_{75}A_{12}W_{0.40}$ are presented in Figure 5.9b, c and d, respectively. It is evident that, majority of fly ash and GGBS particles are fully reacted and embedded in the gelatinous products. Where, partially reacted fly ash embedded with non-homogenous gel matrix is found in sample with increased water content as shown in enlarged portion of Figure 5.9b. The mix characterized by a higher W/GS ratio distinctly exhibits a significantly greater presence of unreacted particles in comparison to the mix with the optimal W/GS ratio. This clearly results in less gel creation within the samples with higher W/GS ratios, accounting for the significant drop in mechanical strength as discussed in section 5.3.2 when more water was added to the mixtures. These findings are consistent with earlier research work (Ban et al. 2017). During polycondensation, higher amount of water evaporates and creates uneven internal pressure resulting in weaker matrix and more voids, leading to high rate of drying shrinkage (Das and Rout 2021). A dense and homogenous matrix is observed in combination with a higher activator content. However, longer micro-cracks were discovered, as seen in Figure 5.9c. These cracks can be attributed to the increased amount of Na_2O concentration in the system at higher dosages of activator that results in higher heat generation during the polymerization process. As a result, the concentration of ionic species rises, impeding ion mobility and slowing the creation of coagulated structures (Haruna et al. 2021). It can be observed that the development of gelatinous products with higher concentration of activator content in the mix is

observed even though in the presence of longer cracks. Dense and uniform matrix with compacted microstructure which contributes to greater strength can be observed in Figure 5.9d, as GGBS content increases in the mix. However, few GGBS particles are left unreacted. This observation potentially elucidates the enhancements observed in drying shrinkage when compared to the OPGM mix with lower GGBS content, these

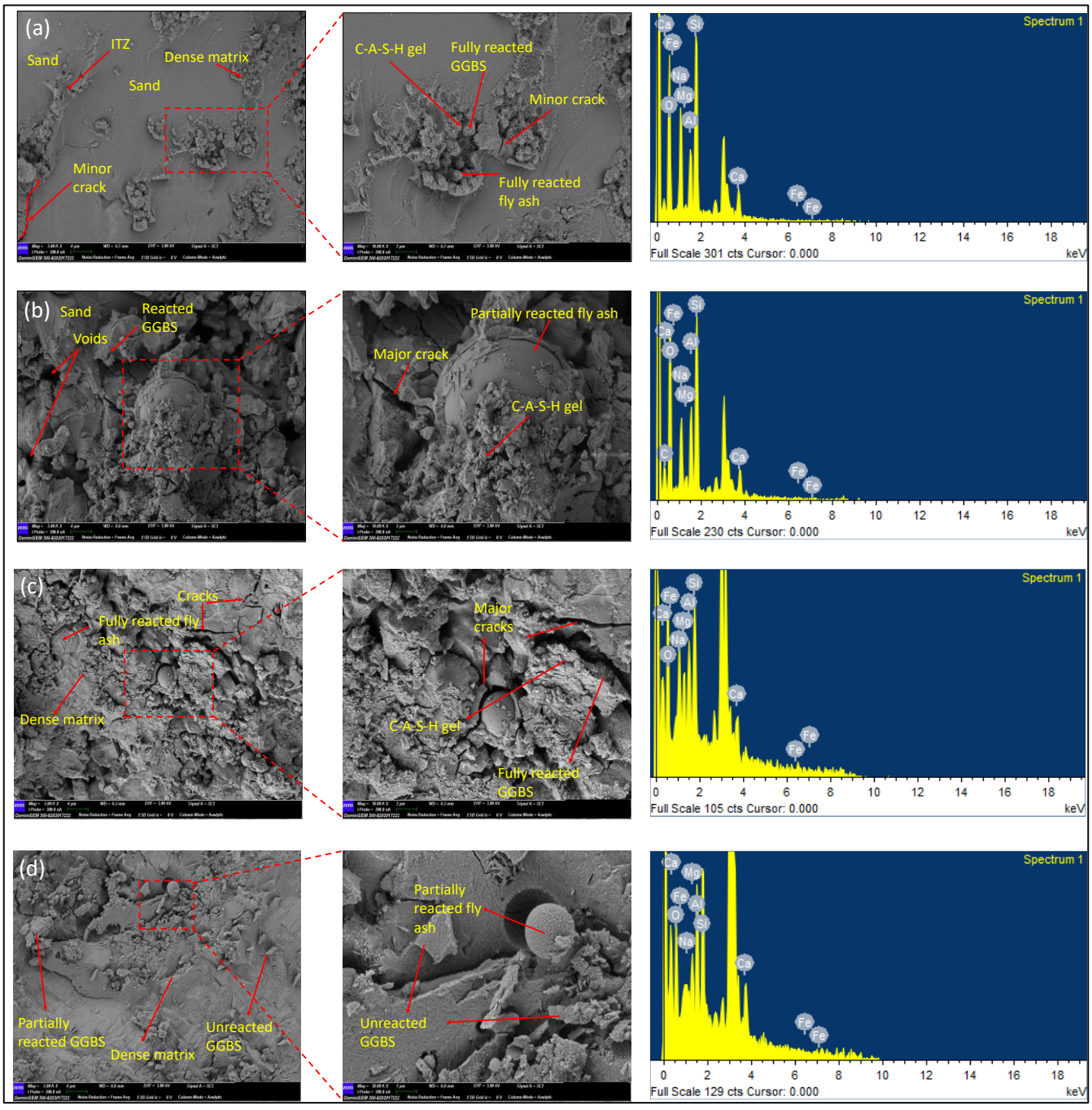

Figure 5.9 SEM microgr aphs and EDS analysis of OPGMs a) $G_{49.81}A_{13.60}W_{0.37}$ b) $G_{50}A_{12}W_{0.45}$, c) $G_{50}A_{16}W_{0.40}$, and d) $G_{75}A_{12}W_{0.40}$.

observations are in agreement with findings of earlier literature (Abdel-Gawwad and Abo-El-Enein 2016). The calcium in gel products is found more in mix composed of higher GGBS content, aluminium and silica phases are found in the gel products which could be C-(N)-A-S-H gels which are in agreement with the earlier studies (Haruna et al. 2021). The homogeneity of gel clusters in sample $G_{49.81}A_{13.60}W_{0.37}$ (Figure 5.9a) is found comparable to the mix with higher GGBS content. The strong interface transitional zone (ITZ) found between sand and binder particles because of densified gelatinous products formed in the ITZ regions is observed in Figure 5.9a. The minor cracks were also observed, these may be due to heat associated during polymerization reaction (Askarian et al. 2019). However, the optimum mix exhibits the dense and compacted mictrostrucres with fewer unreacted particles and better gel clusters which are associated with strength enhancements of the OPGMs compared to other mixes.

The EDS chemical analysis observations reveals that the products have high content of calcium, silica, aluminium, and sodium phases with interparticle bonds among elements. The existence of these substances indicates the presence of C-(N)-A-S-H gels. The high amount of Ca and Si elements found in the mix that comprise of high GGBS content were compared to other mixes with 50% GGBS content. This implies that more GGBS in the system leads to formation of higher amount of gelatinous products in the mix, which are responsible for strength development of the OPGMs. The optimized mix also is composed of higher amount of Ca and Si elements. The Ca/Si ratio and Al/Si of $G_{49.81}A_{13.60}W_{0.37}$ mix are 0.80 and 0.56, respectively. This signifies the presence of C-A-S-H gel, which is responsible for strength gain and to achieve the dense and compacted microstructures. However, as shown in Figure 5.9 (a, b, c, and d), surplus amounts of Ca, Fe, and Mg were found as remnants in the mix. These residual traces did not completely dissolve throughout the reaction process and had the same composition and form as conventional geopolymers. These findings are consistent with earlier research findings (Puligilla and Mondal 2013). It is noteworthy that SEM and EDS studies have found supportive evidence to the optimization technique which proves the accuracy of designing the optimum mix proportions with better performance of engineering properties and microstructure characterizations.

5.5.2 XRD – Phase analysis

The XRD peaks of hardened OPGMs specimens at 28 days of curing are shown in Figure 5.10. The XRD spectra of the samples were taken for diffraction angle 2θ = 10° - 70°. It can be observed that the peak intensities were noticeably reduced as compared to XRD spectra of aluminosilicate precursors. This implies that moderate level of reaction has occurred between the components. In the XRD spectra, new crystalline peaks were discovered, which are formed while geopolymerization takes place. The hardened mortar contains significant crystalline phases such as quartz and mullite which are consistent with the fly ash crystalline phases and indicates that not all fly ash particles are taking part in the reaction and are left unreacted. Further, the absence of several sharp peaks in the XRD pattern of hardened OPGMs, compared to fly ash, suggests the presence of geopolymer synthesis. Certain crystalline structures are transformed into amorphous inorganic substances during the geopolymerization process.

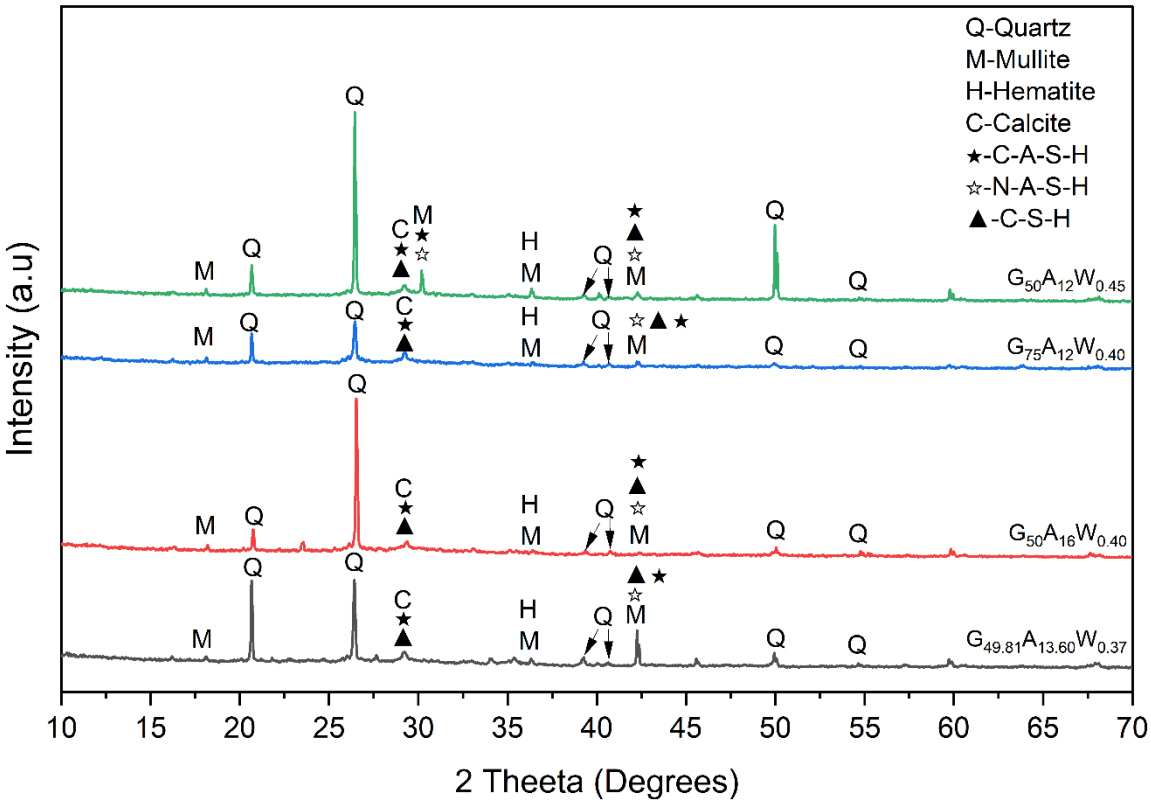

Figure 5.10 XRD spectra of OPGMs ($G_{50}A_{12}W_{0.45}$, $G_{75}A_{12}W_{0.40}$, $G_{50}A_{16}W_{0.40}$, and $G_{49.81}A_{13.60}W_{0.37}$) after 28 days of ambient curing.

The OPGM mixes had a broadly distributed amorphous phases found in the range of 20° 2θ to 40° 2θ when compared with the raw aluminosilicates XRD spectra suggests the production of alkaline aluminosilicate geopolymer gels. The only promising distinction between the mixture's peaks is a shift in peak intensity at around 29° 2θ. This change resembles the existence of C-S-H gel as well as the calcium carbonate phase. The presence of new crystalline phases corresponding to calcium (or sodium) aluminosilicate complex (C-(N)-A-S-H) is indicated by the XRD spectra. These phases are important in improving the compressive and flexural strengths of OPGM mixes, which agree well with previous studies (Lee and Lee 2015)(Kim et al. 2013). As seen in Figure 5.10, $G_{75}A_{12}W_{0.40}$ mix with of higher amount of GGBS replacement is associated with more CaO content that accelerates the formation of C-S-H gel that quickens the dissolution of Si and Al species in the precursor. This improved dissolution increases the geopolymers functioning greatly (Prusty and Pradhan 2020) that contribute to the strength gain of OPGM mixes. The appearance of an XRD peak coincident with a hump has been attributed to reflection from the poorly-crystalline C-S-H phase (Ban et al. 2017). The mix comprises of higher activator content $G_{50}A_{16}W_{0.40}$ also shows the similar XRD spectra, however, it exhibits relatively high crystallinity gels due to excessive activator dosage which is in line with earlier reported literature (Guo et al. 2019). Further, few noticeable small peaks were observed which resembles the presence of undissolved activator particles (Dong et al. 2020). However, the XRD spectra of optimized mix $G_{49.81}A_{13.60}W_{0.37}$ shows better peak intensities with gelatinous products presence and fewer crystalline peaks indicating lesser unreacted aluminosilicate precursors, and exhibiting dense and compacted microstructure as observed in SEM analysis.

5.5.3 TGA/DTG analysis

The thermogravimetric analysis (TGA) and differential thermogravimetry (DTG) analysis of the selected OPGM compositions are shown in Figure 5.11. The TGA and DTG further confirms the reaction products in OPGM mixes. The weight loss in TGA was considered from temperatures ranging 50 °C to 900 °C. At about 900 °C, the mix $G_{50}A_{12}W_{0.45}$ exhibited the largest weight loss of 22%, although the difference in the overall weight losses of the other three combinations are comparatively negligible.

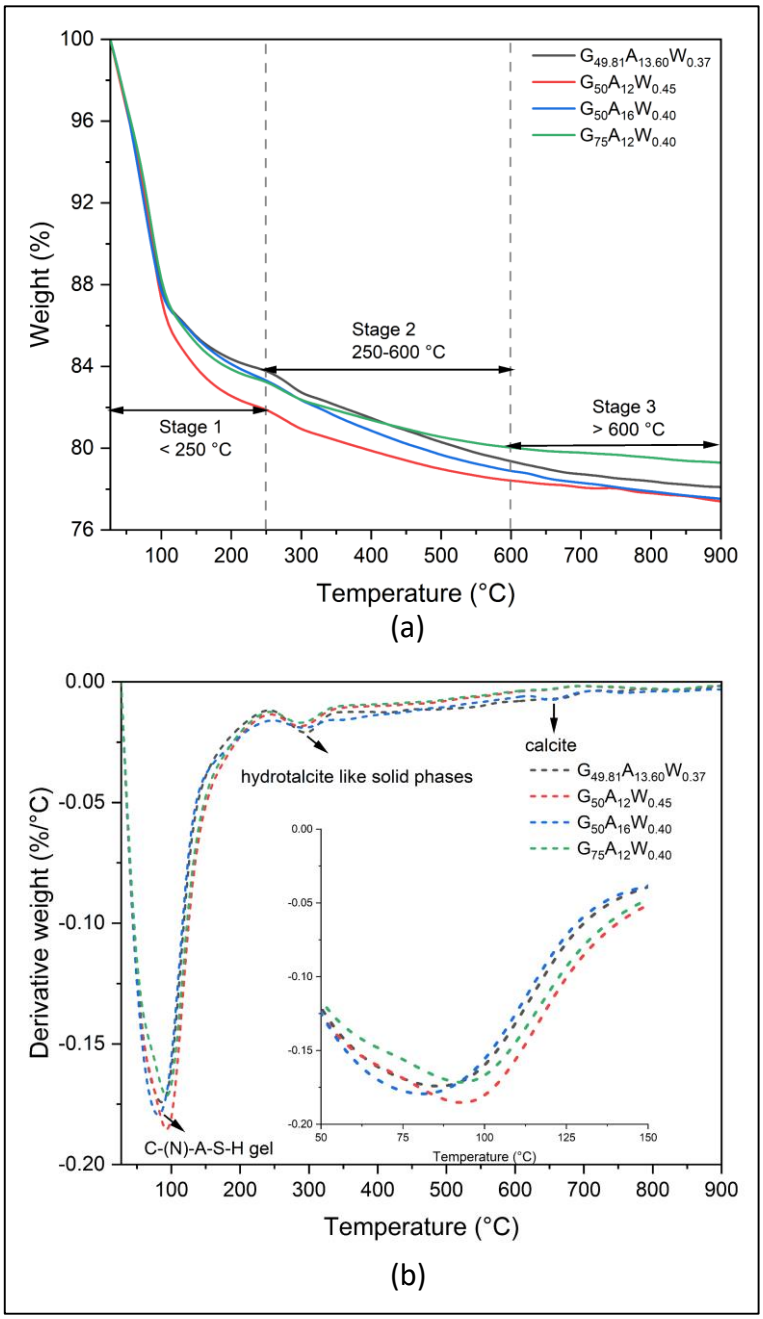

Figure 5.11 a) TGA and b) DTG, of OPGMs ($G_{50}A_{12}W_{0.45}$, $G_{75}A_{12}W_{0.40}$, $G_{50}A_{16}W_{0.40}$, and $G_{49.81}A_{13.60}W_{0.37}$) after 28 days of ambient curing.

Three major stages of weight losses are visible in the TGA curves of OPG systems; a) stage 1, up to 250 °C, is attributed to the weight loss of free and bound water from gelatinous products, b) stage 2, occurring between 250 to 600 °C, is primarily associated with the loss of chemically-bonded water and dehydroxylation of hydrotalcite-like solid phases, and c) stage 3, above 600 °C indicates the decomposition

of calcite phases and transition of gelatinous products to some crystalline phases, which are in line with studies (Abdollahnejad et al. 2020a; Adesanya et al. 2020; Alzaza et al. 2021; Ma et al. 2019; Ren et al. 2021). The lesser rate of mass loss is observed in the mix $G_{75}A_{12}W_{0.40}$ with higher GGBS content, where the higher mass loss is observed in the mix $G_{50}A_{12}W_{0.45}$ which comprises of 50% fly ash and higher water content (Abdollahnejad et al. 2020b). The mass loss up to 250 °C includes the weight loss of bound water in gelatinous material that resembles the presence of C-(N)-A-S-H gels and can serve as a quantifiable measure of the hydration degree, as it is closely linked to the C-(N)-A-S-H gels (Ren et al. 2021). After reaching 250 °C, the mass loss rate decelerated due to the presence of chemically bonded water and OH groups (Abdollahnejad et al. 2020a).

In the DTG curves of OPGMs, a single significant hump resembling gelatinous minerals is observed around 100 °C. This endothermic peak is attributed to the dehydration of C-(N)-A-S-H gels in OPGMs (Alzaza et al. 2021). The disparities observed in the major endothermic peaks of the DTG curves suggest that additional gel formation might have taken place due to variations in constituents of OPGMs. Another endothermic peak around 300 °C, indicates the dehydroxylation of hydrotalcite-like solid phases. A small dip after 600 °C shows the decomposition of calcite phases, which are observed by XRD spectra. The results achieved from TGA and DTG suggested that, there is significant amount of gel products are formed, transition of gels to crystalline phases, and decomposition of residues at higher temperatures in OPG mortar mixes, and there are no much significant difference between the optimized mix and other mixes.

5.5.4 FTIR – Chemical analysis

The FTIR spectra obtained to explore the behaviour and reaction of Si and Al species, along with calcium compounds of precursors, when interacting with solid activators in one-part geopolymer mortars are shown in Figure 5.12. The newly detected peaks ranged in frequency range from 1649 to 463 cm^{-1}, indicating the presence of slag particles in one-part geopolymers. The occurrence of the asymmetric bending vibration of Si-O-Si in the region of around 463 cm^{-1} and the Al-O bond at 784 cm^{-1} in OPGM mixes at 28 days is attributable to unreacted precursor materials (Askarian et al. 2019).

The FTIR spectra indicate a broad stretching vibration in the 664 cm^{-1} to1232 cm^{-1} region, with a centre peak at 990 cm^{-1}, which is commonly designated to the (Si-O-Si) and (Si-O-Al) groups, respectively. These peaks indicate the reactivity level of the source ingredients and are commonly observed in silicate compounds, these findings point to the development of C-(N)-A-S-H gels (Askarian et al. 2019; Liu et al. 2020; Ma et al. 2019). The uneven crest positions of Si-O, Al-O, Si-O-Si, or Si-O-Al bonds are beneficial for interpreting the geopolymerization mechanism (Mohammed et al. 2019b). However, the major vibration band around 1090 cm^{-1} is attributable to fly ash, while the band at 996 cm^{-1} is due to GGBS. The asymmetric stretching vibration of Si-O-Si(Al) bonds is connected with these vibrations (Jang and Lee 2016; Liu et al. 2016). The precise displacement of wavenumbers and the magnitude of the shift are contingent upon the Si/Al ratio of the precursors and the specific conditions of the reaction (Zhang et al. 2017). The variation in intensity might be linked to the quantity of reaction products generated, with minimal influence stemming from the development of a geopolymeric network.

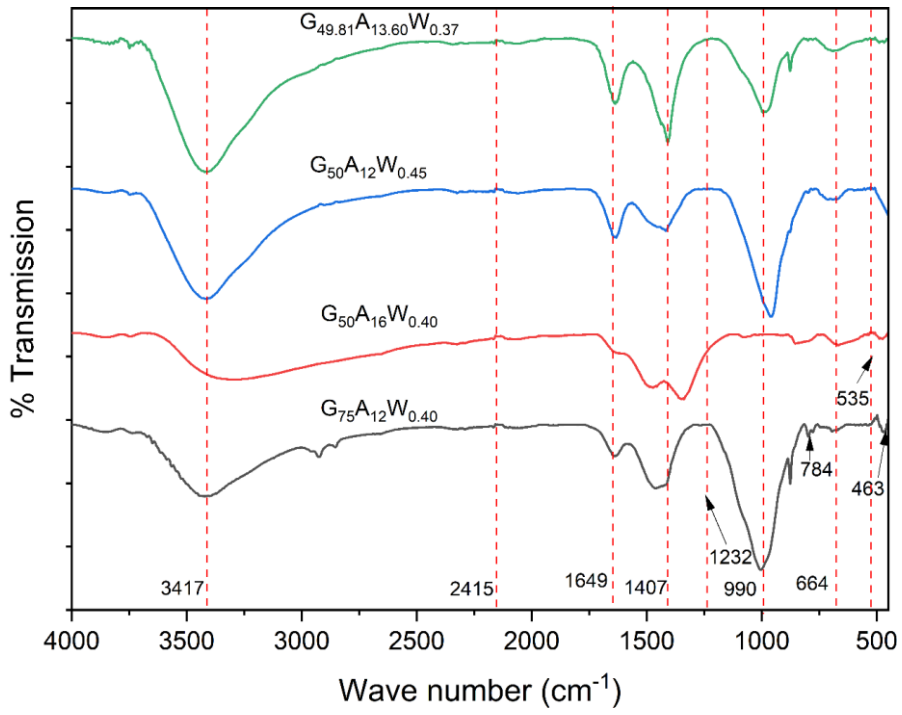

Figure 5.12 FTIR spectra of OPGMs ($G_{50}A_{12}W_{0.45}$, $G_{75}A_{12}W_{0.40}$, $G_{50}A_{16}W_{0.40}$, and $G_{49.81}A_{13.60}W_{0.37}$) after 28 days of ambient curing.

The stretching vibration of CO_3^{2-} corresponds to the band spanning around 1407 cm^{-1} suggesting the existence of carbonate groups in the OPGM mixtures (Puligilla and Mondal 2015; Zhang et al. 2017). The stretching vibration is ascribed to H-OH groups in the range of 3250-3650 cm^{-1}, confirming the existence of alkali hydroxides (Ma et al. 2019). The absorption peak at 535 cm^{-1} is generated as a result of symmetric bending vibrations of O-Si-O bonds, which are induced by both the solid anhydrous sodium metasilicate activator and the presence of water molecules. The stretching vibrations around 1649 cm^{-1} and bending vibrations around 463 cm^{-1} wavenumbers corresponds to O-H stretching and SiO_4 tetrahedral deformations (Shah et al. 2020). The FTIR of OPGMs are for various factors are found to be same, only the intensity of resonance is different which is associated with gelatinous products formed while geopolymerization. Further, the FTIR spectrum of the optimum mix $G_{49.81}A_{13.60}W_{0.37}$ shows peaks that are consistent with the SEM and XRD investigations suggesting the formation of C-(N)-A-S-H gel, which contribute significantly to the CpS of this mixture.

5.6 CLOSURE

In this chapter, the experimental programme and optimization studies on one-part geopolymer mortars are reported. Further, the microstructural characterization studies like SEM, XRD, TGA and FTIR are reported with respect to the microstructural changes, mineral phases, thermal mass loss and molecular bonding of one-part geopolymer mortar mixes.

CHAPTER 6

ONE-PART GEOPOLYMER CONCRETES

6.1 GENERAL

This chapter focuses on the experimental evaluation and optimization of one-part geopolymer concretes. The fresh and hardened properties of one-part geopolymer concrete mixes are discussed in detail. The microstructural observations on changes in structural and chemical compositions of one-part geopolymer concrete are discussed. Further, the ecological and cost analysis studies are reported.

6.2 MIX PROPORTIONS DESIGNED BY RESPONSE SURFACE METHOD

The OPG concrete experimentation involved the use of low calcium fly ash, GGBS, anhydrous sodium metasilicate powder, fine and coarse aggregates, and water. In this work, OPGC mixes were developed by considering three influential factors, each with three different levels. The factors considered include the replacement of GGBS with 25%, 50%, and 75% of the volume of fly ash, along with activator dosages of 8%, 12%, and 16% based on the mass of the binder, while maintaining W/GS ratios of 0.35, 0.40, and 0.45. Using a 3-level factorial design approach, a total of 27 different mixes were formulated. Table 6.1 provides a comprehensive overview of the mix proportions for OPGCs. Mix proportions are labelled for ease of reference, such as $G_{75}A_{12}W_{0.30}$, where G_{75} corresponds to 75% GGBS substitution, A_{12} represents a 12% activator dosage, and $W_{0.30}$ indicates a W/GS ratio of 0.30.

6.3 RESULTS AND DISCUSSION

The test results obtained for the OPGC mixes of various fly ash/GGBS ratios and dosages of activator content at different water to geopolymer solids ratios are presented in Figure 6.1 - Figure 6.6.

6.3.1 Workability

Workability assesses the ease with which homogeneous concrete can be mixed, placed, and finished. The slump values of all OPGC mixes are shown in Figure 6.1.

Table 6.1 Mix proportions for 1 m^3 of one-part geopolymer concretes.

Mix ID	Fly ash (%)	GGBS (%)	Activator (%)	W/GS	Fly ash (kg/m^3)	GGBS (kg/m^3)	Activator (kg/m^3)	Fine aggregate (kg/m^3)	Coarse aggregate (kg/m^3)		Water (kg/m^3)	*P/A
									20-10 mm	10-4.75 mm		
$G_{25}A_8W_{0.30}$	75	25	8	0.3	317	139	36	616	704	469	137	0.35
$G_{50}A_8W_{0.30}$	50	50	8	0.3	197	260	36	626	716	477	137	0.35
$G_{75}A_8W_{0.30}$	25	75	8	0.3	92	364	36	639	730	487	137	0.34
$G_{25}A_{12}W_{0.30}$	75	25	12	0.3	317	139	54	609	696	464	137	0.37
$G_{50}A_{12}W_{0.30}$	50	50	12	0.3	197	260	54	619	708	472	137	0.36
$G_{75}A_{12}W_{0.30}$	25	75	12	0.3	92	364	54	632	723	482	137	0.35
$G_{25}A_{16}W_{0.30}$	75	25	16	0.3	317	139	73	602	689	459	137	0.38
$G_{50}A_{16}W_{0.30}$	50	50	16	0.3	197	260	73	613	701	467	137	0.37
$G_{75}A_{16}W_{0.30}$	25	75	16	0.3	92	364	73	626	715	477	137	0.37
$G_{25}A_8W_{0.35}$	75	25	8	0.35	317	139	36	594	679	453	160	0.38
$G_{50}A_8W_{0.35}$	50	50	8	0.35	197	260	36	605	691	461	160	0.37
$G_{75}A_8W_{0.35}$	25	75	8	0.35	92	364	36	617	706	470	160	0.36
$G_{25}A_{12}W_{0.35}$	75	25	12	0.35	317	139	54	587	672	448	160	0.39
$G_{50}A_{12}W_{0.35}$	50	50	12	0.35	197	260	54	598	684	456	160	0.39
$G_{75}A_{12}W_{0.35}$	25	75	12	0.35	92	364	54	611	698	465	160	0.38
$G_{25}A_{16}W_{0.35}$	75	25	16	0.35	317	139	73	581	664	443	160	0.41
$G_{50}A_{16}W_{0.35}$	50	50	16	0.35	197	260	73	591	676	451	160	0.40
$G_{75}A_{16}W_{0.35}$	25	75	16	0.35	92	364	73	604	691	460	160	0.39
$G_{25}A_8W_{0.40}$	75	25	8	0.4	317	139	36	572	655	436	183	0.41
$G_{50}A_8W_{0.40}$	50	50	8	0.4	197	260	36	583	667	444	183	0.40
$G_{75}A_8W_{0.40}$	25	75	8	0.4	92	364	36	596	681	454	183	0.39

$G_{25}A_{12}W_{0.40}$	75	25	12	0.4	317	139	54	566	647	431	183	0.42
$G_{50}A_{12}W_{0.40}$	50	50	12	0.4	197	260	54	576	659	439	183	0.41
$G_{75}A_{12}W_{0.40}$	25	75	12	0.4	92	364	54	589	673	449	183	0.41
$G_{25}A_{16}W_{0.40}$	75	25	16	0.4	317	139	73	559	639	426	183	0.44
$G_{50}A_{16}W_{0.40}$	50	50	16	0.4	197	260	73	570	651	434	183	0.43
$G_{75}A_{16}W_{0.40}$	25	75	16	0.4	92	364	73	582	666	444	183	0.42
* P/A : Paste to aggregate ratio												

The observed results suggest that the slump value of the mix is primarily influenced by the W/GS ratio, irrespective of the GGBS content and activator dosage in the mixture. The workability of all the mixtures exhibited a direct correlation with the ratio of paste to aggregate. Where slump value of 255 mm reported for the mix with 0.44 paste to aggregate ratio and 40 mm slump recoded for mix with 0.34 paste to aggregate ratio. The workability of the mixtures improves with an increase in the W/GS ratio. The highest slump value in the mix $G_{25}A_{16}W_{0.40}$ reaching 255 mm, was observed in the mixture with a W/GS ratio of 0.40, featuring 16% activator, 25% GGBS content. In contrast, a slump value of 115 mm was recorded for the mixture with a W/GS ratio of 0.30, while maintaining the same activator and GGBS content. Workability exhibits an increase of approximately 70-85% when the W/GS ratio varies from 0.30 to 0.35 and 130-155% when it is 0.40, irrespective of the activator and GGBS content within the mixture. The phenomenon can be attributed to the inverse correlation between the water content and viscosity present in the mix. Studies conducted previously have demonstrated that an increase in water content results in a decrease in viscosity, which in turn leads to higher workability of the mix. This finding is consistent with earlier literature (Neupane, 2016).

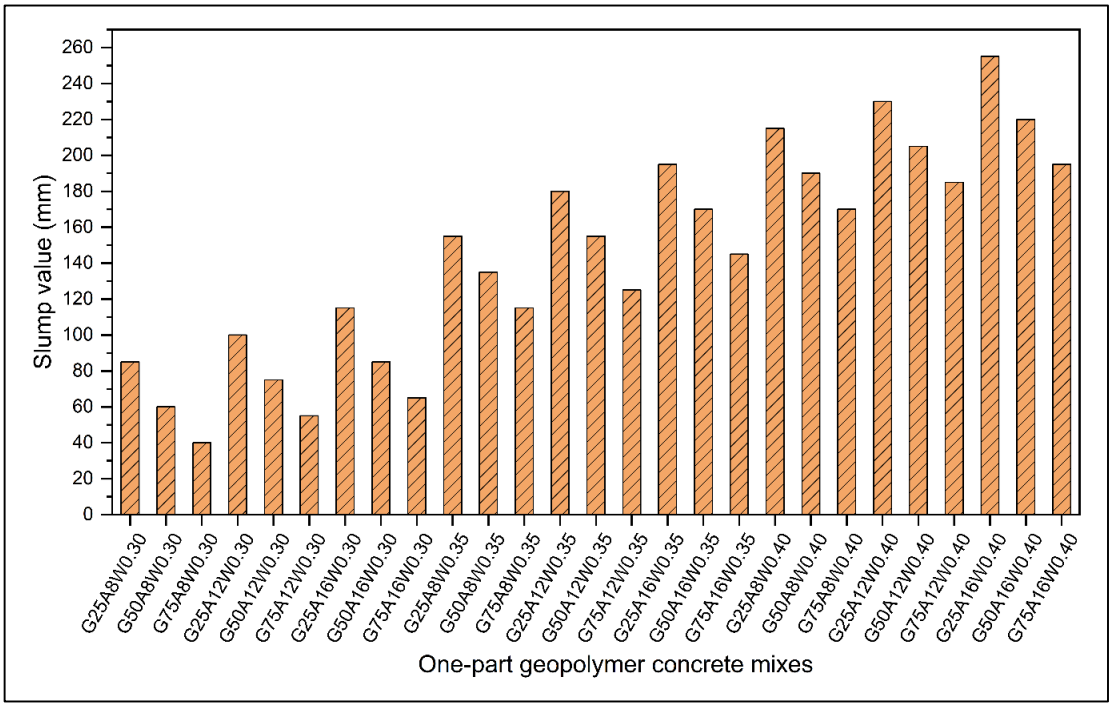

Figure 6.1 Slump values of one-part geopolymer concretes.

The slump value of the OPGCs was observed to decrease with the increase in GGBS content, as shown in Figure 6.1. This trend remained consistent regardless of the activator content and W/GS ratio used. As the GGBS replacement level ranges from 25% to 50% and 75%, the slump value of the OPGCs experiences a reduction of about 30% and 55%, respectively. The mix $G_{75}A_8W_{0.30}$ with a high GGBS content, a lower activator dosage, and W/GS ratio achieved the lowest slump value of 40 mm. It's evident that GGBS had an adverse impact on the workability of the OPGC mixes, a finding consistent with the conclusions drawn in earlier research works (Li et al. 2020; Perumal et al. 2021; Prusty and Pradhan 2020). The phenomenon can be ascribed to the augmented specific surface area and non-uniform shape of the slag particles, which impede the fluidity and expeditious reaction kinetics of such particles. (Yousefi Oderji et al. 2019). The observed trend in Figure 6.1reveals that the OPGC slump values exhibited an increase of roughly 16% and 35% when the activator dosage was changed from 8% to 12% and 16%, respectively. This increase was observed irrespective of the W/GS ratio. The observed phenomena might be explained by the excessive presence of anhydrous Na_2SiO_3, which impedes the dissolving of raw materials with high modulus. As a result, the mix becomes less cohesive (Jafari Nadoushan and Ramezanianpour 2016).

6.3.2 Compressive strength of OPGC

The compressive strength (CpS) results of OPGCs across different parameters and levels are presented in Figure 6.2. The CpS of all blends at the end of the 7-day curing period was found to be around 65-70% of the CpS of OPGC after 28 days. The CpS of OPGCs exhibited a significant drop when the ratio of W/GS rises. The increase in the W/GS ratio poses a hindrance to the geopolymerization process, leading to a decrease in strength. The OPGC mix $G_{25}A_8W_{0.40}$ exhibited the lowest 28-day CpS of 14.3 MPa. This result can be attributed to the higher W/GS ratio of 0.40 and the presence of 75% fly ash as precursor, with least activator concentration. The OPGC mix $G_{75}A_{12}W_{0.30}$, which consisted of a lower W/GS ratio of 0.30, 12% activator dosage, and 75% GGBS content, achieved the maximum CpS of 72.7 MPa. Nevertheless, the fluctuation in CpS that is found as the W/GS ratio increases can be related to the substantial impact of variations in the proportions of fly ash and GGBS within the mixes of OPGC (Ma et al.

2023; Neupane 2016; Srinivasa et al. 2023). It is observed that as the W/GS increases from 0.30 to 0.35 and 0.40, the CpS experiences a decrease ranging from 11% to 20% and 15% to 30% respectively. The decrease in strength can be attributed to the increase in the W/GS ratio, which leads to an elevation in the water content within the mixture. This, in turn, impacts the polymerization process. The determination of the water content in a geopolymer mixture is found upon the quantity necessary to facilitate the thorough disintegration of the activator. Excessive water beyond the specified requirement results in increased porosity, thereby causing a decrease in strength (Ye et al. 2016; Yousefi Oderji et al. 2019).

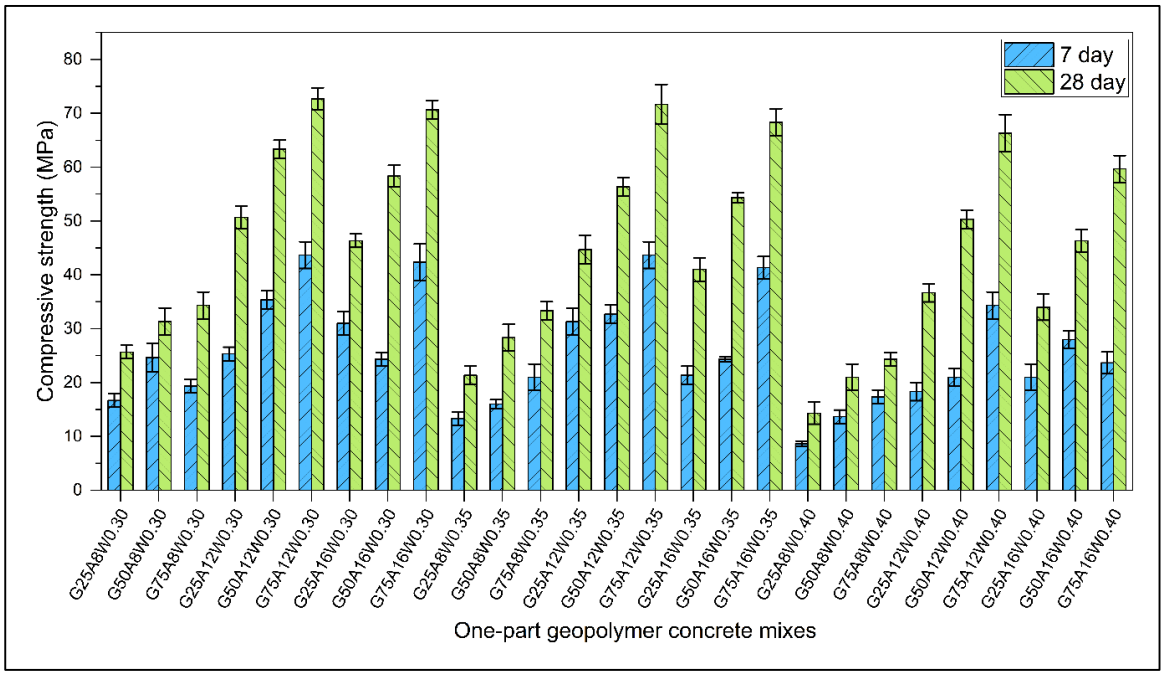

Figure 6.2 Compressive strength results of one-part geopolymer concretes.

The activator dosage has significant impact in variation of CpS of the OPGC mixes. It is observed that the development of CpS is roughly 2 - 2.5 times greater when the activator dosage is increased from 8% to 12%, irrespective of the W/GS ratio and slag concentration. When the activator component is decreased, the degree of polycondensation is lowered, resulting in a drop in the strength of the OPGC mixes. In contrast, a higher activator concentration results in a greater dissolution of Ca, Si, and Al species, hence amplifying the amount of the geopolymerization reaction. As a consequence, a stable aluminosilicate network is formed, accompanied by the generation of C-S-H gel within the composite. Consequently, the blends exhibit

increased CpS (Askarian et al. 2019; Elzeadani et al. 2022). Nevertheless, an increase in the activator concentration over 12% leads to a marginal decrease in the CpS of OPGC mixes. The observed behavior can be attributed to a higher dose of activator, particularly an excessive amount of Na_2O, which hinders the development of binding phases and increases the possibility of activator leaching and efflorescence. These factors contribute to the degradation of the matrix and a subsequent reduction in strength. From Figure 6.2, the data clearly demonstrates that an increase in GGBS content results in an increase in CpS of the OPGC mixes. This relationship holds true regardless of the activator level and W/GS ratio in the mixes. The CpS exhibited an increase ranging from 15% to 25% when the GGBS percentage was increased from 25% to 50% in the concrete mixes. Furthermore, a higher rise of 30% to 55% in CpS was seen when the GGBS content was further increased to 75%. The utilisation of GGBS as a substitute material significantly impacts the strength characteristics of the OPGCs (Haruna et al. 2020a; Hassan et al. 2019; Kadhim et al. 2021; Perumal et al. 2022). The significant disparity in CpS seen across different OPGC mixes at a given age can primarily be attributed to the noteworthy influence of the amount of GGBS replacement. This is due to greater substitution of GGBS leads to an increased Ca concentration in the mixture, hence enhancing the CpS of OPGC mixtures. The presence of a substantial amount of Ca contributes to the increased formation of C-A-S-H gel, which is influenced by the presence of an alkali activator and occurs simultaneously with the formation of N-A-S-H gel (Mohammed et al. 2019a). In addition, larger Ca levels accelerate the polycondensation mechanism, leading to the creation of tetrahedral Si and Al structures. These structures combine to form a three-dimensional network that leads to increased CpS of OPGCs. However, from the observations of test results of the OPGC mixes, the GGBS content and the amount of activator are significant factors in the strength growth of OPGCs.

6.3.3 Flexural strength of OPGC

The flexural strength (FrS) of concrete is a crucial parameter employed to evaluate the degree of cracking caused by applied load and deformation in various structural and non-structural contexts. The FrS test is an indirect method used to assess the tensile strength of concrete. The examination assesses the ability of an unenhanced concrete

beam or slab to withstand failure caused by bending. The flexural strength of concrete may serve as an approximation for its tensile strength, as it typically exceeds its corresponding splitting tensile strength. The FrS results for OPGC mixes are depicted in Figure 6.3. The FrS of the OPGC mixtures exhibited a similar pattern to that observed in the CpS. The FrS of OPG concrete exhibited a range of values, with the least strength recorded as 2.33 MPa for the $G_{25}A_8W_{0.40}$ mixture, and the maximum strength observed as 6.3 MPa for the $G_{75}A_{12}W_{0.30}$ mixture. The FrS exhibited an inverse relationship with the paste-aggregate ratio, whereby a drop in the ratio resulted in a rise in FrS, and conversely, an increase in the ratio led to a decrease in FrS. Where FrS of 6.3 MPa reported for the mix with 0.35 paste to aggregate ratio and 2.3 MPa recoded for mix with 0.41 paste to aggregate ratio. The similar trend was observed in earlier literature (Haruna et al. 2020b). It is noteworthy to observe that the total aggregate content exerts minimal influence on the FrS of OPGC.

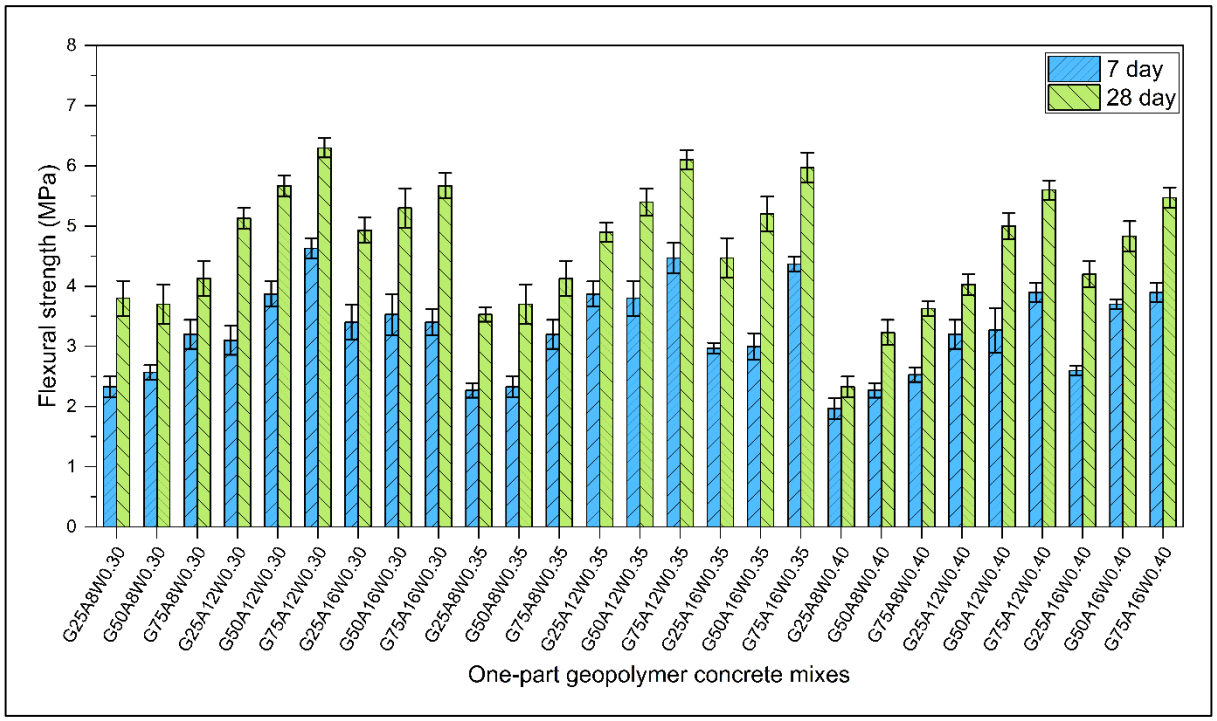

Figure 6.3 Flexural strength results of one-part geopolymer concretes.

The FrS of OPGCs exhibited a significant drop when the ratio of W/GS rises. The OPGC mixture $G_{25}A_8W0_{.40}$ demonstrated the FrS of 2.3 MPa after 28 days. The observed outcome can be ascribed to the elevated W/GS ratio of 0.40 and the use of 75% fly ash as a precursor, accompanied by the lowest concentration of activator. The

OPGC mix $G_{75}A_{12}W_{0.30}$, which consisted of a lower W/GS ratio of 0.30, 12% activator dosage, and 75% GGBS content, achieved the maximum FrS of 6.3 MPa. It is observed that as the W/GS increases from 0.30 to 0.35 and 0.40, the FrS experiences a decrease ranging from 7% to 21% and 18% to 32% respectively. It is noted that, FrS increases by roughly 35% when the activator dosage is raised from 8% to 12%, regardless of the W/GS ratio and slag content. From Figure 6.3, the data clearly demonstrates that an increase in GGBS content results in an increase in FrS of the OPGC mixes. The FrS has shown a notable escalation, varying between 8% and 15%, as GGBS was augmented from 25% to 50% in the concrete compositions. Furthermore, a larger rise of 20% to 35% in FrS was noticed when the GGBS content was further increased to 75%. However, the proportion of fly ash to GGBS has significant effects on early age and later age FrS of the OPGC mixes. Where the mixes with high Ca content exhibits better performance due to heightened pozzolanic reaction of the Ca rich precursors at later stages. The early and later age FrS development can be correlated to the CpS of the OPGC mixes.

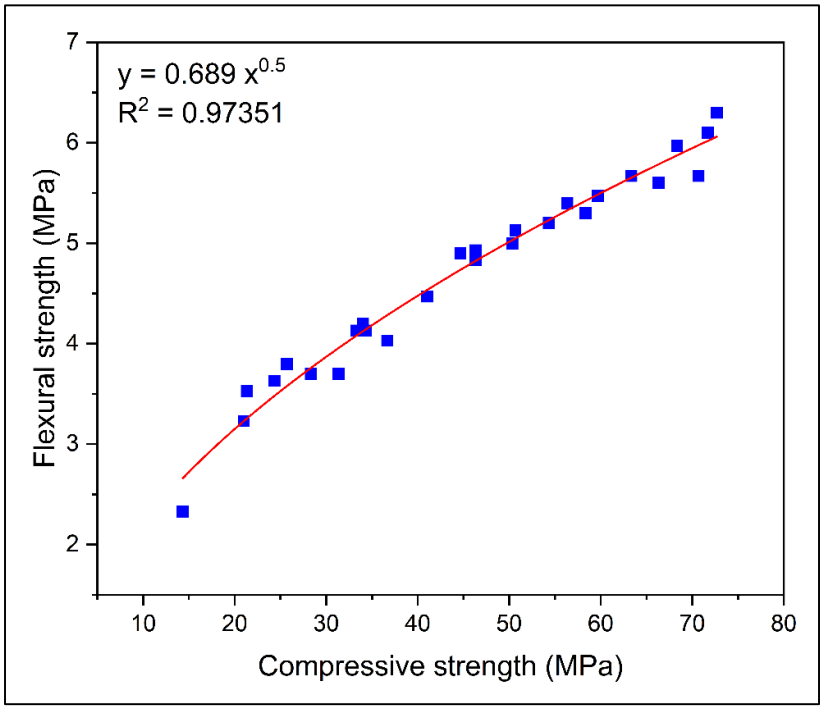

Figure 6.4 Correlation between 28-day flexural and compressive strength of one-part geopolymer concretes.

A power regression analysis was performed to examine the relationship between the CpS and FrS of one-part geopolymer concretes using experimental data. The

investigation yielded regression analysis results, including correlation coefficients and sample data, which are depicted in Figure 6.4. The results of the regression analysis demonstrate a statistically significant power link between CpS and FrS. This is supported by a very significant correlation coefficient, with an R^2 value of 0.97351, in the context of CpS and FrS. The R^2 value obtained from the calculation serves as an indicator of the regression line's ability to elucidate the fluctuations observed in the y variable, FrS. The relationship obtained for the FrS and CpS based on the present experimental results is as follows;

$$f_r = 0.69\sqrt{f_c} \quad (6.1)$$

Where, f_r = Flexural strength of concrete, f_c = Compressive strength of concrete

Some earlier findings suggest the relation between FrS and CpS are as follows;

Nath and Sarker (Nath and Sarker 2017): $f_r = 0.89\sqrt{f_c}$ (6.2)

Suggested higher value of FrS of normal strength concrete.

Sofi et al. (Sofi et al. 2007): $f_r = 0.6\sqrt{f_c}$ (6.3)

There exists a notable resemblance between the equation under consideration and the AS 3600 standard.

Diaz-Loya et al. (Diaz-Loya et al. 2011): $f_r = 0.69\sqrt{f_c}$ (6.4)

Proposed following relationship of Frs and CpS of conventional geopolymer concrete.

The correlation observed in this work between the FrS and CpS of one-part geopolymer concrete closely aligns with the established relationship between FrS and CpS of geopolymer concrete given in Eq.6.4 and OPC-based concrete, as indicated by the suggested constant factor of 0.7 in code IS 456 (BIS 456:2000). Nevertheless, due to the scarcity of data regarding OPG mixes, the developed prediction model can be successfully utilised to estimate the FrS of OPG mixes by considering its CpS.

6.3.4 Split tensile strength of OPGC

The split tensile strength (SpS) test provides a measure of a concrete's ability to resist tensile forces, which is crucial in various structural applications. Concrete exhibits

intrinsic weakness in tension, with its tensile strength being notably inferior to its compressive strength. SpS experiment facilitates the comprehension of the mechanical response of concrete under tensile loading conditions. The capacity to detect the propensity for fracture in concrete components is crucial for guaranteeing the longevity and security of constructions. The SpS results for OPGC mixes are shown in Figure 6.5. The SpS of the OPGC mixtures displayed a comparable trend to that observed in the CpS. The SpS of OPG concrete exhibited a range of values, with the least strength recorded as 1.5 MPa for the $G_{25}A_8W_{0.40}$ mixture, and the maximum strength observed as 3.8 MPa for the $G_{75}A_{12}W_{0.30}$ mixture. The SpS demonstrated a negative correlation with the paste-aggregate ratio, such that a decrease in the ratio corresponded to an increase in SpS and vice-versa. SpS of 3.8 MPa was reported for the mixture with a paste to aggregate ratio of 0.35, whereas a value of 1.5 MPa was recorded for the mixture with a paste to aggregate ratio of 0.41. Similar trend was noted in previous works reported (Haruna et al. 2020b). It's worth noting that the overall amount of aggregate has little impact on the SpS of OPGC. This is attributed to the substantial binder content in the mixtures, which results in a gradual development of strength.

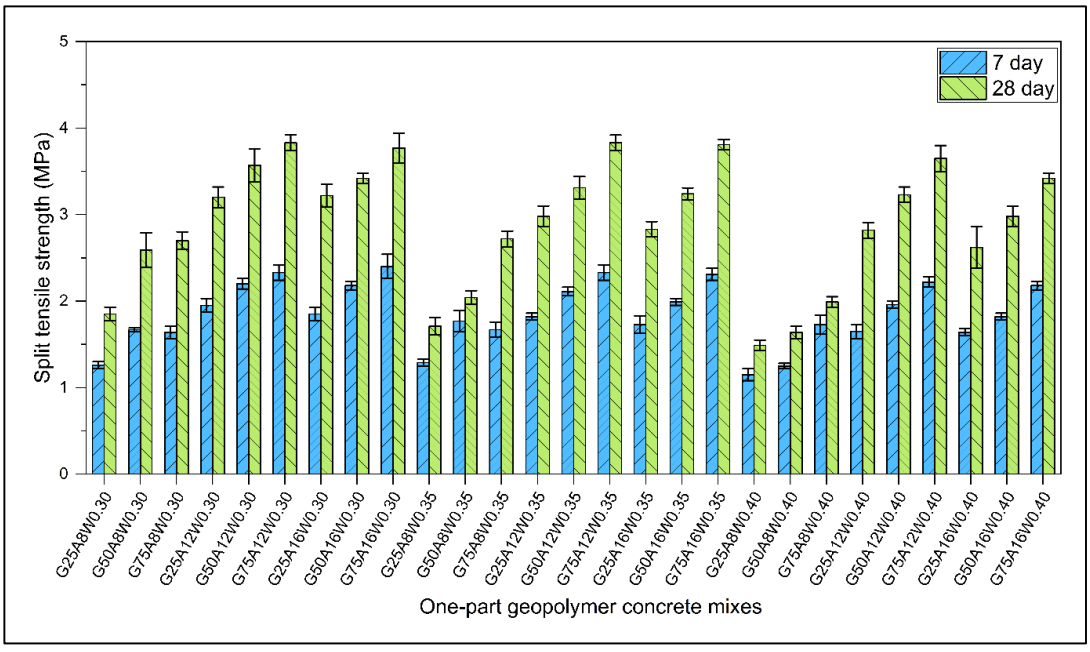

Figure 6.5 Split tensile strength results of one-part geopolymer concretes.

The SpS of OPGCs exhibited a notable decrease when the ratio of W/GS increased. The OPGC mixture with the composition $G_{25}A_8W_{0.40}$ exhibited a SpS of 1.5

MPa after a curing period of 28 days. The observed result can be attributed to the higher W/GS ratio of 0.40 and the utilisation of 75% fly ash as a precursor, coupled with the lowest concentration of activator. The OPGC mix $G_{75}A_{12}W_{0.30}$, which comprises of a lower W/GS ratio of 0.30, 12% activator dosage, and 75% GGBS content, achieved the maximum SpS of 3.8 MPa. It is observed that as the W/GS increases from 0.30 to 0.35 and 0.40, the SpS experiences a decrease ranging from 10% to 25% and 20% to 35% respectively. SpS increases by roughly 35% as the activator dosage rise from 8% to 12%, regardless of the W/GS ratio and GGBS content. The data presented in Figure 6.5 demonstrate conclusively that an increase in GGBS content leads to an increase in SpS of OPGC mixtures. The SpS increased noticeably, from 10% to 25%, when GGBS was increased from 25% to 50% in the concrete mixtures. When the GGBS concentration was raised to 75%, an even greater increase in FrS of 15% to 35% was observed. Early age and later age SpS of the OPGC mixes are both significantly affected by the fly ash to GGBS ratio. The CpS of the OPGC mixtures is related to both the early and late age development of SpS.

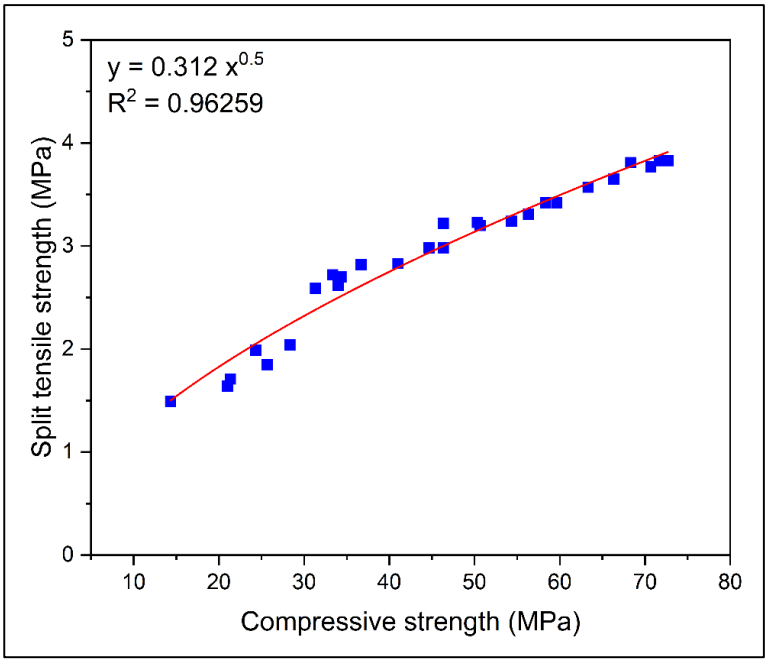

Figure 6.6 Correlation between 28-day split tensile and compressive strength of one-part geopolymer concretes.

A power regression analysis was performed to examine the relationship between the CpS and SpS of one-part geopolymer concretes using experimental data. The

investigation yielded regression analysis results, including correlation coefficients and sample data, is shown in Figure 6.6. The results of the regression analysis demonstrate a statistically significant power link between CpS and SpS. This is supported by a very significant correlation coefficient, with an R^2 value of 0.96259, in the context of CpS and SpS. The R^2 value derived from the computation functions as a metric for assessing the explanatory power of the regression line in capturing the variations observed in the dependent variable, SpS. The relationship obtained for the SpS and CpS based on the present experimental results is as follows;

$$f_S = 0.31\sqrt{f_c} \quad (6.5)$$

Where, f_s = Split tensile strength of concrete, f_c = Compressive strength of concrete

Some earlier findings suggest the relation between SpS and CpS are as follows;

Australian Standards 3600 (2009): $f_S = 0.36\sqrt{f_c}$ (6.6)

(for f_c: 20 MPa to 100 MPa geopolymer concrete)

Sofi et al. (Sofi et al. 2007): $f_S = 0.5\sqrt{f_c}$ (6.7)

Proposed following relationship of SpS and CpS of conventional geopolymer concrete.

Concrete Institute of Australia (2011): $f_S = 0.4\sqrt{f_c}$ (6.8)

Suggests a similar equation to AS 3600 (2009) for geopolymer concrete.

The correlation observed in this work between the SpS and CpS of one-part geopolymer concrete closely aligns with the established relationship between SpS and CpS of geopolymer concrete given in Eq. 6.6. However, the developed prediction model may be successfully used to estimate the SpS of OPGC mixes by considering its CpS, despite the lack of data regarding OPGC mixes.

6.4 OPTIMIZATION PROGRAMME

6.4.1 Modelling and statistical evaluation

Response surface method was employed to conduct a multi-objective optimization analysis based on the preceding test outcomes. The purpose of this analysis was to

determine the most optimal solution while balancing several competing objectives. The RSM method was chosen due to its versatility and ability to model complex systems. By utilizing the previous test results, the analysis was able to take into account the various constraints and parameters involved. This approach allowed for a more informed decision-making process and an optimized outcome. The primary objective was to determine the optimal values for GGBS substitution, activator dosage, and W/GS ratio. The study aimed to identify the most appropriate combination of these three parameters to achieve the desired outcome. The study on optimization prioritized attaining a slump value of 125 mm while simultaneously maximizing the strength attributes of OPGCs. To identify the most appropriate polynomial function that accurately fit the data obtained from the experiments, the "Design Expert" software was utilized. The resulting model derived from the polynomial function was then used to analyze the experimental results. To perform nonlinear fitting of different models, model summary statistics, deviation's sum of squares, and fitting error are utilized. To formulate the quadratic polynomial models, the coefficients of the parameters were estimated using multiple regression analysis. Employing analysis of variance, helps in assessing the reliability of outcomes and comparing the means and effects of multiple factors. The general polynomial regression model is shown in Eq.6.9. The regression models established for all responses are presented in Eqs.6.10-6.13, displaying the actual coefficients. Additionally, the coded coefficients for each response can be found in Table 6.2.

$$Response = a + b\times A + c\times B + d\times C + e\times AB + f\times AC + g\times BC + h\times A^2 + i\times B^2 + j\times C^2 \quad (6.9)$$

$$Slump\ value = -863.00926 - 0.744444\times A + 3.78472\times B + 4463.88889\times C - 0.025000\times AB - 0.666667\times AC + 6.25\times BC + 0.003111\times A^2 - 0.034722\times B^2 - 4555.55556\times C^2 \quad (6.10)$$

$$Compressive\ strength = -180.18148 - 0.263878\times A + 28.02250\times B + 375.13333\times C + 0.038900\times AB + 0.688667\times AC - 1.52500\times BC - 0.000292\times A^2 - 1.08462\times B^2 - 718.22222\times C^2 \quad (6.11)$$

$$Flexural\ strength = -10.21704 - 0.037933 \times A + 1.49083 \times B + 41.34444 \times C + 0.001067 \times AB + 0.126667 \times AC + 0.433333 \times BC + 0.000023 \times A^2 - 0.062639 \times B^2 - 85.55556 \times C^2 \quad (6.12)$$

$$Split\ tensile\ strength = -5.15769 + 0.009967 \times A + 1.12299 \times B + 6.50556 \times C - 0.000025 \times AB + 0.006667 \times AC + 0.262500 \times BC + 0.000036 \times A^2 - 0.04444 \times B^2 - 21.1111 \times C^2 \quad (6.13)$$

Table 6.2 Coded coefficients of responses.

Coefficients		**Response**			
		Workability	**Compressive strength**	**Flexural strength**	**Split tensile strength**
Coded	*a*	151.85	58.28	5.48	3.40
	b	-24.17	10.37	0.5378	0.3889
	c	15.56	13.61	0.7700	0.5878
	d	65.83	-5.57	-0.3506	-0.2394
	e	-2.50	3.89	0.1067	-0.0025
	f	-0.8333	0.8608	0.1583	0.0083
	g	1.25	-0.3050	0.0867	0.0525
	h	1.94	-0.1822	0.0144	0.0222
	i	-0.5556	-17.35	-1.00	-0.7111
	j	-11.39	-1.80	-0.2139	-0.0528

Where a-j represents coefficients, while A, B, and C represents GGBS content, activator dosage, and W/GS ratio, respectively. To ensure that each regression analysis yielded reliable results within an acceptable range, a range of statistical metrics, including p-values, lack of fit evaluations, and R^2 (regression coefficient) values, were calculated. Table 6.3 displays the model terms utilized in the calculations, along with the outcomes of the ANOVA conducted for each response, and provides descriptive statistics for each model. As indicated by the findings presented in Table 6.3, all response models and individual factors exhibit statistical significance at the 95% confidence level, as evidenced by p-values below 0.05. The F-value represents the relationship between the mean square effect and the mean square error, similar to the ratio of the average variation among groups to the average variation within groups (Bingol et al. 2010). The model F-value of 1277.61, 164.06, 99.21, and 76.28 for workability, CpS, FrS, and SpS, respectively, indicates that the likelihood of an F-value of this magnitude occurring solely due to random noise is only 0.01% (Li et al. 2021). The higher F-values for GGBS content, activator dosage, and W/GS ratio, which are

364.17, 627.43, and 105.23, respectively, indicate that these independent variables have a substantial impact on the CpS of OPGCs. The assertion is supported by a P-value below 0.050, indicating that these independent variables had a substantial impact on workability, CpS, FrS, and SpS of OPGCs.

Table 6.3 ANOVA models.

Model	**Responses**			
	Workability	**Compressive strength**	**Flexural strength**	**Split tensile strength**
p-value (model)	<0.0001	<0.0001	<0.0001	<0.0001
F-value	1277.61	164.06	99.21	76.28
R^2	0.9985	0.9886	0.9813	0.9758
Adjusted R^2	0.9977	0.9826	0.9714	0.9630
Predicted R^2	0.9963	0.9684	0.9474	0.9317
Adeq precision	121.4635	42.1303	34.9222	31.1005
Std. deviation	2.86	2.31	0.1671	0.1379
Mean	145.19	45.39	4.68	2.91
C.V (%)	1.97	5.08	3.57	4.75
p-value (Prob > F) of factors, their interrelations and squares				
A: GGBS (%)	<0.0001	<0.0001	<0.0001	<0.0001
B: Activator (%)	<0.0001	<0.0001	<0.0001	<0.0001
C: W/GS	<0.0001	<0.0001	<0.0001	<0.0001
AB	0.0075	<0.0001	0.0410	0.9507
AC	0.3263	0.2132	0.0044	0.8367
BC	0.1478	06526	0.0901	0.2048
A^2	0.1137	0.8488	0.8348	0.6980
B^2	0.6398	<0.0001	<0.0001	<0.0001
C^2	<0.0001	0.0735	0.0060	0.3617

The R^2 value of workability, CpS, FrS, and SpS of OPGCs was 0.9985, 0.9886, 0.9813 and 0.9758, respectively. The R^2 value measures the degree of correlation between the actual experimental outcomes and the predicted results generated by the model equation. Consequently, as R^2 approaches a value of one, it signifies an enhancement in the accuracy of the model equation's predictions. The predicted R^2 of 0.9963, 0.9684, 0.9474, and 0.9317 for workability, CpS, FrS, and SpS, respectively are in reasonable agreement with the adjusted R^2 of 0.9977, 0.9826, 0.9714, and 0.9630, respectively. The difference between the models' predicted R^2 and adjusted R^2 values falls below the 0.2 threshold, indicating that their adeptness and reliability are well within acceptable parameters. This information suggests that the models have been appropriately constructed and are capable of providing accurate results (Shi et al. 2022).

According to Table 6.3, all the models exhibit precision values greater than 4, indicating their appropriateness for exploring the design space. The CV% (coefficient of variation) values of 1.96, 5.08, 3.57, and 4.75 for responses workability, CpS, FrS, and SpS, respectively, demonstrate that the constructed model is more robust. This information suggests that the models are suitable for further exploration and application.

The present study showcases the 3D response surface plots of the workability, CpS, FrS, and SpS models in Figure 6.7. The aforementioned plots demonstrate the influence of independent factors such as GGBS content, activator dosage, and W/GS ratio on the responses, including workability, CpS, FrS, and SpS. Notably, these plots exhibit the individual effects of the aforementioned factors, as well as their interaction effects. The plots, therefore, provide valuable insights into the impact of different factors on the responses, which can be particularly useful in the selection and optimization of the independent variables for the desired responses. The residual normal probability plots pertaining to all the response models are presented in Figure 6.8. These plots demonstrate the extent to which the data is sufficient and distributed as per the expected parameters. The analysis of the residual normal probability plots provides important insights into the adequacy of the data, thereby contributing significantly to the reliability and validity of the findings. The plots, therefore, hold great significance in the domain of research, particularly in the context of statistical analysis. The plots indicate that the data points conform to a linear trend, exhibiting normal distribution of the residuals post the appropriate transformation of the response variables. These observations, therefore, validate the reliability and accuracy of the results obtained through the analysis of the response models. The effectiveness and accuracy of the developed models have been assessed through graphical analysis, where the predicted results are plotted on the y-axis and the actual results on the x-axis.

In Figure 6.9, the graphical representation clearly demonstrates the precision of the response model, with each data point closely following the straight line. The consistent alignment of the dataset with the straight line serves as strong evidence of the agreement between the test and predicted outcomes, confirming that the existing models fit the data well and are reliable. This graphical analysis is a valuable tool for

evaluating the efficacy of the developed models, significantly enhancing the quality and credibility of the research findings.

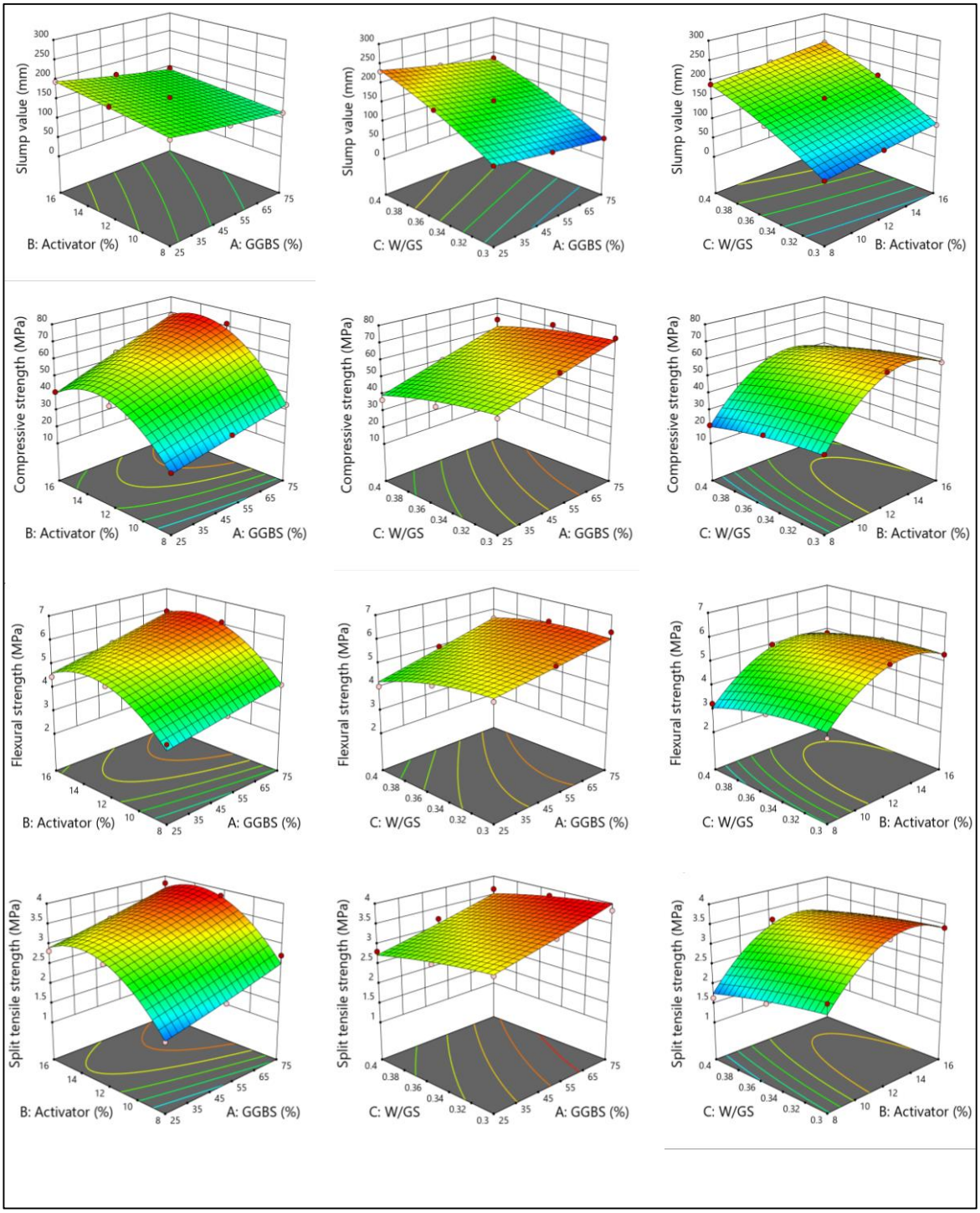

Figure 6.7 Response surface plots for one-part geopolymer concrete mixes.

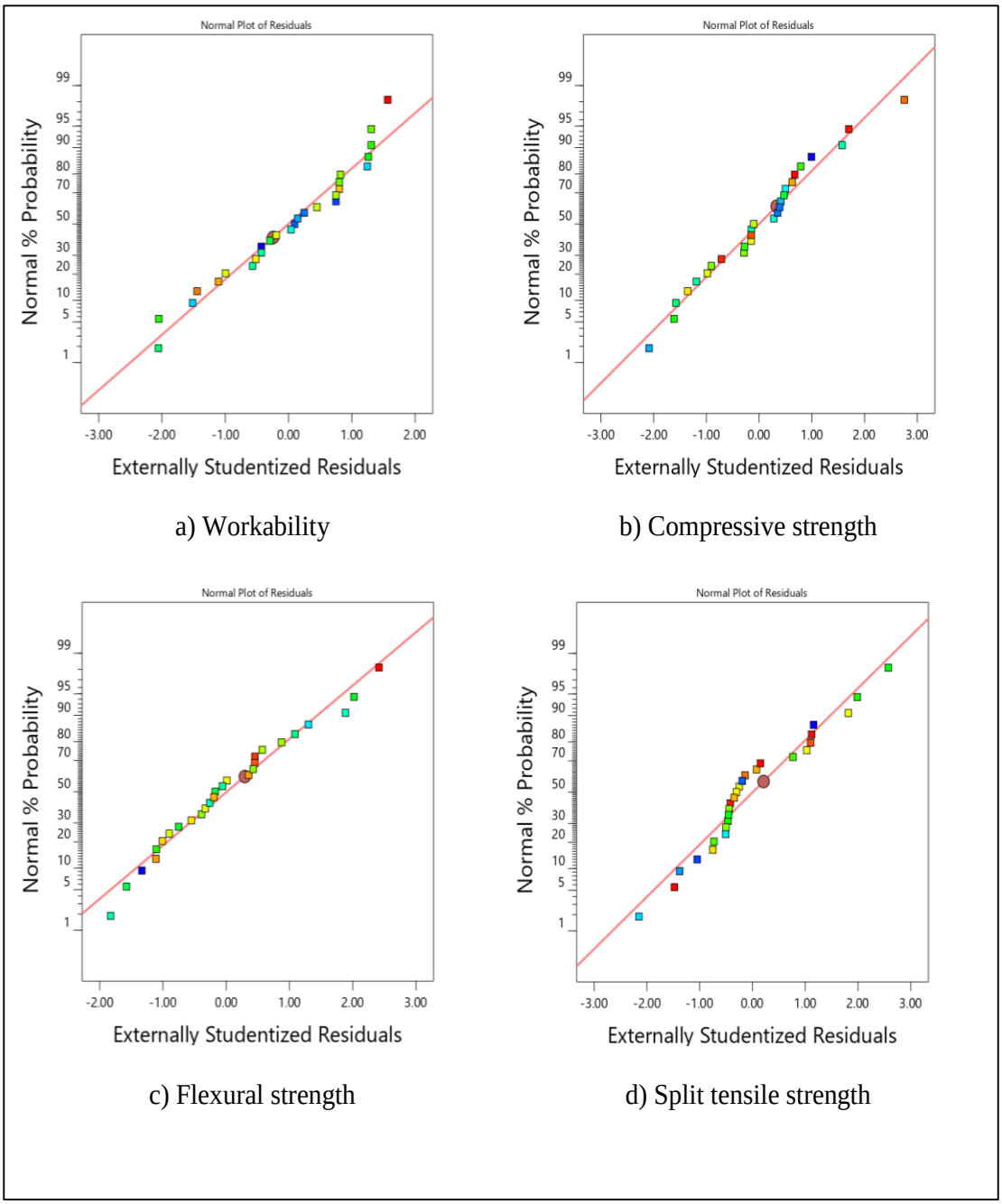

Figure 6.8 (a)-(d) Normal probability plots of response models of one-part geopolymer concretes.

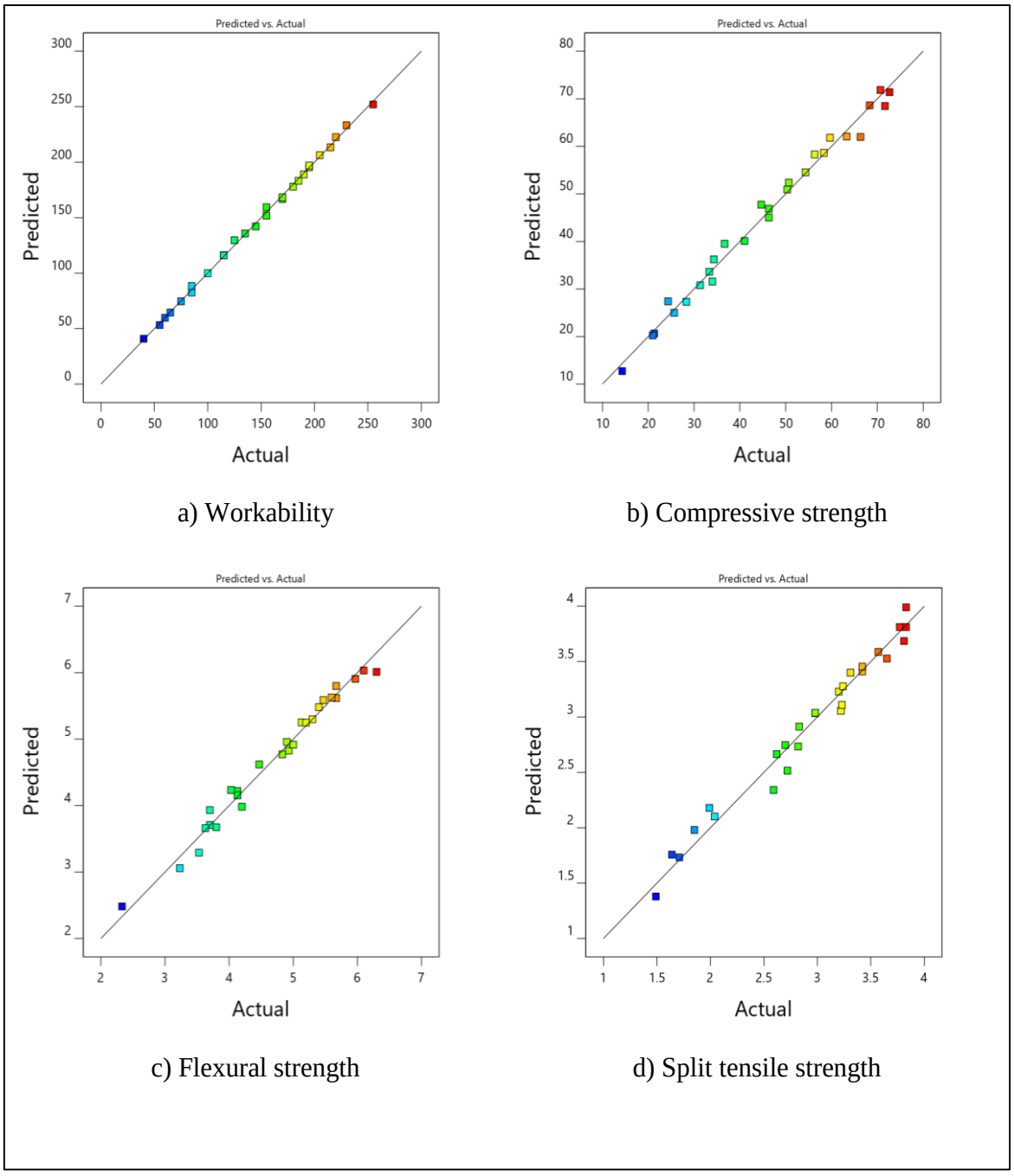

Figure 6.9 (a)-(d). Predicted and actual values of one-part geopolymer concrete responses.

6.4.2 Optimization and validation study

In order to investigate the collective impact of various factors on the properties of OPGCs, as well as to establish a correlation between the considered variables and their respective responses, the response surface method was employed. In order to determine the optimal values for the GGBS content, activator dosage, and W/GS, a variety of computational techniques, including multi-objective optimization, response surface fitting models, and the desirability function were employed. The objective was to achieve a workability of 125 mm, while maximizing the compressive, flexural, and split tensile strength of the developed one-part geopolymer concretes. The equal importance to all of these factors was assigned, recognizing that each plays a critical role in determining the overall quality and performance of the material. The aim of optimization research is to identify the most desirable values of independent factors that lead to achieving the best performance criteria. The desirability function (D) evaluates a single solution by assigning a numerical value between 0 and 1, with 0 indicating an undesirable response value and 1 indicating the desired response value. In multi-objective optimization, the primary objective is to achieve the highest possible value for the desirability function. This approach seeks to balance multiple objectives efficiently, often with competing interests, to identify the most desirable outcome. The optimization goals and benchmarks are given in Table 6.4. The obtained optimum mix proportions is as follows: 75% GGBS, 13.75% of activator dosage, and 0.34 as W/GS ratio. The results demonstrate a high degree of reliability, as indicated by the function value of 0.996. Furthermore, based on the obtained results, the expected outcome can be viewed as highly dependable. It's important to highlight that the function value serves as a dependable performance metric that offers a comprehensive evaluation of the system's overall performance. These findings underscore the system's robustness, which can be attributed to its inherent design and operational attributes.

Table 6.5 presents the solutions obtained from the numerical optimization aimed at optimizing a specific objective. The obtained results demonstrate that the model used for predicting the optimum OPGCs proportions is highly accurate, with a prediction error of less than 10%. This implies that the model's predictions are reliable and can be used to optimize the OPGCs mix proportions. In order to validate the model's

accuracy, response prediction values and their absolute deviations from the test values were calculated using individual response models. Table 6.5 shows the error percentage between experimental and predicted values. The greatest deviation was observed in the workability response, at 8%, which falls below the 10% threshold, signifying a high level of accuracy for the model (Shi et al., 2022). Figure 6.10 illustrates the optimization ramps, providing a visual representation of the independent variables and responses examined in the study.

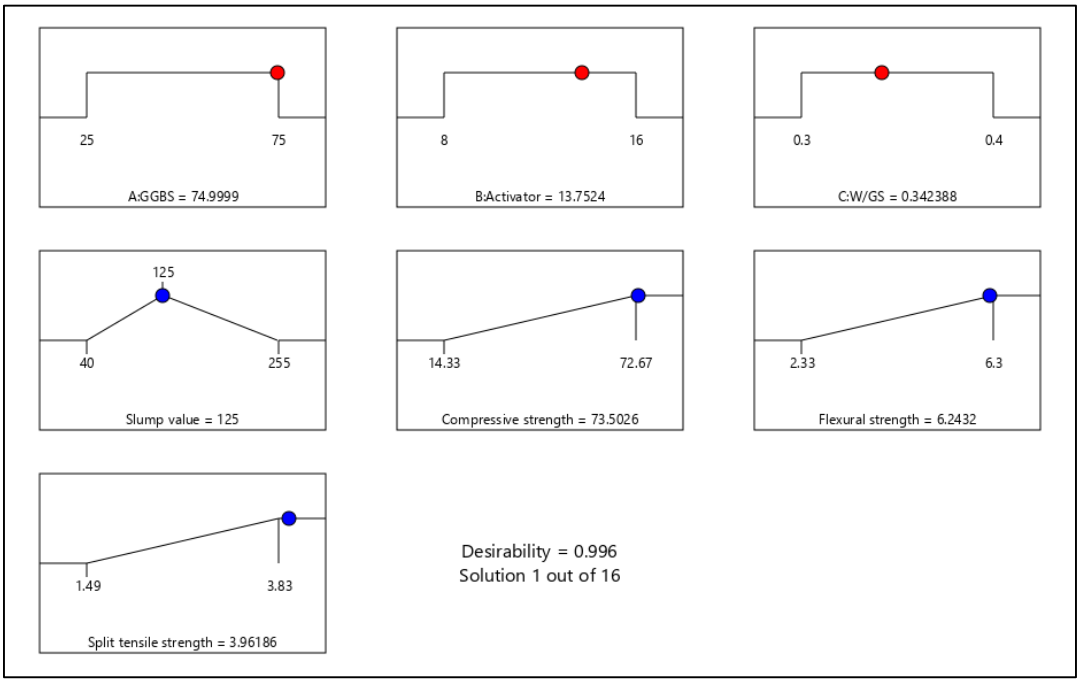

Figure 6.10 Optimization ramps.

Table 6.4 Optimization goals and benchmarks.

Independent variables and responses	**Goal**	**Lower limit**	**Upper limit**	**Target value**
A: GGBS (%)	In range	25	75	-
B: Activator (%)	In range	8	16	-
C: W/GS	In range	0.35	0.45	-
R_1: Workability (mm)	Target	35	255	125
R_2: Compressive strength (MPa)	Maximize	14.3	72.6	-
R_3: Flexural strength (MPa)	Maximize	2.33	6.30	-
R_4: Split tensile strength (MPa)	Maximize	1.49	3.83	-

Table 6.5 Optimum mix model verification.

Responses	GGBS (%)	Activator (%)	W/GS	Predicted value	Test value	Error (%)
Workability (mm)	75	13.75	0.34	125	135	8.00
Compressive strength (MPa)	75	13.75	0.34	73.5	70.2	4.42
Flexural strength (MPa)	75	13.75	0.34	6.2	5.8	6.89
Split tensile strength (MPa)	75	13.75	0.34	3.9	3.6	7.32

6.5 MICROSTRUCTURAL, PHASE AND CHEMICAL ANALYSIS

The microstructural characterization like SEM, EDS, XRD, TGA/DTG and FTIR were studied for selected OPGC mixes. In order to investigate the influence of individual and interaction factors on the microstructural characteristics of OPGCs, the test samples are analyzed for characterization after a curing period of 28 days. The chosen mixes are $G_{25}A_8W_{0.30}$, $G_{50}A_{12}W_{0.35}$, and $G_{75}A_{16}W_{0.40}$, to observe and compare the microstructural changes with the proposed optimized mix i.e., $G_{75}A_{13.75}W_{0.34}$.

6.5.1 SEM morphology and EDS analysis

The SEM micrographs and EDS results of the selected OPGCs are shown in Figure 6.11. The SEM and EDS micrographs of selected mixes are $G_{25}A_8W_{0.30}$, $G_{50}A_{12}W_{0.35}$, and $G_{75}A_{16}W_{0.40}$, are shown in Figure 6.11a, b, and c, respectively. To observe the microstructural changes in proposed optimized mix of $G_{75}A_{13.75}W_{0.34}$, the SEM and EDS micrographs are shown in Figure 6.11d. In Figure 6.11a, it is clear that many fly ash particles are either unreacted or only partially reacted because the mixture lacks the necessary activator and water content for the reaction to take place. However, the particles that come into contact with the activator are able to react with the available water and produce the gelatinous products necessary for development of early and later age strength, even though the mix with lower activator content fails to sufficiently distribute the activator over the entire volume of the mix. As can be seen in Figure 6.11a, only a small fraction of GGBS particles can be detected. The GGBS have a high Ca concentration, hence the lack of Ca in this blend prevents them from gaining strength. However, few voids are identified in the micrograph, which can be later reasoned for strength decline in the mix. The mixture exhibited a uniform and consolidated appearance as the level of GGBS replacement, activator concentration,

and w/GS ratio increased, as depicted in Figure 6.11b. Noticeably, a significant proportion of fly ash and GGBS particles have undergone a complete reaction and are incorporated into the gelatinous products.

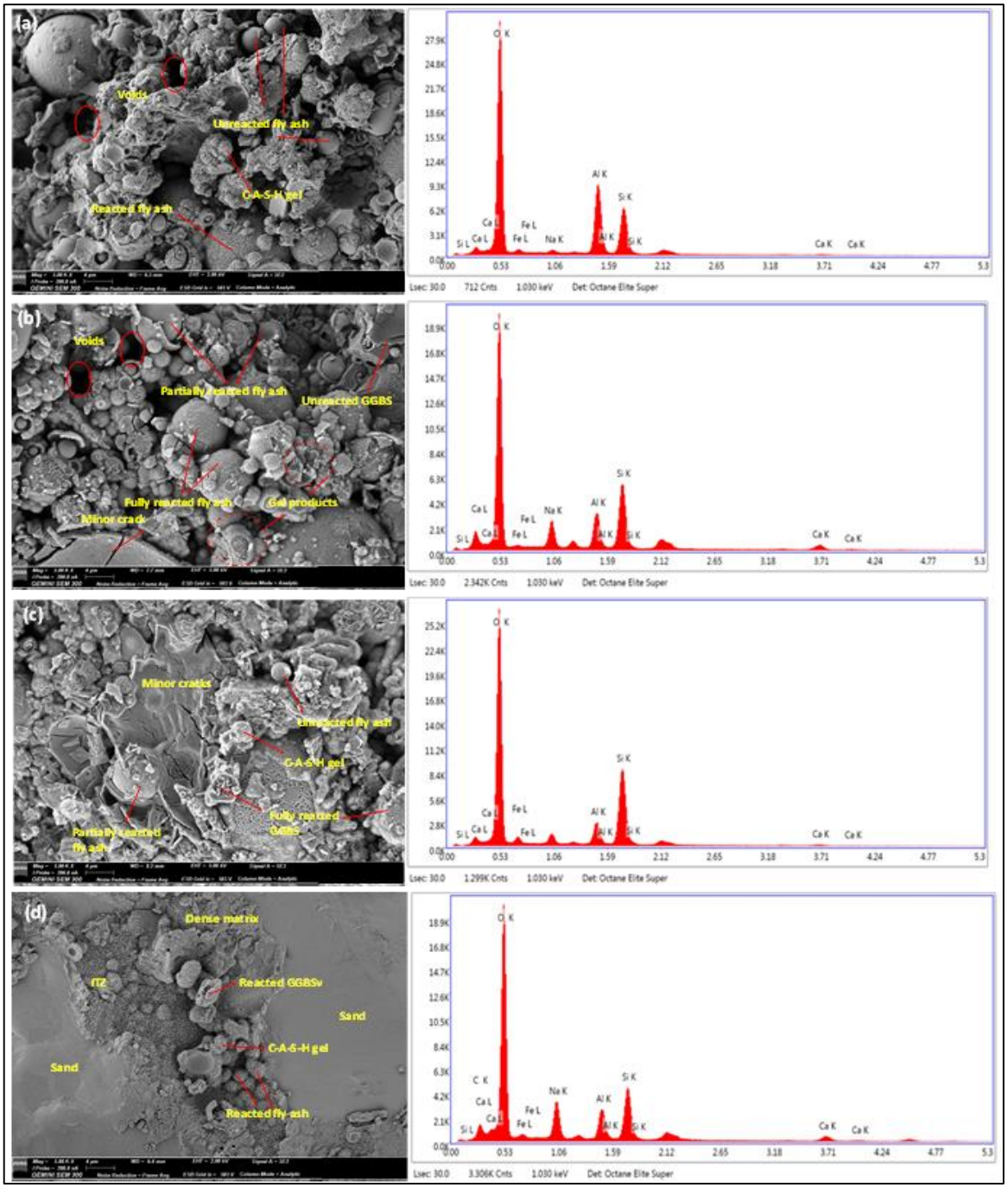

Figure 6.11 SEM micrographs and EDS analysis of OPGCs a) $G_{25}A_8W_{0.30}$ b) $G_{50}A_{12}W_{0.35}$ c) $G_{75}A_{16}W_{0.40}$, and d) $G_{75}A_{13.75}W_{0.34}$.

The partially reacted fly ash contained within a non-homogeneous gel matrix can be observed in SEM micrographs having higher water content. Further, in Figure 6.11c, it is clear that an increase in the W/GS ratio results in a much higher concentration of unreacted particles compared to the ideal W/GS ratio mixture. This certainly accounts for the dramatic loss in mechanical strength when more water was added to the mixtures, as the W/GS ratios for these samples are much greater. These results agree with previous studies (Ban et al. 2017). As the water evaporates during polycondensation, the resulting uneven internal pressure weakens the matrix and increases the number of voids, ultimately reducing the material's strength (Das and Rout 2021). A compact and uniform matrix is observed when combined with a higher concentration of activator. Nevertheless, it was observed that there were longer micro-cracks, as depicted in Figure 6.11c. The observed cracks can be ascribed to the elevated concentration of Na_2O in the system at higher levels of activator dosage, leading to an augmented heat generation during the process of polymerization. Consequently, the increase in concentration of ionic species hinders the movement of ions, thereby decelerating the formation of coagulated structures.

The occurrence of gelatinous product development with increased activator concentration in the mixture is evident, despite the existence of longer fractures. Figure 6.11c and d exhibits a matrix that is both dense and uniform, characterised by a compacted microstructure. This particular microstructural attribute is known to enhance the overall strength of the material. The observed increase in GGBS concentration within the mixture is directly associated with this phenomenon. The level of homogeneity observed in the gel clusters of proposed optimized mix is similar to that of the mixture containing a higher proportion of GGBS, observed in Figure 6.11d. The gel products have a larger concentration of calcium in mixtures containing a greater proportion of GGBS. Additionally, the gel products contain aluminium and silica phases, which are consistent with the presence of C-(N)-A-S-H gels, as observed in previous research (Vu et al. 2020; Yousefi Oderji et al. 2019; Zhang et al. 2021). It can be noticed in Figure 6.11d, the densified gelatinous products generated in the forming a strong interface transitional zone (ITZ) zone between sand and binder particles are clearly visible. Nevertheless, the proposed optimized mix combination demonstrates dense and compact microstructures, characterised by a reduced presence of unreacted

particles and improved gel clusters where these factors contribute to the enhanced strength of the OPGCs in comparison to alternative mixtures.

The chemical analysis findings conducted using EDS indicate that the products exhibit a significant presence of calcium, silica, aluminium, and sodium phases, characterised by interparticle linkages between these elements. The presence of these compounds serves as an indication of the existence of C-(N)-A-S-H gels. The mixture containing a high proportion of GGBS exhibits elevated levels of Ca and silicon Si elements in comparison to other mixtures containing 50% GGBS content. This suggests that an increased presence of GGBS in the system results in the production of a greater quantity of gelatinous substances within the mixture, which play a crucial role in the development of strength in the OPGCs. The Ca/Si ratio and Al/Si of proposed optimized mix $G_{75}A_{13.75}W_{0.34}$ mix are 0.72 and 0.77, respectively. This indicates that C-A-S-H gel is present that increases the strength and produce compact microstructures. Nevertheless, as depicted in Figure 6.11 (a, b, c, and d), there were detectable residues of Ca, Fe, and Mg present in excess quantities within the mixture. These remaining traces did not entirely dissolve during the reaction process and had the identical composition and form as typical geopolymers. These findings align with previous research findings (Puligilla and Mondal 2013). The findings of the SEM and EDS analysis provide support for the optimisation technique, demonstrating the accuracy of developing optimal mix proportions that yield improved engineering attributes and microstructure characterizations.

6.5.2 XRD – Phase analysis

The XRD peaks of hardened OPGCs specimens at 28 days of curing are shown in Figure 6.12. The XRD spectra of the samples were obtained for diffraction angle 2θ = 10° - 70°. The XRD spectra of the aluminosilicate precursors exhibited higher peak intensities in comparison to the observed spectra, indicating a substantial reduction in peak intensities. This suggests that a moderate quantity of reactivity has taken place between the components. The XRD spectra revealed the presence of novel crystalline peaks, which arise during the process of geopolymerization. The hardened concrete exhibits notable crystalline phases, including quartz and mullite, which align with the crystalline phases found in the fly ash. This observation suggests that not all

fly ash particles are actively participating in the reaction and remain unreacted. Moreover, the lack of several distinct peaks observed in the XRD pattern of hardened OPGCs, in contrast to fly ash, indicates the occurrence of geopolymerization. During the process of geopolymerization, specific crystalline structures undergo a transformation into amorphous inorganic substances.

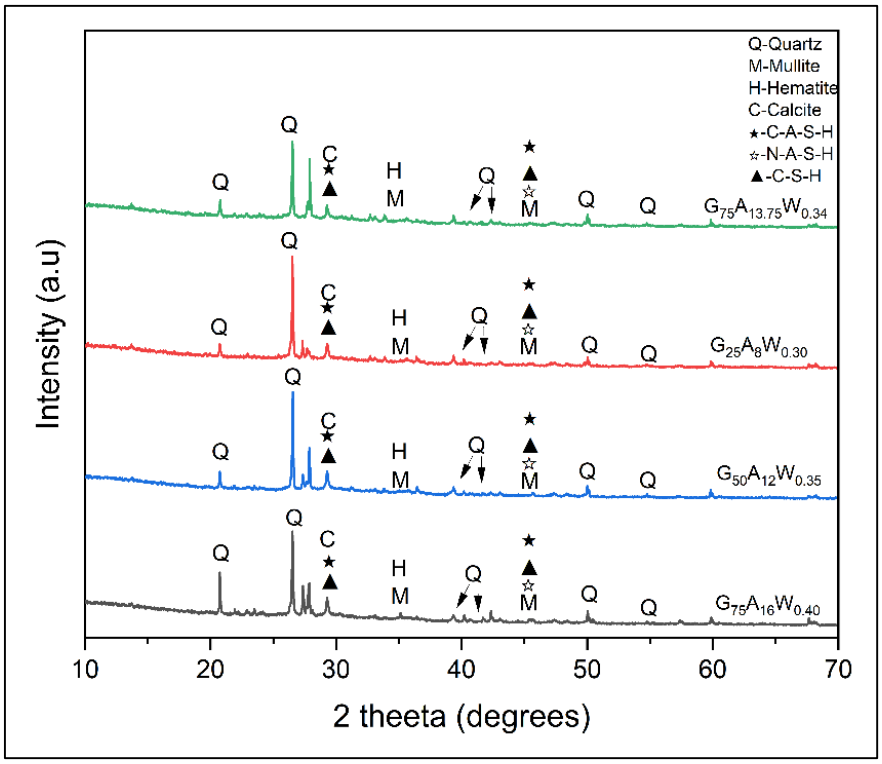

Figure 6.12 XRD spectra of OPGCs ($G_{75}A_{13.75}W_{0.34}$, $G_{25}A_{8}W_{0.30}$, $G_{50}A_{12}W_{0.35}$, $G_{75}A_{16}W_{0.40}$) after 28 days of ambient curing.

The XRD spectra of the OPGC mixes revealed the presence of amorphous phases, which were observed within the 20° 2θ to 40° 2θ range. This finding indicates the formation of alkaline aluminosilicate geopolymer gels in the processed aluminosilicates. The sole discernible differentiation among the peaks of the mixture is an alteration in the strength of the peak, occurring approximately at 29° 2θ. This alteration bears similarity to the presence of the C-S-H gel, alongside the calcium carbonate phase. The X-ray XRD spectra revealed the existence of novel crystalline phases associated with the Ca or Na aluminosilicate complex, known as C-(N)-A-S-H. The aforementioned stages play a crucial role in enhancing the strengths of OPGC mixtures, consistent with findings from earlier studies (Kim et al. 2013; Lee and

Lee 2015). The OPGC mix with high dosage of activator and GGBS content exhibited better peak intensities indicating the formation of C-(N)-S-H alongside C-S-H gel. However, excessive activator dosage results in gels with rather high crystallinity (Ban et al. 2017; Guo et al. 2019; Prusty and Pradhan 2020). The proposed optimized mix demonstrate comparable peak intensities in the presence of gelatinous products, suggesting a reduction in unreacted aluminosilicate precursors. Additionally, a decrease in crystalline peaks indicates a more compact and dense microstructure, as revealed through SEM analysis.

6.5.3 TGA/DTG analysis

The thermogravimetric analysis (TGA) and differential thermogravimetry (DTG) analysis of the selected OPGC mixes are shown in Figure 6.13. The use of TGA and DTG provides additional confirmation for the reaction products in OPGC mixes. The weight loss in TGA was considered from temperatures ranging 50 °C to 900 °C. At a temperature of around 900 °C, the mixture $G_{75}A_{16}W_{0.40}$ demonstrates the most significant weight reduction of 26%. However, the disparities in the overall weight reductions of the remaining three combinations are rather insignificant. The TGA curves of OPG systems exhibit three prominent stages of weight loss. The first stage, which takes place up to 250 °C, is characterised by the reduction in weight due to the evaporation of both free and bound water present in gelatinous products. The second stage, occurring between 250 to 600 °C, is primarily attributed to the elimination of chemically-bonded water and the dehydroxylation process of solid phases similar to hydrotalcite. Finally, the third stage, observed above 600 °C, signifies the decomposition of calcite phases and the transformation of gelatinous products into certain crystalline phases, which agree with the findings of earlier research reported (Abdollahnejad et al. 2020a; Adesanya et al. 2020; Alzaza et al. 2021; Ma et al. 2019). The mix G25A8W0.30 exhibits a comparatively reduced rate of mass loss during its initial phases, followed by a substantial increase in mass loss during the later stages. The weight reduction up to a temperature of 250 °C encompasses the loss of moisture that is chemically bound inside a gelatinous substance, which exhibits similarities to the presence of C-(N)-A-S-H gels. This weight loss can be utilised as a measurable indicator of the level of hydration, as it is strongly associated with the C-(N)-A-S-H

gels (Ren et al. 2021). Upon reaching a temperature of 250 °C, the rate of mass loss exhibited a deceleration, which can be attributed to the existence of chemically linked water and hydroxyl (OH) groups. The DTG curves of OPGCs exhibit a distinct peak at approximately 100 °C, which has resemblance to the thermal behaviour of gelatinous minerals. The observed endothermic peak can be ascribed to the process of dehydration occurring in the C-(N)-A-S-H gels within the OPGCs (Alzaza et al. 2021). The presence of discrepancies in the prominent endothermic peaks found in the DTG curves indicates the possibility of extra gel formation occurring as a result of differences in the composition of OPGC mixes. An additional endothermic peak observed at around 400-500 °C signifies the dehydroxylation process of hydrotalcite-like solid phases. The XRD spectra exhibit the observation of calcite phases undergoing decomposition, as indicated by a small decline in temperature after reaching 700 °C. The findings obtained from TGA and DTG indicate that a substantial quantity of gel products are produced, the transition of gels to crystalline phases occurs, and the decomposition of residues takes place at elevated temperatures in OPGC mixes.

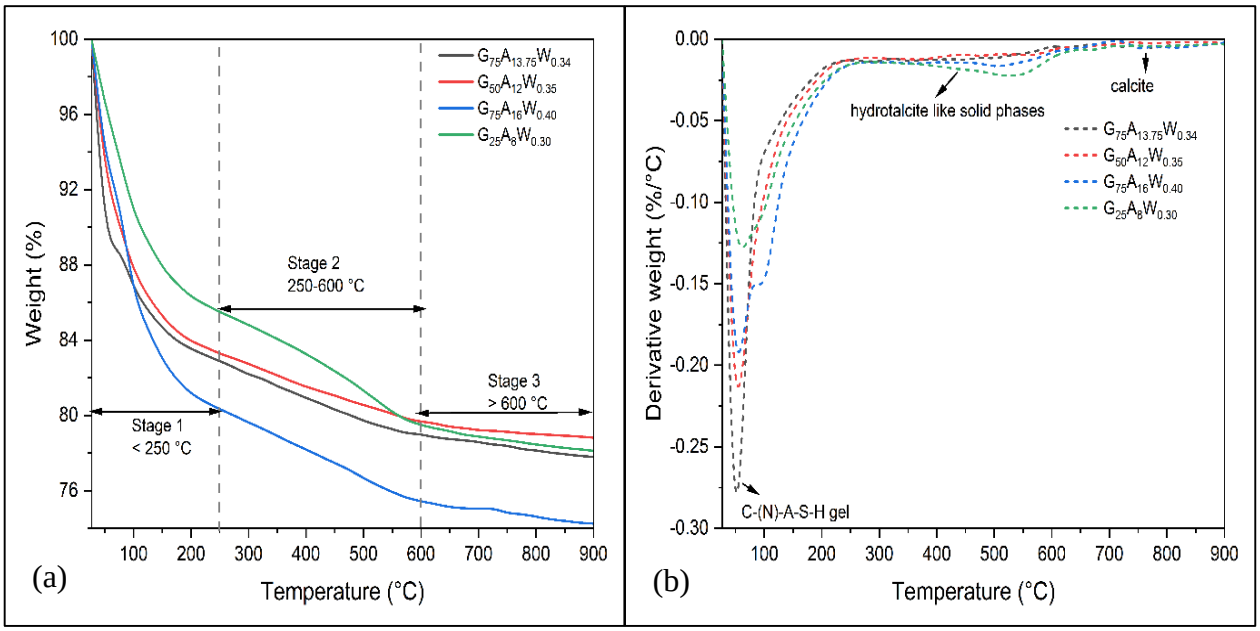

Figure 6.13 a) TGA and b) DTG of OPGCs ($G_{75}A_{13.75}W_{0.34}$, $G_{25}A_{8}W_{0.30}$, $G_{50}A_{12}W_{0.35}$, $G_{75}A_{16}W_{0.40}$) after 28 days of ambient curing.

6.5.4 FTIR – Chemical analysis

The FTIR spectra acquired for the purpose of investigating the behaviour and reaction of Si and aluminium Al species, as well as Ca compounds from precursors, during their interaction with solid activators in OPGC mixes are shown in Figure 6.14. The frequency range of the identified peaks extended from 1649 cm^{-1} to 536 cm^{-1}, suggesting the existence of slag particles within the one-part geopolymers. The presence of the asymmetric bending vibration of Si-O-Si at about 536 cm^{-1} and the Al-O bond at 778 cm^{-1} in OPGC mixes after 28 days can be attributed to the presence of unreacted precursor materials.

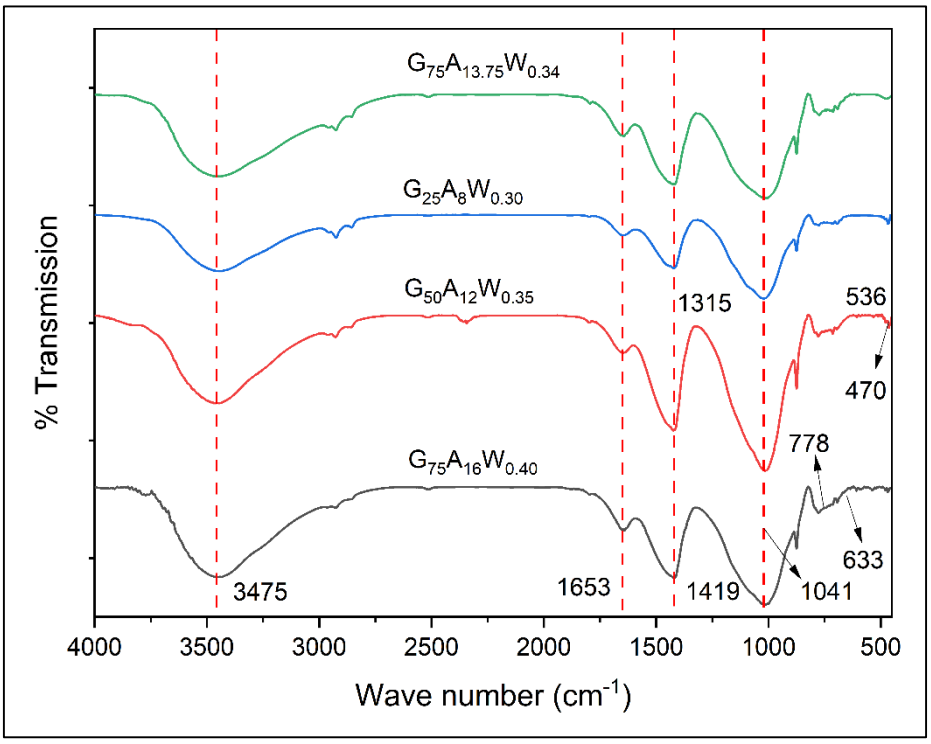

Figure 6.14 FTIR spectra of OPGCs ($G_{75}A_{13.75}W_{0.34}$, $G_{25}A_{8}W_{0.30}$, $G_{50}A_{12}W_{0.35}$, $G_{75}A_{16}W_{0.40}$) after 28 days of ambient curing.

The FTIR spectra reveal a broad stretching vibration spanning from 633 cm^{-1} to 1315 cm^{-1}, with a prominent peak at 1041 cm^{-1}. This peak is typically associated with the (Si-O-Si) and (Si-O-Al) groups. The peaks indicate the reactivity degree exhibited by the source constituents, a phenomenon frequently observed in silicate compounds. These findings support the formation and growth of C-(N)-A-S-H gels (Askarian et al. 2019; Liu et al. 2020; Ma et al. 2019). Nevertheless, the primary vibrational peak at

approximately 1041 cm^{-1} can be attributed to the presence of fly ash. The vibrational mode associated with the asymmetric stretching of Si-O-Si(Al) bonds is correlated with these vibrational phenomena (Jang and Lee 2016; Liu et al. 2016). The precise wavenumber shift and the extent of the change depend on the Si/Al ratio of the precursors and the conditions of the reaction. The intensity range may be related to the yield of reaction products, with the formation of a geopolymeric network having a negligible effect (Zhang et al. 2017). The band at 1419 cm^{-1} is consistent with the stretching vibration of CO_3^{2-}, indicating the presence of carbonate groups in the OPGC mixes (Puligilla and Mondal 2015). H-OH groups are responsible for the stretching vibration between 3200 and 3750 cm^{-1}, which is evidence of the presence of alkali hydroxides (Ma et al. 2019). The presence of water molecules and the activator, solid anhydrous sodium metasilicate, cause symmetric bending vibrations of O-Si-O bonds, which in turn form the absorption peak at 536 cm^{-1}. O-H stretching and SiO_4 tetrahedral deformations are represented by stretching vibrations at 1653 cm^{-1} and bending vibrations at 470 cm^{-1}, respectively (Shah et al. 2020). The FTIR of OPGCs are consistent across a wide range of conditions; the degree of reverberation, which is linked to the gelatinous products created during polymerization, varies. Moreover, the FTIR spectrum of the proposed optimized mixture $G_{75}A_{13.75}W_{0.34}$ exhibits peaks that align with the findings from SEM and XRD analyses, indicating the presence of C-(N)-A-S-H gel.

6.6 ECOLOGICAL AND COST ANALYSIS OF OPGC MIXES

The ecological impacts of concretes were assessed by calculating the embodied energy (EE) and embodied carbon dioxide emission (ECO_2e) associated with them. The EE refers to the amount of energy consumed, while ECO_2e represents the quantity of CO_2 emissions generated during the many stages of a product's life cycle, including raw material extraction, transport, manufacturing, assembly, installation, disassembly, and deconstruction. The data on EE, ECO_2e and cost per unit kg of raw materials used in the development of OPGC mixes are given in Table 6.6 obtained by previous literature (Mithun and Narasimhan 2016; Yaragal et al. 2020) (Xu et al. 2021). The total EE, ECO_2e and cost for the selected OPGC mixes are shown in Figure 6.15. The EE and ECO_2e increases with increase in activator content and GGBS. However, the role water

shows negligible variations in the EE and ECO_2e of OPGC mixes. The cost of OPGC mixes per cubic meter is highly relay on the activator dosage since the cost of activator is high. The OPGC mix with lower level of factors shows less EE, ECO_2e and cost whereas the mix with higher level of factors shows high EE, ECO_2e and cost. The proposed optimization mix shows EE of 1323 MJ/m^3, ECO_2e 155 ECO_2e/m^3, and cost of 106 $\$/m^3$. However, these parameters are less compared to OPC based concrete reported in the literature (Mithun and Narasimhan 2016). Hence OPGC mixes can be considered are eco-friendly materials. The cost OPGC is 15-25% more compared to OPC based concrete, which is in line with earlier reports (Luukkonen et al. 2018a).

Table 6.6 EE, ECO_2e and material costs of raw ingredients.

Raw materials	EE in MJ per kg	ECO_2e in $kgCO_2e$ per kg	Cost in $ per ton
GGBS	1.6	0.083	26
Fly ash	0.1	0.01	3.6
Activator	8.93	1.86	1200
FiAg	0.081	0.0051	12
CoAg	0.083	0.0048	12
Water	0.2	0.0008	0.12

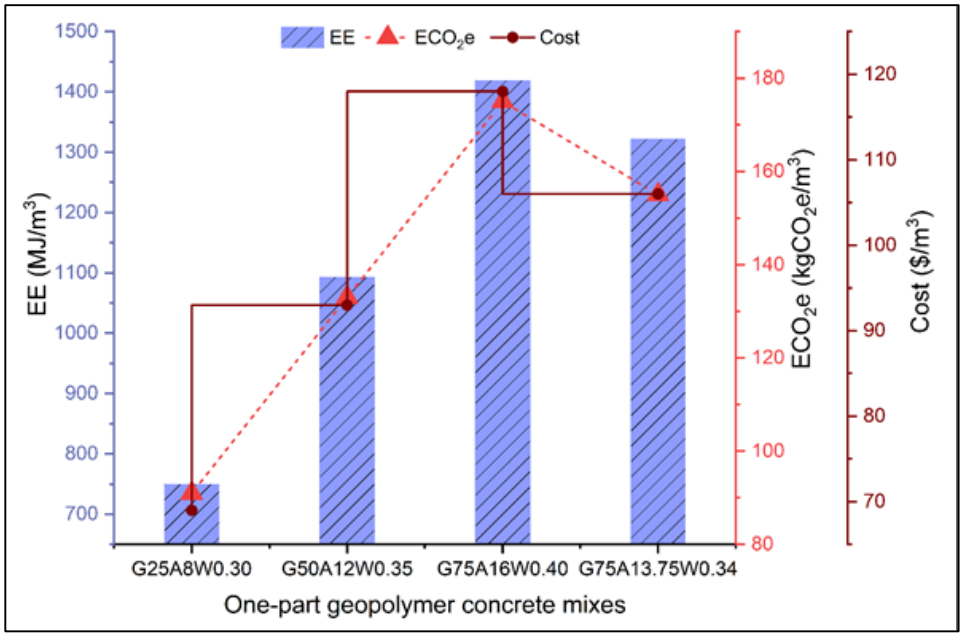

Figure 6.15 EE (MJ/m^3), ECO_2e (ECO_2e/m^3) and cost ($\$/m^3$) of OPGC ($G_{75}A_{13.75}W_{0.34}$, $G_{25}A_8W_{0.30}$, $G_{50}A_{12}W_{0.35}$, $G_{75}A_{16}W_{0.40}$) mixes.

6.7 CLOSURE

In this chapter the experimental evaluation and optimization of one-part geopolymer concretes are reported. The fresh and hardened properties of one-part geopolymer concrete mixes and their correlations are obtained and reported. Further, the microstructural characterization studies like SEM, XRD, TGA and FTIR are reported with respect to the microstructural changes, mineral phases, thermal mass loss and molecular bonding of one-part geopolymer concrete mixes. Finally, the ecological and cost analysis studies are discussed.

CHAPTER 7

PERFORMANCE OF ONE-PART GEOPOLYMER MIXES AT ELEVATED TEMPERATURES

7.1 GENERAL

Concrete can be exposed to high temperatures when employed in the construction of furnaces and reactors. Elevated temperatures can have a detrimental impact on concrete by causing a breakdown in the bonds among hydration products, leading to a reduction in its compressive strength. This decrease in compressive strength can subsequently affect various other mechanical properties of the concrete. Therefore, investigating the concrete performance at elevated temperatures is essential to determine its suitability for use in furnaces and reactors and to assess its condition when exposed to higher temperatures. The present study discusses about the performance of OPG mixes when it is exposed to elevated temperatures ranging from 200 ℃ to 800 ℃.

In the course of the performance studies on OPG mixtures, to observe the higher temperature effect on activator dosage, a fixed composition was established for OPG paste system comprising fixed amount of aluminosilicate precursors and W/GS ratio with varied activator content. OPG paste developed with optimum mix proportions is also considered for the study. The Details of mix proportions of OPG pastes are presented in Table 7.1. The percentage of weight loss and residual compressive strengths were recorded for the OPG pastes.

Table 7.1 Mix proportions of OPG pastes considered for elevated temperature studies.

Sl. No	Mix ID	Fly ash (%)	GGBS (%)	Activator (%)	W/GS
1	$G_{50}A_{8}W_{0.30}$	50	50	8	0.30
2	$G_{50}A_{12}W_{0.30}$	50	50	12	0.30
3	$G_{50}A_{16}W_{0.30}$	50	50	16	0.30
4	$G_{51.39}A_{12.35}W_{0.32}$	48.61	51.39	12.35	0.32

Further, the effect of elevated temperatures on OPG mortars and OPG concretes are studied for the mixes presented in Table 7.22 and Table 7.3, respectively. The weight loss and residual compressive strengths for OPG mortars and concretes. Additionally ultrasonic pulse velocity values were recorded for OPG concrete mixes only. The test specimen were subjected to elevated temperatures ranging from 200 ℃ to 800 ℃ using programmable electrical muffle furnace. Total 60 OPG mixes were considered for the elevated temperatures study. Detailed methodology on conducting elevated temperature studies can be obtained in the methodology chapter.

Table 7.2 Mix proportions of OPG mortars considered for elevated temperature studies.

Sl. No	Mix ID	FA (%)	GGBS (%)	Activator (%)	W/GS	FA (kg/m^3)	GGBS (kg/m^3)	Activator (kg/m^3)	Water (kg/m^3)	Sand (kg/m^3)
1	$G_{25}A_8W_{0.35}$	75	25	8	0.35	569.3	245.4	70.8	309.9	1943
2	$G_{50}A_8W_{0.35}$	50	50	8	0.35	379.5	490.8	75.7	331.1	1943
3	$G_{75}A_8W_{0.35}$	25	75	8	0.35	189.8	736.2	80.5	352.3	1943
4	$G_{25}A_{12}W_{0.35}$	75	25	12	0.35	544.5	234.7	106.3	309.9	1943
5	$G_{50}A_{12}W_{0.35}$	50	50	12	0.35	363.0	469.5	113.5	331.1	1943
6	$G_{75}A_{12}W_{0.35}$	25	75	12	0.35	181.5	704.2	120.8	352.3	1943
7	$G_{25}A_{16}W_{0.35}$	75	25	16	0.35	519.8	224.1	141.7	309.9	1943
8	$G_{50}A_{16}W_{0.35}$	50	50	16	0.35	346.5	448.1	151.4	331.1	1943
9	$G_{75}A_{16}W_{0.35}$	25	75	16	0.35	173.3	672.2	161.0	352.3	1943
10	$G_{25}A_8W_{0.40}$	75	25	8	0.40	569.3	245.4	70.8	354.2	1943
11	$G_{50}A_8W_{0.40}$	50	50	8	0.40	379.5	490.8	75.7	378.4	1943
12	$G_{75}A_8W_{0.40}$	25	75	8	0.40	189.8	736.2	80.5	402.6	1943
13	$G_{25}A_{12}W_{0.40}$	75	25	12	0.40	544.5	234.7	106.3	354.2	1943
14	$G_{50}A_{12}W_{0.40}$	50	50	12	0.40	363.0	469.5	113.5	378.4	1943
15	$G_{75}A_{12}W_{0.40}$	25	75	12	0.40	181.5	704.2	120.8	402.6	1943
16	$G_{25}A_{16}W_{0.40}$	75	25	16	0.40	519.8	224.1	141.7	354.2	1943
17	$G_{50}A_{16}W_{0.40}$	50	50	16	0.40	346.5	448.1	151.4	378.4	1943
18	$G_{75}A_{16}W_{0.40}$	25	75	16	0.40	173.3	672.2	161.0	402.6	1943
19	$G_{25}A_8W_{0.45}$	75	25	8	0.45	569.3	245.4	70.8	398.5	1943
20	$G_{50}A_8W_{0.45}$	50	50	8	0.45	379.5	490.8	75.7	425.7	1943
21	$G_{75}A_8W_{0.45}$	25	75	8	0.45	189.8	736.2	80.5	452.9	1943
22	$G_{25}A_{12}W_{0.45}$	75	25	12	0.45	544.5	234.7	106.3	398.5	1943
23	$G_{50}A_{12}W_{0.45}$	50	50	12	0.45	363.0	469.5	113.5	425.7	1943
24	$G_{75}A_{12}W_{0.45}$	25	75	12	0.45	181.5	704.2	120.8	452.9	1943
25	$G_{25}A_{16}W_{0.45}$	75	25	16	0.45	519.8	224.1	141.7	398.5	1943
26	$G_{50}A_{16}W_{0.45}$	50	50	16	0.45	346.5	448.1	151.4	425.7	1943
27	$G_{75}A_{16}W_{0.45}$	25	75	16	0.45	173.3	672.2	161.0	452.9	1943
28	$G_{49.81}A_{13.60}W_{0.37}$	50.19	49.81	13.6	0.37	487.2	491.5	154.4	419.6	1943

Table 7.3 Mix proportions of OPG concretes considered for elevated temperature studies.

Mix ID	Fly ash (%)	GGBS level (%)	Activator (%)	W/GS	Fly ash (kg/m^3)	GGBS (kg/m^3)	Activator (kg/m^3)	Fine aggregate (kg/m^3)	Coarse aggregate (kg/m^3)		Water (kg/m^3)
									20-10 mm	10-4.75 mm	
$G_{25}A_8W_{0.30}$	75	25	8	0.3	317	139	36	616	704	469	137
$G_{50}A_8W_{0.30}$	50	50	8	0.3	197	260	36	626	716	477	137
$G_{75}A_8W_{0.30}$	25	75	8	0.3	92	364	36	639	730	487	137
$G_{25}A_{12}W_{0.30}$	75	25	12	0.3	317	139	54	609	696	464	137
$G_{50}A_{12}W_{0.30}$	50	50	12	0.3	197	260	54	619	708	472	137
$G_{75}A_{12}W_{0.30}$	25	75	12	0.3	92	364	54	632	723	482	137
$G_{25}A_{16}W_{0.30}$	75	25	16	0.3	317	139	73	602	689	459	137
$G_{50}A_{16}W_{0.30}$	50	50	16	0.3	197	260	73	613	701	467	137
$G_{75}A_{16}W_{0.30}$	25	75	16	0.3	92	364	73	626	715	477	137
$G_{25}A_8W_{0.35}$	75	25	8	0.35	317	139	36	594	679	453	160
$G_{50}A_8W_{0.35}$	50	50	8	0.35	197	260	36	605	691	461	160
$G_{75}A_8W_{0.35}$	25	75	8	0.35	92	364	36	617	706	470	160
$G_{25}A_{12}W_{0.35}$	75	25	12	0.35	317	139	54	587	672	448	160
$G_{50}A_{12}W_{0.35}$	50	50	12	0.35	197	260	54	598	684	456	160
$G_{75}A_{12}W_{0.35}$	25	75	12	0.35	92	364	54	611	698	465	160
$G_{25}A_{16}W_{0.35}$	75	25	16	0.35	317	139	73	581	664	443	160
$G_{50}A_{16}W_{0.35}$	50	50	16	0.35	197	260	73	591	676	451	160
$G_{75}A_{16}W_{0.35}$	25	75	16	0.35	92	364	73	604	691	460	160
$G_{25}A_8W_{0.40}$	75	25	8	0.4	317	139	36	572	655	436	183
$G_{50}A_8W_{0.40}$	50	50	8	0.4	197	260	36	583	667	444	183
$G_{75}A_8W_{0.40}$	25	75	8	0.4	92	364	36	596	681	454	183
$G_{25}A_{12}W_{0.40}$	75	25	12	0.4	317	139	54	566	647	431	183
$G_{50}A_{12}W_{0.40}$	50	50	12	0.4	197	260	54	576	659	439	183

$G_{75}A_{12}W_{0.40}$	25	75	12	0.4	92	364	54	589	673	449	183
$G_{25}A_{16}W_{0.40}$	75	25	16	0.4	317	139	73	559	639	426	183
$G_{50}A_{16}W_{0.40}$	50	50	16	0.4	197	260	73	570	651	434	183
$G_{75}A_{16}W_{0.40}$	25	75	16	0.4	92	364	73	582	666	444	183
$G_{75}A_{13.75}W_{0.34}$	25	75	13.75	0.34	92	364	62	611	699	466	156

7.2 PHYSICAL OBSERVATION

Visual observations initially reveal the impact of elevated temperature on OPG specimens. These observations include alterations in color, shifts in dimensions, surface cracks, void formation, and spalling. Subsequently, destructive testing is conducted to assess the residual strength of the specimens. These physical observations serve as fundamental indicators of the extent of specimen deterioration and can be correlated with real-world field conditions. The dimensions of the OPG specimen were documented prior to exposing them to elevated temperatures. No significant distortions were detected in the OPG specimens across all mixes exposed to temperatures as high as 800°C.

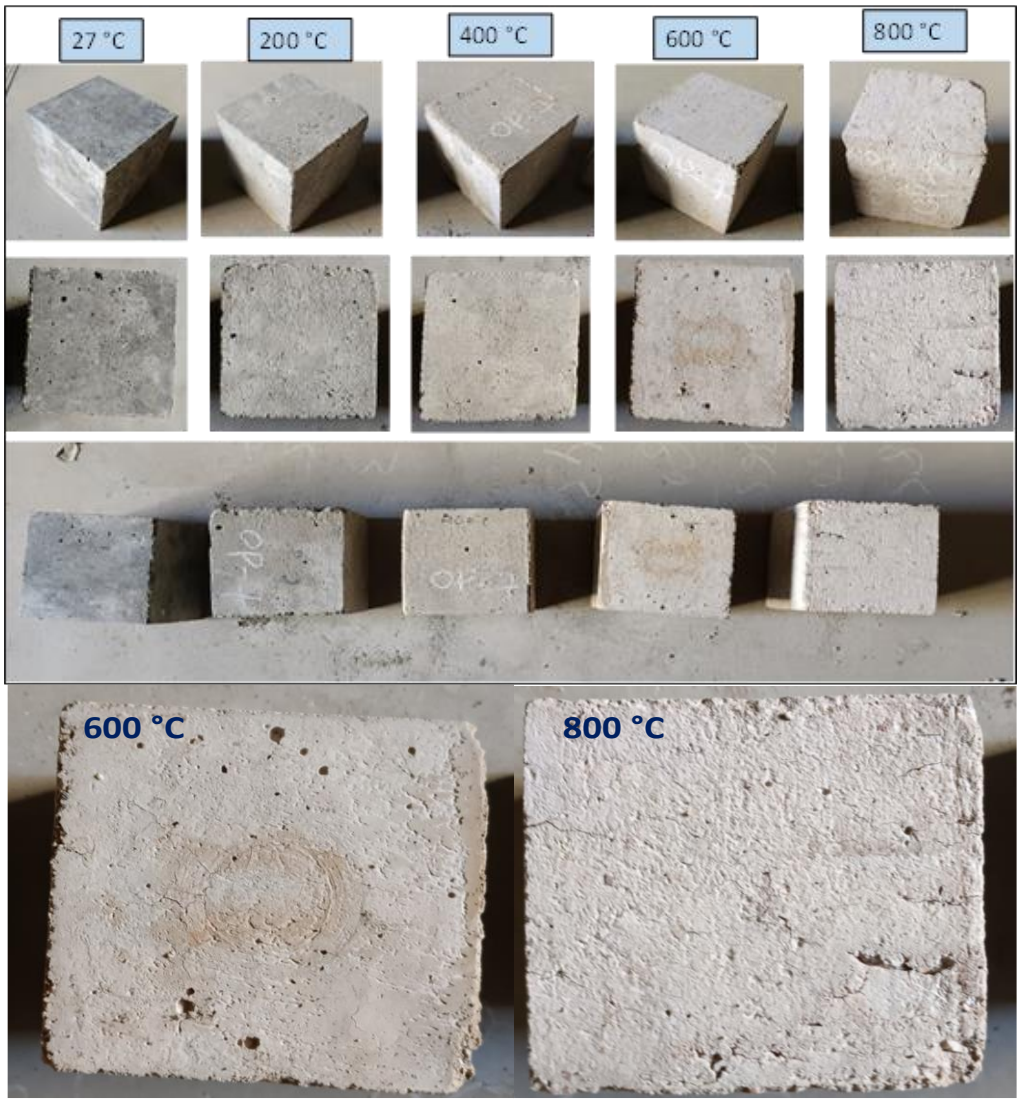

Figure 7.1 OPG concrete specimen after exposure to elevated temperatures.

The OPG specimen exposed to elevated temperatures demonstrates alterations in both color and texture across its surface. The variation in color can be attributed to changes in texture, chemical composition, and the destruction of crystals that occur during elevated temperatures (Yaragal et al. 2012). The images of the OPG concrete specimen of different mixes are presented in Figure 7.1. The alteration in color of the concrete specimen can be observed as the temperature increases from 27 °C to 800 °C, with uniform intervals of 200 °C across all specimens with varying mix proportions. The typical grey hue of the specimen at room temperature gradually fades as the temperature rises, eventually reaching a whitish-grey shade at 400 °C. As the exposure temperature continues to rise, a transition in color from whitish-grey to brownish or yellowish-grey is observed.

During exposure to elevated temperatures, one of the main distresses observed in specimens is spalling, which refers to the significant disintegration or separation of a portion of the specimen from its main body. During the current investigation, spalling is not observed in any specimen across various elevated temperatures. The absence of spalling is attributed to the quality of materials used and the mix proportion employed.

7.3 WEIGHT LOSS OF OPG MIXES AT ELEVATED TEMPERATURES

The weight of OPG mixes exhibits a decreasing trend with escalating temperatures. The weight retention ratios for OPG paste mixes under varying temperature conditions are graphically depicted in Figure 7.2. Notably, OPG paste composed of lower level of activator dosage exhibited the most substantial weight loss, registering an approximate 15% reduction. Conversely, as the activator content increases, better weight retention was observed. The OPG paste developed with optimum mix proportions exhibited better weight retention compared to mixes composed of lower and higher level of activator dosage at elevated temperatures. The average weight loss in mix comprised of lower level of activator dosage is 5, 11, 14, and 17% for 200, 400, 600 and 800 °C, respectively. On other side, the average weight loss in mix with higher level of activator dosage is 4, 10, 12, 14% for 200, 400, 600 and 800 °C, respectively. This decrease in weight loss due to reduced voids in mixes comprised of higher level of activator

dosages. However, the optimum paste mix shows better weight retention at higher rate of temperature not exceeding 15% of weight loss.

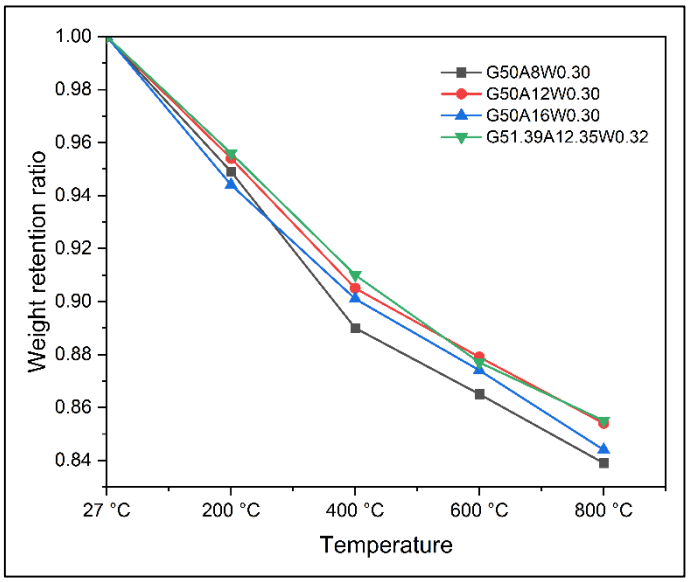

Figure 7.2 Weight retention variation of OPG pastes with temperature.

In case of OPG mortar and concretes, the weight of specimen exhibits a decreasing trend with escalating temperature. The weight retention ratios for OPG mortar and concrete mixes under varying temperature conditions are graphically depicted in Figure 7.3 and Figure 7.4, respectively. It can be observed that, OPG blends composed exclusively of fly ash exhibited the most substantial weight loss, registering an approximate 15% reduction. Conversely, as the GGBS content increases, better weight retention was observed. Specifically, in the case of mixes comprise of higher fly ash content, weight reductions of approximately 5, 10, 14, and 17% were observed at temperatures of 200, 400, 600, and 800 °C, respectively. Contrarily, mixes comprised of higher GGBS content experienced maximum weight losses of 12% at 800°C. It is worth noting that the weight retention in optimum mixes better than that of other blends after exposure to temperatures exceeding 600°C, though the difference is insignificant.

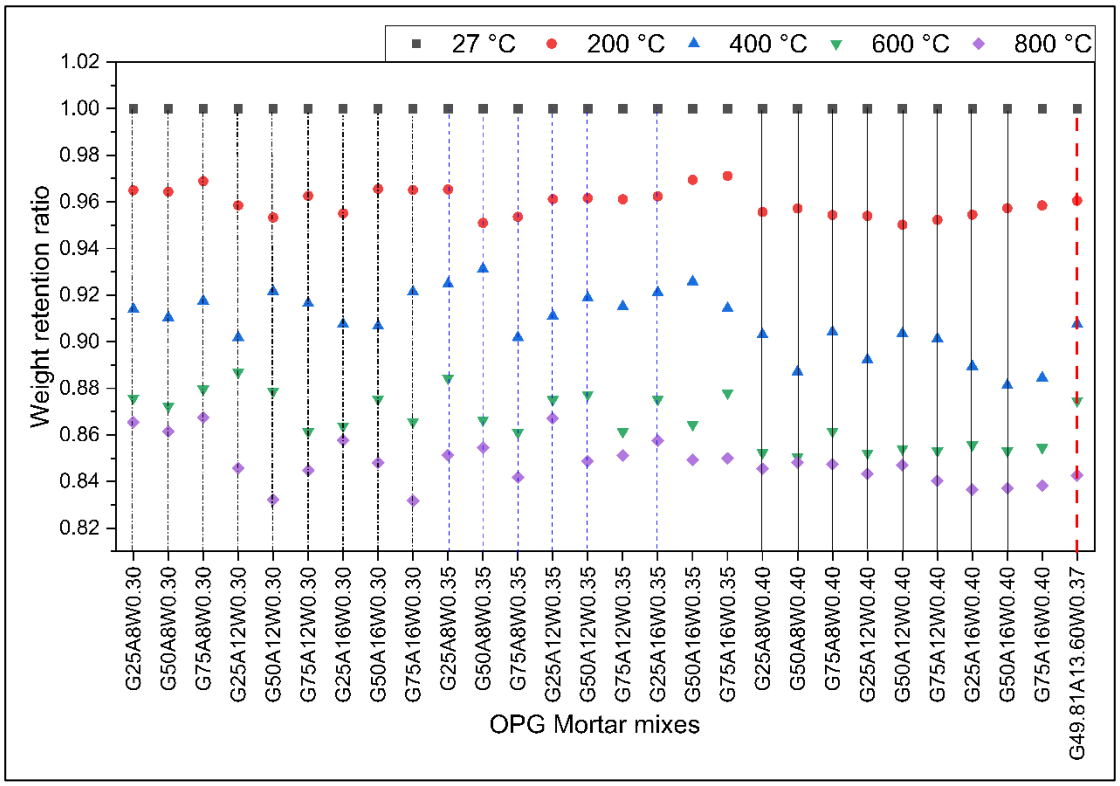

Figure 7.3 Weight retention variation of OPG mortars with temperature.

Approximately 60% of weight loss was uniformly observed across all OPG mixes within the temperature range of 27°C to 400°C. This phenomenon can be attributed to the evaporation of free water present in the mortar and concrete matrix (Burciaga-Díaz and Escalante-García 2017). Beyond 400°C, while the weight loss in OPG mixes continued, the rate of reduction notably decelerated. The weight loss experienced in OPG mixes between 400°C and 600°C can be primarily attributed to the evaporation of chemically bound water within the matrix (Tu and Zhang 2023). Comparatively, the weight loss in mixes comprised of higher W/GS surpasses that of mixes comprised of lower W/GS ratio. However, OPG mortar and concrete mixes produced from obtained optimum mix proportions shows better weight retention at higher rate of temperature not exceeding 15% of weight loss. These mixes possesses a higher C-(N)-A-S- H gel products, owing to its higher GGBS content and sufficient activator dosages for their geopolymerization reaction mechanism.

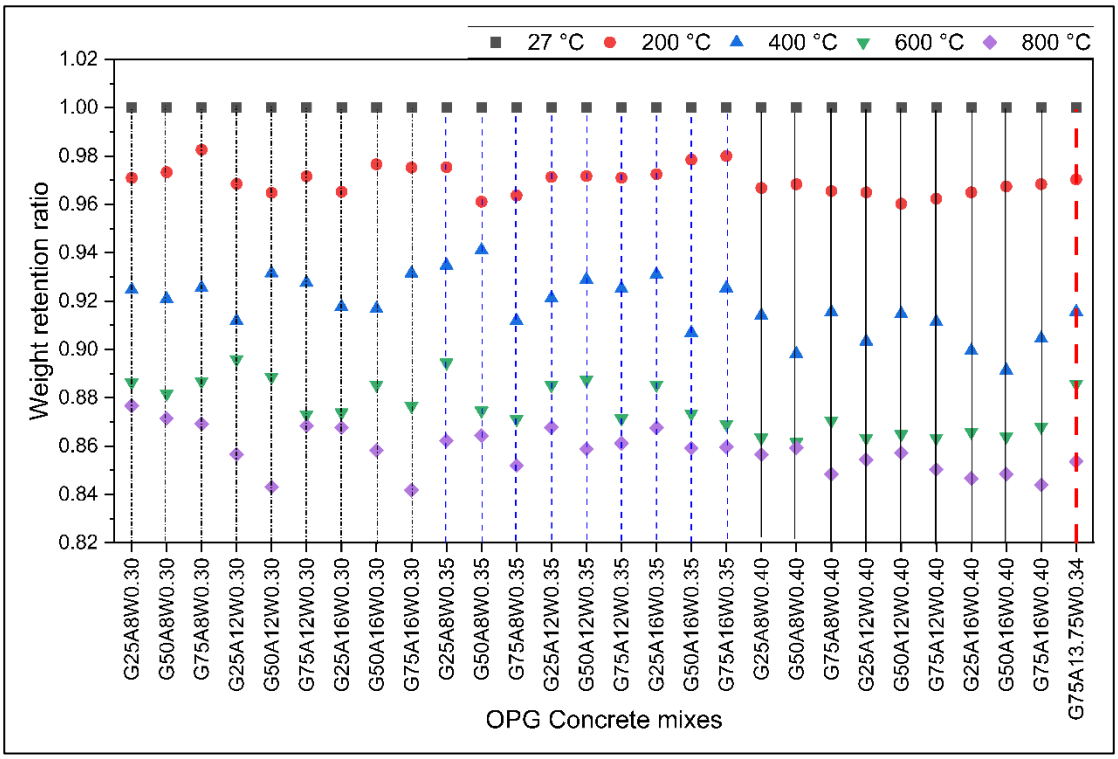

Figure 7.4 Weight retention variation of OPG concretes with temperature.

7.4 ULTRASONIC PULSE VELOCITY (UPV) RESULTS OF OPG MIXES AT ELEVATED TEMPERATURES

UPV test is a non-destructive testing technique to assess the quality of concrete. UPV test was conducted to determine the severity of damage when OPG concrete mixes were exposed to elevated temperatures, and results are presented in Table 7.4. The normalized UPV values of all mixes at elevated temperatures are presented in Table 7.5. At ambient temperature, the UPV values of the mixes comprising of higher fly ash content exceeds that of the contrary mixes, primarily attributed to the enhanced void-filling characteristics facilitated by the incorporation of fly ash. However, upon exposure to elevated temperatures, the UPV of the all mixes decreases. At a temperature of 27 ℃, the UPV value of the mix $G_{25}A_{12}W_{0.30}$ is 5.16 km/sec, whereas for the mixes $G_{50}A_{12}W_{0.30}$ and $G_{75}A_{12}W_{0.30}$ the UPV values are 5.24 and 5.59 km/sec. It can be observed that as GGBS content increases the UPV values increases when at 12% activator dosage and 0.30 W/GS. The mix comprises of higher GGBS content exhibits dense microstructure after sufficient hydration take place.

Table 7.4 UPV values of OPG mixes at elevated temperatures (in km/sec).

Sl.No	Mixes	Temperature (℃)				
		27	200	400	600	800
1	$G_{25}A_8W_{0.30}$	4.38	4.47	4.21	3.14	2.68
2	$G_{50}A_8W_{0.30}$	4.45	4.85	4.29	3.35	2.67
3	$G_{75}A_8W_{0.30}$	4.56	4.97	4.35	3.61	2.72
4	$G_{25}A_{12}W_{0.30}$	5.16	5.29	4.84	4.12	2.91
5	$G_{50}A_{12}W_{0.30}$	5.24	5.34	4.91	4.35	2.99
6	$G_{75}A_{12}W_{0.30}$	5.59	5.62	5.01	4.48	3.48
7	$G_{25}A_{16}W_{0.30}$	5.04	5.21	4.67	4.02	2.85
8	$G_{50}A_{16}W_{0.30}$	5.14	5.38	4.69	4.14	2.91
9	$G_{75}A_{16}W_{0.30}$	5.24	5.41	4.67	4.18	2.99
10	$G_{25}A_8W_{0.35}$	4.25	4.38	3.97	2.91	1.65
11	$G_{50}A_8W_{0.35}$	4.48	4.85	4.02	2.98	1.79
12	$G_{75}A_8W_{0.35}$	4.5	4.75	4.14	3.14	2.01
13	$G_{25}A_{12}W_{0.35}$	4.76	4.97	4.38	3.48	2.69
14	$G_{50}A_{12}W_{0.35}$	4.98	5.07	4.47	4.01	2.69
15	$G_{75}A_{12}W_{0.35}$	5.47	5.74	5.24	4.29	2.78
16	$G_{25}A_{16}W_{0.35}$	4.85	4.91	4.38	3.21	1.68
17	$G_{50}A_{16}W_{0.35}$	4.67	4.82	4.28	3.69	1.99
18	$G_{75}A_{16}W_{0.35}$	5.38	5.41	4.74	4.15	2.05
19	$G_{25}A_8W_{0.40}$	4.15	4.23	3.67	2.71	1.54
20	$G_{50}A_8W_{0.40}$	4.22	4.29	3.84	2.69	1.62
21	$G_{75}A_8W_{0.40}$	4.34	4.41	3.71	2.79	1.72
22	$G_{25}A_{12}W_{0.40}$	4.46	4.59	4.09	3.51	2.08
23	$G_{50}A_{12}W_{0.40}$	4.21	4.41	3.49	2.65	1.66
24	$G_{75}A_{12}W_{0.40}$	5.18	5.29	4.97	3.97	2.97
25	$G_{25}A_{16}W_{0.40}$	4.58	4.89	4.21	3.35	1.94
26	$G_{50}A_{16}W_{0.40}$	4.98	5.21	4.46	3.63	2.13
27	$G_{75}A_{16}W_{0.40}$	5.26	5.46	4.74	3.98	2.34
28	$G_{75}A_{13.75}W_{0.34}$	5.51	5.65	4.86	4.13	2.98

Notably, at 200 ℃, the UPV values of all the mixes, exhibit an improvement. At 200 ℃, the UPV values of mixes with increasing GGBS content with unaltered W/GS and activator dosages shows increment by 8% and 11% at GGBS level of 50% and 75% respectively. However, at 200 ℃ some of the specimen with a greater content of fly ash shows increment in UPV values which can be attributed to the pozzolanic

activity of fly ash (Ishak et al. 2019). The UPV values of mixes with increasing W/GS ratio irrespective of GGBS and activator dosage shows decrement by 2% and 5% at W/GS ratio of 0.35 and 0.40, respectively compared to mixes with W/GS 0.30. This is due to, the higher water level in the mixes leads to more porous microstructures in OPG concrete. As the temperature continues to rise beyond 200℃, the UPV values of all mixtures exhibit a declining trend. This decrease can be attributed to the formation of internal pores and cracks within the specimen.

Table 7.5 Normalized UPV values at elevated temperatures.

Sl.No	Mixes	Temperature (℃)				
		27	200	400	600	800
1	$G_{25}A_8W_{0.30}$	1	1.021	0.951	0.717	0.612
2	$G_{50}A_8W_{0.30}$	1	1.090	0.942	0.753	0.600
3	$G_{75}A_8W_{0.30}$	1	1.090	0.954	0.792	0.596
4	$G_{25}A_{12}W_{0.30}$	1	1.025	0.938	0.798	0.564
5	$G_{50}A_{12}W_{0.30}$	1	1.019	0.937	0.830	0.571
6	$G_{75}A_{12}W_{0.30}$	1	1.005	0.896	0.801	0.623
7	$G_{25}A_{16}W_{0.30}$	1	1.034	0.927	0.798	0.565
8	$G_{50}A_{16}W_{0.30}$	1	1.047	0.912	0.805	0.566
9	$G_{75}A_{16}W_{0.30}$	1	1.032	0.891	0.798	0.571
10	$G_{25}A_8W_{0.35}$	1	1.031	0.934	0.685	0.388
11	$G_{50}A_8W_{0.35}$	1	1.083	0.897	0.665	0.400
12	$G_{75}A_8W_{0.35}$	1	1.056	0.920	0.698	0.447
13	$G_{25}A_{12}W_{0.35}$	1	1.044	0.920	0.731	0.565
14	$G_{50}A_{12}W_{0.35}$	1	1.018	0.898	0.805	0.540
15	$G_{75}A_{12}W_{0.35}$	1	1.049	0.958	0.784	0.508
16	$G_{25}A_{16}W_{0.35}$	1	1.012	0.903	0.662	0.346
17	$G_{50}A_{16}W_{0.35}$	1	1.032	0.916	0.790	0.426
18	$G_{75}A_{16}W_{0.35}$	1	1.006	0.881	0.771	0.381
19	$G_{25}A_8W_{0.40}$	1	1.019	0.884	0.653	0.371
20	$G_{50}A_8W_{0.40}$	1	1.017	0.910	0.637	0.384
21	$G_{75}A_8W_{0.40}$	1	1.016	0.855	0.643	0.396
22	$G_{25}A_{12}W_{0.40}$	1	1.029	0.917	0.787	0.466
23	$G_{50}A_{12}W_{0.40}$	1	1.048	0.829	0.629	0.394
24	$G_{75}A_{12}W_{0.40}$	1	1.021	0.959	0.766	0.573
25	$G_{25}A_{16}W_{0.40}$	1	1.068	0.919	0.731	0.424
26	$G_{50}A_{16}W_{0.40}$	1	1.046	0.896	0.729	0.428
27	$G_{75}A_{16}W_{0.40}$	1	1.038	0.901	0.757	0.445
28	$G_{75}A_{13.75}W_{0.34}$	1	1.025	0.882	0.750	0.541

It can be observed that, at 400℃ the UPV values of all mixes decreases by approximately 7% compared to their respective UPV values at 27 ℃. Notably, the $G_{75}A_{12}W_{0.30}$, $G_{75}A_{12}W_{0.35}$ and $G_{75}A_{12}W_{0.40}$ mixes exhibit superior performance relative to the other mixtures at a temperature of 400℃, with UPV values of 5.01, 5.24 and 4.97 km/sec, respectively, showing a decrease of approximately 5% compared to their values at 27℃. In contrast, the specimen with lower fly ash content experiences a more pronounced reduction in UPV values.

After being subjected to temperatures of 600 ℃ and 800 ℃, all mixtures experienced a substantial reduction in their UPV values. The primary reason for this reduction is believed to be the formation of internal cracks induced by thermal stresses (Tu and Zhang 2023). It can be observed that, at 600 ℃ and 800 ℃, the UPV values of all mixes decreases by approximately 25-30% and 40-50%, respectively compared to their respective UPV values at 27 ℃. . However, OPG concrete mix produced from obtained optimum mix proportions shows better UPV values at higher rate of temperature not exceeding 50% of decrement at 800 ℃, due to its high compacted and dense microstructures.

Table 7.6 Quality of concrete according to UPV values.

S.no	UPV (km/sec)	Concrete quality grading
1	Above 4.5	Excellent
2	3.5 to 4.5	Good
3	3.0 to 3.5	Medium
4	2.0 to 3.0	Poor
5	Less than 2.0	Very Poor

The quality of the concrete specimen can be classified according to the guidelines outlined in IS:13311(Part 1): 1992, as presented in Table 7.6. Up to 400℃, all mixes fall within the 'Good' quality range. At 600 ℃, some of the mixes fall into the 'poor' quality category, while majority of the mixes maintain UPV values that categorize them as 'Medium' quality. At 800 ℃, majority mixtures classified as 'Very Poor' quality, whereas few mixes remains within the 'Poor' quality range.

Upon analyzing the UPV values, it is evident that the OPG concrete mixtures capable of comfortably withstanding temperatures up to 600 ℃ without a significant decrease in quality. Even at 800 ℃, it performs considerably well.

7.5 RESIDUAL COMPRESSIVE STRENGTH OF OPG MIXES AT ELEVATED TEMPERATURES

All OPG mix specimen were furnace cooled after subjecting to elevated temperatures. The specimen were subjected to compression strength test to record residual compressive strength of OPG mixes. The residual compressive strength of OPG paste, mortar and concrete mixes are shown in Figure 7.5, 7.6, and 7.7 respectively. The residual compressive strength of all OPG mixes are recorded at 27 ℃, 200 ℃, 400 ℃, 600 ℃, and 800 ℃. As shown in Figure 7.5, the residual compressive strength of all OPG paste mixes of varied activator dosage increases by approximately 10%, when the paste specimen were subjected to 200 ℃. After, elevating the temperature to 400 ℃, 600 ℃ and 800 ℃, the residual compressive strength drops by approximately 15%, 50%, and 80%, respectively. It is noteworthy that an increase in the content of activator positively impacts the compressive strength of OPG paste mixes at elevated temperatures.

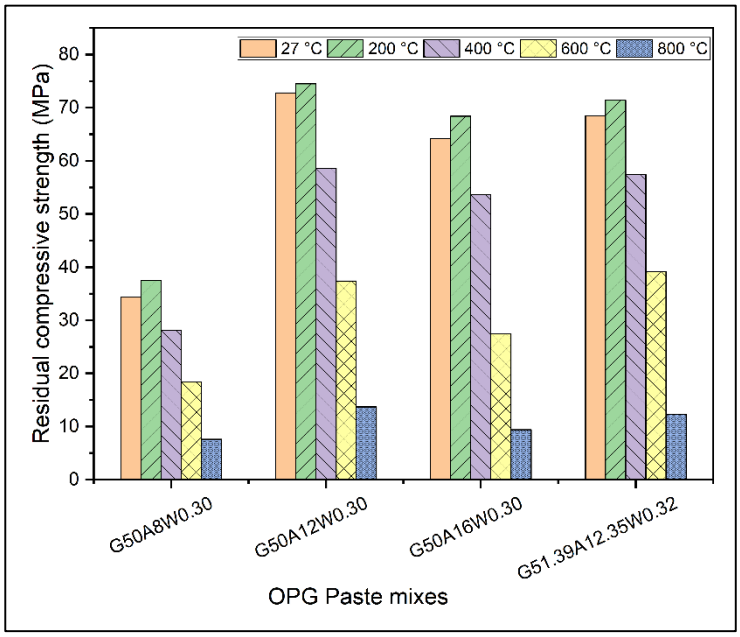

Figure 7.5 Residual compressive strength of OPG Pastes at elevated temperatures.

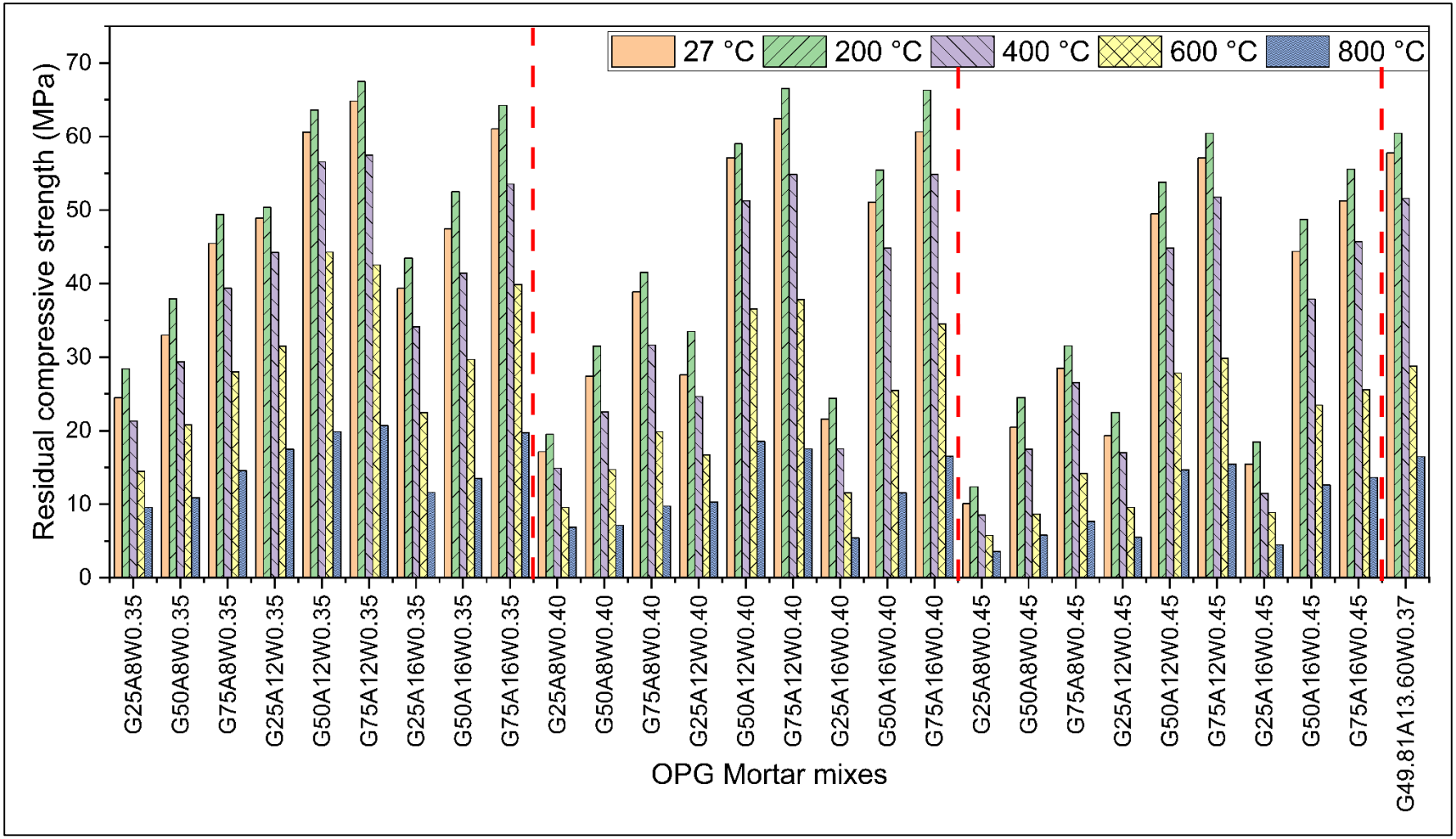

Figure 7.6 Residual compressive strength of OPG mortars at elevated temperatures.

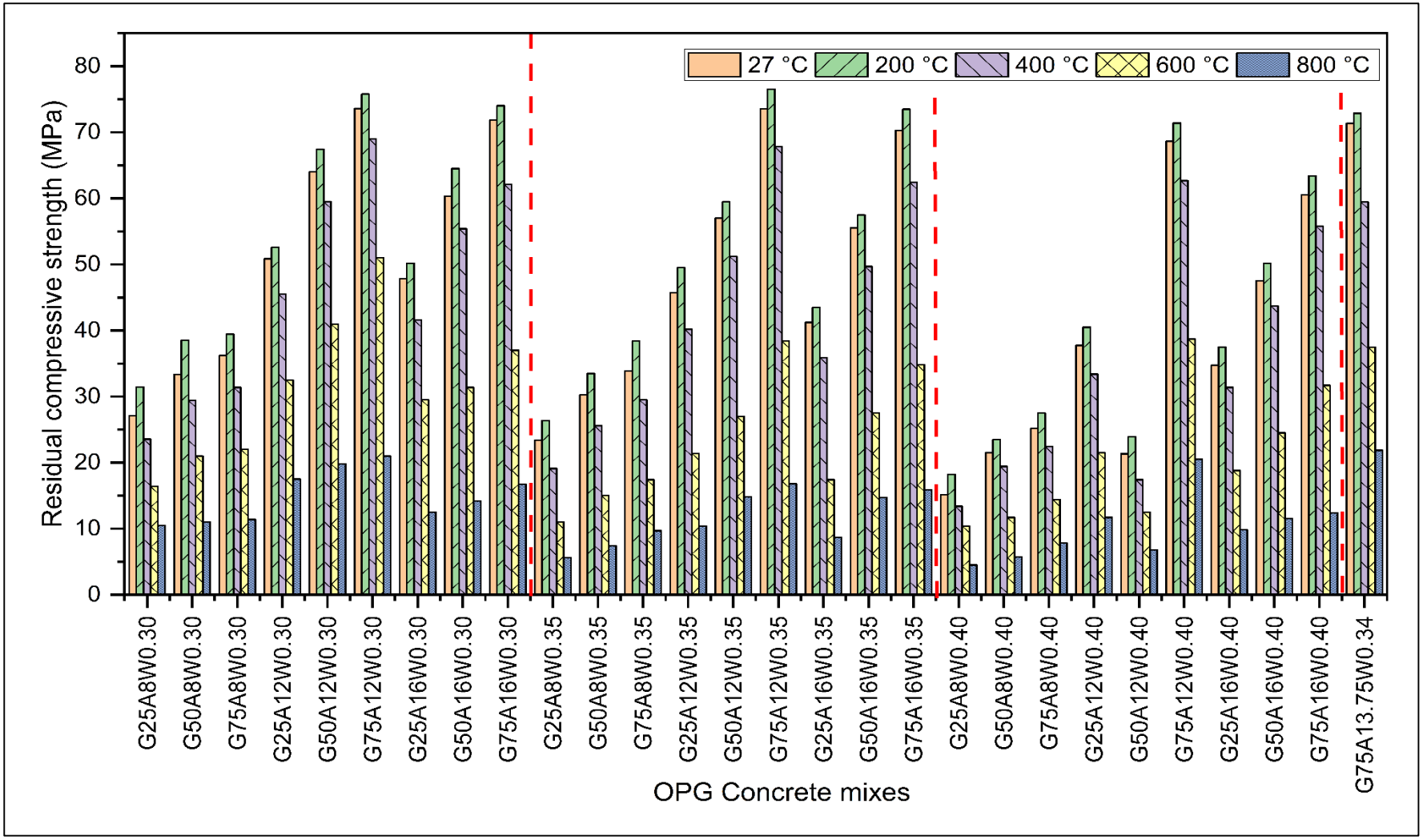

Figure 7.7 Residual compressive strength of OPG concretes at elevated temperature.

The mix $G_{50}A_{12}W_{0.30}$ achieved residual compressive strength 74.5 MPa at 200 ℃. After, elevating to higher temperatures the compressive strength diminish rate is low compared to other mixes. This is due to at lower activator content, the reduced degree of polycondensation leads to a decrease in strength of the OPG mixes. On the contrary, an increased activator leads to a more extensive dissolution of Al, Si, and Ca species, thereby enhancing the extent of the geopolymerization process. This leads to the development of a stable aluminosilicate network, along with the formation of C-S-H gel within the mixture, resulting in higher compressive strength for the blends, which could able to resist the higher temperature. The OPG paste mix produced with optimum mix proportion also performed better at elevated temperature.

After exposure to a temperature of 200 °C, the residual compressive strength of OPG mortar and concrete mixes showed a slight increase of 8-10% compared to their initial strength at 27 °C. This increase in compressive strength is attributed to the autoclave effect. At 200 °C, the elevated temperature may facilitate further activation of the geopolymer matrix. This can lead to additional formation or strengthening of the gel structures (e.g., N-A-S-H and C-A-S-H gels), which could temporarily improve strength. The temperature range might also promote the densification of the matrix, contributing to the observed increase in compressive strength. The temperature of 200 ℃ may lead to the removal of free moisture and bound water from the matrix, potentially reducing porosity and leading to higher strength measurements. This process could consolidate the material and increase density (Chethan et al. 2020). Additionally, mixes with higher levels of fly ash exhibited a significant improvement, with a 15-20% increase in residual compressive strength relative to their ambient temperature strength, compared to other mixes. Optimized OPG mortar and concrete mixes also demonstrated a similar trend of increased residual compressive strength. This enhancement is due to the hydration of unhydrated fly ash components, resulting in greater strength gains compared to other mixes. The residual compressive strength of OPG concrete mixes, namely $G_{25}A_8W_{0.30}$, $G_{25}A_8W_{0.35}$, and $G_{25}A_8W_{0.40}$ exhibited substantial increases post-exposure to 200 ℃, by 16%, 13%, and 20%, respectively as illustrated in Figure 7.7. However, the mixes with higher GGBS level shows a significant resistance to elevated temperatures irrespective of the activator dosage and W/GS ratio, but the strength gain percentage at post-exposure of 200 ℃ is less than

10%. As the fly ash content decreases, the observed increment in compressive strength after exposure to 200 ℃ diminishes. This trend suggests a correlation between fly ash content reduction and a corresponding decrease in the incremental improvement of compressive strength under elevated temperature conditions. Further insights into the microstructural analysis provide a comprehensive understanding of the underlying reasons for this observed behavior.

Upon exposure to temperatures beyond 200 ℃, both OPG mortar and concrete mixes experienced a decline in compressive strength. The residual compressive strength of both mortar and concrete mixes decreases by 10-15%, at 400 ℃. It is noteworthy that, higher rate of compressive strength loss found in mixes comprising of higher level of water content. The mixes comprised of higher level of GGBS content shows lower rate of strength diminish at 400 ℃. Upon exposure to the elevated temperature of 600 ℃, the compressive strength of mortar and concrete specimen experienced further reduction. The residual compressive strength of both mortar and concrete mixes decreases by 35-50%, at 600 ℃. This is due to internal cracks development which leads to disturb the structural integrity of the specimen. Further, exposure to the elevated temperature of 800 ℃, the compressive strength of all specimen exhibited a significant and drastic reduction. The residual compressive strength of both mortar and concrete mixes decreases by 60-75%, at 800 ℃. This is because of development of major cracks through the pores formed by evaporation structural water content in the matrix. This cracks propagates further and weaken the interfacial transition zone between binder and the aggregates. At 800 ℃, the specimen matrix strength diminishes due to reduced structural integrity of gel products that ultimately results in strength reduction of the specimen (Chethan et al. 2020). However, the optimized OPG mortar and concrete mixes performs better compared to other mixes at elevated temperatures.

7.6 MICRO-STRUCTURAL STUDIES

SEM analysis was employed to examine morphological changes in OPG mixes after exposure to elevated temperatures. The SEM images of optimized OPG concrete mix following exposure to different elevated temperatures are depicted in Figure 7.8.

SEM micrographs of optimized concrete mix shows the variation in structural matrix of specimen. When subjected to 200 °C, the porous network in alkali-activated fly ash allows the release of pore pressure induced by water evaporation, without the formation of major cracks. Simultaneously, further alkali activation occurs, leading to strength gain as newly formed gels fill the cracks and voids left by free water (Amran et al. 2022). Post-exposure to 200 °C, OPG mixes maintain stability with no significant loss of structural integrity and no apparent alteration of crystalline phases. This indicates that the mixes retain their structural integrity and do not undergo significant changes in morphology or crystalline phases at 200 ℃ temperature.

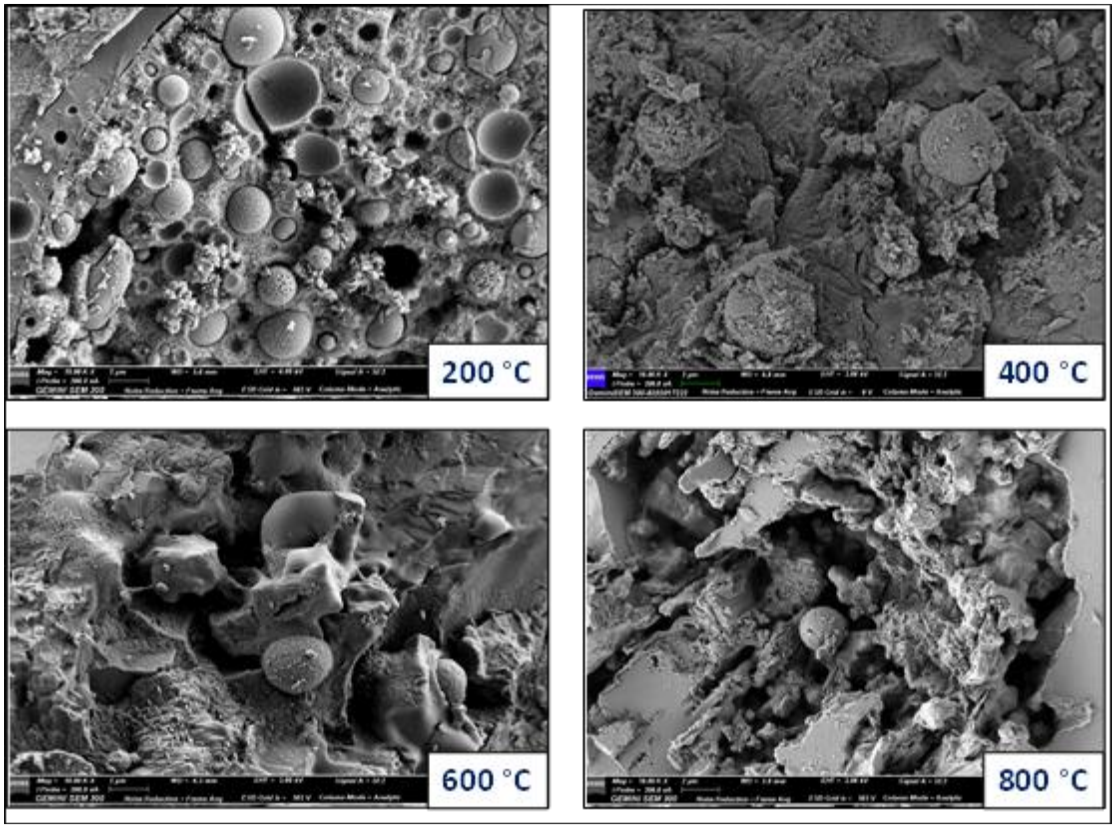

Figure 7.8 SEM micrographs of optimized OPG concrete mix.

The OPG mixes contain additional hydrated phases attributed to the high calcium content in GGBS. The presence of these additional phases can potentially impair thermal resistance and stability. This phenomenon is linked to the instability of CSH gel at elevated temperatures, as highlighted in previous literature (Rivera et al. 2016). It is noteworthy that, based on the literature, no apparent development of new phases occurred in OPG mixes containing GGBS until the temperature increased to 200 °C.

This information suggests that the introduction of elevated temperatures triggered the formation of new phases in OPG mixes, potentially influencing their thermal characteristics and stability, particularly in mixes containing GGBS.

It can be observed that in Figure 7.8, the development of minor cracks in the matrix after exposing to 400 °C. Notably, there was no apparent change in the stability of hydration products in matrix up to 400 ℃. This stability might be a contributing factor to the relatively lesser strength loss observed after exposure to 400 ℃ (Rivera et al. 2016). As the GGBS content increases in OPG mixes, the loss in strength also increases due to the decomposition of CSH gel formed as a result of the calcium content in GGBS. However, the matrix experienced a substantial loss in strength when exposed to 600 °C and 800 °C. It is seen that in micrographs of 600 °C and 800 °C, diminish of structural integrity of gel products and formation of larger pores which are responsible for decline in strength of the matrix. Additionally, the C-A-S-H gel produced from slag is fully dehydrated, while the N-A-S-H gel generated from fly ash undergoes partial crystallization. This contributing to the degradation of mechanical properties in OPG mixes at elevated temperatures. The combination of these factors results in the observed cracks and decline in mechanical strength at elevated temperatures.

7.7 CLOSURE

This chapter provides a comprehensive overview of the performance of OPG mixes under elevated temperatures. The comparative analysis of weight retention, UPV values and residual compressive strength of OPG paste, mortar and concrete mixes after exposure to elevated temperatures are discussed. The discussion is further enriched by an examination of SEM images, offering insights into the reasons behind the observed variations in the mechanical properties of OPG mixes. This multi-faceted analysis contributes to a thorough understanding of the behavior and resilience of OPG mixes under the influence of elevated temperatures.

CHAPTER 8

CONCLUSIONS AND RECOMMENDATIONS

8.1 CONCLUSIONS OF THE PRESENT WORK

In this study, the optimization and characterization of one-part geopolymer pastes, mortars, and concretes at ambient condition has been carried out. RSM was employed to study the effect of individual and combined factors on OPG systems. The desirability function is used to perform multi-objective optimization based on the proposed model. The important conclusions drawn from this study are as follows:

1. GGBS substitution significantly influences the fresh and hardened properties of one-part geopolymer systems. Higher GGBS increases CaO, promoting polymerization and rapid generation of C-A-S-H gel, resulting in dense microstructures, increased strength, and reduced flowability and setting time.
2. The W/GS ratio increases water content, causing severe shrinkage, decreased strength, and increased setting time. Activator content significantly affects strength development: higher dosages create dense microstructures but longer micro-cracks, while lower dosages leave more unreacted particles, inhibiting strength development.
3. The ideal mix parameters of one-part geopolymer paste, according to RSM multi-objective optimization, are 51.4% GGBS substitution, 0.32 w/s, and 12.4% activator content, with 191 mm of slump flow, 68.6 MPa of 28 day compressive strength, 59 and 191 min of initial and final setting times, respectively. Validation test findings show less than 10% deviation from projected values.
4. According to multi-objective optimization, the optimum mix proportions obtained for one-part geopolymer mortars are 49.81% GGBS substitution, 0.37 w/s, and 13.6% activator content, with 170 mm flowability, 57.7 MPa of 28 day compressive strength, 5.8 MPa of 28 day flexural strength, and 1626 microstrain of 180 days drying shrinkage. Validation test results show maximum of 6.6% deviation from the predicted test results.

5. Response models of flowability, setting time, compressive strength, flexural strength and drying shrinkage developed are quadratic polynomial models, showing a strong relationship between the factors and the responses. The model shows high prediction accuracy and also high the correlation coefficient.
6. Multi-objective optimization identified the optimal one-part geopolymer concrete mix: 75% GGBS, W/GS ratio of 0.34, and 13.8% activator dosage. This mix achieved a slump of 125 mm, 28-day compressive strength of 73.5 MPa, flexural strength of 6.2 MPa, and split tensile strength of 3.9 MPa. Validation tests showed a maximum 10% deviation from predicted values, confirming the model's accuracy and RSM's effectiveness. The measured results were a slump of 135 mm, 28-day compressive strength of 70.3 MPa, flexural strength of 5.8 MPa, and split tensile strength of 3.7 MPa.
7. The prediction models for workability, compressive strength, flexural strength, and split tensile strength are proposed using quadratic polynomial equations, indicating a close relation between the components and the resulting responses. Excellent fitting accuracy and strong precision in outcome prediction are obtained from these models.
8. SEM analysis of the proposed optimized mixture reveals compact and dense microstructures, as well as the presence of C-(N)-A-S-H gel and robust ITZ areas. The creation of C-(N)-A-S-H gel, in addition to C-S-H gel, has been demonstrated by XRD spectra of selected mixtures. The creation of gel products is of significant importance in the development of strength properties of OPGC mixes.
9. XRD reveals that the higher GGBS level in the mix results in the formation of more C-(N)-A-S-H gel, which also conforms the observations made by FTIR spectroscopy, that alterations in the structural aluminosilicates Si-O-Si(Al) resulting from a polymerization reaction, which subsequently creates gelatinous substances responsible for enhancing strength in the OPGCs.
10. All OPG specimens maintained structural stability without spalling after exposure to temperatures up to 800°C. They retained 20-25% of their strength at 800°C and 40-50% at 600°C.

11. The EE and ECO_2e increase with increase in activator content and GGBS. The cost of OPG concrete mixes per cubic meter is highly dependent on the activator dosage as the cost of activator is higher. The proposed optimization mix shows EE of 1323 MJ/m^3, ECO_2e 155 ECO_2e/m^3, and cost of 106 $\$/m^3$. The cost OPG concrete mixes is about 15-25% more and is much more eco-friendly sustainable alternative as compared to OPC based concretes.

8.2 RECOMMENDATIONS

1. **Practical Implementation**: To achieve optimal fresh and hardened properties in one-part geopolymer systems, it is recommended to use approximately 50% GGBS substitution for pastes and mortars, and up to 75% for concrete mixes. This balance optimizes the formation of C-A-S-H gel, enhancing strength and reducing setting time while maintaining workability.
2. **Workability and Strength:** Maintaining a lower W/GS ratio (around 0.32 for paste and 0.34-0.37 for mortar and concrete) is crucial to prevent severe shrinkage and achieve higher compressive strength. Adjustments should be made based on specific application requirements to balance workability and mechanical properties.
3. **Activator Dosage:** It is advisable to use around 12.4-13.8% activator content for different mixes to achieve dense microstructures and optimal strength. Higher dosages may lead to micro-cracking, while lower dosages may result in unreacted particles. Given the higher cost and environmental impact of activators, optimization should aim to use the minimum effective dosage to balance cost, environmental sustainability, and performance.
4. **Optimization Tools:** Utilize RSM and desirability functions in the design and optimization of geopolymer mixes. This approach allows for the identification of optimal mix proportions and enhances the predictability of outcomes.
5. **High-Temperature Applications**: Given the demonstrated thermal stability up to 800 °C, one-part geopolymer materials are recommended for applications involving high-temperature exposure. Conduct further studies to explore

potential applications in fire-resistant construction and high-temperature industrial processes.

6. **Environmental and Economic Impact:** Emphasize the use of one-part geopolymer concretes as a more sustainable alternative to traditional OPC-based concretes. While the cost of OPG concretes is higher, efforts should be made to optimize the production process to reduce costs.

8.3 CONTRIBUTIONS OF THE STUDY

This research has made significant contributions to the field of one-part geopolymers (OPG), including:

1. **Optimization Methodology:** A comprehensive approach to optimizing OPG mixes, which establishes a new benchmark for future studies.
2. **Elevated Temperature Studies:** For the first time, the performance of OPGs under elevated temperatures has been investigated, providing valuable data and insights not previously available in the literature.
3. **Ecological and Cost Benefits:** Analysis of the ecological impact and cost-effectiveness of OPGs, highlighting their potential as a sustainable and economical alternative to traditional materials.

8.4 SCOPE FOR FUTURE WORK

The present investigation has focused on the production of one-part geopolymer pastes, mortars and concretes and performance of produced mixes at elevated temperatures.

There is scope for future investigation in the following areas,

1. Due to the absence of a standardized mix design for OPGC mixes, a comprehensive and systematic study is necessary. This involves developing a robust mix design methodology tailored specifically for various types of concrete, such as self-compacting concrete and high-performance concrete.
2. A crucial area for further exploration is evaluating the durability properties of OPGC under various environmental and service conditions. This includes

investigating its resistance to freeze-thaw cycles, chemical exposure, and abrasion.

3. A comprehensive investigation into the long-term properties of OPGC is essential for evaluating its structural integrity and performance over extended periods. This includes examining factors such as creep, shrinkage, and long-term strength development.

REFERENCES

Abdel-Gawwad, H. A., and Abo-El-Enein, S. A. (2016). "A novel method to produce dry geopolymer cement powder." *HBRC J.*, 12(1), 13–24.

Abdollahnejad, Z., Luukkonen, T., Mastali, M., Giosue, C., Favoni, O., Ruello, M. L., Kinnunen, P., and Illikainen, M. (2020a). "Microstructural Analysis and Strength Development of One-Part Alkali-Activated Slag/Ceramic Binders Under Different Curing Regimes." *Waste and Biomass Valorization*, 11(6), 3081–3096.

Abdollahnejad, Z., Mastali, M., Woof, B., and Illikainen, M. (2020b). "High strength fiber reinforced one-part alkali activated slag/fly ash binders with ceramic aggregates: Microscopic analysis, mechanical properties, drying shrinkage, and freeze-thaw resistance." *Constr. Build. Mater.*, 241, 118129.

Abdollahnejad, Z., Pacheco-Torgal, F., Aguiar, J. B., and Jesus, C. (2015). "Durability performance of fly ash based one-part geopolymer mortars." *Key Eng. Mater.*, 634, 113–120.

Adesanya, E., Ohenoja, K., Maria, A. Di, Kinnunen, P., and Illikainen, M. (2020). "Alternative alkali-activator from steel-making waste for one-part alkali-activated slag." *J. Clean. Prod.*, 274, 123020.

Ali, M., Liebscher, M., Hempel, S., Yang, J., and Mechtcherine, V. (2018). "Correlation of microstructural and mechanical properties of geopolymers produced from fly ash and slag at room temperature." *Constr. Build. Mater.*, 191, 330–341.

Ali Shah, S. F., Chen, B., Ahmad, M. R., and Haque, M. A. (2021). "Development of Cleaner One-part geopolymer from lithium slag." *J. Clean. Prod.*, 291, 125241.

Alzaza, A., Ohenoja, K., and Illikainen, M. (2021). "One-part alkali-activated blast furnace slag for sustainable construction at subzero temperatures." *Constr. Build. Mater.*, 276, 122026.

Amran, M., Huang, S. S., Debbarma, S., and Rashid, R. S. M. (2022). "Fire resistance of geopolymer concrete: A critical review." *Constr. Build. Mater.*, 324(February), 126722.

Askarian, M., Tao, Z., Adam, G., and Samali, B. (2018). “Mechanical properties of ambient cured one-part hybrid OPC-geopolymer concrete.” *Constr. Build. Mater.*, 186, 330–337.

Askarian, M., Tao, Z., Samali, B., Adam, G., and Shuaibu, R. (2019). “Mix composition and characterisation of one-part geopolymers with different activators.” *Constr. Build. Mater.*, 225, 526–537.

Aydin, S. (2013). “A ternary optimisation of mineral additives of alkali activated cement mortars.” *Constr. Build. Mater.*, 43, 131–138.

Ban, C. C., Ken, P. W., and Ramli, M. (2017). “Mechanical and Durability Performance of Novel Self-activating Geopolymer Mortars.” *Procedia Eng.*, 171, 564–571.

Bernal, S. A., and Provis, J. L. (2014). “Durability of alkali-activated materials: Progress and perspectives.” *J. Am. Ceram. Soc.*, 97(4), 997–1008.

Bingol, D., Tekin, N., and Alkan, M. (2010). “Brilliant Yellow dye adsorption onto sepiolite using a full factorial design.” *Appl. Clay Sci.*, 50(3), 315–321.

BIS 456:(2000). (2000). “Indian Standard PLAIN AND REINFORCED CONCRETE.” 31(July 2000).

Bong, S. H., Nematollahi, B., Xia, M., Nazari, A., and Sanjayan, J. (2020). “Properties of one-part geopolymer incorporating wollastonite as partial replacement of geopolymer precursor or sand.” *Mater. Lett.*, 263, 127236.

Burciaga-Díaz, O., and Escalante-García, J. I. (2017). “Comparative performance of alkali activated slag/metakaolin cement pastes exposed to high temperatures.” *Cem. Concr. Compos.*, 84, 157–166.

Chen, K., Wu, D., Zhang, Z., Pan, C., Shen, X., Xia, L., and Zang, J. (2022). “Modeling and optimization of fly ash–slag-based geopolymer using response surface method and its application in soft soil stabilization.” *Constr. Build. Mater.*, 315, 125723.

Chethan, K. B., Yaragal, S. C., and Das, B. B. (2020). “Ferrochrome ash – Its usage potential in alkali activated slag mortars.” *J. Clean. Prod.*, 257, 120577.

Chindaprasirt, P., Silva, P. De, Sagoe-Crentsil, K., and Hanjitsuwan, S. (2012). “Effect

of SiO 2 and Al 2O 3on the setting and hardening of high calcium fly ash-based geopolymer systems." *J. Mater. Sci.*, 47(12), 4876–4883.

Cülfik, M. S., and Özturan, T. (2002). "Effect of elevated temperatures on the residual mechanical properties of high-performance mortar." *Cem. Concr. Res.*, 32(5), 809–816.

Das, D., and Rout, P. K. (2021). "Synthesis, Characterization and Properties of Fly Ash Based Geopolymer Materials." *J. Mater. Eng. Perform.*, 30(5), 3213–3231.

Davidovits, J. (1991). "Geopolymers." *J. Therm. Anal.*, 37(8), 1633–1656.

Davidovits, J. (1994). "Properties of Geopolymer Cements." *First Int. Conf. Alkaline Cem. Concr.*, 131–149.

Davidovits, J. (1999). "Chemistry of geopolymeric systems, terminology." *Geopolymer*, sn, 9–39.

Davidovits, J. (2005). "Geopolymer, Green Chemistry and Sustainable Development Solutions: Proceedings of the World Congress Geopolymer, Geopolymer Institute."

DeRousseau, M. A., Kasprzyk, J. R., and Srubar, W. V. (2018). "Computational design optimization of concrete mixtures: A review." *Cem. Concr. Res.*, 109(December 2017), 42–53.

Diaz-Loya, E. I., Allouche, E. N., and Vaidya, S. (2011). "Mechanical properties of fly-ash-based geopolymer concrete." *ACI Mater. J.*, 108(3), 300–306.

Dong, M., Elchalakani, M., and Karrech, A. (2020). "Development of high strength one-part geopolymer mortar using sodium metasilicate." *Constr. Build. Mater.*, 236, 117611.

Duran Atiş, C., Bilim, C., Çelik, Ö., and Karahan, O. (2009). "Influence of activator on the strength and drying shrinkage of alkali-activated slag mortar." *Constr. Build. Mater.*, 23(1), 548–555.

Duxson, P., Fernández-Jiménez, A., Provis, J. L., Lukey, G. C., Palomo, A., and Deventer, J. S. J. Van. (2007). "Geopolymer technology: The current state of the art." *J. Mater. Sci.*, 42(9), 2917–2933.

Duxson, P., and Provis, J. L. (2008). “Designing precursors for geopolymer cements.” *J. Am. Ceram. Soc.*, 91(12), 3864–3869.

Elzeadani, M., Bompa, D. V, and Elghazouli, A. Y. (2022). “One part alkali activated materials: A state-of-the-art review.” *J. Build. Eng.*, 57(June), 104871.

Fu, Y., Cai, L., and Yonggen, W. (2011). “Freeze–thaw cycle test and damage mechanics models of alkali-activated slag concrete.” *Constr. Build. Mater.*, 25(7), 3144–3148.

Geraldo, R. H., Gonçalves, J. P., and Camarini, G. (2022). “Production Process of an Eco-Friendly One-Part Alkali-Activated Binder.” *Mater. Res.*, 25, 1–13.

Gluth, G. J. G., Lehmann, C., Rübner, K., and Kühne, H. C. (2013). “Geopolymerization of a silica residue from waste treatment of chlorosilane production.” *Mater. Struct. Constr.*, 46(8), 1291–1298.

Guo, S., Ma, C., Long, G., and Xie, Y. (2019). “Cleaner one-part geopolymer prepared by introducing fly ash sinking spherical beads: Properties and geopolymerization mechanism.” *J. Clean. Prod.*, 219, 686–697.

Guo, W., Wang, S., Xu, Z., Zhang, Z., Zhang, C., Bai, Y., and Zhao, Q. (2021). “Mechanical performance and microstructure improvement of soda residue–carbide slag–ground granulated blast furnace slag binder by optimizing its preparation process and curing method.” *Constr. Build. Mater.*, 302(August), 124403.

Hajimohammadi, A., and Deventer, J. S. J. van. (2017). “Characterisation of One-Part Geopolymer Binders Made from Fly Ash.” *Waste and Biomass Valorization*, 8(1), 225–233.

Hajimohammadi, A., Provis, J. L., and Deventer, J. S. J. Van. (2008). “One-part geopolymer mixes from geothermal silica and sodium aluminate.” *AIChE Annu. Meet. Conf. Proc.*

Hajimohammadi, A., Provis, J. L., and Deventer, J. S. J. Van. (2010). “Effect of alumina release rate on the mechanism of geopolymer gel formation.” *Chem. Mater.*, 22(18), 5199–5208.

Hajimohammadi, A., Provis, J. L., and Deventer, J. S. J. Van. (2011). “The effect of silica availability on the mechanism of geopolymerisation.” *Cem. Concr. Res.*, 41(3), 210–216.

Haruna, S., Mohammed, B. S., and Wahab, M. M. . (2020a). “Effect of GGBS Slag on Setting Time and Compressive Strength of One-Part Geopolymer Binders.” *J. Infrastruct. Facil. Asset Manag.*, 2(2).

Haruna, S., Mohammed, B. S., Wahab, M. M. A., Kankia, M. U., Amran, M., and Gora, A. M. (2021). “Long-term strength development of fly ash-based one-part alkali-activated binders.” *Materials (Basel).*, 14(15), 1–14.

Haruna, S., Mohammed, B. S., Wahab, M. M. A., and Liew, M. S. (2020b). “Effect of paste aggregate ratio and curing methods on the performance of one-part alkali-activated concrete.” *Constr. Build. Mater.*, 261, 120024.

Hassan, H. S., Abdel-Gawwad, H. A., Vásquez-García, S. R., Israde-Alcántara, I., Flores-Ramirez, N., Rico, J. L., and Mohammed, M. S. (2019). “Cleaner production of one-part white geopolymer cement using pre-treated wood biomass ash and diatomite.” *J. Clean. Prod.*, 209, 1420–1428.

Hiremath, P. N., and Yaragal, S. C. (2018). “Performance evaluation of reactive powder concrete with polypropylene fibers at elevated temperatures.” *Constr. Build. Mater.*, 169, 499–512.

Huseien, G. F., Sam, A. R. M., Shah, K. W., Asaad, M. A., Tahir, M. M., and Mirza, J. (2019). “Properties of ceramic tile waste based alkali-activated mortars incorporating GBFS and fly ash.” *Constr. Build. Mater.*, 214(X), 355–368.

IS:516-6. (2021). “Hardened concrete - Methods of test.” *Bur. Indian Stand. New Dehli*, 54(August), 1–20.

IS 10086. (2021). “Moulds for Use in Tests of Cement, Concrete and Pozzolana — Specification.” (December).

IS 1199 (Part 5). (2018). “Fresh Concrete — Methods of Sampling, Testing and Analysis.” 1199(December).

IS 4031 (Part 5). (2002). “Methods of Physical Tests for Hydraulic Cement Methods of Physical Tests for Hydraulic Cement.” *Bur. Indian Stand.*, 4031(1), 2–7.

Ishak, S., Lee, H. S., Singh, J. K., Ariffin, M. A. M., Lim, N. H. A. S., and Yang, H. M. (2019). “Performance of fly ash geopolymer concrete incorporating bamboo ash at elevated temperature.” *Materials (Basel).*, 12(20), 1–17.

Jafari Nadoushan, M., and Ramezanianpour, A. A. (2016). “The effect of type and concentration of activators on flowability and compressive strength of natural pozzolan and slag-based geopolymers.” *Constr. Build. Mater.*, 111, 337–347.

Jang, J. G., and Lee, H. K. (2016). “Effect of fly ash characteristics on delayed high-strength development of geopolymers.” *Constr. Build. Mater.*, 102, 260–269.

Jiang, X., Zhang, Y., Xiao, R., Polaczyk, P., Zhang, M., Hu, W., Bai, Y., and Huang, B. (2020). “A comparative study on geopolymers synthesized by different classes of fly ash after exposure to elevated temperatures.” *J. Clean. Prod.*, 270, 122500.

Kadhim, A., Sadique, M., Al-Mufti, R., and Hashim, K. (2021). “Developing one-part alkali-activated metakaolin/natural pozzolan binders using lime waste.” *Adv. Cem. Res.*, 33(8), 342–356.

Karahan, O., and Yakupoğlu, A. (2011). “Resistance of alkali-activated slag mortar to abrasion and fire.” *Adv. Cem. Res.*, 23(6), 289–297.

Kaya, M. (2022). “The effect of micro-SiO2 and micro-Al2O3 additive on the strength properties of ceramic powder-based geopolymer pastes.” *J. Mater. Cycles Waste Manag.*, 24(1), 333–350.

Kaya, M., Uysal, M., Yilmaz, K., Karahan, O., and Atis, C. D. (2020). “Mechanical properties of class C and F fly ash geopolymer mortars.” *Gradjevinar*, 72(4), 297–309.

Ke, X., Bernal, S. A., Ye, N., Provis, J. L., and Yang, J. (2015). “One-part geopolymers based on thermally treated red Mud/NaOH blends.” *J. Am. Ceram. Soc.*, 98(1), 5–11.

Kim, M. S., Jun, Y., Lee, C., and Oh, J. E. (2013). “Use of CaO as an activator for producing a price-competitive non-cement structural binder using ground granulated blast furnace slag.” *Cem. Concr. Res.*, 54, 208–214.

Kong, D. L. Y., and Sanjayan, J. G. (2010). “Effect of elevated temperatures on geopolymer paste, mortar and concrete.” *Cem. Concr. Res.*, 40(2), 334–339.

Lee, N. K., and Lee, H. K. (2015). “Reactivity and reaction products of alkali-activated, fly ash/slag paste.” *Constr. Build. Mater.*, 81, 303–312.

Li, K., Zeng, Q., Luo, M., and Pang, X. (2014). “Effect of self-desiccation on the pore structure of paste and mortar incorporating 70% GGBS.” *Constr. Build. Mater.*, 51, 329–337.

Li, L., Lu, J. X., Zhang, B., and Poon, C. S. (2020). “Rheology behavior of one-part alkali activated slag/glass powder (AASG) pastes.” *Constr. Build. Mater.*, 258, 120381.

Li, X., Wang, Z., and Jiao, Z. (2013). “Influence of curing on the strength development of calcium-containing geopolymer mortar.” *Materials (Basel).*, 6(11), 5069–5076.

Li, Z., Lu, D., and Gao, X. (2021). “Optimization of mixture proportions by statistical experimental design using response surface method - A review.” *J. Build. Eng.*, 36(November 2020), 102101.

Liu, Y., Qin, Z., and Chen, B. (2020). “Experimental research on magnesium phosphate cements modified by red mud.” *Constr. Build. Mater.*, 231, 117131.

Liu, Y., Zhu, W., and Yang, E. H. (2016). “Alkali-activated ground granulated blast-furnace slag incorporating incinerator fly ash as a potential binder.” *Constr. Build. Mater.*, 112, 1005–1012.

Luo, Y., Li, S. H., Klima, K. M., Brouwers, H. J. H., and Yu, Q. (2022). “Degradation mechanism of hybrid fly ash/slag based geopolymers exposed to elevated temperatures.” *Cem. Concr. Res.*, 151(October 2021).

Luukkonen, T., Abdollahnejad, Z., Yliniemi, J., Kinnunen, P., and Illikainen, M. (2018a). “One-part alkali-activated materials: A review.” *Cem. Concr. Res.*, 103(September 2017), 21–34.

Luukkonen, T., Abdollahnejad, Z., Yliniemi, J., Kinnunen, P., and Illikainen, M. (2018b). “Comparison of alkali and silica sources in one-part alkali-activated blast furnace slag mortar.” *J. Clean. Prod.*, 187, 171–179.

Luukkonen, T., Sreenivasan, H., Abdollahnejad, Z., Yliniemi, J., Kantola, A., Telkki, V. V., Kinnunen, P., and Illikainen, M. (2020). "Influence of sodium silicate powder silica modulus for mechanical and chemical properties of dry-mix alkali-activated slag mortar." *Constr. Build. Mater.*, 233, 117354.

Ma, B., Zhu, Z., Huo, W., Yang, L., Zhang, Y., Sun, H., and Zhang, X. (2023). "Assessing the viability of a high performance one-part geopolymer made from fly ash and GGBS at ambient temperature." *J. Build. Eng.*, 75(June), 106978.

Ma, C., Long, G., Shi, Y., and Xie, Y. (2018). "Preparation of cleaner one-part geopolymer by investigating different types of commercial sodium metasilicate in China." *J. Clean. Prod.*, 201, 636–647.

Ma, C., Zhao, B., Guo, S., Long, G., and Xie, Y. (2019). "Properties and characterization of green one-part geopolymer activated by composite activators." *J. Clean. Prod.*, 220, 188–199.

Madlool, N. A., Saidur, R., Hossain, M. S., and Rahim, N. A. (2011). "A critical review on energy use and savings in the cement industries." *Renew. Sustain. Energy Rev.*, 15(4), 2042–2060.

Mastali, M., Kinnunen, P., Dalvand, A., Mohammadi Firouz, R., and Illikainen, M. (2018). "Drying shrinkage in alkali-activated binders – A critical review." *Constr. Build. Mater.*, 190, 533–550.

Matalkah, F., Xu, L., Wu, W., and Soroushian, P. (2017). "Mechanochemical synthesis of one-part alkali aluminosilicate hydraulic cement." *Mater. Struct. Constr.*, 50(1), 1–12.

Melo Neto, A. A., Cincotto, M. A., and Repette, W. (2008). "Drying and autogenous shrinkage of pastes and mortars with activated slag cement." *Cem. Concr. Res.*, 38(4), 565–574.

Mermerdaş, K., Algın, Z., Oleiwi, S. M., and Nassani, D. E. (2017). "Optimization of lightweight GGBFS and FA geopolymer mortars by response surface method." *Constr. Build. Mater.*, 139, 159–171.

Mithun, B. M., and Narasimhan, M. C. (2016). “Performance of alkali activated slag concrete mixes incorporating copper slag as fine aggregate.” *J. Clean. Prod.*, 112, 837–844.

Mohammed, B. S., Fang, O. C., Anwar Hossain, K. M., and Lachemi, M. (2012). “Mix proportioning of concrete containing paper mill residuals using response surface methodology.” *Constr. Build. Mater.*, 35, 63–68.

Mohammed, B. S., Haruna, S., Mubarak bn Abdul Wahab, M., and Liew, M. S. (2019a). “Optimization and characterization of cast in-situ alkali-activated pastes by response surface methodology.” *Constr. Build. Mater.*, 225, 776–787.

Mohammed, B. S., Haruna, S., Wahab, M. M. A., Liew, M. S., and Haruna, A. (2019b). “Mechanical and microstructural properties of high calcium fly ash one-part geopolymer cement made with granular activator.” *Heliyon*, 5(9), e02255.

Mohammed, B. S., Khed, V. C., and Nuruddin, M. F. (2018). “Rubbercrete mixture optimization using response surface methodology.” *J. Clean. Prod.*, 171, 1605–1621.

Nadeem, A., Memon, S. A., and Lo, T. Y. (2013). “Mechanical performance, durability, qualitative and quantitative analysis of microstructure of fly ash and Metakaolin mortar at elevated temperatures.” *Constr. Build. Mater.*, 38, 338–347.

Nath, P., and Sarker, P. K. (2014). “Effect of GGBFS on setting, workability and early strength properties of fly ash geopolymer concrete cured in ambient condition.” *Constr. Build. Mater.*, 66, 163–171.

Nath, P., and Sarker, P. K. (2017). “Flexural strength and elastic modulus of ambient-cured blended low-calcium fly ash geopolymer concrete.” *Constr. Build. Mater.*, 130, 22–31.

Nematollahi, B., Sanjayan, J., Qiu, J., and Yang, E. H. (2017a). “Micromechanics-based investigation of a sustainable ambient temperature cured one-part strain hardening geopolymer composite.” *Constr. Build. Mater.*, 131, 552–563.

Nematollahi, B., Sanjayan, J., Qiu, J., and Yang, E. H. (2017b). “High ductile behavior of a polyethylene fiber-reinforced one-part geopolymer composite: A micromechanics-

based investigation." *Arch. Civ. Mech. Eng.*, 17(3), 555–563.

Nematollahi, B., Sanjayan, J., and Shaikh, F. U. A. (2015). "Synthesis of heat and ambient cured one-part geopolymer mixes with different grades of sodium silicate." *Ceram. Int.*, 41(4), 5696–5704.

Neupane, K. (2016). "'Fly ash and GGBFS based powder-activated geopolymer binders: A viable sustainable alternative of portland cement in concrete industry.'" *Mech. Mater.*, 103, 110–122.

Oderji, S. Y., Chen, B., Shakya, C., Ahmad, M. R., and Shah, S. F. A. (2019). "Influence of superplasticizers and retarders on the workability and strength of one-part alkali-activated fly ash/slag binders cured at room temperature." *Constr. Build. Mater.*, 229, 116891.

Ouellet-Plamondon, C., and Habert, G. (2015). *Life cycle assessment (LCA) of alkali-activated cements and concretes*. *Handb. Alkali-Activated Cem. Mortars Concr.*, Woodhead Publishing Limited.

Pacheco-Torgal, F., Castro-Gomes, J., and Jalali, S. (2008). "Alkali-activated binders: A review. Part 1. Historical background, terminology, reaction mechanisms and hydration products." *Constr. Build. Mater.*, 22(7), 1305–1314.

Palacios, M., and Puertas, F. (2007). "Effect of shrinkage-reducing admixtures on the properties of alkali-activated slag mortars and pastes." *Cem. Concr. Res.*, 37(5), 691–702.

Palomo, A., Grutzeck, M. W., and Blanco, M. T. (1999). "Alkali-activated fly ashes: A cement for the future." *Cem. Concr. Res.*, 29(8), 1323–1329.

Pangdaeng, S., Phoo-ngernkham, T., Sata, V., and Chindaprasirt, P. (2014). "Influence of curing conditions on properties of high calcium fly ash geopolymer containing Portland cement as additive." *Mater. Des.*, 53, 269–274.

Peng, M. X., Wang, Z. H., Shen, S. H., and Xiao, Q. G. (2014). "Synthesis, characterization and mechanisms of one-part geopolymeric cement by calcining low-quality kaolin with alkali." *Mater. Struct. Constr.*, 48(3), 699–708.

Peng, M. X., Wang, Z. H., Xiao, Q. G., Song, F., Xie, W., Yu, L. C., Huang, H. W., and Yi, S. J. (2017). “Effects of alkali on one-part alkali-activated cement synthesized by calcining bentonite with dolomite and Na 2 CO 3.” *Appl. Clay Sci.*, 139, 64–71.

Perumal, P., Nguyen, H., Carvelli, V., Kinnunen, P., and Illikainen, M. (2022). “High strength fiber reinforced one-part alkali activated slag composites from industrial side streams.” *Constr. Build. Mater.*, 319, 126124.

Perumal, P., Sreenivasan, H., Luukkonen, T., Kantola, A. M., Telkki, V. V., Kinnunen, P., and Illikainen, M. (2021). “High strength one-part alkali-activated slag blends designed by particle packing optimization.” *Constr. Build. Mater.*, 299, 124004.

Prusty, J. K., and Pradhan, B. (2020). “Multi-response optimization using Taguchi-Grey relational analysis for composition of fly ash-ground granulated blast furnace slag based geopolymer concrete.” *Constr. Build. Mater.*, 241, 118049.

Puligilla, S., and Mondal, P. (2013). “Role of slag in microstructural development and hardening of fly ash-slag geopolymer.” *Cem. Concr. Res.*, 43(1), 70–80.

Puligilla, S., and Mondal, P. (2015). “Co-existence of aluminosilicate and calcium silicate gel characterized through selective dissolution and FTIR spectral subtraction.” *Cem. Concr. Res.*, 70, 39–49.

Qu, F., Li, W., Tao, Z., Castel, A., and Wang, K. (2020). “High temperature resistance of fly ash/GGBFS-based geopolymer mortar with load-induced damage.” *Mater. Struct. Constr.*, 53(4).

Rajput, S. P. S., and Datta, S. (2019). “A review on optimization techniques used in civil engineering material and structure design.” *Mater. Today Proc.*, 26, 1482–1491.

Ranjbar, N., Kuenzel, C., Spangenberg, J., and Mehrali, M. (2020). “Hardening evolution of geopolymers from setting to equilibrium: A review.” *Cem. Concr. Compos.*, 114, 103729.

Rashad, A. M. (2013). “A comprehensive overview about the influence of different additives on the properties of alkali-activated slag - A guide for Civil Engineer.” *Constr. Build. Mater.*, 47(2013), 29–55.

Rashad, A. M., and Sadek, D. M. (2017). “An investigation on Portland cement replaced by high-volume GGBS pastes modified with micro-sized metakaolin subjected to elevated temperatures.” *Int. J. Sustain. Built Environ.*, 6(1), 91–101.

Rasuli, M. I., Tajunnisa, Y., Yamamura, A., and Shigeishi, M. (2022). “A consideration on the one-part mixing method of alkali-activated material: problems of sodium silicate solubility and quick setting.” *Heliyon*, 8(1), e08783.

Rattanasak, U., Pankhet, K., and Chindaprasirt, P. (2011). “Effect of chemical admixtures on properties of high-calcium fly ash geopolymer.” *Int. J. Miner. Metall. Mater.*, 18(3), 364–369.

Rehan, R., and Nehdi, M. (2005). “Carbon dioxide emissions and climate change: Policy implications for the cement industry.” *Environ. Sci. Policy*, 8(2), 105–114.

Ren, J., Sun, H., Li, Q., Li, Z., Ling, L., Zhang, X., Wang, Y., and Xing, F. (2021). “Experimental comparisons between one-part and normal (two-part) alkali-activated slag binders.” *Constr. Build. Mater.*, 309(March), 125177.

Rivera, O. G., Long, W. R., Weiss, C. A., Moser, R. D., Williams, B. A., Torres-Cancel, K., Gore, E. R., and Allison, P. G. (2016). “Effect of elevated temperature on alkali-activated geopolymeric binders compared to portland cement-based binders.” *Cem. Concr. Res.*, 90, 43–51.

Rockström, J., Steffen, W., K. Noone, Å. Persson, Chapin, F. S., E. F. Lambin, T. M. Lenton, M. Scheffer, C. Folke, H. J. Schellnhuber, B. Nykvist, C. A. de Wit, T. Hughes, S. van der Leeuw, H. Rodhe, S. Sörlin, P. K. Snyder, R. Costanza, U. Svedin, M. Falkenmark, L. Karlberg, R. W. Corell, J. Fabry, V., J. Hansen, B. Walker, D. Liverman, K. Richardson, P. Crutzen, and J. A. Foley. (2009). “A safe operation space for humanity.” *Nature*, 461(September), 472–475.

Ruiz-Santaquiteria, C., Fernández-Jiménez, A., Skibsted, J., and Palomo, A. (2013). “Clay reactivity: Production of alkali activated cements.” *Appl. Clay Sci.*, 73(1), 11–16.

Ryu, G. S., Lee, Y. B., Koh, K. T., and Chung, Y. S. (2013). “The mechanical properties of fly ash-based geopolymer concrete with alkaline activators.” *Constr. Build. Mater.*,

47, 409–418.

Sadeghian, G., Behfarnia, K., and Teymouri, M. (2022). “Drying shrinkage of one-part alkali-activated slag concrete.” *J. Build. Eng.*, 51(December 2021), 104263.

Shah, S. F. A., Chen, B., Oderji, S. Y., Haque, M. A., and Ahmad, M. R. (2020). “Improvement of early strength of fly ash-slag based one-part alkali activated mortar.” *Constr. Build. Mater.*, 246, 118533.

Shahmansouri, A. A., Nematzadeh, M., and Behnood, A. (2021). “Mechanical properties of GGBFS-based geopolymer concrete incorporating natural zeolite and silica fume with an optimum design using response surface method.” *J. Build. Eng.*, 36(December 2020), 102138.

Shi, X., Zhang, C., Wang, X., Zhang, T., and Wang, Q. (2022). “Response surface methodology for multi-objective optimization of fly ash-GGBS based geopolymer mortar.” *Constr. Build. Mater.*, 315, 125644.

Singh, B., Ishwarya, G., Gupta, M., and Bhattacharyya, S. K. (2015). “Geopolymer concrete: A review of some recent developments.” *Constr. Build. Mater.*, 85, 78–90.

Sofi, M., Deventer, J. S. J. van, Mendis, P. A., and Lukey, G. C. (2007). “Engineering properties of inorganic polymer concretes (IPCs).” *Cem. Concr. Res.*, 37(2), 251–257.

Srinivasa, A. S., Swaminathan, K., and Yaragal, S. C. (2023). “Microstructural and optimization studies on novel one-part geopolymer pastes by Box-Behnken response surface design method.” *Case Stud. Constr. Mater.*, 18(February), e01946.

Sturm, P., Gluth, G. J. G., Brouwers, H. J. H., and Kühne, H. C. (2016). “Synthesizing one-part geopolymers from rice husk ash.” *Constr. Build. Mater.*, 124, 961–966.

Thomas, R. J., Lezama, D., and Peethamparan, S. (2017). “On drying shrinkage in alkali-activated concrete: Improving dimensional stability by aging or heat-curing.” *Cem. Concr. Res.*, 91, 13–23.

Tu, W., and Zhang, M. (2023). “Behaviour of alkali-activated concrete at elevated temperatures: A critical review.” *Cem. Concr. Compos.*, 138(January), 104961.

Vu, T. H., Gowripalan, N., Silva, P. De, Paradowska, A., Garbe, U., Kidd, P., and

Sirivivatnanon, V. (2020). “Assessing carbonation in one-part fly ash/slag geopolymer mortar: Change in pore characteristics using the state-of-the-art technique neutron tomography.” *Cem. Concr. Compos.*, 114(April), 103759.

Wang, J., Dai, Y., and Gao, L. (2009). “Exergy analyses and parametric optimizations for different cogeneration power plants in cement industry.” *Appl. Energy*, 86(6), 941–948.

Wang, K. tuo, Du, L. qiu, Lv, X. sen, He, Y., and Cui, X. min. (2017). “Preparation of drying powder inorganic polymer cement based on alkali-activated slag technology.” *Powder Technol.*, 312, 204–209.

Wang, Y. S., Alrefaei, Y., and Dai, J. G. (2021). “Roles of hybrid activators in improving the early-age properties of one-part geopolymer pastes.” *Constr. Build. Mater.*, 306(September), 124880.

Xu, L. Y., Qian, L. P., Huang, B. T., and Dai, J. G. (2021). “Development of artificial one-part geopolymer lightweight aggregates by crushing technique.” *J. Clean. Prod.*, 315(January), 128200.

Yang, K. H., Song, J. K., Ashour, A. F., and Lee, E. T. (2008). “Properties of cementless mortars activated by sodium silicate.” *Constr. Build. Mater.*, 22(9), 1981–1989.

Yaragal, S. C., Babu Narayan, K. S., and Adari, S. (2012). “Strength characteristics of concrete exposed to elevated temperatures and cooled under different regimes.” *J. Struct. Fire Eng.*, 3(4), 301–310.

Yaragal, S. C., Chethan Kumar, B., and Jitin, C. (2020). “Durability studies on ferrochrome slag as coarse aggregate in sustainable alkali activated slag/fly ash based concretes.” *Sustain. Mater. Technol.*, 23, e00137.

Yazici, Ş., Sezer, G. N., and Şengül, H. (2012). “The effect of high temperature on the compressive strength of mortars.” *Constr. Build. Mater.*, 35, 97–100.

Ye, N., Yang, J., Liang, S., Hu, Y., Hu, J., Xiao, B., and Huang, Q. (2016). “Synthesis and strength optimization of one-part geopolymer based on red mud.” *Constr. Build. Mater.*, 111, 317–325.

Yong-Jie, H., Cheng-Yong, H., Yun-Ming, L., Bakri Abdullah, M. M. Al, Yeng-Seng, L., Ern-Hun, K., Shee-Ween, O., Wan-En, O., Hui-Teng, N., and Yong-Sing, N. (2023). "Strength optimization and key factors correlation of one-part fly ash/ladle furnace slag (FA/LFS) geopolymer using statistical approach." *J. Build. Eng.*, 63(PA), 105480.

Yousefi Oderji, S., Chen, B., Ahmad, M. R., and Shah, S. F. A. (2019). "Fresh and hardened properties of one-part fly ash-based geopolymer binders cured at room temperature: Effect of slag and alkali activators." *J. Clean. Prod.*, 225, 1–10.

Zhang, B., He, P., and Poon, C. S. (2020). "Optimizing the use of recycled glass materials in alkali activated cement (AAC) based mortars." *J. Clean. Prod.*, 255, 120228.

Zhang, H. Y., Liu, J. C., and Wu, B. (2021). "Mechanical properties and reaction mechanism of one-part geopolymer mortars." *Constr. Build. Mater.*, 273.

Zhang, Z., Zhu, Y., Yang, T., Li, L., Zhu, H., and Wang, H. (2017). "Conversion of local industrial wastes into greener cement through geopolymer technology: A case study of high-magnesium nickel slag." *J. Clean. Prod.*, 141, 463–471.

Zhou, S., Ma, C., Long, G., and Xie, Y. (2020). "A novel non-Portland cementitious material: Mechanical properties, durability and characterization." *Constr. Build. Mater.*, 238, 117671.

APPENDIX

Sample Mix Design of One-part Geopolymer Concrete Mixes

Input parameters

Specific gravity of GGBS	=	2.91
Density of GGBS	=	1100 kg/m^3 (Loose)
	=	1250 kg/m^3 (Vibrated)
Specific gravity of Fly ash	=	2.25
Density of Fly ash	=	700 kg/m^3 (Loose)
	=	1120 kg/m^3 (Vibrated)
Specific gravity of solid activator	=	2.64
Specific gravity of sand	=	2.65
Water absorption of sand	=	Nil
Maximum size of coarse aggregates	=	20 mm
Specific gravity of Coarse aggregates (20-10 mm)	=	2.71
Specific gravity of Coarse aggregates (10-4.75 mm)	=	2.69
Water to geopolymer solids ratio (W/GS)	=	0.35
Fly ash to GGBS ratio	=	50:50

The aggregates are used in saturated surface dry condition.

Estimation of ingredients for 1 m^3 of one-part geopolymer concrete

Step 1: Selection of Binder Content and Water Binder Ratio

Assumed precursor content = 450 kg/m^3

Assumed Water/binder ratio = 0.4

Step 2: Calculations for fly ash and GGBS (solid precursors) required for 1 m^3 of OPG concrete

Volume of concrete = 1 m^3

Total weight of Precursor = 450 kg/m^3

Fly ash volume = 0.5 × (450/2.2×1000) = 0.1023 m^3

GGBS volume = 0.5 × (450/2.9×1000) = 0.0776 m^3

Total volume of precursor = 0.1799 m^3

Weight of fly ash = 0.1023 × 0.5 × 2.2 × 1000 = 197 kg/m^3

Weight of GGBS = 0.0776 × 0.5 × 2.9 × 1000 = 260 kg/m^3

Total weight precursors = 197 + 260 = 457 kg/m^3

Step 3: Calculation for water content required

Considered water to geopolymer solid ratio (W/GS) = 0.40

Quantity of water required = 0.40 × Total weight of solid precursors

= 0.40 × 457

Total quantity of water required = 183 kg/m^3.

Step 4: Calculations for solid activators required

Dosage of solid activator = 12% of the total weight of solid precursors

Weight of solid activator

Solid sodium silicate powder having 48% Na_2O, 47% SiO_2 and 5% of water by weight.

Hence, 1 kg of solid sodium silicate powder contains 0.48 kg of Na_2O, 0.47 kg of SiO_2 and 0.05 kg of water.

Since, water content is less than 5% by weight, is not considered as additional water content.

Modulus (Ms) of solid sodium silicate powder = SiO_2/Na_2O = 47/48 = 0.98

Weight of the solid activator = Total weight of solid precursors × Dosage of solid

Activator/100

= 457 × 12/100

Weight of the solid activator = 55 kg/m^3.

Step 5: Calculation of Total Aggregate Quantity

Volume of Paste $= \left[\frac{197}{2.2} + \frac{260}{2.9} + \frac{183}{1} + \frac{55}{2.61}\right] \times \frac{1}{1000} = 0.385\ m^3$

Volume of Aggregate $=$ 1-0.385 $= 0.615\ m^3$

The Proportioning of Fine aggregate: Coarse aggregate = 35:65

Weight of fine aggregate $= 0.615 \times 2.65 \times 1000 \times 0.35$

= 570 kg/m^3

The Proportioning of Coarse aggregate: (20-10 mm) : (10-4.75 mm) = 60:40

Weight of coarse aggregate (20-10 mm) $= 0.615 \times 2.71 \times 1000 \times 0.65 \times 0.6$

= 650 kg/m^3

Weight of coarse aggregate (10-4.75 mm) $= 0.615 \times 2.69 \times 1000 \times 0.65 \times 0.4$

= 430 kg/m^3

Step 6: Mix calculations

a)	Weight of fly ash	=	197 kg/m^3
b)	Weight of GGBS	=	260 kg/m^3
c)	Weight of solid activator	=	55 kg/m^3
d)	Weight of water	=	183 kg/m^3
e)	Weight of fine aggregate	=	570 kg/m^3
f)	Weight of coarse aggregate (20-10 mm)	=	650 kg/m^3
g)	Weight of coarse aggregate (20-10 mm)	=	430 kg/m^3
	Total weight of OPG concrete	**=**	**2345 kg/m^3**

LIST OF PUBLICATIONS BASED ON PRESENT RESEARCH WORK

Journal:

1. **Anil Sagar Srinivasa**, K. Swaminathan, Subhash C. Yaragal and R. Rakesh Kumar Reddy (2023). "Multi-objective optimization of one-part geopolymer mortars adopting response surface method." *Construction and Building Materials.* https://doi.org/10.1016/j.conbuildmat.2023.133772 (Q1, IF: 7.4, SCIE/Scopus)
2. **Anil Sagar Srinivasa**, K. Swaminathan, and Subhash C. Yaragal (2023). "Microstructural and optimization studies on novel one-part geopolymer pastes by Box-Behnken response surface design method." *Case Studies in Construction Materials*. https://doi.org/10.1016/j.cscm.2023.e01946 (Q1, IF: 6.2, SCIE/Scopus)
3. **Anil Sagar Srinivasa**, K. Swaminathan, and Subhash C. Yaragal (2023). "Influence of solid activator on setting time and compressive strength properties of fly ash/slag based one-part geopolymer pastes." *Indian Journal of Environmental Protection.* (Scopus)

Proceedings:

1. **Anil Sagar Srinivasa**, K. Swaminathan, and Subhash C. Yaragal (2023). "Effect of slag and solid activator on flowability and compressive strength of fly ash based one-part geopolymer pastes." *Materials Today: Proceedings.* https://doi.org/10.1016/j.matpr.2023.03.481. (Scopus)

Book chapters:

1. **Anil Sagar Srinivasa**, K. Swaminathan, Subhash C. Yaragal, and Rakesh Kumar Reddy (2023). "Experimental studies on the development of one-part geopolymer binders at higher dosage of sodium metasilicate powder". *International conference on "Climate Resilient Construction and Building Materials (ICCRCBM - 2023)" held at NITK, Surathkal, India on March 03-05, 2023.* (Accepted to publish in springer book chapter) (Scopus)
2. **Anil Sagar Srinivasa**, K. Swaminathan, and Subhash C. Yaragal (2022).

"Effect of water to geopolymer solids ratio on properties of fly ash and slag-based one-part geopolymer binders". *International conference on "Advances in Civil Engineering 2022 (ICAC-2022)" held at LSKBJ College of Engineering, Chandwad, Nashik, India on December 20-22, 2022.* (Accepted for publication in an Open Access Edited Book)

3. **Anil Sagar Srinivasa**, K. Swaminathan, and Subhash C. Yaragal (2023). "Mechanical strength properties of fly ash/slag based one-part geopolymer mortars". *International Conference On Sustainable Infrastructure: Innovation, Opportunities and Challenges– 2023 (SIIOC – 2023)" held at NITK, Surathkal, India on April 20-21, 2023.* (Accepted to publish in springer book chapter) (Scopus)

CURRICULUM VITAE

Name : Anil Sagar S

Contact No. : 9741785597

Email : anilsagars1993@gmail.com

Date of Birth : 27 – 07 – 1993

Educational Qualifications

Degree	**Institution**	**University**	**Year of passing**	**Division**
B.E (Civil)	Government college of Engineering, Kushalanagar, Karnataka	VTU, Belagavi	2014	1st Class with Distinction
M.Tech (Structures)	Government SKSJTI, Bangalore, Karnataka	VTU, Belagavi	2017	1st Class with Distinction

Teaching Experience

Name of Institution	**Position held**	**Period**
MITS, Madanapalle, AP	Assistant Professor	July – 2017 to July – 2018

Research Publications

	International	**National**
Journal papers	6	3
Conference Publications	7	-